N°: 40504 Year: 2011

A dissertation submitted in the partial fulfilment of the requirement for the award of

DOCTOR OF PHILOSOPHY (PhD)

in

MATERIALS SCIENCE

from

UNIVERSITY OF SCIENCE AND TECHNOLOGY, LILLE

by

Saad NAUMAN

GEOMETRICAL MODELLING AND CHARACTERIZATION OF 3D WARP INTERLOCK COMPOSITES AND THEIR ON-LINE STRUCTURAL HEALTH MONITORING USING FLEXIBLE TEXTILE SENSORS

March, 2011

Presented before the jury on 24th March 2011, comprising of

Dr. Christophe BINETRUY	Professeur, Ecole de Mines de Douai, France	President of jury
Dr. George STYLIOS	Professeur, Heriot Watt University, United Kingdom	Rapporteur
Dr. Emmanuelle VIDAL-SALLE	Maitre de conférences, INSA de Lyon, France	Rapporteur
Dr. Damien SOULAT	Maitre de conférences, Polytech Orleans, France	Examinateur
Dr. Ahmed RACHID	Professeur, Université de Picardie Jule Verne, France	Examinateur
Dr. Vladan KONCAR	Professeur, ENSAIT, Roubaix, France	Directeur de la thèse
Dr. François BOUSSU	Maitre de conférences, ENSAIT, Roubaix, France	Co-encadrant de la thèse
Dr. Irina CRISTIAN	Maitre de conférences, ENSAIT, Roubaix, France	Co-encadrant de la thèse

ACKNOWLEDGEMENTS

A PhD thesis is never a solitary effort but is the result of collaboration and intensive team work. Many people have actively participated during the course of present research work in their personal and institutional capacities.

First of all I express my sincere gratitude to **Higher Education Commission, Pakistan** and **Ecole Nationale Supérieure des arts et Industries Textiles, Roubaix (France)** for showing their trust in me and giving me an opportunity to carry out research, which not only fostered my technical outlook but contributed manifolds to the development of my multicultural horizon.

I would like to thank **Prof. Vladan KONCAR, Dr. François BOUSSU and Dr. Irina CRISTIAN** for giving me continuous guidance and unconditional support during the entire project work. It has been a great experience for me to work under their supervision.

Many thanks are due to the technical staff of GEMTEX and the weaving department for their sincere efforts for the completion of this project. I would like to personally thank the staff and researchers at **Ecole de Mines de Douai** including **Patrick LAPEYRONNIE**, who delivered their kind assistance right from the beginning of whole exercise. Moreover thanks are also due to **Pierre-Marie ROGIER** for his help and assistance during some very important research work without which the completion of this thesis could not have been possible.

Many others should be thanked for their support. Though not all of them physically helped me, they stood by me in very trying times with numerous words of encouragement and much needed moral support. When I felt that I was unable to finish, they pushed me along and would not let me give up, for they knew failure was not an option I would be able to live with.

Finally, I would like to thank, though words might not suffice, from the depth of my heart, my parents, family and friends in Pakistan for supporting me in my endeavours for completing this thesis.

March 2011 **Saad NAUMAN**

TABLE OF CONTENTS

CHAPTER 3

CHAPTER 4

LIST OF FIGURES

LIST OF TABLES

LIST OF PUBLICATIONS

2007

F. Boussu, X. Legrand, S. Nauman, and P. Bruniaux, "**Comparison of the geometrical and mechanical models used for the textile composite structures**," in *CORTEP International Conference* Iasi, Romania, 2007.

2008

F. Boussu, X. Legrand, S. Nauman, and V. Koncar, "**Geometric modelling of 3D angle interlock fabrics**," in *AUTEX International Textile Conference* Biella, Italy, 2008.

F. Boussu, X. Legrand, S. Nauman, and C. Binetruy, "**Mouldability of angle interlock fabric**," in *9th international Conference on Flow Processes in Composite Materials* Montreal, Canada, 2008.

S. Nauman, F. Boussu, X. Legrand, and V. Koncar, "**Geometrical modelling of 3D textile composite application to warp interlock carbon fabrics**," in *13th European Conference on Composite Materials* Stockholm, Sweden, 2008.

2009

S. Nauman, I. Cristian, F. Boussu, X. Legrand, and V. Koncar, "**Weaving of 3D interlock layer to layer carbon-glass reinforcement on a conventional loom**," in *2nd international Conference on textile and Clothing* Lahore, Pakistan, 2009.

F. Boussu, I. Cristian, and S. Nauman, "**Technical performance of yarns inside a 3D woven fabric**," in *ITC International Conference on Latest Advancements in High Tech Textiles and Textile-based Materials* Gent, Belgium, 2009.

F. Boussu, S. Nauman, I. Cristian, X. Legrand, and V. Koncar, "**Geometrical characterization of orthogonal / layer-layer woven interlock carbon reinforcement**," in *AUTEX World Textile Conference* Çesme, İzmir, Turkey, 2009.

X. Legrand, F. Boussu, S. Nauman, I. Cristian, P. Lapeyronnie, L.-G. P., and C. Binetruy, "**Forming behaviour of warp interlock composite**," in *ESAFORM Conference* Twente University, Netherlands, 2009.

S. Nauman, F. Boussu, I. Cristian, and V. Koncar, "**Impact of 3D woven structure onto the high performance yarn properties**," in *2nd ITMC conference on Intelligent Textiles and Mass Customisation* Casablanca, Morocco, 2009.

X. Legrand, F. Boussu, S. Nauman, I. Cristian, P. Lapeyronnie, P. Le Grognec, and C. Binetruy, "**Forming behaviour of warp interlock composite**," *International Journal of Material Forming*, vol. 2, pp. 177-180, 2009.

2010

S. Nauman, I. Cristian, F. Boussu, and V. Koncar, "**Design and Optimization of piezoresistive sensors for Structural health monitoring of carbon fibre reinforced 3D woven composites**," in *7th IBCAST* Islamabad, Pakistan, 2010.

Y. Nawab, S. Nauman, I. Cristian, F. Boussu, and V. Koncar, “**Study of Mouldability of 3D Woven Multilayer Interlock, Carbon-Epoxy Composites**,” in *7th IBCAST* Islamabad, Pakistan, 2010.

S. Nauman, I. Cristian, F. Boussu, and V. Koncar, "**Application of 3D Geometrical Modelling approach on Multilayer angle interlock carbon reinforcements**," in *AUTEX 2010 World Textile Conference* Vilnius, Lithuania, 2010.

S. Nauman, I. Cristian, F. Boussu, and V. Koncar, "**In situ strain sensing in Three dimensional woven preform based composites using flexible tensile sensor**," in *TEXCOMP* Lille, France, 2010.

S. Nauman, P. Lapeyronnie, I. Cristian, F. Boussu, and V. Koncar, "**On line measurement of structural deformations in composites**," *IEEE Sensors Journal,* vol. PP, 2010.

2011

S. Nauman, I. Cristian and F. Boussu, “**Geometrical Modelling Of Angle Warp Interlock Fabrics,”** *accepted for publication in Journal of Textile Institute.*

I. Cristian, S. Nauman, F. Boussu, and V. Koncar, "**A study of strength transfer from tow to textile composite using different reinforcement architectures,**" *accepted for publication in Journal of Applied Composite Materials.*

GENERAL INTRODUCTION

Motivations

A material composed of two or more distinct phases (matrix phase and dispersed or reinforcing phase) and having bulk properties significantly different form those of any of the constituents is defined as a composite material.

Composite materials can be adapted to the intended application area and conceived according to the desired mechanical performance of the structure. Due to this fact, composite materials find broad potential in structural applications. Structural composite materials are being developed in many different domains such as: aeronautics, marine, automotive, civil engineering and all the others where specific properties related to weight are important.

Currently, fibre reinforced composites (i.e. composites having fibres as the reinforcing phase) are being widely used in high performance structural applications. Various techniques can be used to manufacture these fibrous reinforcements. Weaving technique which is one of the traditional textile technologies is used to manufacture interlaced fibrous assemblies to serve as reinforcements for composite materials. A suitable design of the reinforcement coupled with the use of high performance fibres and a compatible matrix are essential for high performance composite structural part.

Woven interlock reinforcements are unique as they can be manufactured on a conventional adapted loom. In this way a single complex net shaped preform having through the thickness reinforcing fibres, to minimize delamination can be produced in a single manufacturing step.

An unlimited number of interlock architectures can be designed owing to the versatility of the weaving technology. Therefore it is important for academic and practical purposes that a clear classification of the interlock structures be adopted. Various different classifications exist in the literature. The one adopted and further elaborated here is particularly interesting as it can be used for the mathematical description of interlocks.

Since a composite owes its mechanical strength to the reinforcement properties, it is important to design reinforcement according to the end use of the composite. Complete understanding of the reinforcement properties, its manufacturing process and the nature of matrix are critical. Moreover, woven structures are hierarchically organized. Three hierarchy levels are usually associated with textiles namely macro (structural parts ranging from a cm to several meters), meso (yarns and tows in mm) and micro (fibres in µm). At each level, different degrees of approximations are needed to describe the textile structure. Geometrical modelling at meso structural level is advantageous as it can be used to describe all the essential parameters of a fabric while avoiding unrealistic approximations of the macro scale and unnecessary complications at the micro scale. It is important that the woven reinforcement geometry be modelled keeping in view the technological constraints, so that the resultant geometrical description becomes realistic. Weaving parameters should be coupled with the geometry at meso structural level in order to obtain a sufficiently accurate and user friendly model.

Manufacturing process not only influences the geometry of tows inside the reinforcement, but also their mechanical properties. Due to mechanical stresses and deformations induced during manufacturing process, tow to tow friction and abrasion between tows and the loom parts, the tows lose their properties significantly. Moreover tow strength changes significantly along the complete production line of a woven composite i.e., from tow to its integration in warp and weft to form a reinforcement and finally to the composite that is formed by resin impregnation. It is important that this evolution be studied and the influence of weaving parameters be well understood on the final reinforcement and composite properties.

In addition to the understanding of mechanical behaviour of a composite in laboratory, it is important that some sort of system be put in place so as to monitor the state or 'health' of the structure during service life of the structural part or component. This scheme is termed as structural health monitoring.

A generic design procedure for a structural health monitoring system comprises of several interrelated steps. These steps can be represented as follows

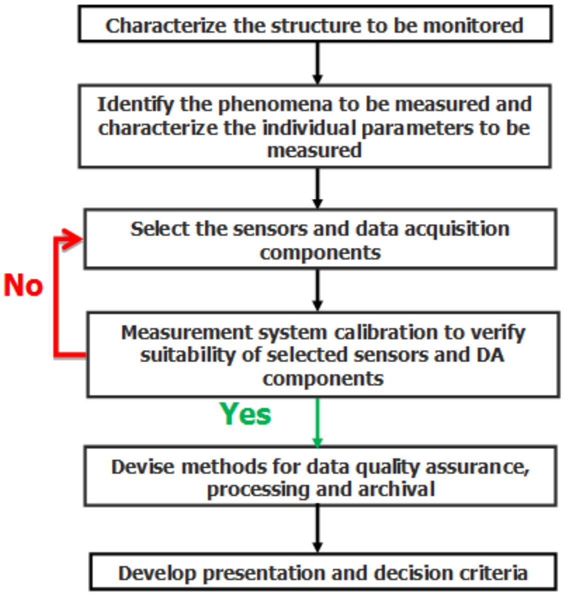

Generic procedure for health monitoring design

This design procedure can serve as a reference for our research and can guide us through various steps required for designing a system for in situ measurements in a composite reinforced with warp interlocks.

Therefore having studied the global tensile behaviour of composites, the next step is introducing sensing mechanism in the composite so as to measure in-situ local deformations. In the context of textile materials these sensors should be compatible with the reinforcement and its manufacturing process. In this way the cost of integration of sensors can be reduced considerably as it is one step insertion during manufacturing. Moreover any sensor that follows the geometry of the reinforcement is expected to follow the deformation pattern when the composite is subjected to stresses. Strategically located in-situ sensor can also give useful information about the deformation pattern of the reinforcement inside the composite during loading.

Main contributions

In reference to the aforementioned scope of the research, the thesis provides following contributions

- After the review of modelling approaches used to model geometry of interlock structures, a comprehensive study of the interlock geometries has been carried out. Samples of woven interlocks have been analysed. A simple meso structural modelling approach has been proposed which can be correlated to the structural parameters of a warp interlock reinforcement and its geometrical parameters can be calculated henceforth.
- A complete study of the mechanical properties of tows from its virgin state to its final integration in the reinforcement and finally to the composite formation has been carried out for a class of interlock structures. A coefficient called strength transfer coefficient has been proposed which can be used to understand and compare the impact of weaving parameters on the final composite properties.
- A novel flexible textile sensor along with data amplification and treatment module has been developed for real time in-situ structural health monitoring of textile composites. The sensors were inserted during weaving on a modified loom. The system was tested during quasi static tensile loading.

Thesis overview

This thesis is composed of two main parts. The first part deals with the geometrical modelling and deformation study of warp interlock woven fabrics. The second part is concerned with the real time in situ structural health monitoring of textile composites.

A brief overview of all the chapters is presented in the following;

The **first chapter** introduces 3D fabrics and their classification. An overview of geometrical modelling techniques and studies on mechanical deformations in 3D composites has also been given.

Having understood the importance of geometrical description, the **second chapter** of this thesis focuses on establishing and defining a model for geometrical description of 3D Interlock preforms woven with multifilament tows. This is followed by the description of weaving of 3D interlock reinforcements and their analysis.

The **third chapter** deals with the study of complete track of tow properties from tow to global composite mechanical properties. A coefficient which allows estimation of mechanical properties has been proposed and results have been presented for different woven reinforcement architectures.

The **fourth chapter** presents an overview of sensing mechanisms in intelligent textiles and composites. Different sensing systems have been described and compared. This is followed by a brief description of structural health monitoring.

The **fifth chapter** deals with the development and implementation of real time in situ measurement system for structural health monitoring of composites using flexible textile sensors.

The thesis ends with a conclusion of the theoretical and practical work presented in the previous parts. A perspective has also been given on the possibilities of further expanding the research presented in this thesis.

PART 1:

GEOMETRICAL MODELLING AND DEFORMATION STUDY OF WARP INTERLOCK WOVEN FABRICS

Chapter 1

State Of The Art

1.1. 3D-Weaving and 3D-Woven Fabrics

Weaving is defined as the action of producing fabrics by the interlacement of warp and weft threads [1]. The process of interlacement is carried out and completed on the loom by three sequential primary motions; shedding, picking and beat up. A woven fabric is produced by interlocking two sets of yarns, the warp and the weft, which are at right angles to each other in the plane of the cloth. The warp is along the length and the weft along the width of the fabric [2]. Due to its versatility weaving process can be used to produce so called 2D, 2.5 D and 3D fabrics [3]. In the following these three types have been defined.

- ***2D-fabrics:*** In 2D-fabrics the constituent yarns are disposed in one plane or two dimensions. A single layer warp and weft (i.e., two sets of yarns) are used to carry out the weaving process.
- ***2.5D-fabrics:*** In 2.5D or pile fabrics the constituent yarns are supposedly disposed in two mutually perpendicular plane relationships. In order to carry out the weaving process single layer ground warp, pile warp and weft (i.e., three sets of yarns) are used.
- ***3D-fabrics:*** In 3D fabrics the constituent yarns are disposed in three mutually perpendicular plane relationships. A multilayer warp and weft (i.e., two sets of yarns) or multilayer ground warp, binder warp and weft (i.e., three sets of yarns) are used.

1.1.1. Classification of 3D fabrics

Following two approaches can be used to classify woven 3D fabrics [4].

- **Based on Type of Weaving Process.** According to Khokhar [3] there are mainly three types of manufacturing systems to produce woven 3D fabrics. Thus on the basis of manufacturing method employed, three dimensional fabrics can be classified as:
    - 2D weaving – 3D fabrics;
    - 3D weaving – 3D fabrics and
    - NOOBing
- **Based on Type of 3D Structures:**
    - 3D Solid – further classified as warp and weft interlocks depending on whether the warp or weft is used to bind/interlock different layers together.
    - 3D Profiled – further classified as Hollow, Shell and Nodal type (Fig. 1.1)

Fig. 1.1: 3D Profiled fabrics (A) Hollow (B) Shell and (C) Nodal Type [5]

1.1.2. 3-D Structures obtained by 2D weaving

3D solid structures are integrated woven structures with interlacing yarns in three mutually perpendicular directions. When produced using 2D weaving process such woven fabrics are termed as 2D-woven/3D-fabrics. As mentioned above in such 2D woven 3D structures the interlocking yarn may be disposed in warp or weft directions. Such solid 3D fabrics may be termed as warp interlock or weft interlock respectively.

In warp interlocks, different layers of the multi-layer warp are interconnected. In the production of such 3D fabrics constituting two sets of yarns i.e., warp and weft, multi-layer warp is displaced in the fabric-thickness direction by the operation of shedding to form a shed across the fabric width direction in order to enable interlacement with the weft. This manner of producing a 3D fabric constituting two sets of yarns and also the functioning of the weaving device is in complete accordance with the principle of 2D weaving. For convenience this approach of producing a 'simple' interlaced 3D fabric by employing the 2D weaving principle may be referred to as the multi-layer or warp interlock weaving [3].

In the present work, the terms interlock weaves or structures will be used to refer to warp interlock as the dissertation is primarily concerned with the study of such fabrics.

1.1.3. Classification of interlock weaves/ Multilayer fabrics

In order to define interlock fabrics, several different classification methodologies have been adopted in the literature [6]. The one used here is proposed by Yi and Ding [7]. This classification approach is particularly unique as it allows a generic description of all interlocks and as will be shown later, permits the derivation of mathematical notions for the general definition of all interlock structures.

According to the orientation of binder warp yarns, 3D-solid woven structures can be classified into angle interlock and orthogonal interlock, or into through-the-thickness and layer-to-layer, if the penetration depth of binding is considered. Consequently, 3D solid woven fabrics can be classified into four types (Fig. 1-A, 1-B, 1-C and 1-D):

A. Angle interlock/Through-the-thickness binding;
B. Angle interlock/Layer-to-layer binding;
C. Orthogonal interlock/Layer-to-layer binding and
D. Orthogonal interlock/Through-the-thickness binding.

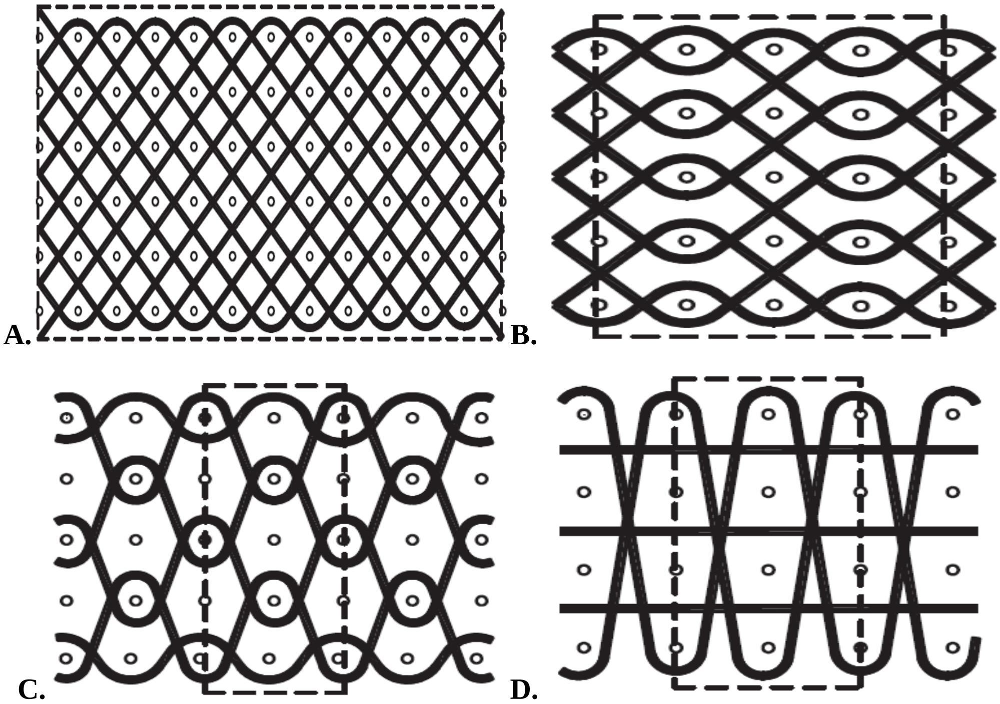

Fig. 1.2: Classes of 3D solid woven fabrics
A - Angle interlock/Through-the-thickness binding; B - Angle interlock/Layer-to-layer binding; C - Orthogonal interlock/ Layer-to-layer binding; D-Orthogonal interlock/Through-the-thickness binding [7]

In order to further elaborate the scheme of interlock classification given here, it is important that certain notions be defined beforehand. In case of an interlock fabric, the crimp angle, crimp amplitude and crimp frequency depend upon two geometrical factors called *'step'* and *'depth'* of binder warp. Moreover in a multilayer fabric the number of layers of warp and weft is not the same. In the technical literature the number of layers of a multilayer fabric usually refers to the number of layers of weft tows conceived to lay one above another. Therefore in this chapter the number of layers of a multilayer fabric will be refereed to as 'n_{wft}' i.e., number of layers of weft tows in a multilayer fabric.

Step 'x' refers to yarn movement in horizontal direction. In the case of warp interlock structures, the number of transversal weft yarns of a single layer crossed by a single longitudinal warp yarn between two consecutive interlacing points. It should be recalled that in a woven fabric an interlacing point is described as a place in the fabric where a warp yarn crosses over then under a weft yarn [8]. Step determines crimp frequency.

Depth 'y' refers to yarn movement in vertical axis i.e. the number of layers of transversal weft yarns that an interlocking warp yarn traverses in vertical direction. It determines crimp amplitude. Schematic of warp path having different values of step and depth has been given in Fig. 1.3.

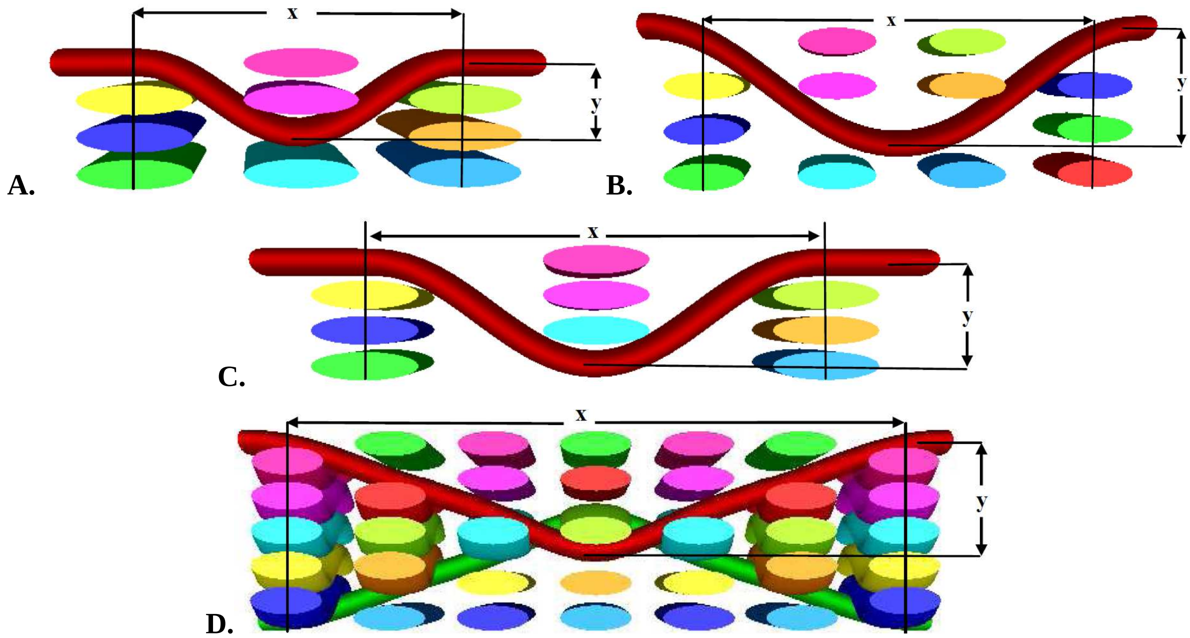

Fig. 1.3: Definition of step and depth for different interlock architectures

(A) x=1, y=2 (B) x=2, y=2 (C) x=1, y=3 (D) x=5, y=3

An interlock fabric can be designed to correspond to one of the four classes. Each of the four classes can be defined in terms of step 'x', depth 'y' and the number of layers 'n_{wft}', as shown in Table 1.1. Where x, y and n_{wft} are positive integers and $n_{wft} \geq 3$, as a true interlock structure can only be woven when number of weft layers is greater than 2.

Table 1.1: Description of different interlock classes in terms of binding depth and step

	Layer to layer		Through the thickness	
	Step (x)	Depth (y)	Step (x)	Depth (y)
Orthogonal	$1 \leq x < \infty$	$2 \leq y < n_{wft}$	$1 \leq x < \infty$	$y = n_{wft}$
Angle	$1 < x < \infty$	$2 \leq y < n_{wft}$	$1 < x < \infty$	$y = n_{wft}$

1.1.4. Advantages of Interlock/Multilayer woven reinforcements in composites

Owing to their special architecture 3D woven reinforcements exhibit following features.

- They form integral structures to near net shape [9-12]. In 3D woven fabrics, layers are joined together by filaments. Thus the reinforcement becomes a solid entirety and it is difficult for the layers to separate. Additionally filaments in a 3D woven structure are arranged in crosswise, lengthwise and thickness directions. This particular fibre architecture provides strength in three directions and 3D textile preforms form fully integrated continuous fibre assemblies having multi-axial in plane and out-of-plane fibre orientations. This has led to their usage in structural applications in aerospace, aircraft and automotive industries [12].
- 3D reinforcements provide enhanced delamination resistance [11, 12], resistance to crack propagation [11, 12], impact/fracture resistance, damage tolerance and dimensional stability [10, 12]. In laminated composites, delamination is the main failure mode under impulsive loading or ballistic impact. 3D textile structural composites are much tougher between layers and are characterized by better through the thickness properties as many reinforcing yarns exist in through-the-thickness direction [10]. This leads to the higher impact damage tolerance of 3D structural composites as compared to 2D laminates [12].
- 3D composites also have improved post-impact mechanical properties than that of 2D laminates [12].
- 3D composites possess high strain to failure in both tension and compression [10-12].
- 3D composites are also characterized by ease of fabrication via near-net-shape design and manufacturing of composite preforms, thus minimizing the need for cutting and joining parts and eventual use of resin transfer moulding of 3D preforms [4, 10, 12]. Not only can this reduce cycle times, since in making up composite parts no cutting and manual lay-up of single 2D pieces is required, but will result in better surface quality of the products. That's why 3D woven fabric reinforced composite materials have been widely used in engineering as they are less expensive and simpler to manufacture.
- 3D woven reinforcements are also characterized by easier and more efficient moulding, since, because the textile is already shaped, there are no forces to affect fibre placing during the moulding process, which results in better surface quality of products [4].
- Through-thickness properties can be adjusted by controlling the amount of z yarns. The variation of properties could also be achieved by hybriding [4, 12].

1.2. Modelling of 3D woven fabrics

Fibre orientations in a woven fabric determine its mechanical properties. Usually composite reinforcement is made from multifilament tows. These tows consist of parallel strands of filaments. Inside a tow they can be approximated to lie parallel to tow axis. Thus their influence can be studied by studying tow orientations at meso structural scale [13]. The tow orientations are related to fabric structure and weaving parameters. All of these can be broadly termed as fabric parameters. The interaction between fabric parameters can be obtained by considering a geometrical model of the fabric [14].

Several researches conducted have shown that the internal geometry of the reinforcement is an important factor influencing the composite manufacturing process and the service life of the composite structural part [11]. For the former, impregnation of the reinforcement is governed by its porosity (size, distribution and connectivity of pores). For the latter, load transfer from the matrix to the reinforcement is governed by the fibre orientation, which plays a paramount role in determining composite stiffness and stress-strain concentration loci. Determination of composite strength is correlated with the resin rich zones and fabric/matrix interfaces which are distributed in the composite volume according to the reinforcement geometry [15-18]. In order to better understand and predict the properties of a composite, it is critical that tow orientations and fibre volume fraction of the reinforcement be determined beforehand. This not only gives an “à priori” idea about the performance of the composite material but also allows us to vary the fibre volume fraction and crimp in warp and weft directions according to the end use and performance criteria of the composite material.

Geometrical modelling approach applied at mesostructural level coupled with certain weaving parameters known to textile technologists and the raw material properties can be employed to formulate a geometrical model of the multi layer reinforcement. Research in this field was pioneered by Peirce [19, 20]. Lomov has worked extensively on the subject and has developed textile geometry pre-processor for WiseTex® software package [21]. TexGen® developed by Sherburn [22] is another software package that allows geometrical modelling of textile reinforcements. But there is nevertheless a dearth of research work on the geometries of real 3D woven structures as the weaving technology parameters are numerous and they tend to influence the geometry of the structure in various ways.

Recently some geometrical models have been proposed for 3D fabrics [23-25] but either the tow trajectory is too unrealistic or the scope of the model is too limited. Quinn et al. [26] have calculated fibre volume fractions of 3D orthogonal structures. The binder tow path that they adopted was vertical. Authors have reported that fibre volume in z direction shows poor correlation because of the idealized yarn path adopted. Quinn et al. [27] have used lenticular tow sections for the calculation of preform thickness, areal density and fibre volume fractions for orthogonal woven preforms. Authors have concluded that the lenticular path gives accurate results. Buchanan et al. [23] have calculated fibre volume fractions for angle warp interlock weaves but they have assumed an idealized step shaped tow path which is a source of error in the calculations.

Taking into account the importance of geometrical description, this chapter focuses on the study and characterization of 3D Warp interlock reinforcements woven with carbon and glass multifilament tows. On the basis of this characterization a meso scale geometrical model has been developed and is used to calculate basic fabric parameters.

1.2.1. Classification of Models

In the following different approaches used for modelling the geometry of woven fabrics have been described briefly [28]:

A. Continuum models;
B. Mesostructural models;
C. Numerical models;
D. Mixed element approach.

A. Continuum Models

A continuum model treats a woven fabric as an anisotropic planar continuum with two preferred material directions (Fig. 1.4). Two of the greatest advantages of the continuum models are high computational efficiency and possibility of integration into multi-component system models.

In order to approximate a fabric as a continuum it is important to identify appropriate homogenized material parameters. Different approaches are used in this regard such as empirical testing, both empirical testing and detailed F.E.M. and mixed element modelling of fabric mesostructure.

The greatest inconvenience of continuum models is their inability to capture effects of interactions between yarn groups (crimp interchange, locking and resistance to relative yarn shear).

Examples of such models include Baesu et al. [29], Xue et al. [30] and Ruan and Chou [31], Gommers et al. [32] and Yasser et al. [33]

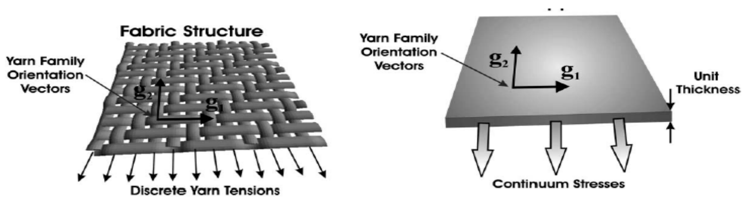

Fig. 1.4: Approximation of a fabric as an anisotropic homogenous material [28]

B. Mesostructural Models

These models use simplified geometrical assumptions to model the fabric at mesostructural level. Such models can be used to predict the mechanical properties of the component yarns of the fabric under specific modes of deformation. One important application of mesostructural models can be the quantification of homogenized material properties for use in continuum models. Analytical models of fabric mesostructure can be used in conjunction with anisotropic continuum models to track the deformations at mesostructural level of fabric hierarchy as the continuum deforms. Such a modelling approach combines the benefits of continuum modelling with the capability of following the evolution of fabric mesostructure in a single modelling step. In this way the scope of continuum models is widened.

One of the limitations of such models is that they are only applicable for special loading modes for which they are developed. Extension of these models to more general load cases is challenging due to the complexity of textile geometry.

In 1937 Peirce [19] described the mesostructural geometry of plain weave fabric whose yarns were approximated as having circular cross sections (Fig. 1.5). This pioneering work was meant to formulate mathematical relations relating the parameters that describe the geometrical configuration of a plain weave fabric.

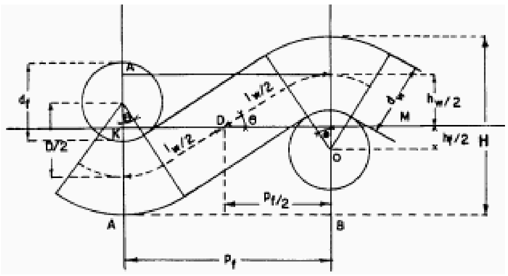

Fig. 1.5: Geometry Proposed by Peirce [19]

Different researchers have used modified forms of Peirce’s geometry to model yarns with non-circular deformable cross sections. Sagar et al. [34]and Hearle et al. [35]is a notable example.

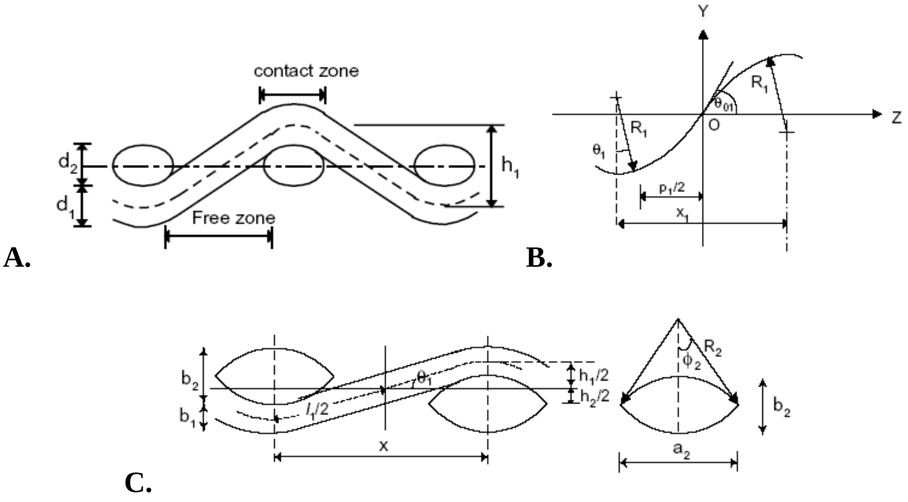

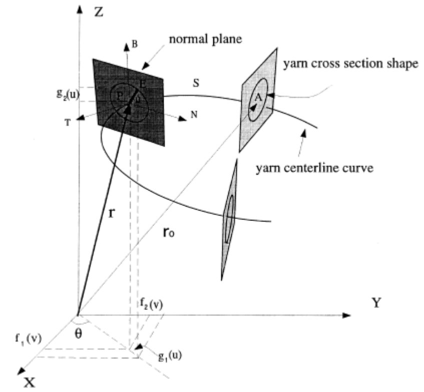

D.

Fig. 1.6: Different meso structural geometrical models based on Peirce's geometry

Kawabata [36-38]developed pin-joined truss geometry for analytical models of fabric (Fig. 1.7). This model is capable of describing biaxial, uniaxial and shear deformation behaviours.

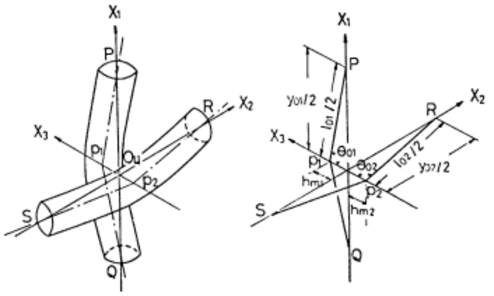

Fig. 1.7: Geometry Proposed by Kawabata [36]

Kato et al. [39] modified the geometry of Kawabata by adding spars to capture the effect of coatings (Fig. 1.8-A). The unit cell thus created was capable of resisting shear deformation. This model was proposed for predicting the constitutive behaviour of a coated fabric composite.

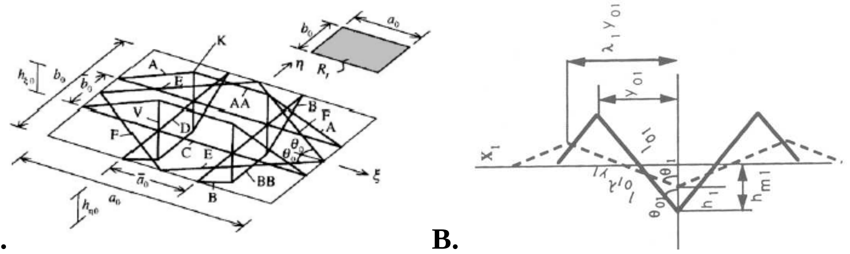

A. **B.**

Fig. 1.8: Geometries based on Kawabata model (A) Kato et al. [39], (B) Realff et al. [40]

Realff et al. [40] built on Kawabata's uniaxial model to include more complex behaviours such as yarn flattening and consolidation (Fig. 1.8-B).

Other examples of such models include Rattensperger et al. [41] (These models do not include yarn bending effects, locking or resistance of the fabric to shear) and Tanov et al. [42] (This model includes shear and locking resistance through diagonal spar elements within the assumed unit cell network but the model does not account for crimp interchange).

C. Numerical Models

Numerical models directly capture the fabric mesostructure by modelling every yarn in the fabric. Such models can capture all yarn interactions and provide a detailed description of all mechanisms of fabric deformation.

Large computational requirements limit the application of numerical models to relatively small systems. Since this approach is not suitable for large or multi component systems, it is used to gain insight into mechanics of fabric deformation at the mesostructural level, to estimate homogenized properties for simpler continuum models or to characterize the interaction of yarns. Since the yarns themselves are not homogenous and are composed of fibres therefore their constitutive behaviour can be a source of model uncertainty.

Examples include Ng et al. [43], Boisse et al. [44] and Nicoletto et al. [45] (Fig. 1.9).

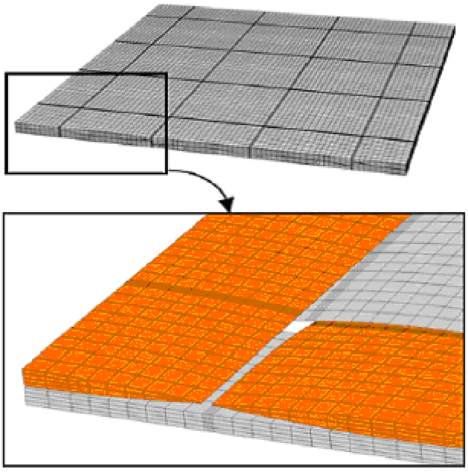

Fig. 1.9: FE Model of a 2 X 2 Twill weave fabric [45]

In order to achieve greater computational efficiency a mix of simpler more efficient finite elements (such as beams and spars) can be used directly to model entire fabric mesostructure.

For instance Reese [46] has used a mixture of truss and solid elements to model 3D textile composites and Cherouat et al. [47] have modelled pre-impregnated woven composites using truss elements and membrane elements.

D. Alternative Approaches

Several different alternative approaches have been proposed by researchers to model selected aspects of the fabric mesostructural behaviour. Such models are not suitable for more general analysis and can only be applied for the specialized aspects of fabric behaviour for which they are meant.

Examples include planar rectangular array of point masses to capture the inertia of fabric, connected by trusses to capture yarn compliances; Roylance et al. [48]and Provot et al. [49] (refer to Fig. 1.10).

Interacting particles to predict the low stress behaviour especially draping of woven fabrics; Breen et al. [50].

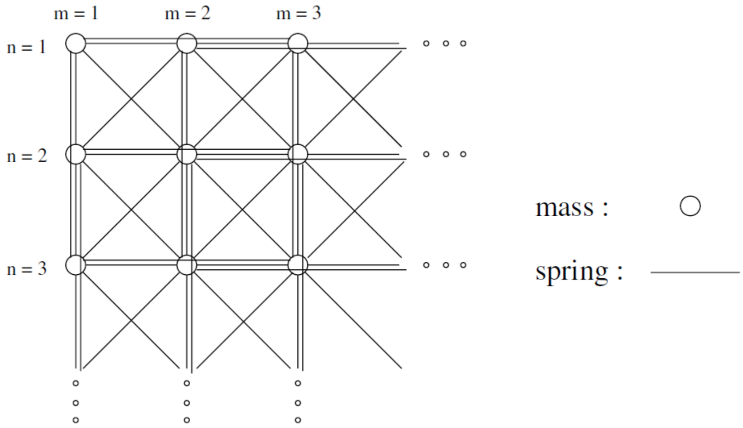

Fig. 1.10: Regular mesh of masses and springs proposed for animating clothed objects [49]

1.2.2. Geometrical Modelling Strategies

Geometrical models can be classified into two categories on the basis of the strategy to model the geometry

Models which require input data measured on composite cross-sections under micro-scope [51]. Particular disadvantage is that prior to manufacturing predictions are not possible and costly manufacturing and testing techniques need to be employed.

Models which employ simple geometrical representation of weave structure [19] so that prior to weaving prediction of fabric geometry is made possible. In such models some important features of fabric geometry are not covered (for instance skewness of yarns in twill weaves or different warp and weft crimp) due to over simplifications. Such models are also termed as à priori models. In order to formulate such models it is important that tow cross section be characterized. In the following different approaches for the characterization of tow cross sections have been explained.

1.2.2.1 General Cross-sectional Profiles

A tow is a bundle of untwisted continuous fibres, also called filaments. Usually tows contain tens or thousands of individual filaments [52].

According to the research work carried out on the subject [53], the cross-sectional geometry of a tow is defined by the arrangement of individual filaments in the tow. The cross-section of the individual filament varies according to the type of fibre. The cross-sections of carbon and glass fibres are usually circular for composites applications (Fig. 1.11).

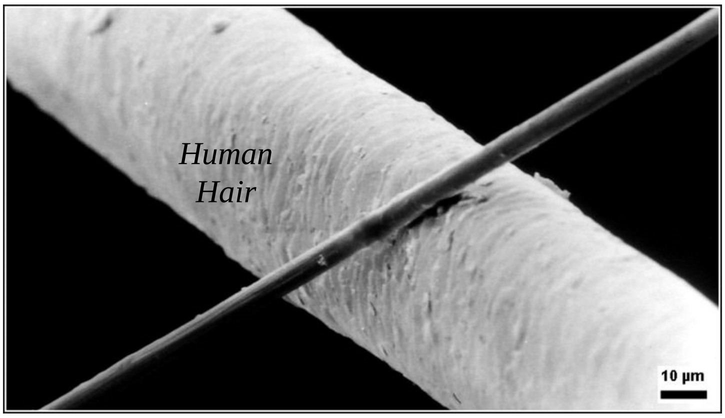

Fig. 1.11: A 6 μm diameter carbon filament (running from bottom left to top right) compared to a human hair [54].

The cross-section is determined during the initial production of tow prior to composite manufacturing. The application of bonding materials called size on the tow restricts fibre movement and results in the formation of a ribbon or a flat tape that is wound on to a package. The cross-sectional shape of the tow in this case is assumed to be rectangular. Sometimes for the purpose of certain idealized calculations, a tow is assumed to have a circular cross section. In such a case the individual filaments are assumed to be held in position to obtain this profile, application of load on the tow can change its profile to an elliptical cross section. The cross section is typically elliptical, lenticular or rectangular in practice.

The rectangular or elliptical cross-section of the tow is defined by its overall dimensions. The thickness of the tow and the width of the tow constitute its dimensions as illustrated in Fig. 1.12 - A, B and C.

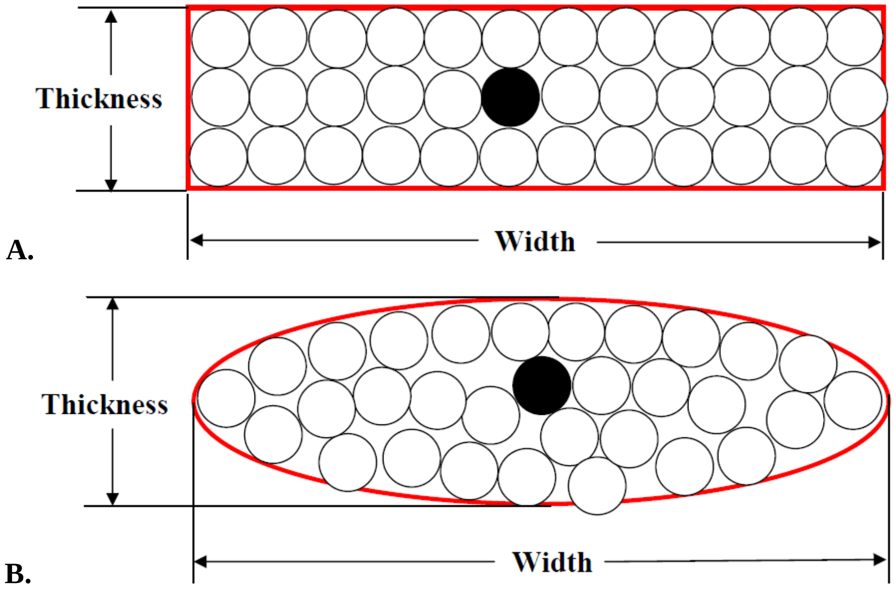

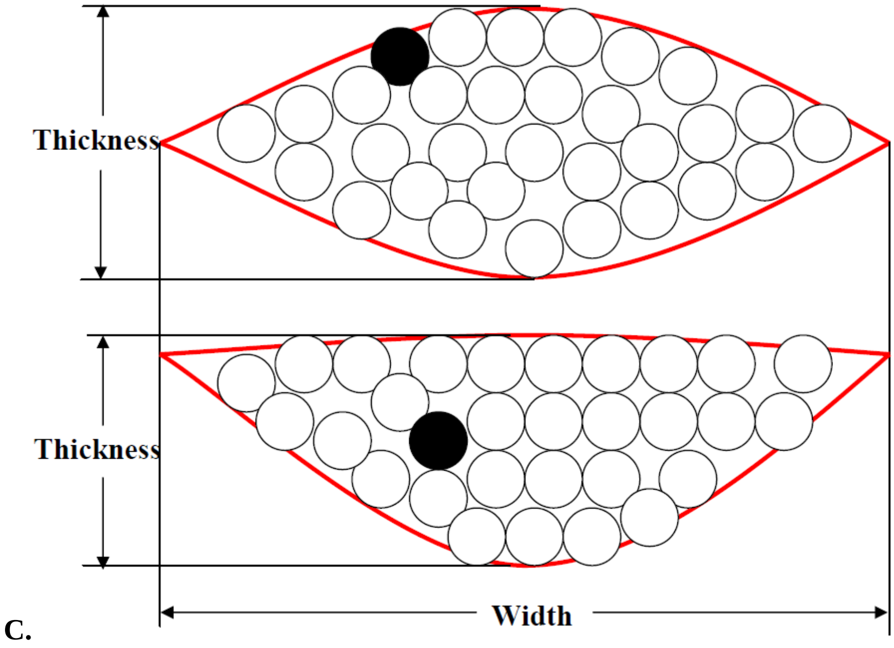

Fig. 1.12: Different tow cross sectional geometries

(A) Rectangular (B) Elliptical (C) Lenticular and half lenticular

1.2.2.2 Fibre Packing inside a tow

The faction of fibres in a three dimensional preform depends on the extent to which fibres pack against one another inside a tow and also on the level to which tows pack against one another in the woven structure [6]. The cross-section of the tow is defined by its overall dimensions at meso scale. However, individual filaments stacked together leave void spaces within the overall cross-section of the tow. Packing factor is thus defined as the ratio of the cross sectional area occupied by the filaments to the cross-sectional area of the tow.

Idealized packing in a tow is achieved when the filaments of a tow are arranged in any orderly and regular pattern, such that they represent the most compact packing configuration [55]. There are two basic forms of idealized packing of circular filaments [6, 56]:

- *Open packing* in which the filaments are arranged in layers between concentric circles; and
- *Close packing* in which the filaments fit into a hexagonal pattern.

A. Open Packing

A single fibre is present at the centre or core of the fibre arrangement in an open packing assembly as shown in Fig. 1.13. In ideal packing, there are no inter-fibre interstices, so six more fibres are packed around this central fibre. Another layer of fibres are packed in a circular arrangement, such that they are in contact with the fibres of the second layer. Subsequent layers are packed and arranged over the previous layers.

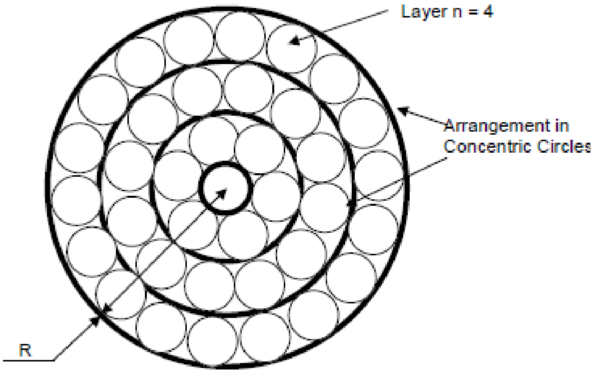

Fig. 1.13: Open Packing arrangement of filaments [53].

Let the fibre at the core = layer number 1,
Radius of circle around nth layer (*R*) = Radius of tow with '*n*' layers
Therefore, the overall radius of the tow,

$$R = (2n-1)R_{filament} \tag{1.1}$$

Where, $R_{filament}$ is the individual filament radius.
Therefore, radius of nth layer from the centre is given as

$$R = 2(n-1)R_{filament} \tag{1.2}$$

If M fibres are closely packed around the circumference of a circle, then the angle subtended at the centre by the distance between centres of the fibres (refer to Fig. 1.14)

$$\rho = \frac{360^\circ}{M} \tag{1.3}$$

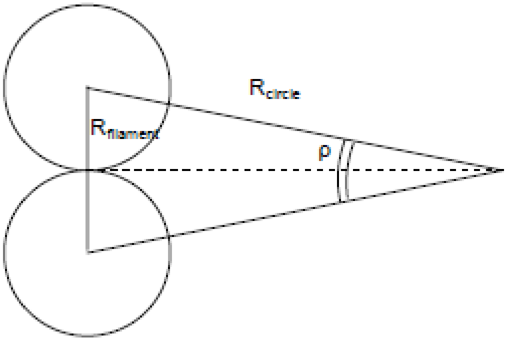

Fig. 1.14: Angle subtended at the centre by M filaments packed in a circle [53].

Hence, radius of circle

$$R_{circle} = R_{filament} \csc\left(\frac{180^{\circ}}{M}\right) \tag{1.4}$$

B. Hexagonal Close Packing

A single fibre present at the centre or core of arrangement of fibres in a close packing assembly has a hexagonal arrangement where all fibres are in contact with adjacent fibres from all directions as shown in Fig. 1.15. Here, the distance between the centre of the core-fibre and the centre of a layer lies between $R = 2(n-1)R_{filament}$ at the corners and $1.732(n-1)R_{filament}$ at the centre of the sides. From the second layer onwards, a constant number of 6 fibres are added in every layer following the expression of $6(n-1)$ fibres in a particular layer, where n is the number of the layer.

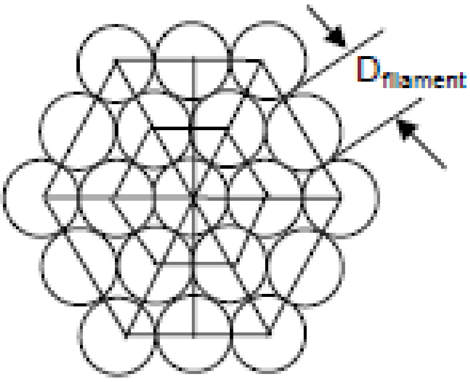

Fig. 1.15: Ideal Hexagonal packing arrangement of filaments [53].

The closest packing configuration is obtained till the 7th layer, which makes a total of 127 fibres. As the layers get added, the yarn outline becomes more complicated and tends to be circular for very large number of fibres. Fig. 1.15 shows hexagonal packing with a single core fibre, but it is also possible to obtain packing on more than one fibre as core in the arrangement. Perfect close packing can be obtained with more than a single core fibre for up to four fibres in the core, but the hexagonal outline no longer remains regular. Increasing the number of core fibres beyond four affects the packing and results in a void at the core if the number of core fibres exceeds five, giving a distorted shape to the whole yarn or tow structure [57].

Let filament diameter = d_f and

Inter-fibre void = u,

Therefore, packing factor is given as

$$P.F. = \left(\frac{\pi}{2\sqrt{3}}\right) \Big/ \left(1+\frac{u}{d_f}\right)^2 \tag{1.5}$$

Hence, considering the tightest fibre arrangement, u = 0. It results in a limit structure whose packing factor $= \frac{\pi}{2\sqrt{3}} = 0.90$. This is the maximum density a tow can have. In a loose structure, we have $u > d_f$, which implies that packing factor, must be < 0.227.

1.3. Tensile properties of 3D woven composites

1.3.1. Failure mechanisms in 3D woven composites

As regards failure mechanisms in 3D woven composites certain studies have been conducted to identify failure mechanisms and modes of deformation.

In his pioneering work Cox et al. [58] have described non linear process of damage propagation in a 3D woven composite in terms of discrete tow rupture events distributed over a band of damage typically 10-20 mm wide. These events have been classified as

- Tow straightening phase
- Rupture phase
- Lock-up phase
- Pull-out phase

In 3D woven composites where delamination is absent, compressive strength is influenced by tow irregularities through the micro-mechanisms of kink band formation. Following sources of tow irregularities were identified:

- Stuffers exhibit appreciable deflections in the out of plane/through thickness direction
- Same kinds of irregularities exist for fillers but their extent is much greater.
- In plane misalignments in stuffers and fillers.
- Local pinching distortions in stuffers and fillers near turning point of warp weavers.

Out of plane waviness is believed to be the critical form of irregularity in kink-band formation in monotonic and cyclic compression.

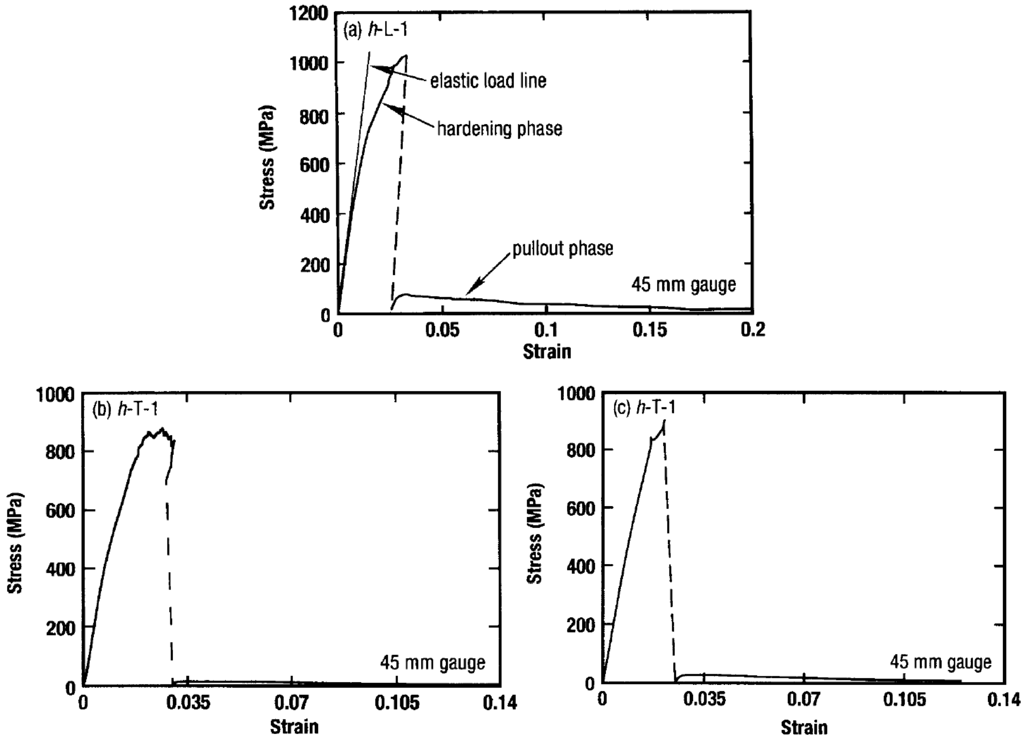

Fig. 1.16: Stress- strain curves for tension tests on carbon/epoxy composites [58]

Non linearity in these curves beyond the elastic regime is due to the fact that the resin in misaligned tow segments deforms plastically in shear which allows reinforcing tows to straighten. It was conjectured that Lock up occurs during the pullout process; Lock up is the result of interaction of waviness and pinching features on adjacent tows. Due to interlocking in 3D woven composites the contact forces between in-plane tows can be especially high. The critical mechanism in the hardening phase is said to be lockup; because of friction greatly enhanced by through-thickness compression and the contact of tow irregularities. Warp weavers play a primary role in the mechanics of lock up. Under axial tension in the stuffer direction, warp weavers develop through thickness compression. This aids lock up by increasing the contact forces between asperities. Warp weavers are not ruptured prior to primary load drop. Primary load drop occurs when warp weavers fail and permit already ruptured stuffers to spring apart and move relatively freely past one another. Warp weavers which follow approximately saw tooth paths, fail at significantly higher strains than the stuffers, which are nominally straight. During the hardening phase, the load is borne predominantly by the stuffers. Without the geometrical distortion of stuffers, neither plastic tow straightening nor lock up would exist. This is the primary reason why the work of fracture of 3D woven composites is very large; about one order of magnitude greater than that of unidirectional or cross plied graphite/epoxy laminates (or any other class of materials).

Callus et al. [59] found that the mechanical properties and failure mechanisms of 3D GRP composites made with orthogonal, layered interlock or offset layered interlock woven fabrics (Fig. 1.17) were the same when loaded in tension, provided the fibre volume fraction in the load direction was taken into account. The authors have reported that this similarity is because of the fact that due to tension variation the crimp in all the three woven architectures was the same.

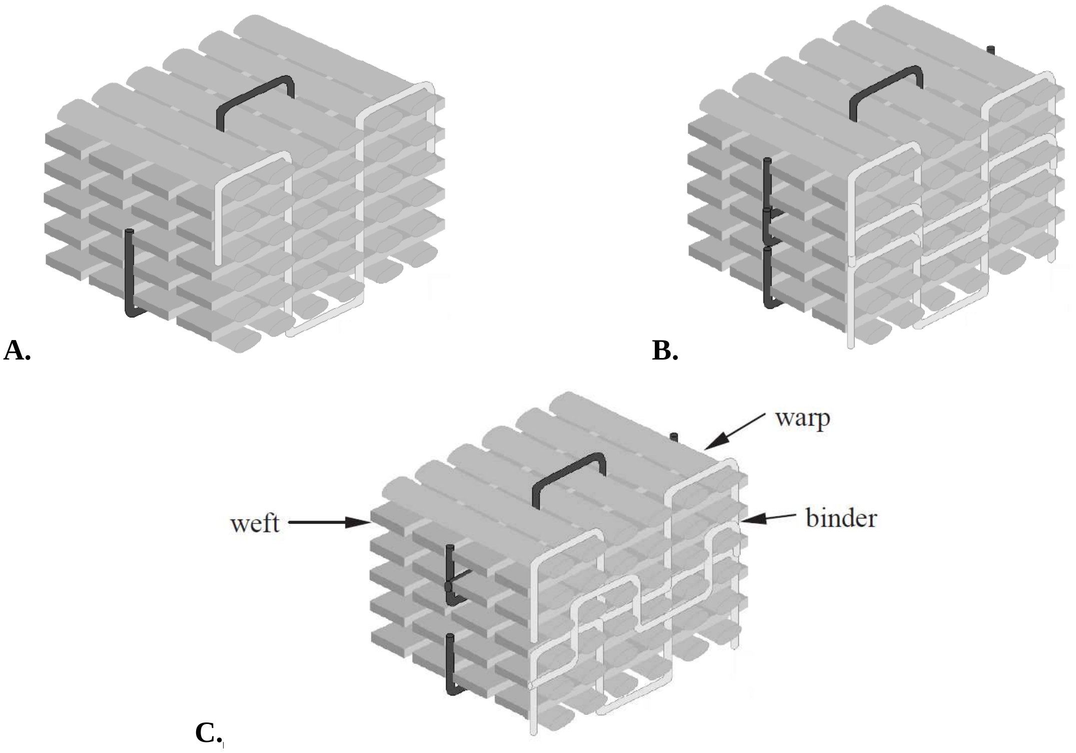

Fig. 1.17: Diagrams illustrating the idealized binder weave paths in the 3D woven: (A) Orthogonal; (B) normal layered interlock; and (C) offset layered interlock composites [59]

Three regions in stress-strain curve were identified (Fig. 1.18):

- ***first region:*** elastic regime; linear increase in curves until a slight kink at 0.3% strain
- ***second region:*** hardening phase; lower rate of increase from 0.3%-1.4%
- ***third region:*** softening phase; the composite experience continuous softening from 1.4-2 % or 2.2% until failure.

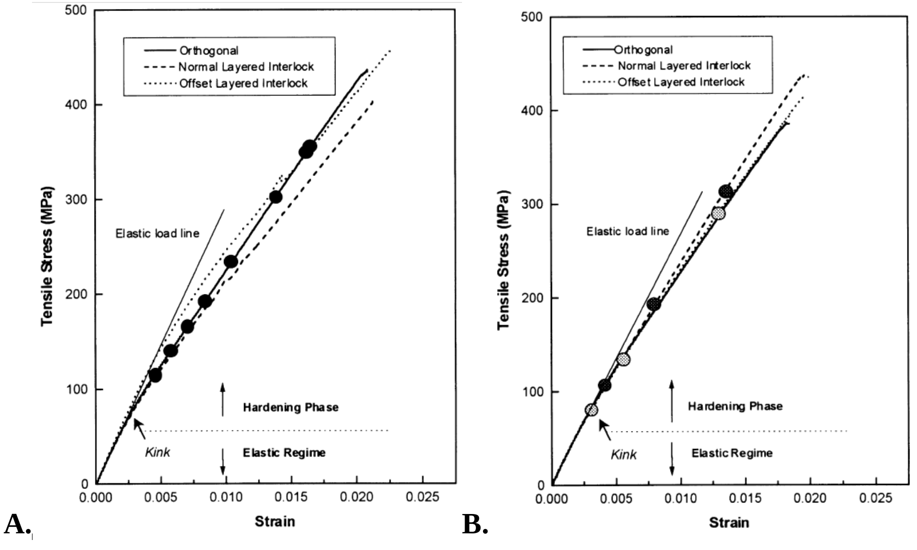

Fig. 1.18: Stress–strain curves for the orthogonal, layered interlock and offset layered interlock composites loaded in the: (A) warp; and (B) weft directions [59].

The points on the curves show the stresses to which the interrupted tensile test specimens were pre-loaded before being examined for damage. The points in Fig. 1.18-A are for the orthogonal composite, and the dark and light points in Fig. 1.18-B are for the normal layered interlock and offset layered interlock composites, respectively [59].

It was concluded that all macroscopic elastic properties follow from the fractions by volume of warp, weft and fillers, measured total fibre volume fractions and the measured composite thickness. Binder path has influence on fibre volume fraction in warp and weft directions. But in the samples studied, binder path had no influence on stiffness or strength of specimens probably because of similar crimp values in all the three architectures.

Internal stresses are generated inside the composite due to mismatch in the coefficients of thermal expansion of fibres and resin during curing. Composite undergoes expansion during consolidation and post curing of the laminate.

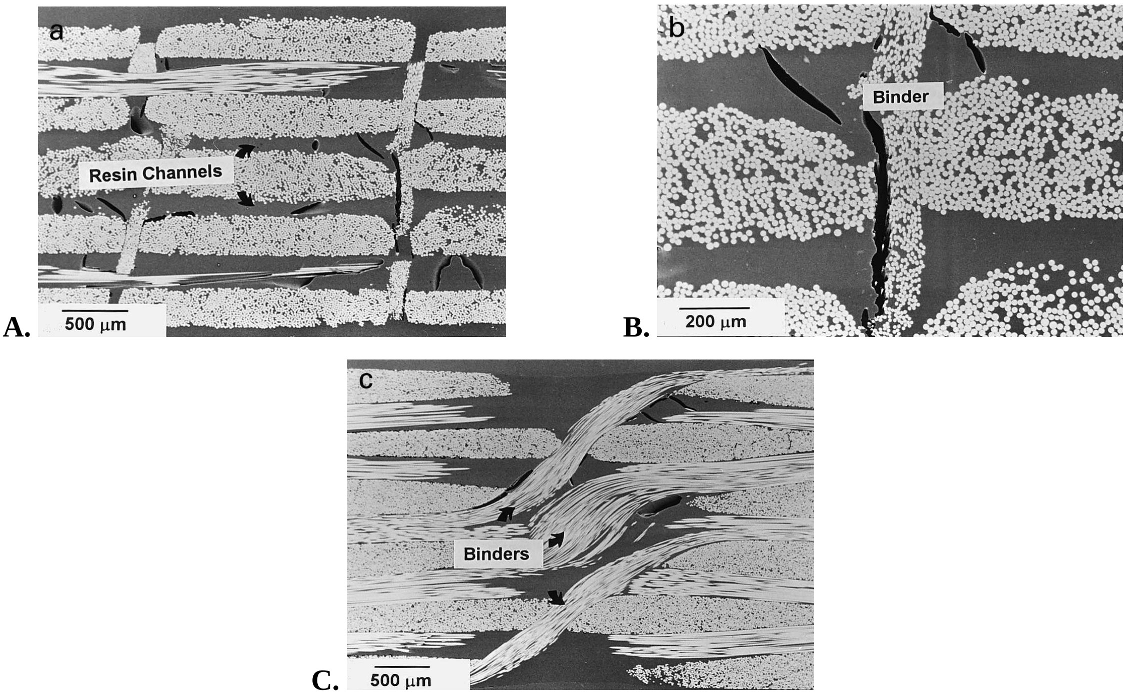

Fig. 1.19: Scanning electron micrographs showing damage produced in the elastic regime: (A) cracking in the resin-rich channels between the tows. Cracking around a binder tow observed from the: (B) warp; and (C) weft directions [59].

The resin between the in-plane tows and around the binder tows in all three 3D composites failed at low strains, but this did not adversely affect the stiffness. It appeared that the reduction in elastic modulus was caused by inelastic straightening of in-plane tows, with the most heavily crimped fibres straightening at relatively low strains, while at higher strains widespread straightening of all the tows caused continuous softening. The failures of composites occurred by the rupture of load-bearing tows within a relatively localized region, and as a result tow lock-up and pullout effects were not observed as were reported by Cox et al. [58].

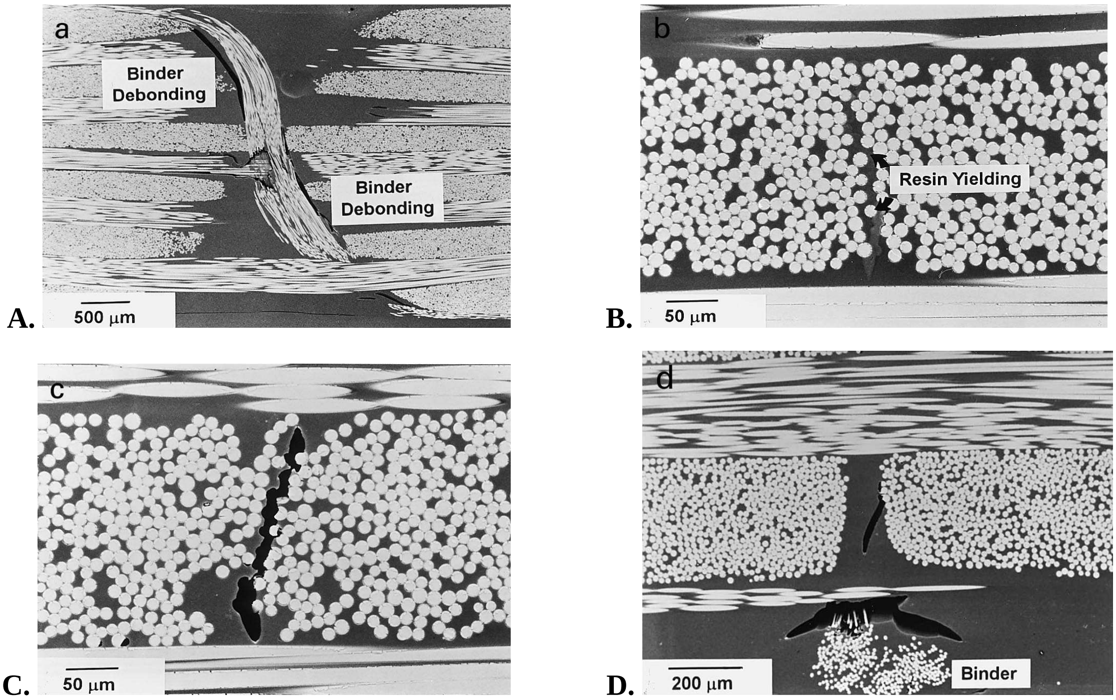

Fig. 1.20 - Damage produced in the hardening phase. (A) Cracking around a binder tows. (B) Plastic yielding of the resin within a warp tow. (C) Cracking of the resin within a warp tow. (D) Cracking between a surface warp tow and the surface leg of a binder tow [59]

In order to understand the effect of binder path on tensile properties Leong et al. [60] have carried out an investigation on the in-plane tensile properties of two orthogonally woven structures with different binder paths. One of the structures was called normal (Fig. 1.21) and the other one was referred to as modified structure (Fig. 1.22). The two structures differ only in the binder path length, with the former having the shorter of the two.

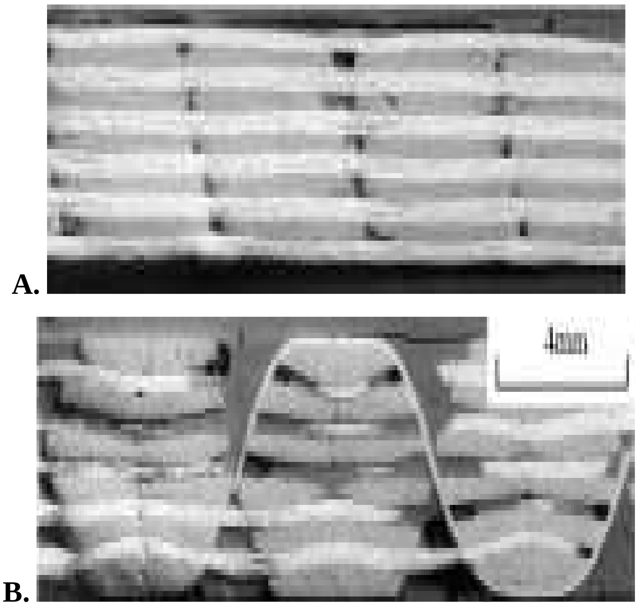

Fig. 1.21: Typical cross-sections of the normal orthogonal weave samples. (A) Sectioned along the warp direction; (B) Sectioned along a weft binder [60].

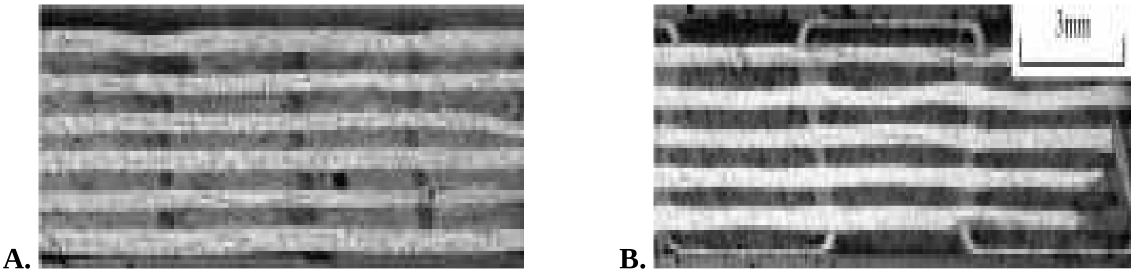

Fig. 1.22: Typical cross-sections of the modified orthogonal weave samples. (A) Sectioned along the warp direction; (B) sectioned along a weft binder [60].

This research revealed that, independent of the fibres used, the in-plane fibre tows in the structure with the longer binder path are less crimped and this, by and large, translates to better or unchanged tensile modulus, strength and strain-to-failure. In addition to fibre fractures, the superior strength of this composite was also observed to promote an extensive amount of longitudinal splitting, thus resulting in a relatively large failure zone. In the structure with the shorter binder path where the in-plane fibres are more crimped, failure is due predominantly to fibre fractures.

Depending on the weaving process some degree of waviness and pinching of the in plane fibre tows is unavoidable. These factors can result in degraded tow rupture strength as high as 30% compared with similar unidirectional tape laminates.

In the normal structure it was found plausible that competing effects of pinching of the warp tows at binder locations vs. the relatively more severe crimping in the weft tows could have been responsible for almost similar strength in the two principle loading directions.

In the modified structure strength and ultimate strain are superior in the warp direction and this is due to absence of pinching by the binder tows.

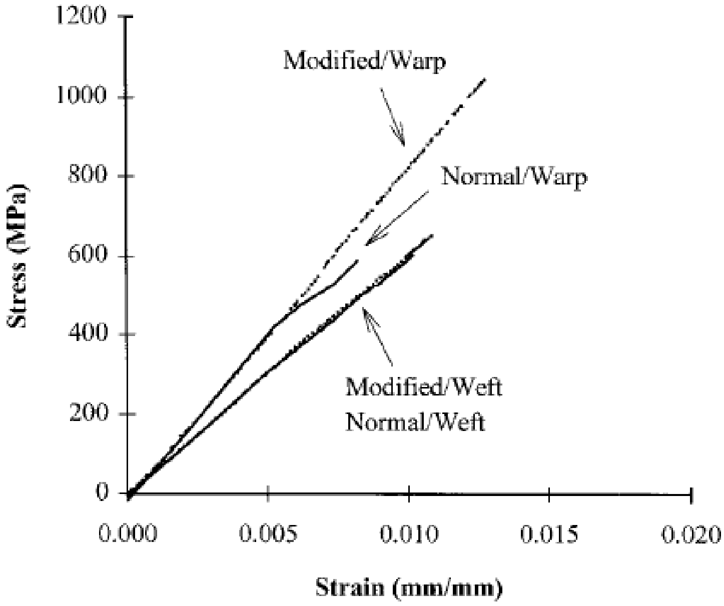

Fig. 1.23: Graph showing representative stress/strain behaviours of the normal and modified weave structures loaded in the warp and weft directions [60].

Failure of the normal structure is relatively contained and it is primarily due to fibre fracture in the load bearing layers of tows (Fig. 1.24-A). For the modified structure, on top of fibre fractures, its superior strength also fuelled an extensive amount of longitudinal splitting, thus resulting in a relatively large failure zone (Fig. 1.24-B). Groups of fibres are pulled out during failure of both structures, despite having good fibre wetting and fibre/matrix adhesion with either fibre.

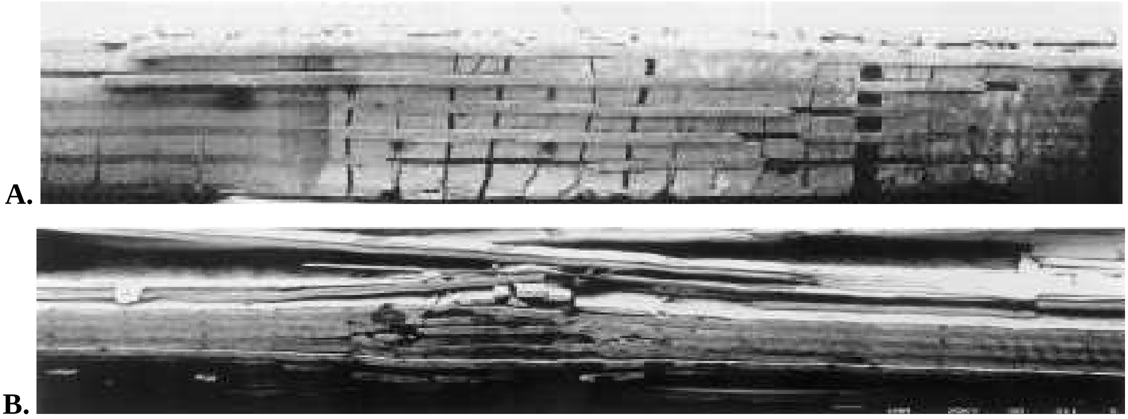

Fig. 1.24: Representative SEM fractographs of the (A) normal, and (B) modified structures, loaded in the warp direction [60]

Recently Quinn et al. [61] examined the failure of 3D woven composites in tension. The study was complemented by an examination of the strain distribution using electronic speckle pattern interferometery (ESPI). The study reports the performance of 3D woven specimens, loaded in tension and shows increased strain in the area where the binder tow enters the subsurface layers of the fabric structure to bind the layers together.

Authors reported that all samples had failure of binder tows visible on the surface of the structure. The failure at the binder region of the structure occurred where the binder tow entered the fabric (Fig. 1.25).

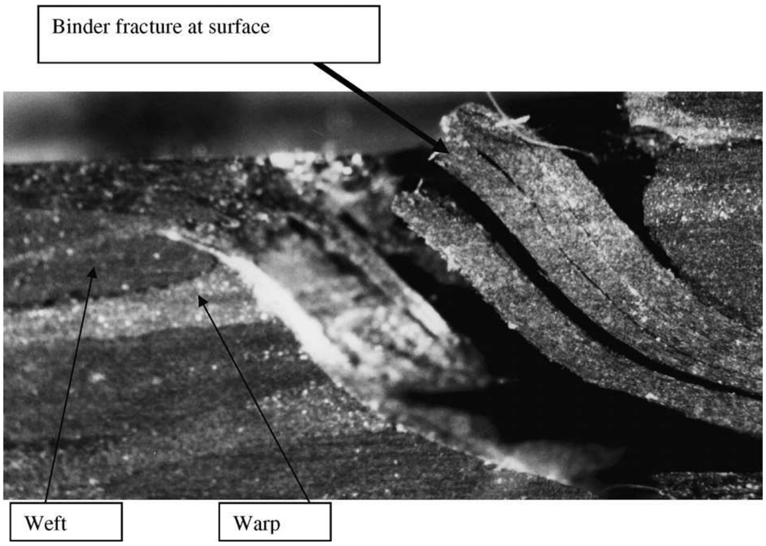

Fig. 1.25: Fracture at the binder turn and subsequent path of fracture along binder (magnification 30x) [61]

Samples failed in brittle manner with no residual strength after the maximum strain was achieved. The warp tows on the surface separated in main fracture area rather than pulling out from the matrix while the warp tows within the inner layer of the composite tended to pullout from the matrix.

Authors have hypothesized that increased localized strain on the surface of the structure brought about by the presence of a resin rich zone at this point caused the failure. The binder tow pinches the weft tows below leaving a depression at the surface of the fabric. During the mould filling process the resin filled this depression and subsequently cured to form the resin rich area. Fracture occurs in resin rich area at the top of the binder and then it moves, as the force on the structure increases in the direction of the binder through the structure.

It was conjectured that the binder tow path has a large influence on the tensile strength and the strain to failure of the sample. This is because of the collimation of weft tows and subsequent resin rich areas left as a result of the movement of the bound warp tows.

Low strain to failure of the structure is due to reduction in the amount of fibre pullout during failure as the failure initiated at binder area, causing low strain to failure for 3D structures. The initial crack weakened the structure and the crack then propagated throughout the structure.

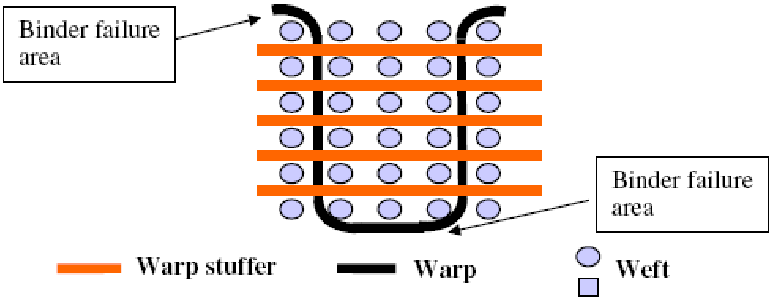

Fig. 1.26: Schematic showing the typical binder path through the structure and the areas of failure [61]

3D woven composites and 2D plied lay ups have comparable modulus values whereas tensile strength of 3D woven composites is somewhat lower (for same fibre volume fraction values). This is because of the following reasons;

- crimp in binder tows which reduces efficiency of the structure in the direction of load
- resin rich areas created by collimation of weft tows
- shearing of binder tow as it entered and left the fabric
- large binders induced resin rich areas around the binders creating areas of concentrated strain

Loading of components in any application is generally never in tension alone and almost always involves a form of more complex loading where the component experiences a combination of forces including flexure, compression, tension and shear. The characterization of performance of 3D woven composites under specific static loading conditions is much more difficult as the material is not isotropic.

Kink band formation occurs prior to the failure of samples. The main reason for failure of 3D woven composites lies in the geometrical irregularity associated with the complex architectures of weave and formation of cracks at low strain in the areas of resin concentration which leads to matrix cracking. Straightening of the stressed tows under uniaxial tensile load is reported to initiate failure.

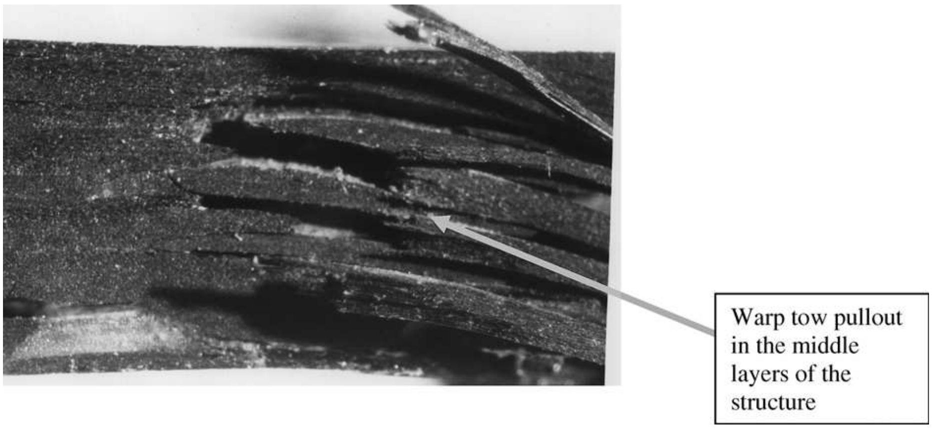

Fig. 1.27: Warp tow pullout within the layers of the composite [61]

Tow misalignment which means that tows can be rearranged in a number of ways under compression, plays a part in lower modulus values of 3D structures.

In a 3D weave, in reality the effects of layer compaction, complexity of the fabric architecture and tension of the binder tows all induce some level of crimp even in straight warp and weft binders.

1.3.2. Effect of weaving on mechanical properties of composites

The tensile strength of carbon multifilament tows undergoes a considerable change from the bobbin to the 3D-woven fabric, owing to the weaving process and the trajectory of yarn inside fabric (amplitude and weave frequency that varies according to the selected weave pattern). Because of the stresses imparted during weaving process and due to the woven fabric architecture (weave structure and yarn density), the breaking strength of an individual yarn is affected after its integration in the fabric. Moreover resin impregnation also contributes to the breaking strength of an individual yarn and to the composite.

In order to quantify the effect of fibre damage induced during weaving on the mechanical performance of tows and their composites, Lee *et al.* [62] have carried out tension tests on (consolidated) tows and woven carbon/epoxy composites. Two commercially-available carbon fibres - Carbon A and Carbon B - were considered.

The tension tests were carried out on consolidated fibre tows sampled from different locations in the loom setup. These included samples from the tensioning, reed, and beat-up stages of weaving. In addition samples from the external and internal warp layers used for the woven preform were also obtained for this investigation.

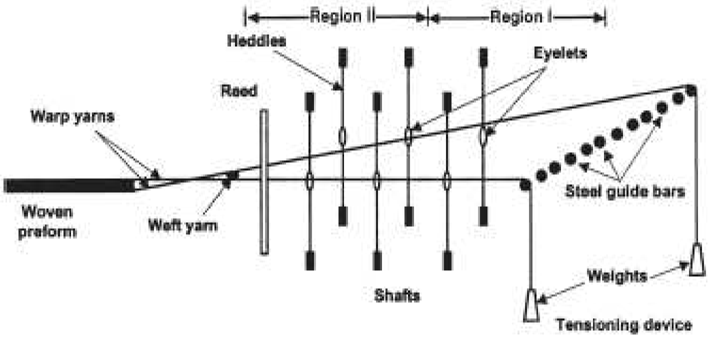

Fig. 1.28: Schematic diagram of handloom setup used by Lee et al. [62]

Authors concluded that tensile properties of fibre composites are detrimentally affected only if the fibres suffer sufficiently large amounts of damage during weaving. According to this research work the reduction in strength and stiffness is caused by fibre damage by

- fibre misalignment
- tow waviness

It was found that stiffness is less sensitive to fibre misalignment as compared to strength. Analysis of damaged samples shows that damaged fibres would result in significant degradation of tensile properties; this effect is less conspicuous when fibres are embedded in a resin matrix which will aid stress redistribution way from the actual locations of the damage in the fibres.

Authors have reported that a reduction of ~30% in the strength of the dry load bearing tows of 3D glass preforms was observed while the weaving damage reduced the strength of single glass composite tow by ~20%. These authors have advocated reduction in crimp percentage by using different geometries as well as improvement in weaving machines and process such as coating of the machinery surface with a wear resistant material having a low coefficient of friction. But for optimum composite tensile properties, the limitation of waviness rather than weaving induced damage in the load bearing fibres is much more important.

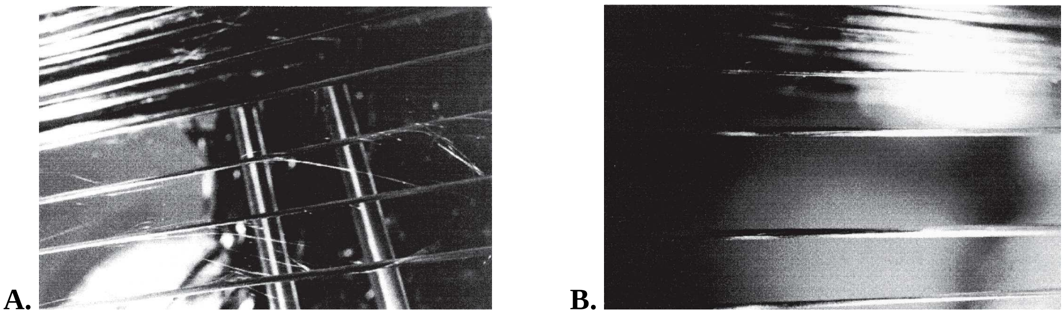

Fig. 1.29: Damage accumulated at tensioning zone (Region I) for:
(A) Carbon A and (B) Carbon B. [62]

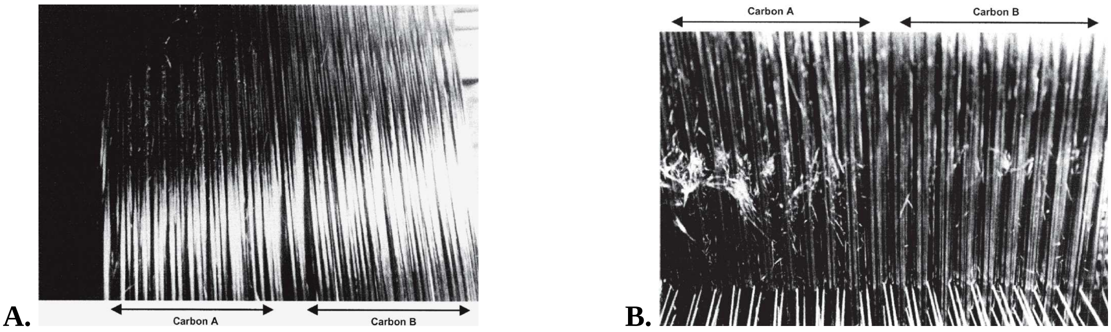

Fig. 1.30: Fibre damage just: (A) ahead of (shaft region), and (B) behind (shaft region), the shaft (Region II) for Carbons A and B [62]

Rudov-Clark et al. [63] have conducted a statistical study to figure out loss in tensile strength and Young’s modulus due to abrasion damage and removal of sizing agent. The study was carried out on fibre glass tows in their pristine form and on the woven structure after the integration of tows in the fabric.

From visual inspection they found out that some fibres are broken during weaving and this causes small reduction to tow stiffness and contributes to large loss in tow strength.

For their study tow samples were taken from;

- as received pristine material
- warp tow samples off warp beams
- warp tow samples after passing through tensioning devices
- warp tow samples extracted from finished fabric after take up stage

Authors have reported that it was not possible to take warp tows from shedding, weft insertion and beat-up operations of the loom because the specimen length was too short to perform tensile tests.

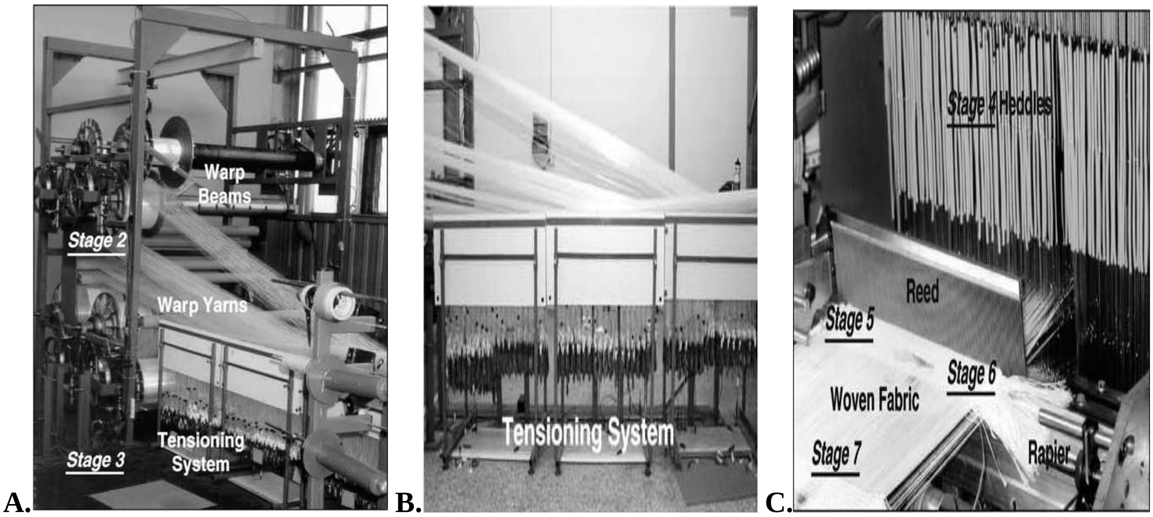

Fig. 1.31: Photographs showing different sections of the Jacquard loom (A) the warp let-off and warp tensioning stages (B) side-view of the tensioning system (C) the shedding, beating and take-up stages [63].

Young's modulus of the tows from tensile tests was measured using the expression

$$E = \frac{PL\rho_f}{w_f \Delta L} \tag{1.6}$$

$P =$ Applied force in the elastic regime of tow

$L =$ Gauge length of the tow specimen

$\rho_f =$ Tow density

$w_f =$ Weight per unit length of tow

$\Delta L =$ Tow extension

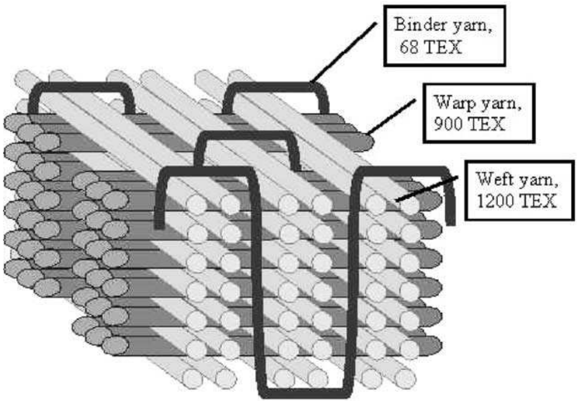

Fig. 1.32: Idealized illustration of the fibre architecture of a 3D orthogonal woven fabric [63]

The conclusions of this study are summarized as follows:

- Fibre to fibre friction and fibre to machine parts abrasion, removes some of the size that coats the glass fibres (Fig. 1.33-A and Fig. 1.33-B). Removing the sizing agent will cause random fibre slacks which can reduce tensile strength.
- Tips of broken glass filaments were jagged as shown in Fig. 1.33-C and 1.33-D, which is indicative of brittle fracture.

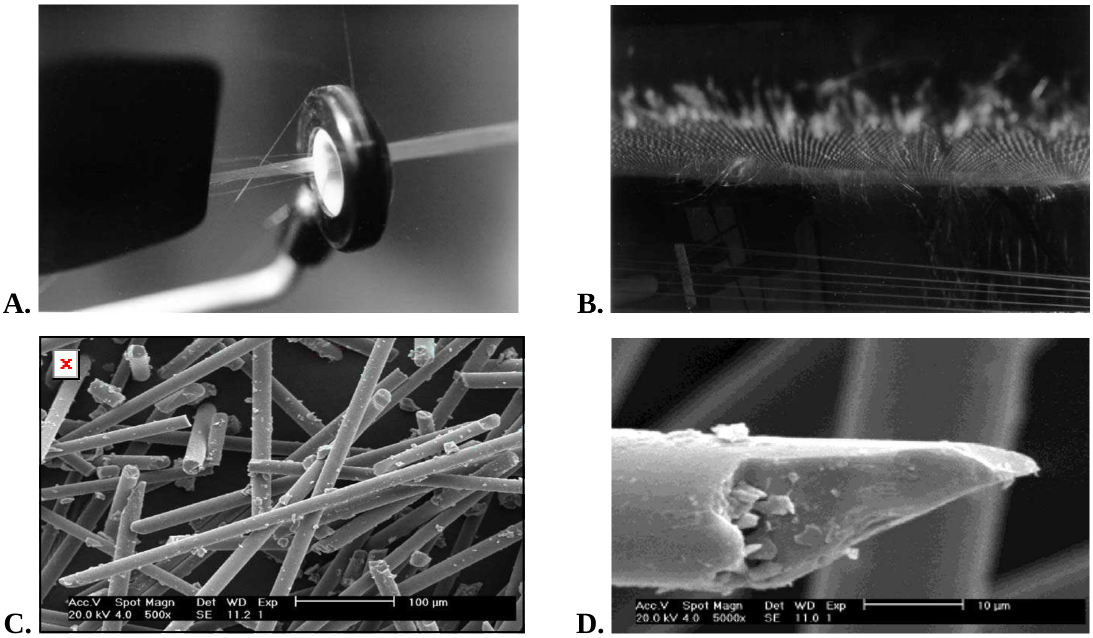

Fig. 1.33: Breakage of fibres A) as the tow passes through a guide on the loom. B) Underside of the 3D woven fabric showing broken fibres protruding from surface C) Scanning electron micrograph showing broken glass fibres collected from the loom D) Scanning electron micrograph showing the fractured tip of a broken glass fibre [63].

- Abrasion causes ultra small scratches on the fibres which reduce strength while not affecting the young’s modulus. Thus abrasion is the main process most responsible for the degradation of tow strength.
- For warp and z-binder tows; total reduction in strength of 30-50% and for Young’s Modulus a much lower reduction in the range of 5-7% was observed.

In a recent paper Archer et al. [64] have conducted a study to assess the damage imparted on load bearing carbon tows in prior to weaving preparatory processes and later on during the 3D weaving process. Tensile tests were performed on three types of commercially available carbon fibre tows. These were 12K, 6K and 3K carbon multifilament tows. Dry specimens of these tows were obtained from different stages of the process namely

- As received virgin tows
- Tows rewound on creel
- Tows obtained after passing through jacquard controller hooks
- Tows extracted from fabric samples

Fabric architectures chosen for this study were layer to layer and a through the thickness angle interlock structure. They were woven on a special jacquard loom at considerably lower production speed of 120 picks/min.

Even though the 12K stuffer tows had minimal crimp whereas 6K and 3K binders had more crimp, the difference in tensile strength caused by weaving damage, between the three tow types was less than 3%. It was reported that in the off the loom samples, the degree of crimp for warp stuffers and weft fillers was less than 0.5% whereas the binders in similar angle interlock and layer to layer interlocks had 4.2% and 3.4% crimp respectively.

An initial degradation of approximately 5% in tensile strength was reported from virgin fibre to rewound fibre. This is because of the fact that rewinding is a high speed process. At the later stages; 1.5% degradation in tensile strength from rewound tows to the tows in the hooks region, and finally 2.8% degradation from the loom to the fabric was reported. This amounts to an average overall degradation of 9.4% from the as received virgin tows to the tows extracted from the woven fabric. The actual weaving process only imparts about 4% knockdown in dry fabrics tensile properties.

In conformity with the findings of Lee et al. [62] weaving damage was found to have little effect on modulus.

1.4. References

[1] M. J. Denton and P. N. Daniels, Textile terms and definitions: Woodhead Publishing Limited, 2002.

[2] A. T. C. Robinson and R. Marks, Woven Cloth Construction: The Textile Institute, 1973.

[3] N. Khokar, "3D-Weaving and Noobing: Characterization of Interlaced and Non-interlaced 3D Fabric Forming Principles," in Polymeric Materials Gothenburg, Sweden: Chalmers University of Technology, 1997.

[4] B. K. Behera and R. Mishra, "3-Dimensional Weaving," Indian Journal of Fiber and Textile Research, vol. 33, pp. 274-287, 2008.

[5] http://www.texeng.co.uk/papers/3D_Weaving.pdf, consulted on 01/01/2010.

[6] T. W. Chou, "Three-dimensional textile Structural Composites," in Microstructural Design of Fiber Composites, New York: Cambridge University Press, 1992.

[7] H. L. Yi and X. Ding, "Conventional Approach on Manufacturing 3D Woven Preforms Used for Composites," Journal of Industrial Textiles, vol. 34, pp. 39-50, July 1 2004.

[8] S. W. Yurgartis and J. Jortner, "Characterisation of yarn shape in woven fabric composites," in Microstructural characterization of fibre-reinforced composites, J. Summerscales, Ed.: Woodhead Publishing Limited, 1998.

[9] F. Ko, "3-D textile reinforcements in composite materials," in 3-D Textile Reinforcements In Composite Materials. vol. null: Woodhead Publishing Limited, 2007.

[10] N. K. Naik, S. N. M. Azad, and P. D. Prasad, "Stress and Failure Analysis of 3D Angle Interlock Woven Composites," Journal of Composite Materials, vol. 36, pp. 93-123, January 1 2002.

[11] S. Z. Sheng and S. Van Hoa, "Modeling of 3D Angle Interlock Woven Fabric Composites," Journal of Thermoplastic Composite Materials, vol. 16, pp. 45-58, January 1 2003.

[12] A. P. Mouritz, M. K. Bannister, P. J. Falzon, and K. H. Leong, "Review of applications for advanced three-dimensional fibre textile composites," Composites Part A: Applied Science and Manufacturing, vol. 30, pp. 1445-1461, 1999.

[13] J. Summerscales, "Microstructural Characterisation of Fibre-Reinforced Composites", Cambridge, UK: Woodhead Publishing Limited, 1998.

[14] B. K. Behera and P. K. Hari, "Geometrical modelling of woven fabric structure," in Woven Textile Structure: Theory and Applications Cambridge, UK: Woodhead Publishing Limited, 2010.

[15] J. Brandt, K. Drechsler, and F. J. Arendts, "Mechanical performance of composites based on various three-dimensional woven-fibre preforms," Composites Science and Technology, vol. 56, pp. 381-386, 1996.

[16] S. V. Lomov, G. Huysmans, Y. Luo, R. S. Parnas, A. Prodromou, I. Verpoest, and F. R. Phelan, "Textile composites: modelling strategies," Composites Part A: Applied Science and Manufacturing, vol. 32, pp. 1379-1394, 2001.

[17] S. V. Lomov, G. Huysmans, and I. Verpoest, "Hierarchy of Textile Structures and Architecture of Fabric Geometric Models," Textile Research Journal, vol. 71, pp. 534-543, June 1, 2001.

[18] I. Verpoest and S. V. Lomov, "Virtual textile composites software WiseTex: Integration with micro-mechanical, permeability and structural analysis," *Composites Science and Technology,* vol. 65, pp. 2563-2574, 2005.

[19] F. T. Peirce, "The Geometry of Cloth Structure," Journal of Textile Institute, 1937.

[20] F. T. Peirce, "Geometrical Principles Applicable to the Design of Functional Fabrics," Textile Research Journal, vol. 17, pp. 123-147, March 1, 1947.

[21] S. V. Lomov, A. V. Gusakov, G. Huysmans, A. Prodromou, and I. Verpoest, "Textile geometry preprocessor for meso-mechanical models of woven composites," Composites Science and Technology, vol. 60, pp. 2083-2095, 2000.

[22] M. Sherburn, "Geometric and Mechanical Modelling of Textiles," PhD thesis, University of Nottingham, 2007.

[23] S. Buchanan, A. Grigorash, J. P. Quinn, A. T. McIlhagger, and C. Young, "Modelling the geometry of the repeat unit cell of three-dimensional weave architectures," Journal of the Textile Institute, vol. 101, pp. 679-685, 2009.

[24] W. Tian, C. Zhu, and S. Wang, "A Geometric Model of Three-dimensional Integrated Cellular Woven Structures," Textile Research Journal, vol. 79, pp. 844-852, June 1, 2009.

[25] Z. Wu, "Three-dimensional exact modeling of geometric and mechanical properties of woven composites," Acta Mechanica Solida Sinica, vol. 22, pp. 479-486, 2009.

[26] J. Quinn, J. B. Hill and R. McIlhagger, “An integrated design system for the manufacture and analysis of 3-D woven preforms” in International Conference on Automated Composites, Bristol , UK, 2001, pp 911-914.

[27] J. Quinn, R. McIlhagger, and A. T. McIlhagger, "A modified system for design and analysis of 3D woven preforms," Composites Part A: Applied Science and Manufacturing, vol. 34, pp. 503-509, 2003.

[28] M. J. King, P. Jearanaisilawong, and S. Socrate, "A continuum constitutive model for the mechanical behavior of woven fabrics," International Journal of Solids and Structures, vol. 42, pp. 3867-3896, 2005.

[29] E. Baesu, "Finite deformations of elastic-plastic filamentary networks," International Journal of Non-Linear Mechanics, vol. 38, pp. 1473-1479, 2003.

[30] P. Xue, X. Peng, and J. Cao, "A non-orthogonal constitutive model for characterizing woven composites," Composites Part A: Applied Science and Manufacturing, vol. 34, pp. 183-193, 2003.

[31] X. Ruan and T.W. Chou, "Experimental and theoretical studies of the elastic behavior of knitted-fabric composites," Composites Science and Technology, vol. 56, pp. 1391-1403, 1996.

[32] B. Gommers, I. Verpoest, and P. Van Houtte, "Modelling the elastic properties of knitted-fabric-reinforced composites," Composites Science and Technology, vol. 56, pp. 685-694, 1996.

[33] Y. A. Gowayed, C. Pastore, and C. S. Howarth, "Modification and application of a unit cell continuum model to predict the elastic properties of textile composites," Composites Part A: Applied Science and Manufacturing, vol. 27, pp. 149-155, 1996.

[34] T. V. Sagar, P. Potluri, and J. W. S. Hearle, "Mesoscale modelling of interlaced fibre assemblies using energy method," Computational Materials Science, vol. 28, pp. 49-62, 2003.

[35] W. J. Shanahan and J. W. S. Hearle, "An Energy Method for Calculations Fabric Mechanics Part 1 and 2," Journal of the Textile Institute vol. 69, pp. 81-91 and 92-100, 1978.

[36] S. Kawabata, M. Niwa, and H. Kawai, "The finite deformation theory of plain weave fabrics part I: The biaxial deformation theory," Journal of the Textile Institute, vol. 64, pp. 21 - 46, 1973.

[37] S. Kawabata, M. Niwa, and H. Kawai, "The finite-deformation theory of plain-weave fabrics part II: The uniaxial-deformation theory," Journal of the Textile Institute, vol. 64, pp. 47 - 61, 1973.

[38] S. Kawabata, M. Niwa, and H. Kawai, "The finite deformation theory of plain weave fabrics part III: The shear deformation theory," Journal of the Textile Institute, vol. 64, pp. 62 - 85, 1973.

[39] S. Kato, T. Yoshino, and H. Minami, "Formulation of constitutive equations for fabric membranes based on the concept of fabric lattice model," Engineering Structures, vol. 21, pp. 691-708, 1999.

[40] M. L. Realff, M. C. Boyce, and S. Backer, "A Micromechanical Model of the Tensile Behaviour of Woven Fabric," Textile Research Journal, vol. 67, pp. 445-459, 1997.

[41] H. Rattensperger, J. Eberhardsteiner, and H. A. Mang, "Numerical investigation of high pressure hydraulic hoses with steel wire braid," in IUTAM Symposium on Computational Mechanics of Solid Materials at Large Strains, 2003, pp. 407-416.

[42] R. R. Tanov and M. Brueggert, "Finite element modeling of non-orthogonal loosely woven fabrics in advanced occupant restraint systems," Finite Elements in Analysis and Design, vol. 39, pp. 357-367, 2003.

[43] S. P. Ng, P. C. Tse, and K. J. Lau, "Numerical and experimental determination of in-plane elastic properties of 2/2 twill weave fabric composites," Composites Part B: Engineering, vol. 29, pp. 735-744, 1998.

[44] P. Boisse, K. Buet, A. Gasser, and J. Launay, "Meso/macro-mechanical behaviour of textile reinforcements for thin composites," Composites Science and Technology, vol. 61, pp. 395-401, 2001.

[45] G. Nicoletto, G. Anzelotti, and E. Riva, "Mesoscopic strain fields in woven composites: Experiments vs. finite element modeling," Optics and Lasers in Engineering, vol. 47, pp. 352-359, 2009.

[46] S. Reese, "Anisotropic elastoplastic material behavior in fabric structures," in IUTAM Symposium on Computational Mechanics of Solid Materials at Large Strains, 2003, pp. 201-210.

[47] A. Cherouat and J. L. Billoët, "Mechanical and numerical modelling of composite manufacturing processes deep-drawing and laying-up of thin pre-impregnated woven fabrics," Journal of Materials Processing Technology, vol. 118, pp. 460-471, 2001.

[48] D. Roylance, P. Chammas, J. Ting, H. Chi, and B. Scott, "Numerical modeling of fabric impact," in Proceedings of the National Meeting of the ASME, 1995.

[49] X. Provot, "Animation Réaliste de Vêtements," in Mathématiques et Informatique: Université René Descartes, Paris V, 1997.

[50] D. E. Breen, D. H. House, and M. J. Wozny, "A Particle-Based Model for Simulating the Draping Behavior of Woven Cloth," Textile Research Journal, vol. 64, pp. 663-685, November 1 1994.

[51] P. Vandeurzen, J. Ivens, and I. Verpoest, "A three-dimensional micromechanical analysis of woven-fabric composites: I. Geometric analysis," Composites Science and Technology, vol. 56, pp. 1303-1315, 1996.

[52] K. K. Chawla, Fibrous Materials. Cambridge: Cambridge University Press, 2005.

[53] N. Anantharamaiah, "Study of Beaming Large High Modulus Fiber Tows," in Department of Textile Engineering. Project report of Master of Science, Raleigh: North Carolina State University, 2002.

[54] "http://www.carbon-fiber-hood.net/cf-information," consulted on 04/07/2010.

[55] E. R. Schwarz, "Certain Aspects of Yarn Structure," Textile Research Journal, vol. 21, pp. 125-136, 1951.

[56] G. W. Du, T.-W. Chou, and P. Popper, "Analysis of 3D Textile Preform for Multi-Directional Reinforcement of Composites," Journal of Materials Sciences, vol. 26, 1991.

[57] J. W. S. Hearle, P. Grosberg, and S. Backer, Structural Mechanics of Fibers, Yarns, and Fabrics vol. 1. New York: Wiley-Interscience, 1969.

[58] B. N. Cox, M. S. Dadkhah, and W. L. Morris, "On the tensile failure of 3D woven composites," Composites Part A: Applied Science and Manufacturing, vol. 27, pp. 447-458, 1996.

[59] P. J. Callus, A. P. Mouritz, M. K. Bannister, and K. H. Leong, "Tensile properties and failure mechanisms of 3D woven GRP composites," Composites Part A: Applied Science and Manufacturing, vol. 30, pp. 1277-1287, 1999.

[60] K. H. Leong, B. Lee, I. Herszberg, and M. K. Bannister, "The effect of binder path on the tensile properties and failure of multilayer woven CFRP composites," Composites Science and Technology, vol. 60, pp. 149-156, 2000.

[61] J. P. Quinn, A. T. McIlhagger, and R. McIlhagger, "Examination of the failure of 3D woven composites," Composites Part A: Applied Science and Manufacturing, vol. 39, pp. 273-283, 2008.

[62] L. Lee, S. Rudov-Clark, A. P. Mouritz, M. K. Bannister, and I. Herszberg, "Effect of weaving damage on the tensile properties of three-dimensional woven composites," Composite Structures, vol. 57, pp. 405-413, 2002.

[63] S. Rudov-Clark, A. P. Mouritz, L. Lee, and M. K. Bannister, "Fibre damage in the manufacture of advanced three-dimensional woven composites," Composites Part A: Applied Science and Manufacturing, vol. 34, pp. 963-970, 2003.

[64] E. Archer, S. Buchanan, A. T. McIlhagger, and J. P. Quinn, "The effect of 3D weaving and consolidation on carbon fiber tows, fabrics, and composites," Journal of Reinforced Plastics and Composites, vol. 29, pp. 3162-3170, 2010.

Chapter 2

A new approach of geometrical modelling of warp interlock fabrics

2.1 Development of the geometrical model

Beyond designing the preforms themselves, there is also a need to develop reinforcement design and analysis systems that can accurately model 3D woven structures in order to be able to better understand, control and predict the performance of composite materials that are made from these reinforcements.

A woven fabric is essentially a hierarchical material [1]. At each level of hierarchy there are different factors which influence its geometry. For a woven fabric, orientations are influenced by its architecture. The architecture of woven fabric is influenced by a multitude of factors corresponding to different levels of hierarchy which include raw material properties (at micro and meso-structural level), warp and weft densities, weave design and weaving parameters (at meso-structural level) and post treatment (at macro structural level) etc.

Orientations of tows in a woven reinforcement determine the mechanical properties of the composite. As mentioned earlier these woven reinforcements are made from the interlacement of multifilament tows. These tows are strands of filaments which run along the tow axis not necessarily parallel to it.

While modelling tow shape at meso-structural scale, it is approximated that the filaments run parallel to the tow axis and thus their influence can be studied by studying tow orientations. At the meso-structural scale the tow shape is characterized by geometry of tow cross section and path followed by the tow axis [2].

Moreover a woven fabric is composed of repeating unit cells or representative volume elements. These unit cells are representative of all the composite geometric and mechanical properties. Modelling of these unit cells is a generic way of predicting reinforcement properties at meso-structural level. Therefore the geometrical model has been developed to calculate tow cross sectional geometry and its trajectory inside a unit cell.

As discussed earlier, in such reinforcements tow shape and crimp are inextricably interrelated and depend on one another. Therefore trajectories of multifilament tows inside the unit cells have been calculated from corresponding cross sectional geometries. The assignment of suitable cross sectional shape functions to warp and weft tows leads to accurate calculation of crimp angles and tow trajectories. In the following the path adopted for the calculation of geometries of different interlock structures has been explained.

2.1.1. Characterization of initial tow cross sectional geometry

As already mentioned, due to the application of binders or size the multifilament tows have an approximately rectangular cross section on the package as shown in Fig. 2.1-A. For convenience it might be assumed that all the filaments are parallel to one another within a tow and they just touch each other so as to acquire homogenous configuration inside a tow.

A simple approach to calculate the initial idealized rectangular dimensions of a virgin tow is described here. Within a rectangular tow, filaments are supposed to be placed one above another so that there are ‘*m*’ rows or ‘levels of filaments’ inside a tow and in each level ‘*n*’ filaments lay next to one another.

In this context two sets of parameters; ‘*known*’ and ‘*calculated*’ can be defined.

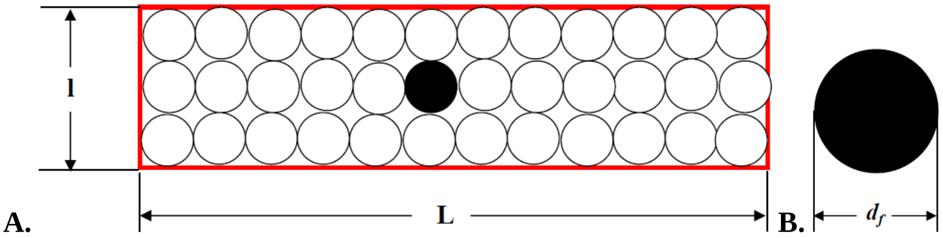

Fig. 2.1: (A) Initial idealized rectangular geometry of the tow coming from package with filaments arranged parallel to one another (B) filament cross section inside a tow

KNOWN PARAMETERS:

- K - Number of filaments in the tow;
- L - Width of tow as measured on the package [mm]
- d_f - Diameter of a single filament [µm]

CALCULATED PARAMETERS:

- n - Number of filaments lying next to each other in each level of the tow:

$$n = \frac{L}{d_f}$$

- m - Number of levels in a tow cross section:

$$m = \frac{K}{n}$$

- l - Thickness of rectangular tow [mm]:

$$l = m \times d_f$$

- a_f - Cross sectional area of each filament [mm^2]:

$$a_f = \frac{\pi}{4} d_f{}^2$$

- $A_{f(Total)}$ - Total area of filaments inside a tow [mm^2]:

$$A_{f(Total)} = K \times a_f$$

- A_{rect} - Area of rectangular tow section [mm^2]:

$$A_{rect} = l \times L$$

- P.F. - Packing factor:

$$P.F. = \frac{A_{f(Total)}}{A_{rect}} \tag{2.1}$$

Table 2.1: Calculated and known parameters for different tows

MANUFACTURER	**SOFICAR TORAYCA**	**HERCULES INC.**	**HEXCEL CORP.**	**VETROTEX**
Designation	FT 300 3000-59A	IM7-GP	AU4C-GP	RC 14 320 P109 160
K	3000	6000	12000	821
L[mm]	1	2	4	2
d_f [µm]	6.82	6.19	6.29	0.014
N	146.62	323.10	635.93	142.86
M	20.46	18.60	18.90	5.75
l [mm]	0.14	0.11	0.12	0.08
a_{f} [mm^2]	3.60×10^{-5}	3.0×10^{-5}	3.10×10^{-5}	0.00015
$A_{f(Total)}$ [mm^2]	0.11	0.18	0.37	0.12
$A_{rect.}$ [mm^2]	0.14	0.22	0.48	0.16
P.F.	0.77	0.82	0.77	0.75

2.1.2. Compacted or final geometry of multifilament tow inside a woven fabric

According to Chou et al. [3] following factors influence packing of fibres in a yarn and packing of yarns in a preform:

- Yarn tension;
- Inter-yarn contact;
- Yarn twist;
- Fibre cross-section;
- Fibre straightness;
- Manufacturing method;
- Preform geometry.

When woven into a fabric, the multifilament tows get compacted. This compaction causes their initial dimensions and geometry to change. The micro-scale geometry i.e. the arrangement of filaments inside a tow determines the meso scale geometry of tows inside the fabric. The arrangement of filaments inside the tow undergoes considerable change from package to fabric. The weaving parameters such as the relative density of warp and weft tows, weave design of the fabric, tension applied during weaving and numbers of layers etc. determine compaction conditions and thus the geometry of a tow inside the fabric. For instance Fig. 2.2 shows that equal compaction on both the tow faces compress the tow into lenticular shape having width ‘w’ and thickness ‘t’.

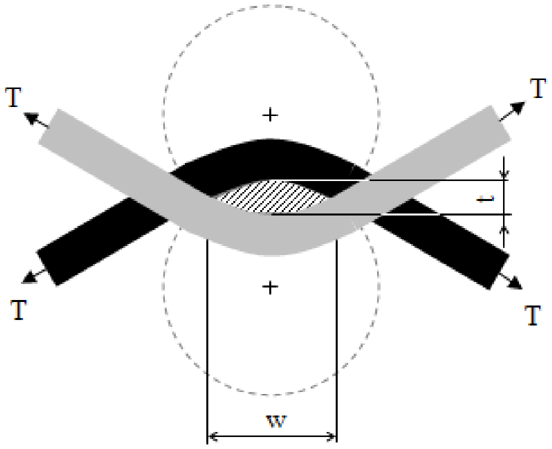

Fig. 2.2: Geometry of a lenticular tow; cross section being compacted into lenticular shape by tensions T

This is because of the fact that filaments are undeformable and rigid. Only their reorganization is possible inside a tow under the influence of compaction forces. Thus meso-structural geometry of a tow changes as filaments reorganize with the change in boundary conditions due to compaction forces. In the absence of compaction, the tows have an irregular cross section. Here such cross sectional shape will be referred to as non-lenticular and will be assigned rectangular shape function.

Photomicrographs of lateral and transversal cross sections of 8 layers warp interlock as a representative case to understand the compaction of tows inside the woven reinforcement are given in

Fig. 2.3-A and 2.3-B respectively. It can be observed that weft tows are non lenticular (Fig. 2.3-A) as there is no compaction acting on them since warp tows are straight and uncrimped, whereas warp tows (Fig. 2.3-B) are lenticular in cross section due to the compaction applied on them by crimped weft tows.

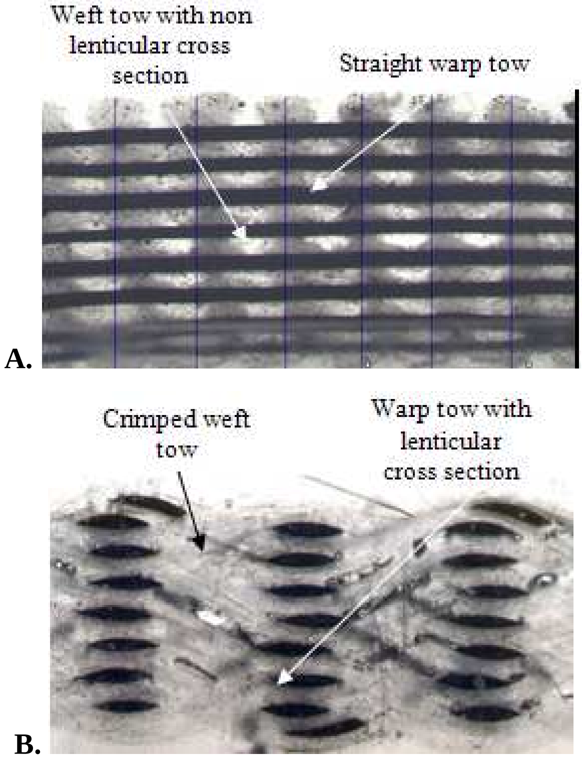

Fig. 2.3: Cross sectional image of 8 layers warp interlock

(A) Longitudinal section showing straight warp tows and non lenticular section of weft tows

(B) Transversal section showing crimped weft tows and lenticular cross section of warp

Fig. 2.4-A and B show different tow trajectories and their influence on tow cross sections as compaction conditions change with the crimp of corresponding tows. Thus it can be inferred that maximum crimp in warp implies lenticular cross section of the weft tows. Whereas minimum crimp in warp implies non lenticular cross section of weft tows and vice versa (Fig. 2.4-A and B). Effect of tow trajectories on their cross sectional profiles will be discussed later in detail.

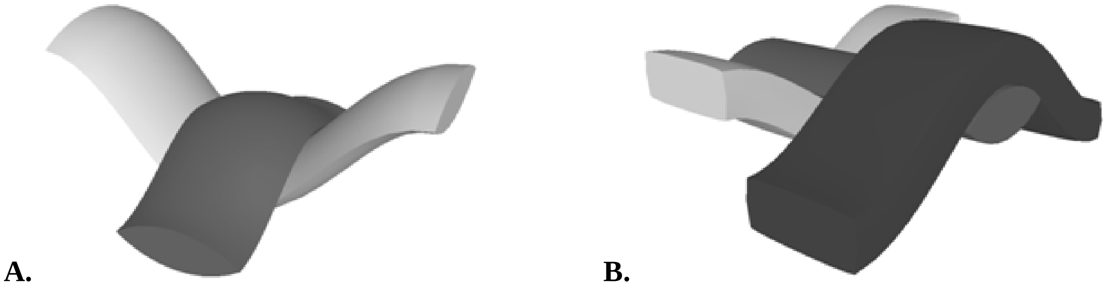

Fig. 2.4: Evolution of tow cross sectional geometry with change in compaction conditions

(A) Both the tows are crimped and apply equal compaction on one another

(B) Only one of the tow groups is crimped and applies compaction on uncrimped tow

2.1.3. Assignment of shape functions-Orthogonal Interlocks/Layer-to-Layer binding

In order to determine warp and weft shape functions for orthogonal interlocks having layer to layer binding, a new notion of geometry called ‘relative fractional cover’ has been introduced. This parameter determines ‘relative tightness’ of the fabric in warp and weft directions. The crimp in warp and weft depends upon the ‘relative tightness’. According to the ‘relative fractional cover’ values calculated using ‘tow’ and ‘weave data’, different shape functions can be assigned to the warp and weft. Once these shape functions have been assigned, we can proceed to calculate crimp in warp and weft. Crimp percentages and crimp angles can be used to calculate all the downstream fabric geometry parameters like areal weight, reinforcement thickness and volume fractions.

Relative fractional cover for layer to layer warp interlocks can be defined as follows;

$$\psi = \frac{e_{wp}}{e_{wft}} = \left[\frac{w_{wp} / S_{wp}}{w_{wft} / S_{wft}} \right] \tag{2.2}$$

Where e_{wp} and e_{wft} are defined as warp and weft fractional cover respectively. For the description of related terms refer to Fig. 2.5.

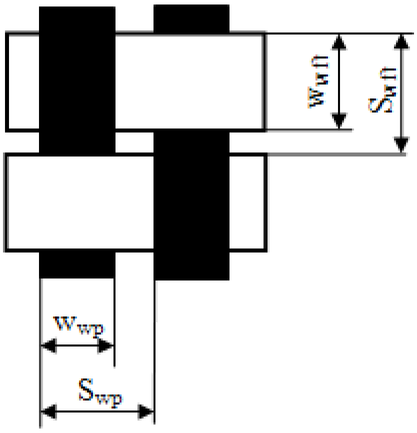

Fig. 2.5: Top view of the unit cell of a layer to layer warp interlock; Definition of relative fractional cover

Widths of warp and weft tows; w_{wp} and w_{wft} are measured on the surface of the fabric. S_{wp} and S_{wft} are warp and weft tow spacing respectively which can also be measured on the surface of the fabric or can be determined prior to weaving from tow aspect ratios and tow densities P_{wp} and P_{wft}.

Relative fractional cover approaches to unity for completely balanced fabrics. For such fabrics both the warp and weft are crimped and thus apply compaction on one another. As a result both the warp and weft tows can be assigned lenticular shape functions. On the other hand very high or very low value of relative fractional cover signifies an unbalanced fabric. In such unbalanced fabrics either the warp or the weft is highly crimped while the other tow group has negligible crimp. Our observations have shown that for relative fractional cover as low as 0.6, both the warp and weft retain considerable crimp. For still lower values of relative fractional cover warp loses almost all the crimp and becomes straight while the weft becomes highly crimped.

It should be noted here that a multilayer woven fabric can not be woven with an arbitrary predetermined value of relative fractional cover. This is because of the fact that tow density in warp is limited by the practical consideration of weavability limit. In a reed the warp tow density can be increased only up to a certain limit beyond which the weaving of the fabric becomes impossible. Therefore relative fractional cover can not be increased much above unity.

No such constraints exist in the weft directions. An orthogonal/Layer-to-layer fabric can be woven with extreme weft densities so that the weft tows are not only in contact with one another but they get deformed due to severe beat up.

2.1.4. Assignment of shape functions - Angle Interlocks

Observations on photomicrographs have shown that in the case of angle interlocks having layer-to-layer binding, both the warp and weft tows retain considerable crimp. That's why both of them can be assigned lenticular cross sections. On the other hand in the case of angle interlocks having through the thickness binding, the warp binder goes through more than two layers of weft tows. In such fabrics the stacking of weft tows one above the other implies that their crimp will be negligible. The warp binder in such fabrics is highly crimped as it penetrates several layers and interlocks them. The crimped warp applies compaction on weft while uncrimped weft is unable to apply such compaction on warp. As a result weft becomes lenticular and the warp non lenticular in cross section. As previously explained once these shape functions are known, all the downstream fabric parameters can be calculated.

2.1.5. Geometrical Model

Having established above premise a geometrical model can be developed based on our observations.

Data provided by the tow manufacturer and the weaver data are used as model input. This data is used to model the unit cell of preform.

The output of the model or 'calculated data' includes all the geometrical parameters comprising of dimensions of the unit cell, warp and weft crimp percentages, areal weight and volume fractions. The model input can be categorized as 'tow data' and 'weaver data'. In the following these have been enumerated.

- **TOW DATA:**

DESCRIPTION	UNIT	TERM
Linear density of warp tows	g/km	Tex_{wp}
Linear density of weft tows	g/km	Tex_{wft}
Either of the aspect ratios or widths of warp and weft tows:		
Aspect ratio of warp tows	-	AR_{wp}
Aspect ratio of weft tows	-	AR_{wft}
Width of warp tows	mm	w_{wp}
Width of weft tows	mm	w_{wft}
Packing factor for warp tows	-	$P.F._{wp}$
Packing factor for weft tows	-	$P.F._{wft}$
Density of warp fibres	g/m^3	ρ_{wp}
Density of weft fibres	g/m^3	ρ_{wft}

- **WEAVER DATA:**

DESCRIPTION	UNIT	TERM
Warp tow spacing	-	S_{wp}
Weft tow spacing	-	S_{wft}
Number of warp tows in the unit cell	-	r_{wp}
Number of weft tows in the unit cell	-	r_{wft}
Number of warp tows per cm	-	P_{wp}
Number of weft tows per cm	-	P_{wft}
Number of layers of weft tows	-	n_{wft}

- **CALCULATED PARAMETERS:**

DESCRIPTION	UNIT	TERM
Relative fractional cover	-	Ψ
(Relative fractional cover will only be calculated for layer to layer warp interlocks)		
Thickness of warp tow inside the fabric	mm	t_{wp}
Thickness of weft tow inside the fabric	mm	t_{wft}
Number of layers of warp tows	-	n_{wp}
Thickness of the fabric	mm	T
Unit cell size in warp direction	mm	$L_{UC(wp)}$
Unit cell size in weft direction	mm	$L_{UC(wft)}$

Warp crimp angle	degrees	Φ_{wp}
Weft crimp angle	degrees	Φ_{wft}
Length of warp in the unit cell	mm	$l_{wp(UC)}$
Length of weft in the unit cell	mm	$l_{wft(UC)}$
Crimp in warp tows	%	c_{wp}
Crimp in weft tows	%	c_{wft}
Areal weight of warp tows	g/m^2	GSM_{wp}
Areal weight of weft tows	g/m^2	GSM_{wft}
Areal weight of the fabric	g/m^2	GSM_{fabric}
Fractional mass of warp	%	FM_{wp}
Fractional mass of weft	%	FM_{wft}
Area of the unit cell	mm^2	a_{UC}
Mass of the unit cell	grams	m_{UC}
Mass of warp in the unit cell	grams	$m_{wp/UC}$
Mass of weft in the unit cell	grams	$m_{wft/UC}$
Volume of warp in the unit cell	mm^3	$V_{wp(UC)}$
Volume of weft in the unit cell	mm^3	$V_{wft(UC)}$
Volume of the unit cell	mm^3	V_{UC}
Total volume fraction	-	FVF
Warp volume fraction	-	FVF_{wp}
Weft volume fraction	-	FVF_{wft}

In order to calculate the tow dimensions inside a fabric, either aspect ratio for both the warp and weft tows; AR_{wp} and AR_{wft} or widths of these tows; w_{wp} and w_{wft} should be known.

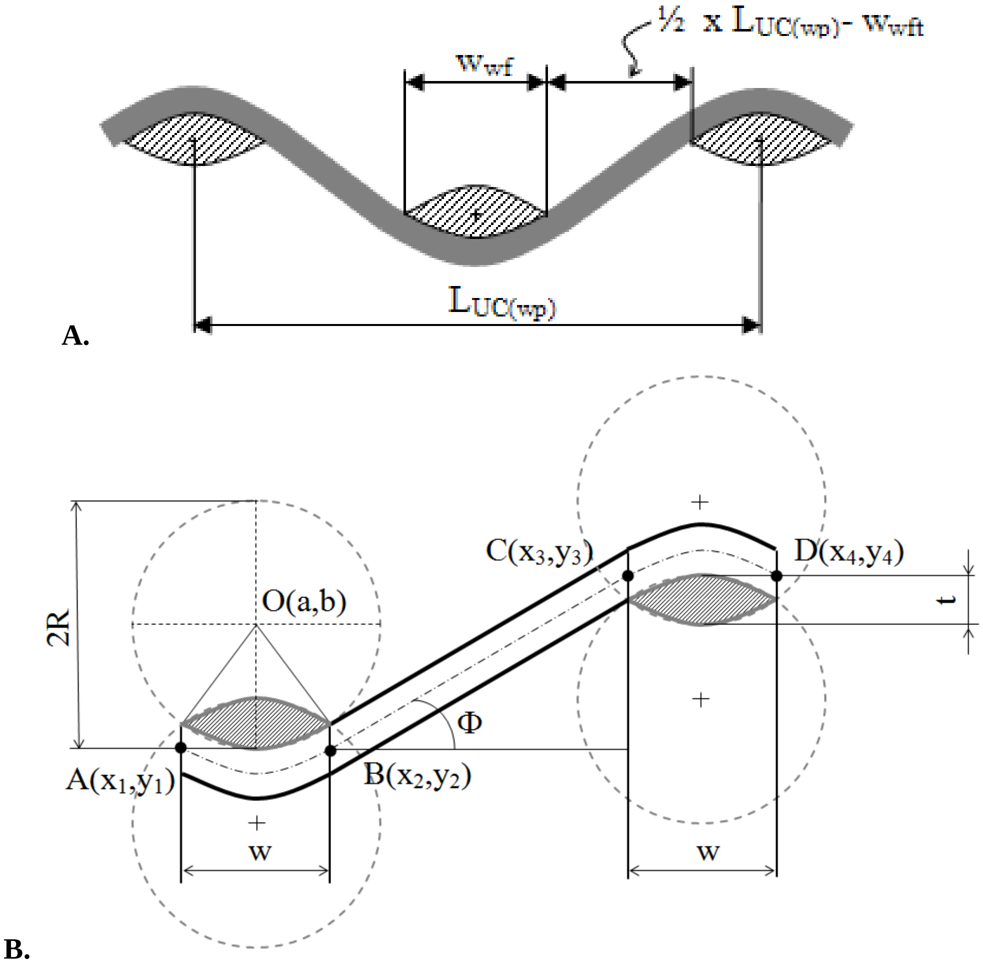

Fig. 2.6: (A) Length of the unit cell in warp direction
(B) Geometry of a lenticular tow

Packing factors for warp and weft tows; $P.F._{wp}$ and $P.F._{wft}$, determine the actual fibrous content inside a multifilament tow. According to Cox et al. [4] the packing factors typically range from 70-80 % for woven reinforcements. Here it will be assumed that 75% of the tow area consists of filaments. Once these parameters are known, following sets of equations 2.3 or 2.4 can be used to calculate thicknesses of warp and weft tows inside the fabric [5].

$$t_{wp} = 2\times\sqrt{\frac{Tex_{wp}}{\rho_{wp}\times AR_{wp}\times PF_{wp}\times\pi\times1000}} \quad \text{and} \quad t_{wft} = 2\times\sqrt{\frac{Tex_{wft}}{\rho_{wft}\times AR_{wft}\times PF_{wft}\times\pi\times1000}} \tag{2.3}$$

$$t_{wp} = \frac{4\times Tex_{wp}}{1000\times\rho_{wp}\times w_{wp}\times PF_{wp}\times\pi} \quad \text{and} \quad t_{wft} = \frac{4\times Tex_{wft}}{1000\times\rho_{wft}\times w_{wft}\times PF_{wft}\times\pi} \tag{2.4}$$

It is understood that in a multilayer woven structure, weft tows are inserted one over another to obtain different layers. The warp tows stay in their vertical plane while following crimped trajectory to link different layers. From weaver specified weave design we know the number of layers of weft tows

(n_{wft}) which for a warp interlock weave is generally taken as the number of layers of the fabric. For any warp interlock fabric, number of layers of warp tows can be calculated as follows:

$$n_{wp} = n_{wft} + 1 \tag{2.5}$$

Having calculated number of layers of warp and weft tows and their respective thicknesses; t_{wp} and t_{wft}, thickness of the fabric *'T'* can be calculated using the following relation:

$$T = (n_{wp} \times t_{wp} + n_{wft} \times t_{wft}) \tag{2.6}$$

The lengths of the unit cell '$L_{UC(wp)}$' and '$L_{UC(wft)}$' in the warp (Fig. 2.6-A) and weft directions respectively (in mm) can be calculated from weaver specified data as follows:

$$L_{UC(wp)} = \frac{r_{wft}}{P_{wft}} \times 10 \tag{2.7}$$

$$L_{UC(wft)} = \frac{r_{wp}}{P_{wp}} \times 10 \tag{2.8}$$

In the case of fabric in which both the warp and weft tows are crimped and their cross sections are lenticular, following set of equations can be used to calculate warp and weft crimp angles in degrees (for derivation consult Appendix 1):

$$\Phi_{wp} = \arctan\left(\frac{2t_{wft} w_{wft}}{w_{wft}{}^{2} - t_{wft}{}^{2}}\right) \tag{2.9}$$

$$\Phi_{wft} = \arctan\left(\frac{2t_{wp} w_{wp}}{w_{wp}{}^{2} - t_{wp}{}^{2}}\right) \tag{2.10}$$

From Fig. 2.6-A and 2.6-B, it is obvious that inside a repeat unit cell each crimped warp and weft tow consists of two lenticular and two straight segments. The sum of these segments gives the length of the tow in the unit cell.

Following set of equations can be used to calculate lengths of crimped warp and weft tows inside a unit cell:

$$l_{wp(UC)} = 2\left[\Phi_{wp}\left\{\frac{w_{wft}{}^{2} + t_{wft}{}^{2}}{2t_{wft}}\right\} + \left\{\frac{1/2 \times L_{UC(wp)} - w_{wft}}{\cos\Phi_{wp}}\right\}\right] \tag{2.11}$$

$$l_{wft(UC)} = 2\left[\Phi_{wft}\left\{\frac{w_{wp}{}^{2} + t_{wp}{}^{2}}{2t_{wp}}\right\} + \left\{\frac{1/2 \times L_{UC(wft)} - w_{wp}}{\cos\Phi_{wft}}\right\}\right] \tag{2.12}$$

In case of architectures where warp is straight i.e., $\Phi_{wp} = 0$, length of the warp tow in the unit cell can be calculated from the following modified formula:

$$l_{wp(UC)} = 2\left[w_{wft} + \left\{\frac{1/2 \times L_{UC(wp)} - w_{wft}}{\cos\Phi_{wp}}\right\}\right] \tag{2.13}$$

Similarly when weft is straight i.e., $\Phi_{wft} = 0$, length of the weft tow in the unit cell can be calculated as follows:

$$l_{wft(UC)} = 2\left[w_{wp} + \left\{\frac{1/2 \times L_{UC(wft)} - w_{wp}}{\cos\Phi_{wft}}\right\}\right] \tag{2.14}$$

Once the dimensions of the unit cell i.e. $L_{UC(wp)}$ and $L_{UC(wft)}$, the lengths of the warp and weft tows inside the unit cell i.e. $l_{wp(UC)}$ and $l_{wft(UC)}$ are known, crimp percentages in respective tows can be calculated using the following equations:

$$c_{wp} = \frac{l_{wp(UC)} - L_{UC(wp)}}{l_{wp(UC)}} \times 100 \tag{2.15}$$

$$c_{wft} = \frac{l_{wft(UC)} - L_{UC(wft)}}{l_{wft(UC)}} \times 100 \tag{2.16}$$

Areal weight of the fabric can be calculated henceforth as follows:

$$GSM_{wp} = \frac{P_{wp} \times Tex_{wp} \times 100}{10 \times (100 - c_{wp})} \tag{2.17}$$

$$GSM_{wft} = \frac{P_{wft} \times Tex_{wft} \times 100}{10 \times (100 - c_{wft})} \tag{2.18}$$

$$GSM_{fabric} = GSM_{wp} + GSM_{wft} \tag{2.19}$$

Fractional masses can be calculated from equations (2.20) and (2.21) as follows:

$$FM_{wp} = \frac{GSM_{wp}}{GSM_{fabric}} \tag{2.20}$$

$$FM_{wft} = \frac{GSM_{wft}}{GSM_{fabric}} \tag{2.21}$$

Area of the unit cell (in mm^2) can be calculated from the dimensions of the unit cell:

$$a_{UC} = L_{UC(wp)} \times L_{UC(wft)} \tag{2.22}$$

Mass of the warp and weft tows (in grams) in the unit cell can be calculated by introducing the values of unit cell area as follows:

$$m_{wp/UC} = \frac{GSM_{wp} \times a_{UC}}{1000000} \tag{2.23}$$

$$m_{wft/UC} = \frac{GSM_{wft} \times a_{UC}}{1000000} \tag{2.24}$$

Mass of the unit cell (in grams) is given as:

$$m_{UC} = \frac{GSM_{fabric} \times a_{UC}}{1000000} \tag{2.25}$$

Volume of warp and weft tows (in mm^3) inside the unit cell can be calculated from equations (2.26) and (2.27) respectively:

$$V_{wp(UC)} = \frac{m_{wp/UC}}{\rho_{wp}} \times 10^9 \tag{2.26}$$

$$V_{wft(UC)} = \frac{m_{wft/UC}}{\rho_{wft}} \times 10^9 \tag{2.27}$$

Volume of the unit cell (in mm^3) can be calculated from the dimensions of the unit cell already calculated:

$$V_{UC} = T \times L_{UC(wp)} \times L_{UC(wft)} \tag{2.28}$$

Fibre volume fraction can be calculated from the volumes of warp and weft tows and the volume of unit cell already calculated. Overall fibre volume fraction is given as:

$$FVF = \frac{V_{wp(UC)} + V_{wft(UC)}}{V_{UC}} \times 100 \tag{2.29}$$

Warp and weft proportions can be calculated from warp and weft volumes already calculated using the following mathematical relationships:

$$FVF_{wp} = \frac{V_{wp(UC)}}{V_{wp(UC)} + V_{wft(UC)}} \times 100 \tag{2.30}$$

$$FVF_{wp} = \frac{V_{wft(UC)}}{V_{wp(UC)} + V_{wft(UC)}} \times 100 \tag{2.31}$$

2.2 Experimental Procedure

The experimental procedure adopted to apply and verify the geometrical model described above consists of two steps

1. weaving of the reinforcements
2. analysis of the woven reinforcements

2.2.1. Weaving of Interlock Reinforcements

All the fabrics belong to different classes of warp interlocks. A specially modified version of “Patronic B 60” dobby type, sampling loom was used to weave these samples (Fig. 2.7-A, B and C).

Weaving was directly done from a rectangular warp creel. 900 bobbins were installed on the creel which corresponds to the maximum warp creel capacity. Pointcarré® software was used to generate lifting plans which were then fed to Selectron® command box to control the dobby loom. These fabrics were woven from 200 Tex 6K (IM7-GP) carbon multifilament tows in warp, supplied by Hercules® and 320 Tex (RC 14 320 P109 160) glass multifilament tows in weft, supplied by Vetrotex® (refer to table 2.1 for initial tow parameters). The use of glass in weft gives necessary contrast required for measurements on photomicrographs.

In order to avoid residual stress in the final product, it is recommended that symmetry of unit cell geometry be ensured. Therefore it is important that the structural design of a 3D woven preform should be made under the following conditions; all the yarn systems be arranged symmetrically in the thickness direction, on both top and bottom of each weft there should be at least one system of warp yarns, and only one kind of binder with the same degree of crimp should be used in order to reduce weaving difficulty [6].

While conceiving a warp interlock fabric, the weft tows are thought to be as rigid bars and the warp yarns are conceived as the crimping or wavy group of threads that while traversing between different layers bind the layers together. Initially we used the similar conception and conceived the warp tows as the 'wavy group' i.e. the group having the maximum crimp and the weft tows as the 'straight group' i.e. having the minimum crimp. All of the weave designs and lifting plans are based on this conception of three dimensional warp interlock fabrics. Weave designs, peg plans and drawing in plans of some of the interlock fabrics woven are given in appendices A2-A7.

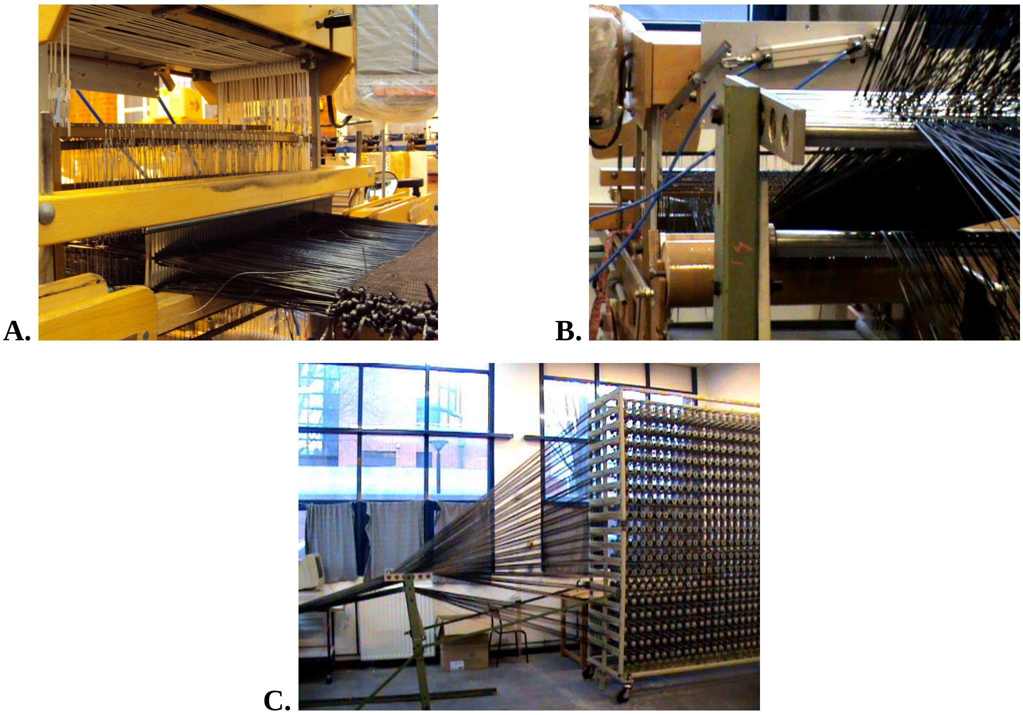

Fig. 2.7: Loom set up (A) Weaving of carbon glass reinforcement on Patronic B60 sampling loom (B and C) Carbon tows coming straight from the creel

2.2.1.1 Calculation of reed count and reed denting order

Conception of the weave is followed by selection of suitable reed count and denting order of warp tows. It is important to keep in mind two basic criteria for the selection of reed count and the corresponding denting order;

1. Reed count suitability from the point of view of avoiding excessive friction and breakage while weaving
2. Reed denting order suitability from the point of view of desired geometry of woven architecture

In the following, weaving of 13 layers Orthogonal Interlock having layer to layer binding (Orth-1.2.13) has been presented as a test case.

Several different reed counts and denting orders were tried to optimize the weaving of 13 layer warp interlock reinforcement. Once a woven architecture has been conceived it is imperative that we have knowledge of tow width so that the optimum denting order for a given reed count may be calculated. Since the warp tows are arranged in the form of vertical blocks inside a reed dent (as will be explained later), therefore in the following, a calculation methodology is given for the selection of reed count as a function of single tow width (Fig. 2.8);

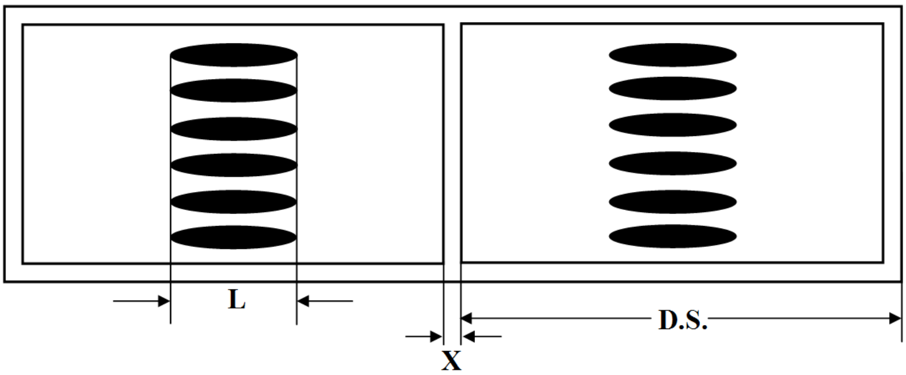

Fig. 2.8: Schematic of reed dent with its dimensions and the warp tows passing through the reed dent

From Fig. 2.8:

L = width of tow as measured directly off the package without any considerable tension and using an ordinary scale

X = thickness of a single reed tooth

R.C. = reed count in dents/cm

D.S. = dent space in mm/dent

F.S. = horizontal free space in reed in mm

Thus:

$$F.S. = (D.S. - L - X) \tag{2.32}$$

We will use the data from table 2.1 for IM7-GP, 200 Tex 6K carbon multifilament tows, which we used in warp for the weaving of 13 layer interlock fabric.

For the reed count we selected on the basis of first criterion:

$L = 2\text{mm}$

$D.S. = 5\text{mm}$

$X = 1\text{mm}$

Thus from equation 2.32:

$F.S. = 2\text{mm}$

And in relation to tow width (L) the free space is:

$$F.S. = \nu \times L$$

$$\nu = \frac{F.S.}{L}$$

For the reed that we selected:

$$\nu = 1$$

Since

$$F.S. = L \tag{2.33}$$

From different trials on the loom we have found that this is the optimum value of '*F.S*' which satisfies the first criteria for the weaving of layer to layer interlock woven architectures from carbon tows.

Again from relations 2.32 and 2.33:

$$D.S. = 2 \times L + X \tag{2.34}$$

Since 'X' should be a fraction of 'D.S.' therefore:

$$X = \beta \times D.S.$$

For the reed that we selected:

$$\beta = \frac{1}{5}$$

Therefore;

$$X = \left(\frac{1}{5}\right) \times D.S. \tag{2.35}$$

From relations 2.34 and 2.35:

$$D.S. = 2 \times L + \left(\frac{1}{5}\right) \times D.S.$$

Therefore:

$$D.S. = 2.5 \times L$$

Since:

$$R.C. = \left(\frac{10}{D.S.} \right)$$

Reed count in dents/cm can be calculated as a function of tow width in mm (L):

$$R.C. = \left(\frac{10}{2.5 \times L} \right)$$

$$R.C. = \left(\frac{4}{L} \right) \tag{2.36}$$

It was noted that the empirical relation deduced above holds good for weaving of the architectures under consideration and is given in order to serve as a guide for the selection of reed counts while weaving flat multifilament tows.

It was found that the reed count of 2 dents per cm is the most suitable as far as the first criteria is concerned.

In order to select the suitable reed denting order according to second criterion, the 13 layers warp interlock reinforcement having layer to layer binding was woven on the loom by varying the following parameters;

- Denting of warp tows in reed
- Warp lifting order

It was found that reed denting as well as warp lifting order has a profound effect on the configuration of the unit cell. In the following table different case studies carried out by varying the reed denting order on the same weave are given:

Table 2.2: Different case studies on layer to layer woven interlock architecture

No	**Characteristics**	**Case 1**	**Case 2**	**Case 3**
1	Fabric width (cm)	37.5	18	37.5
2	Reed dents/cm	2	2	2
3	Total ends	900	900	900
4	Ends/cm	24	48	24
5	Ends/dent	12	24	12
6	Repeat size in warp direction (mm)	10	16	10
7	Repeat size in weft direction (mm)	10	5	1.25
8	Thickness of fabric (mm)	3	4	7
9	Layers in fabric	4	6	13

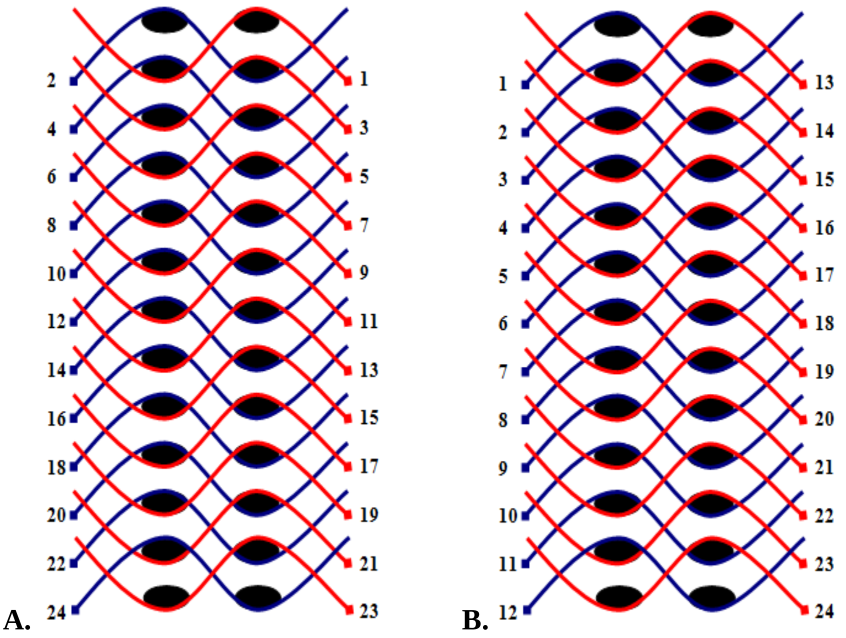

Fig. 2.9: (A) The layer to layer interlock woven and analyzed as case 1 and 2

(B) The layer to layer interlock woven and analyzed as case 3

2.2.1.2 Observations made on photomicrographs

When studied after being woven, following observations were made on the fabric and its photomicrographs

The weft tows were inserted in a diagonal manner for the fabric under discussion as case 1 and 2. Due to the insertion pattern and the order of warp threads, the weft threads are constrained and even after beat up process is complete they only manage to arrange themselves diagonally (Fig. 2.10-A, 2.11-A and 2.11-B). For the woven fabric under study as case 3, the warp numbering order ensures that the weft threads are inserted vertically one over another (Fig. 2.10-B and Fig. 2.11-C).

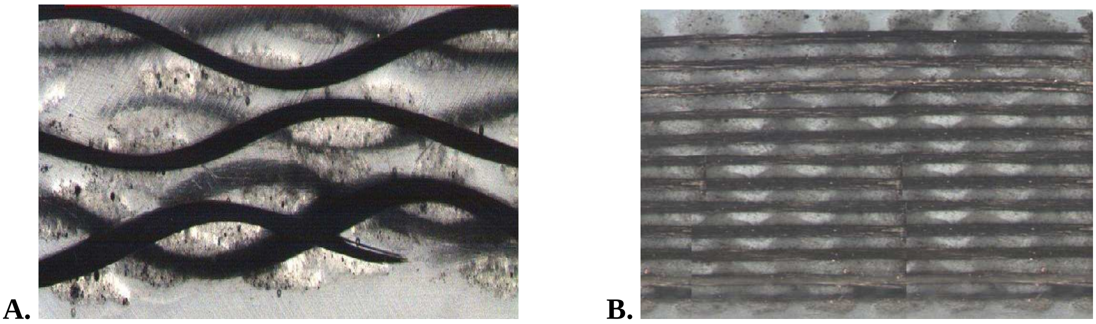

Fig. 2.10: Photomicrographs showing the warp trajectory and weft cross sectional shape in; (A) case 2 (B) case 3

The unit cell size in the weft direction depends upon the reed denting order (see table 2.2). For the cases 1 and 2 the warp tows rearrange themselves and are spread horizontally and occupy the space provided by the reed dent (Fig. 2.11-A and B). There are no vertical blocks of warp tows therefore the fabric has lesser number of layers. When the number of warp tows per dent is increased from 12 to 24, the size of unit cell is reduced to one half and the total number of layers is also increased (see table 2.2). But at the same time the weavability is adversely affected and it was observed that doubling the number of tows increases friction between adjacent warp tows as well as abrasion between warp tows and the metallic dents of reed.

In case 3, due to the vertical placement of warp tows (which is the result of specific warp numbering and reed denting) one over another (Fig. 2.9-B), the fabric has greater number of layers (Fig. 2.11-C). The case 3 fabric is highly unbalanced fabric with respect to warp and weft tow density in the fabric (see table 2.2). A fact that is responsible for the absence of crimp in warp direction (Fig. 2.10-B) and maximum crimp in the weft direction (Fig. 2.11-C).

In case 1 and 2 warp tows have a wavy configuration (Fig. 2.11-A and Fig. 2.12-A) but since the weft tows have a minimal crimp and they don’t apply compaction on warp tows therefore the warp tow cross section is non lenticular (Fig. 2.11-A and B) whereas the weft tow cross section is lenticular (Fig. 2.10-A and Fig. 2.12-A) due to the compaction applied by warp tows. For the fabric under study as case 3 the warp tows get compacted under the pressure of weft tows that have maximum crimp.

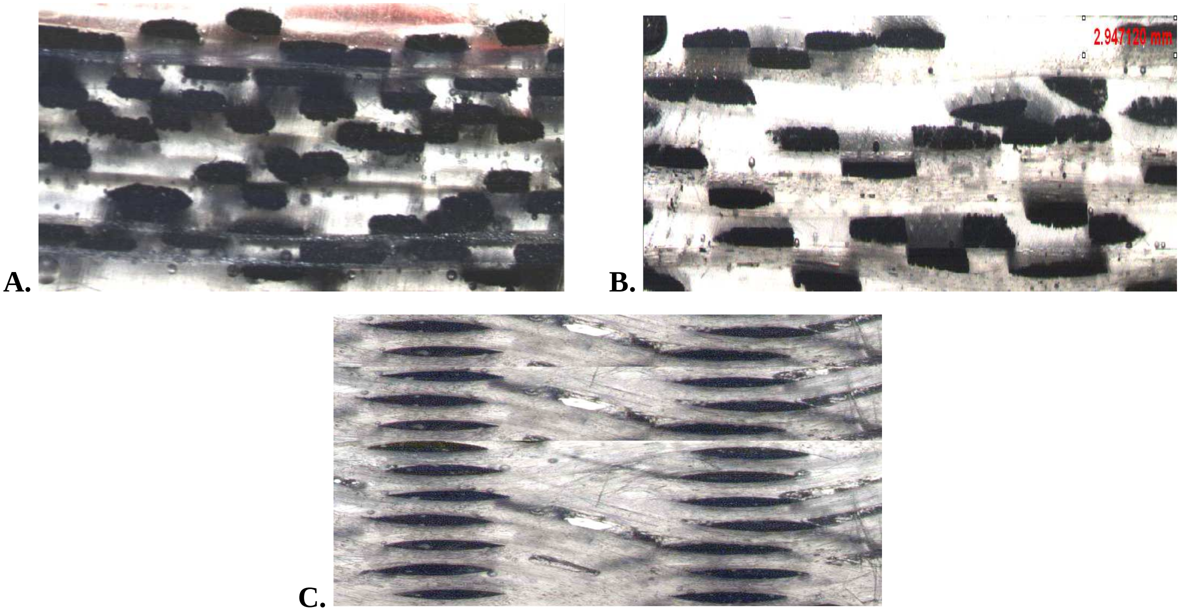

Fig. 2.11: Photomicrographs depicting the weft trajectory and warp cross sectional shape in; (A) case 1(B) case 2 (C) case 3

These warp tows have lenticular cross section as a result (Fig. 2.11-C) while the cross section of weft tows is non lenticular, as the straight warp tows are unable to apply compaction on weft tows (Fig. 2.10-B).

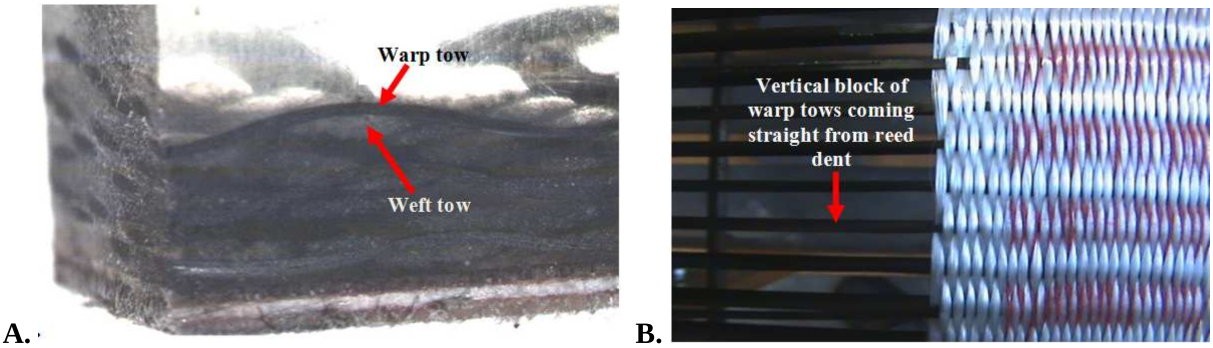

Fig. 2.12: (A) Resin impregnated fabric in case 2 (B) case 3 fabric being woven on loom

The 13 layer warp interlock woven architecture is highly unbalanced with 24 warp tows/cm and 208 weft tows/cm (table 2.7). Due to high density of weft tows, warp tows remain straight (in spite of the conception of fabric as described earlier) while the weft tows have maximum crimp. By varying the warp and weft densities the crimp in the warp or weft direction can be modified. Thus in order to describe the geometry of the layer to layer woven reinforcement two extremes can be defined as:

- Maximum warp crimp and minimum (or zero) weft crimp geometry: $\mathbf{C}_{\max(\text{warp})}$
- Maximum weft crimp and minimum (or zero) warp crimp geometry: $\mathbf{C}_{\max(\text{weft})}$

The 13 layer reinforcement woven for the present study can be identified as $C_{\max(\text{weft})}$. An alternative fabric can be woven to correspond to the other extreme i.e. $C_{\max(\text{warp})}$. It was also observed that the tow cross section also undergoes an evolution with the crimp geometry. In the $C_{\max(\text{weft})}$ architecture the warp tows have a lenticular cross section while the weft tows can be approximated as non lenticular while a $C_{\max(\text{warp})}$ architecture will have lenticular weft cross sections and non lenticular warp cross sections.

By using the weft order as described for case 3, warp and weft blocks (tows stacked one over another in the form of vertical columns) can be achieved. This is imperative in order to achieve high thickness and volume fraction in the desired direction.

Having understood the mechanism of weaving, different warp interlock structures were woven and analyzed in order to validate the model. These structures can be grouped in three categories as follows:

1. Orthogonal Interlock/Layer-to-layer binding
2. Angle Interlock/Layer-to-layer binding
3. Angle Interlock/Through-the-thickness binding

For reference the fabrics have been coded in the following fashion: ***Prefix-x.y.n**$_{wft}$*

The prefix Orth and Ang will be used for orthogonal and angle interlock structures respectively. Whereas the letters x, y and n_{wft} stand for step of interlocking warp, depth of interlocking warp and the total number of layers in the fabric respectively.

Step, depth and fabric layers along with fabric codes are given for three groups of fabrics in tables 2.3-2.5

Table 2.3: Orthogonal Interlocks/Layer-to-layer binding

Code	**Step(x)**	**Depth(y)**	**Layers(n_{wft})**
Orth-1.2.3	1	2	3
Orth-1.2.5	1	2	5
Orth-1.2.7	1	2	7
Orth-1.2.13	1	2	13

Table 2.4: Angle Interlocks/Layer-to-layer binding

Code	**Step(x)**	**Depth(y)**	**Layers(n_{wft})**
Ang-2.2.5	2	2	5
Ang-3.2.7	3	2	7

Table 2.5: Angle Interlocks/ Through-the-thickness binding

Code	**Step(x)**	**Depth(y)**	**Layers(n_{wft})**
Ang-3.3.5	3	3	5
Ang-5.5.5	5	5	5
Ang-7.4.7	7	4	7
Ang-13.7.7	13	7	7

Fig. 2.13-2.22 give the WiseTex® generated geometrical description of all the fabrics described above.

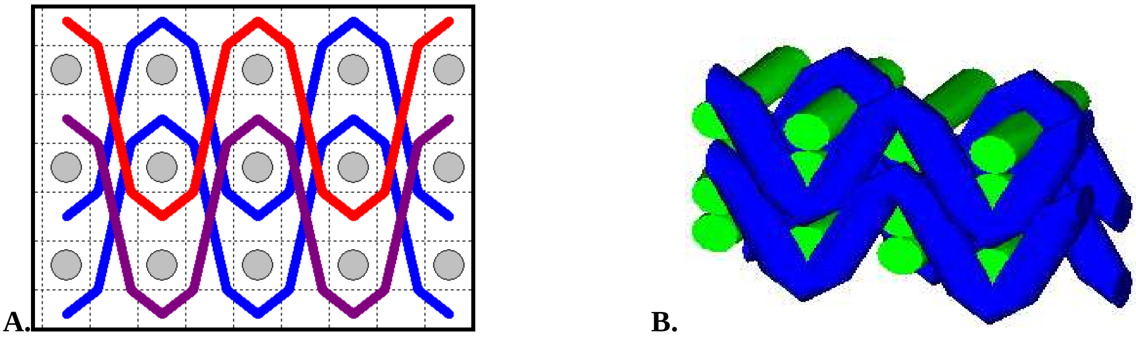

Fig. 2.13: Orth-1.2.3 Weave structure - Wisetex- graphical representation

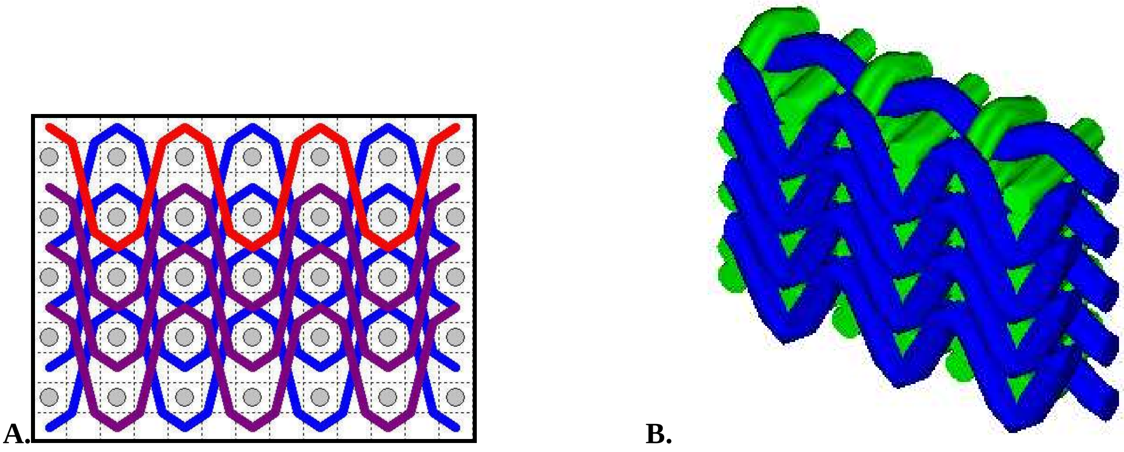

Fig. 2.14: Orth-1.2.5 Weave structure - Wisetex- graphical representation

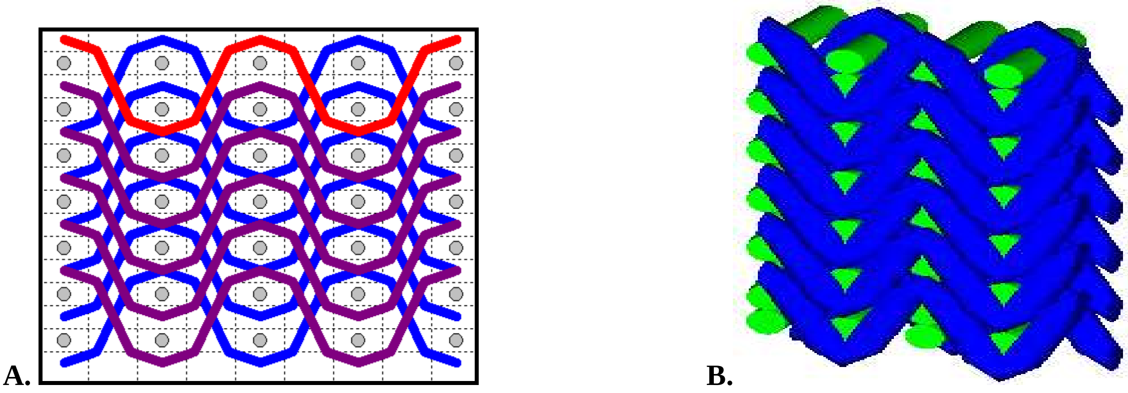

Fig. 2.15: Orth-1.2.7 Weave structure - Wisetex- graphical representation

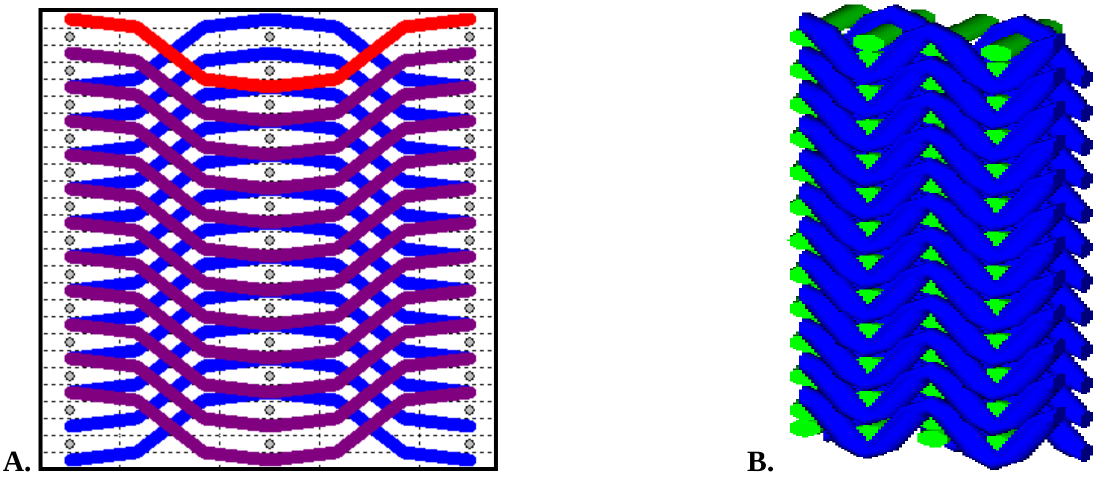

Fig. 2.16: Orth-1.2.13 Weave structure - Wisetex- graphical representation

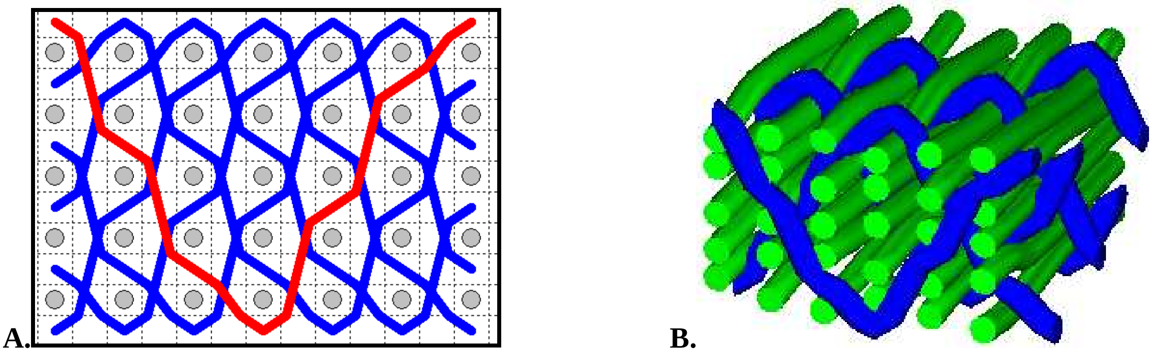

Fig. 2.17: Ang-5.5.5 Weave structure - Wisetex- graphical representation

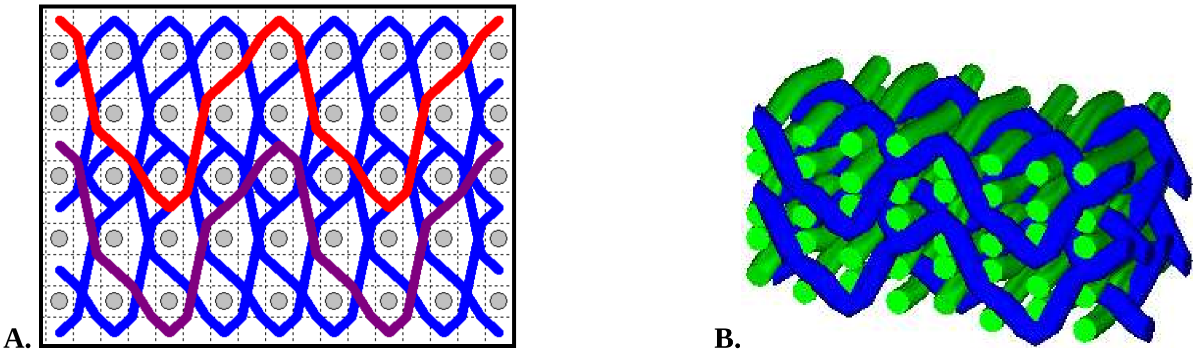

Fig. 2.18: Ang-3.3.5 Weave structure - Wisetex- graphical representation

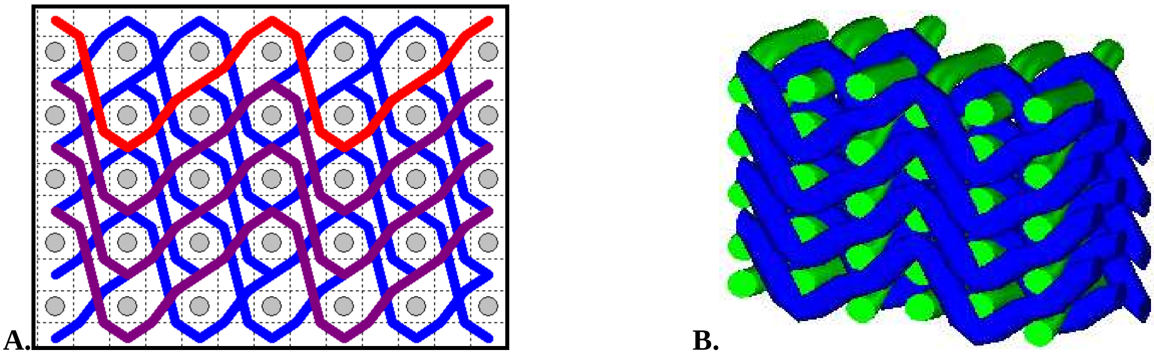

Fig. 2.19: Ang-2.2.5 Weave structure - Wisetex- graphical representation

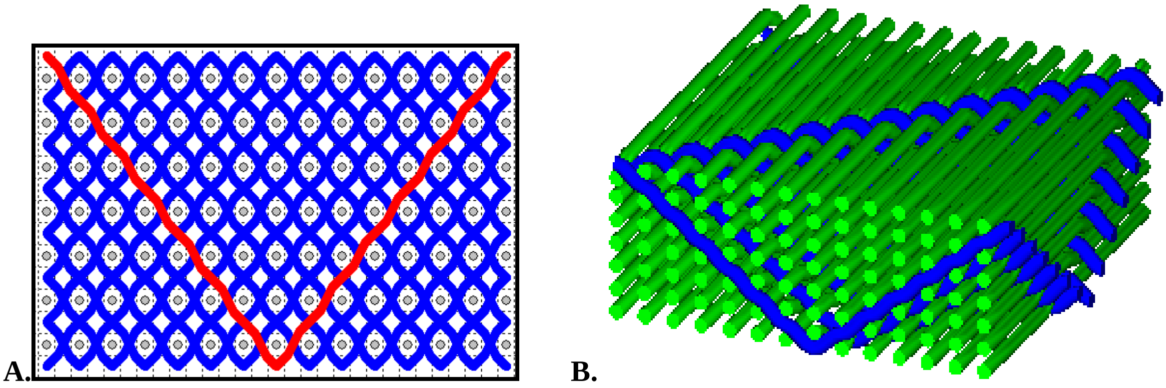

Fig. 2.20: Ang-13.7.7 Weave structure - Wisetex- graphical representation

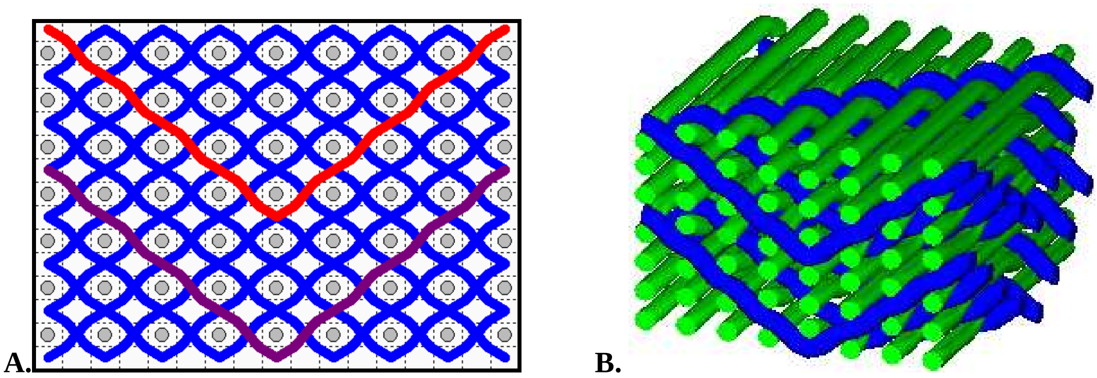

Fig. 2.21: Ang-7.4.7 Weave structure - Wisetex- graphical representation

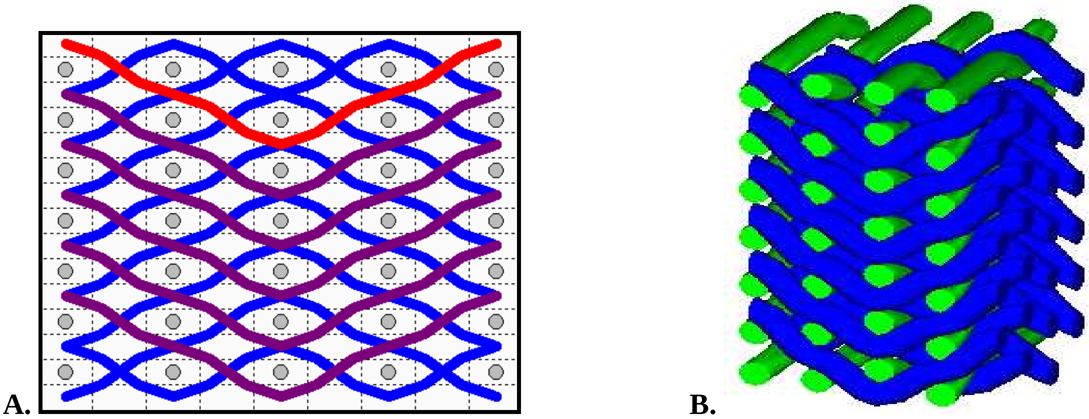

Fig. 2.22: Ang-3.2.7 Weave structure - Wisetex- graphical representation

'Tow data' and *'weaver data'* used as model inputs for all the woven fabrics, is given in tables 2.6 and 2.7 respectively.

Table 2.6: Tow data

Sr. No.	***Fabric Code***	Tex_{wp}	Tex_{wft}	w_{wp} ***(mm)***	w_{wft} ***(mm)***	$P.F._{wp}$	$P.F._{wp}$	ρ_{wp} ***(g/m³)***	ρ_{wft} ***(g/m³)***
1	*Orth-1.2.3*	200	320	1.35	0.44	0.75	0.75	1.76×10^{-6}	2.53×10^{-6}
2	*Orth-1.2.5*	200	320	1.80	1.83	0.75	0.75	1.76×10^{-6}	2.53×10^{-6}
3	*Orth-1.2.7*	200	320	1.42	0.44	0.75	0.75	1.76×10^{-6}	2.53×10^{-6}
4	*Orth-1.2.13*	200	320	1.52	0.44	0.75	0.75	1.76×10^{-6}	2.53×10^{-6}
5	*Ang-2.2.5*	200	320	1.60	1.33	0.75	0.75	1.76×10^{-6}	2.53×10^{-6}
6	*Ang-3.2.7*	200	320	1.48	0.96	0.75	0.75	1.76×10^{-6}	2.53×10^{-6}
7	*Ang-3.3.5*	200	320	1.24	1.33	0.75	0.75	1.76×10^{-6}	2.53×10^{-6}
8	*Ang-3.5.5*	200	320	0.95	1.23	0.75	0.75	1.76×10^{-6}	2.53×10^{-6}
9	*Ang-7.4.7*	200	320	1.17	1.10	0.75	0.75	1.76×10^{-6}	2.53×10^{-6}
10	*Ang-13.7.7*	200	320	1.12	1.21	0.75	0.75	1.76×10^{-6}	2.53×10^{-6}

Table 2.7: Weaver data

Sr. No.	***Fabric Code***	r_{wp}	r_{wft}	P_{wp} ***(tows/cm)***	P_{wft} ***(tows/cm)***	n_{wft}
1	*Orth-1.2.3*	4	6	4	42	3
2	*Orth-1.2.5*	8	10	17	20	5
3	*Orth-1.2.7*	12	14	12	88	7
4	*Orth-1.2.13*	24	26	24	208	13
5	*Ang-2.2.5*	12	15	16	34	5
6	*Ang-3.2.7*	24	28	27	67	7
7	*Ang-3.3.5*	8	20	16	21	5
8	*Ang-3.5.5*	6	30	16	21	5
9	*Ang-7.4.7*	16	56	17	77	7
10	*Ang-13.7.7*	14	98	15	84	7

Fractional cover factor values calculated for four orthogonal interlocks having layer-to-layer binding are given in Table 2.8.

Table 2.8: Relative fractional cover factor for layer-to-layer interlocks

Fabric Code	*Orth-1.2.3*	*Orth-1.2.5*	*Orth-1.2.7*	*Orth-1.2.13*
Fractional C.F.	0.20	0.90	0.32	0.27

A complete flow diagram of the experimental and theoretical approach adopted is given in Fig. 2.23.

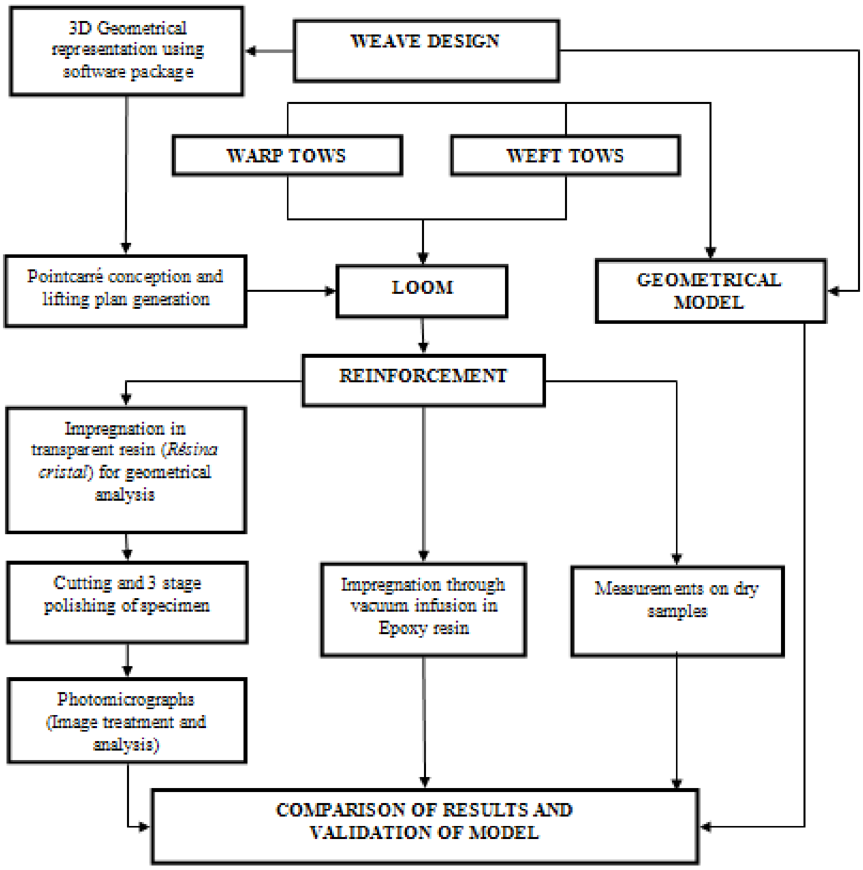

Fig. 2.23: Complete flow diagram of experimental and theoretical approach adopted

2.3 Post weaving analysis

After weaving, the fabric samples were divided in three parts (Fig. 2.23). One was used for dry fabric analysis. The second part was impregnated by vacuum infusion using SR 8100 epoxy resin and SD 8824 hardener supplied by Sicomin®. The composites thus formed were used for fibre volume fraction calculation.

The third part was used for transparent resin impregnation. For this purpose epoxy resin 'Resina Cristal' supplied by Lamplan® was used. This resin polymerizes at room temperature and atmospheric pressure and is used for enveloping fragile materials to allow their visual examination through optical microscopy. These impregnated samples were cut into thin slices of about 1mm thickness with a diamond tipped cutting disk.

Afterwards these specimens underwent three stage polishing in order to obtain smooth and clear surface for visual examination. First of all specimens were polished with 240 grit sand paper disk followed by polishing with 600 grit sand paper disk to render the surface smoother. In the end "Cameo disk Gold®" was used in conjunction with diamond liquid 'BioDIAMANT® 6Mme' supplied by

Lamplan® having monocrystalline 6 µm diamond granules. This procedure was repeated until clear photomicrographs of fabric transversal and lateral sections were obtained with the help of a camera attached to magnifying lens (refer to photomicrographs in Fig. 2.24-2.33). Commercially available software package “Bel Microimage analyzer®” was used for image processing and measurements.

Fabric Thickness was measured on photomicrographs. For each fabric variant, at least 10 measurements were made and their averages were calculated. Similarly warp and weft crimp angles were measured on photomicrographs.

Crimp percentages for warp and weft tows were measured by carefully removing them from dry fabric samples according to ASTM standard D3883-04 [7]. Areal weight of dry fabric samples was measured according to standard test method; ASTM standard D 3776 [8].

Finally fibre volume fractions for the composites made from 3D reinforcements was measured in accordance with ASTM D 3171 standard test method [9].

Relative fractional cover values were calculated for all the Orthogonal Interlocks/layer-to-layer architectures using equation (2.7). These values have been reported in table 2.8.

The highest value calculated for relative fractional cover is 0.90 for Orth-1.2.5. Therefore for the calculation of geometrical parameters using the formulae given above, both the warp and weft tow sections were assumed to be lenticular and the formulae were chosen accordingly for the calculation of geometrical parameters. For all the other architectures the values are much less than 0.6. This implies highly crimped weft and straight warp tows. In the case of these highly unbalanced structures, the warp has been assigned lenticular and weft non lenticular cross section.

All the Calculated and measured geometrical parameters along with their error percentages for the fabrics woven and analyzed have been summarized in tables 2.9-2.11.

Table 2.9: Calculated and measured geometrical parameters for orthogonal interlocks

	Orth-1.2.3			***Orth-1.2.5***			***Orth-1.2.7***			***Orth-1.2.13***		
	C*	**M***	**E***	**C***	**M***	**E***	**C***	**M***	**E***	**C***	**M***	**E***
Thickness (mm)	1.49	1.4	-6.4	1.01	1.01	0	3.31	3.086	-7.2	6.03	6	0.5
Warp crimp angle (^{0})	-	0	-	7.33	8.24	11.04	0	0	0	0	0	0
Weft crimp angle (^{0})	9.61	9.5	-1.1	6.76	7.20	6.1	9.61	9.68	0.72	9.61	9.70	0.93
Crimp in warp (%)	0	0	-	0.43	0.48	10.4	0	0	0	0	0	0
Crimp in weft (%)	1.40	1.50	6.7	0.69	0.60	-0.15	1.40	1.55	9.6	1.40	1.35	-3.7
GSM (g/m^2)	1660.2	1627.9	-1.98	979.4	918.7	-6.61	3095.9	3136.7	1.3	7230.3	7000	-3.3
Total vol. fraction	41.73	43.5	4.07	44.30	42.6	-4.0	41.00	44.5	7.86	49.01	47.20	-3.8

*C – Calculated values; M – Measured values; E – Error (%)

Table 2.10: Calculated and measured geometrical parameters for 5 layered angle interlocks

	Ang-2.2.5			***Ang-3.3.5***			***Ang-3.5.5***		
	C*	**M***	**E***	**C***	**M***	**E***	**C***	**M***	**E***
Thickness (mm)	2.08	1.93	-7.80	1.73	1.62	-6.80	1.53	1.34	-14.20
Warp crimp angle (^{0})	16.01	17.21	7	13.69	13.84	1.1	13.83	11.1	-24.6
Weft crimp angle	0.00	-	-	0.00	-	-	8.67	7.68	-12.9
Crimp in warp (%)	3.44	3.30	-4.2	2.32	2.91	20.3	1.74	1.64	-6.1
Crimp in weft (%)	-	0.25	-	-	0.74	-	1.14	1.23	7.3
GSM (g/m^2)	1003.40	1006.50	0.30	999.60	1003.20	0.30	1426.20	1440.10	0.90
Total vol. fraction	21.83	22.20	1.67	26.02	26.80	2.91	40.52	41.55	2.48

* C – Calculated values; M – Measured values; E – Error (%)

Table 2.11: Calculated and measured geometrical parameters for7 layered angle interlocks

	Ang-3.2.7			***Ang-7.4.7***			***Ang-13.7.7***		
	C*	**M***	**E***	**C***	**M***	**E***	**C***	**M***	**E***
Thickness (mm)	2.22	2.16	-2.8	2.72	2.34	-16.2	2.94	2.67	-10.1
Warp crimp angle (^{0})	15.18	15.97	4.94	20.60	21.81	5.55	25.04	25.95	3.5
Weft crimp angle	10.14	10.02	-1.2	-	0.00	-	-	0.00	-
Crimp in warp (%)	1.39	1.45	4.14	4.57	4.70	2.76	7.94	8.20	3.17
Crimp in weft (%)	1.55	1.62	4.32	-	0	-	-	0	-
GSM (g/m^2)	2735.44	2634.33	-3.84	2827.12	2706.35	-4.46	3025.54	2991.62	-1.13
Total vol. fraction	54.4	52.70	-3.2	50.4	49.08	-2.7	46.87	44.90	-4.4

* C – Calculated values; M – Measured values; E – Error (%)

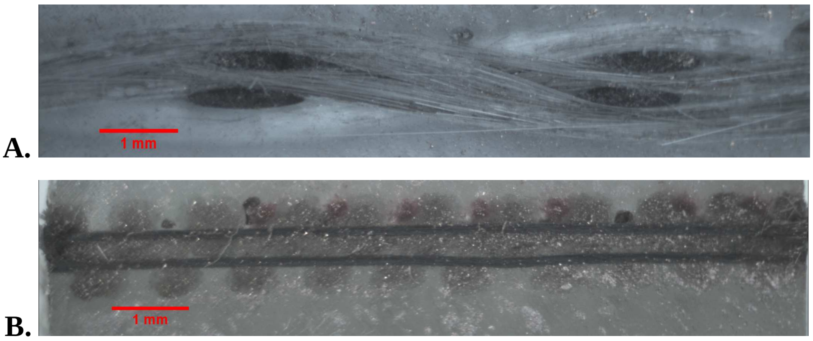

Fig. 2.24: Photomicrograph of Orth-1.2.3, (A) Transversal Section, (B) Longitudinal Section

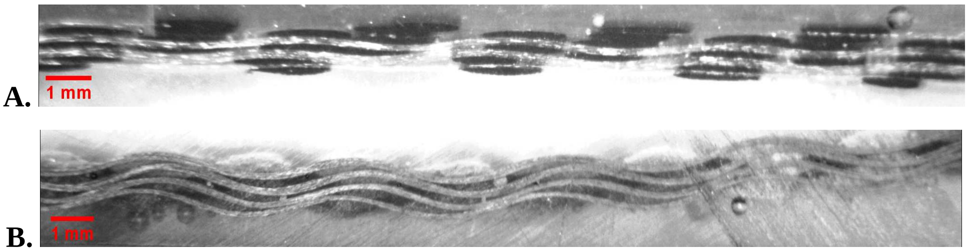

Fig. 2.25: Photomicrograph of Orth-1.2.5, (A) Transversal Section, (B) Longitudinal Section

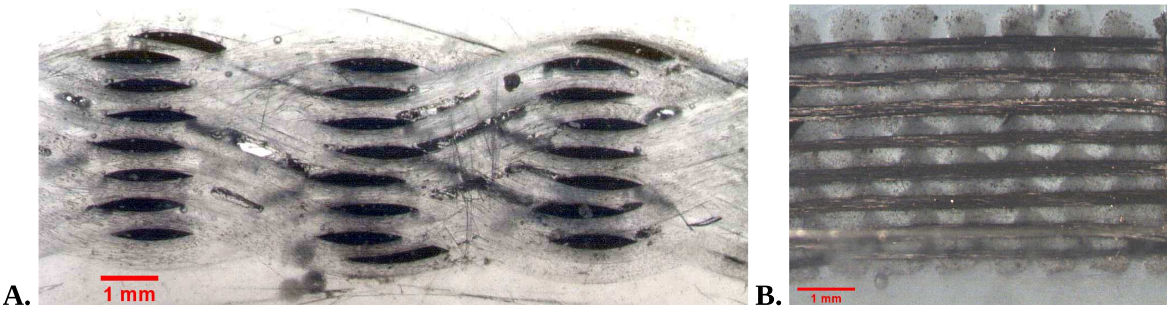

Fig. 2.26: Photomicrograph of Orth-1.2.8, (A) Transversal Section, (B) Longitudinal Section

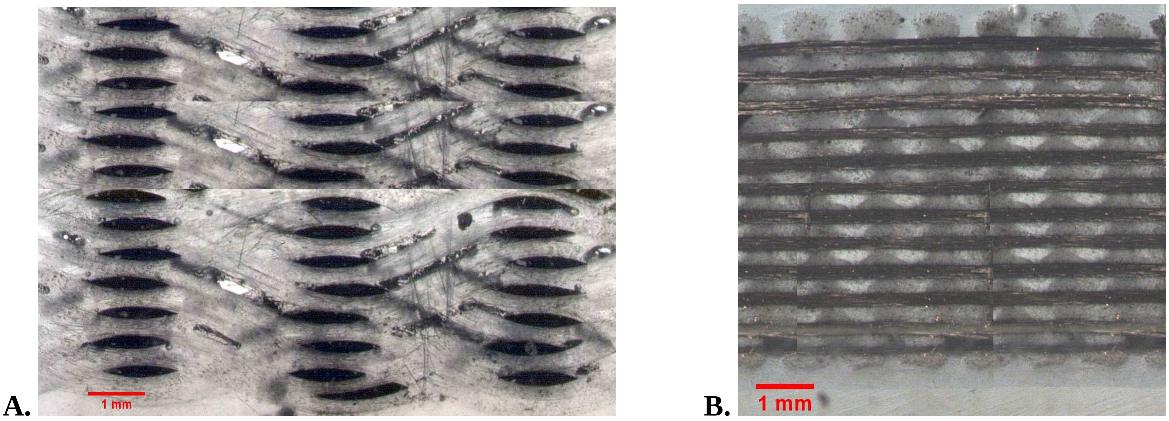

Fig. 2.27: Photomicrograph of Orth-1.2.13, (A) Transversal Section, (B) Longitudinal Section

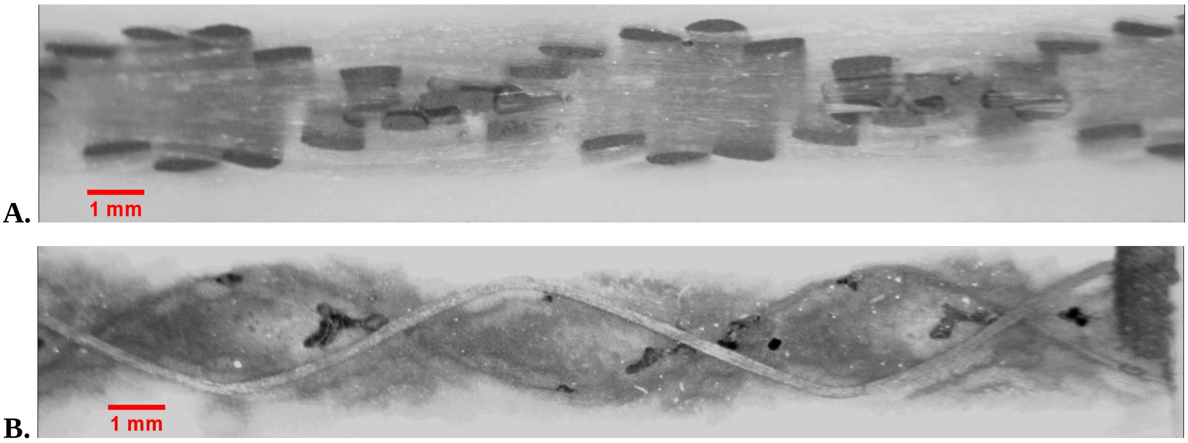

Fig. 2.28: Photomicrograph of Ang-13.7.7, (A) Transversal Section, (B) Longitudinal Section

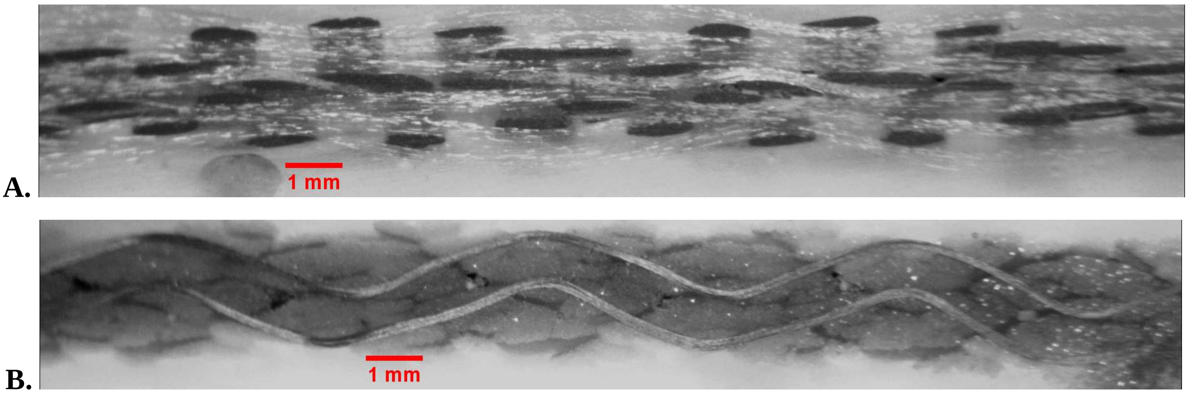

Fig. 2.29: Photomicrograph of Ang-7.4.7, (A) Transversal Section, (B) Longitudinal Section

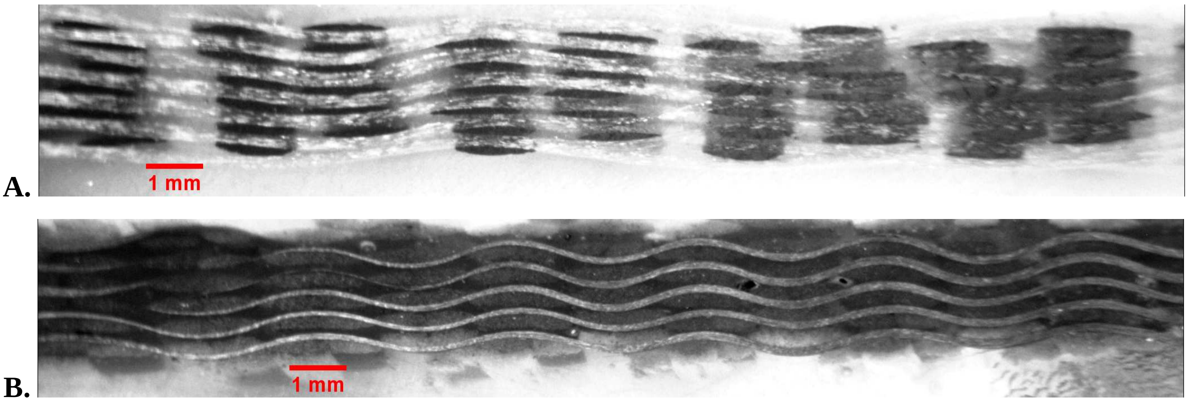

Fig. 2.30: Photomicrograph of Ang-3.2.7, (A) Transversal Section, (B) Longitudinal Section

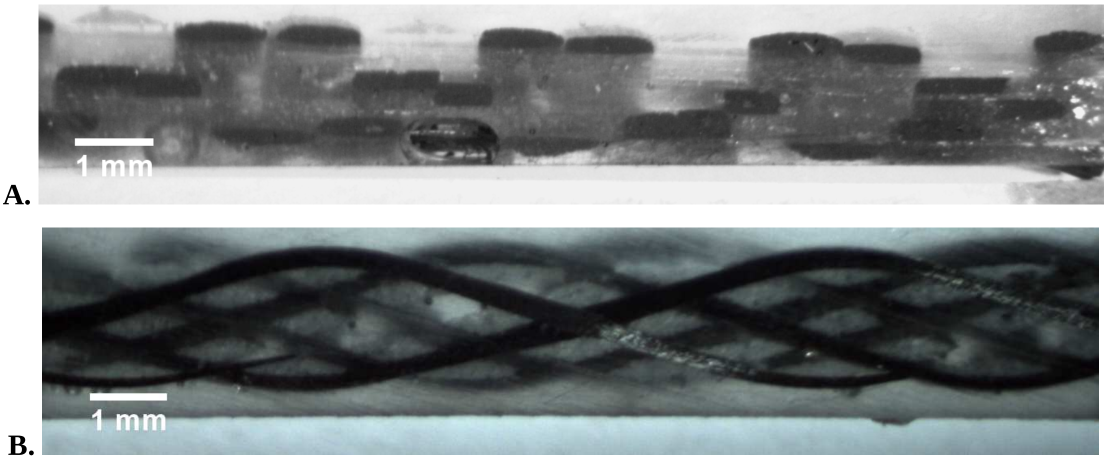

Fig. 2.31: Photomicrograph of Ang-5.5.5, (A) Transversal Section, (B) Longitudinal Section

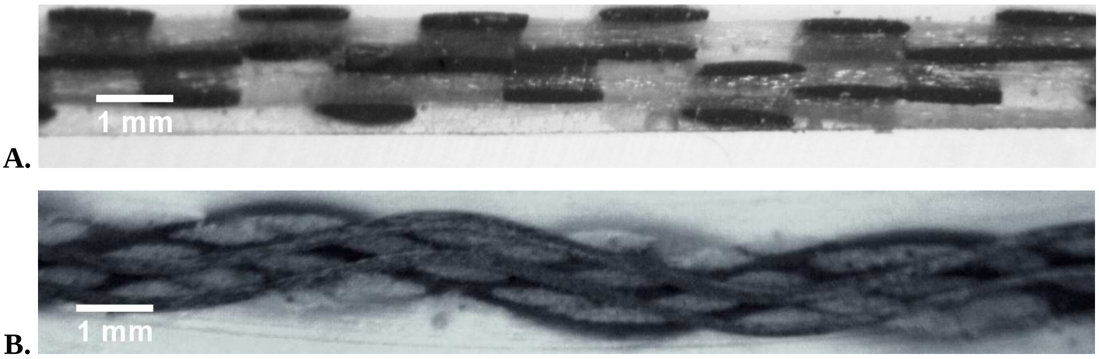

Fig. 2.32: Photomicrograph of Ang-3.3.5, (A) Transversal Section, (B) Longitudinal Section

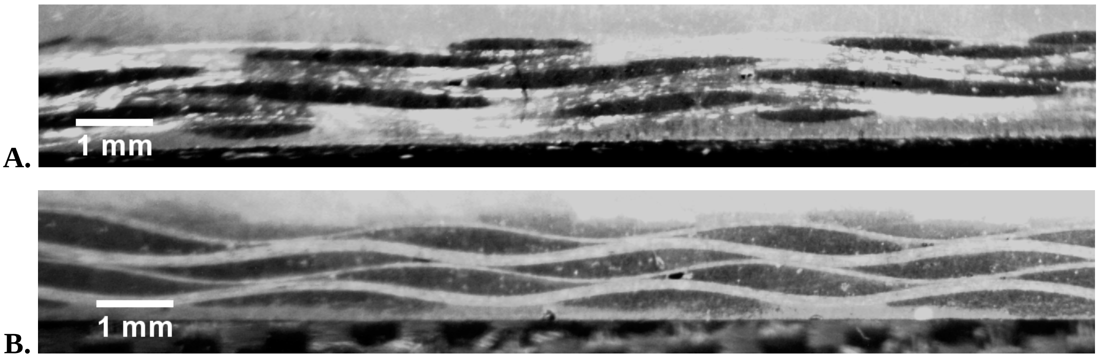

Fig. 2.33: Photomicrograph of Ang-2.2.5, (A) Transversal Section, (B) Longitudinal Section

2.4 Conclusion

In this chapter weaving of 3D woven interlock reinforcements has been described in detail. Issues related to their weaving have been explained. The weaving technique has a profound influence on the geometry of structure obtained. A mesostructural geometrical modelling approach has been developed which helps in describing tow path in the reinforcement. This approach though simple takes into account the effect of weaving parameters on geometry.

There are various sources of error which cause the measured and calculated values to diverge. Firstly it is because of the fact that not all the weft tows lie on top of one another. Visual examination of photomicrographs of some of the architectures shows that warp tows do not stay in vertical columns (refer to Fig. 2.25 and Fig. 2.33), which explains lower measured value of fabric thickness as compared to the calculated one. This anomaly affects the calculated values of all the downstream geometrical parameters. Better control of weaving process is required in order to produce preforms having geometries that agree closely with the initial conception. Moreover vacuum infusion also influences the fabric thickness. The vacuum infusion process tends to compress the reinforcements. Therefore the fibre volume fractions measured using the modelling approach does not always agree with the measured values. It was observed that the weft tows in through the thickness angle interlock architectures are not straight, and have very low crimp when measured as described above. This low crimp is caused by the compression of weft where warp tows come in contact with them, rather than weft tow waviness. However these localised compressions of weft tows have not significantly contributed to *high end* reinforcement parameters such as areal weight and fibre volume fraction.

Nevertheless the geometrical model is able to predict crimp percentages, areal weights and volume fractions reasonably accurately.

The overall results show that an approximation regarding the cross sectional shape of warp and weft tows which corresponds closely to the reality at mesostructural level is necessary in order to understand and predict the geometry of the fabric. Relative fractional cover is a useful technological parameter to assign suitable warp and weft cross sectional shapes for prior to weaving modelling of orthogonal/layer to layer warp interlocks. Another advantage is the generic nature of the geometrical approach as it can be applied to other classes of warp interlocks as well.

2.5 References

[1] S. V. Lomov, G. Huysmans, Y. Luo, R. S. Parnas, A. Prodromou, I. Verpoest, and F. R. Phelan, "Textile composites: modelling strategies," Composites Part A: Applied Science and Manufacturing, vol. 32, pp. 1379-1394, 2001.

[2] S. W. Yurgartis and J. Jortner, "Characterisation of yarn shape in woven fabric composites," in Microstructural characterization of fibre-reinforced composites, J. Summerscales, Ed.: Woodhead Publishing Limited, 1998.

[3] T. W. Chou, "Three-dimensional textile Structural Composites," in Microstructural Design of Fiber Composites New York: Cambridge University Press, 1992.

[4] B. N. Cox and G. Flanagan, "Handbook of analytical methods for textile composites (Contractor Report)" NASA 4750, 1997.

[5] S. Buchanan, A. Grigorash, J. P. Quinn, A. T. McIlhagger, and C. Young, "Modelling the geometry of the repeat unit cell of three-dimensional weave architectures," Journal of the Textile Institute, vol. 101, pp. 679-685, 2009.

[6] H. L. Yi and X. Ding, "Conventional Approach on Manufacturing 3D Woven Preforms Used for Composites," Journal of Industrial Textiles, vol. 34, pp. 39-50, July 1 2004.

[7] "ASTM D3883 - 04 Standard Test Method for yarn crimp and yarn take-take up in woven fabrics," West Conshohocken, PA, USA: ASTM, 2008.

[8] "ASTM D3776 / D3776M Standard Test Methods for Mass Per Unit Area (Weight) of Fabric," West Conshohocken, PA., USA: ASTM, 2010.

[9] "ASTM D3171 - 09 Standard Test Methods for Constituent Content of Composite Materials," West Conshohocken, PA, USA: ASTM, 2010.

Chapter 3

Study of global deformations in 3D-woven interlocks

3.1 Introduction

The tensile strength of carbon multifilament tows undergoes a considerable change from the bobbin to the 3D-woven composite, owing to stresses imparted during the manufacturing process. This evolution of tow mechanical properties also depends on the trajectory of tow inside the reinforcement as tow path has a profound effect on the final reinforcement and composite mechanical properties. In order to quantify this 'evolution' and to understand the influence of warp tow path on final mechanical properties, three variants of angle interlock reinforcements having 5 weft layers were woven from carbon tows. These architectures were conceived such that the depth of the binding tow was progressively decreased from the first to the third variant. Tensile strength tests were performed on carbon tows extracted from virgin bobbins and from weaving loom. Tensile tests were also performed on dry reinforcements woven from these carbon tows and finally on resin impregnated composites. In this way a complete track of the mechanical properties of tows was maintained. Finally strength transfer coefficient was calculated which allows an estimation of the influence of weave architecture and the infusion process on mechanical properties of composite materials. The approach adopted for the study of mechanical properties has been summarised in Fig. 3.1.

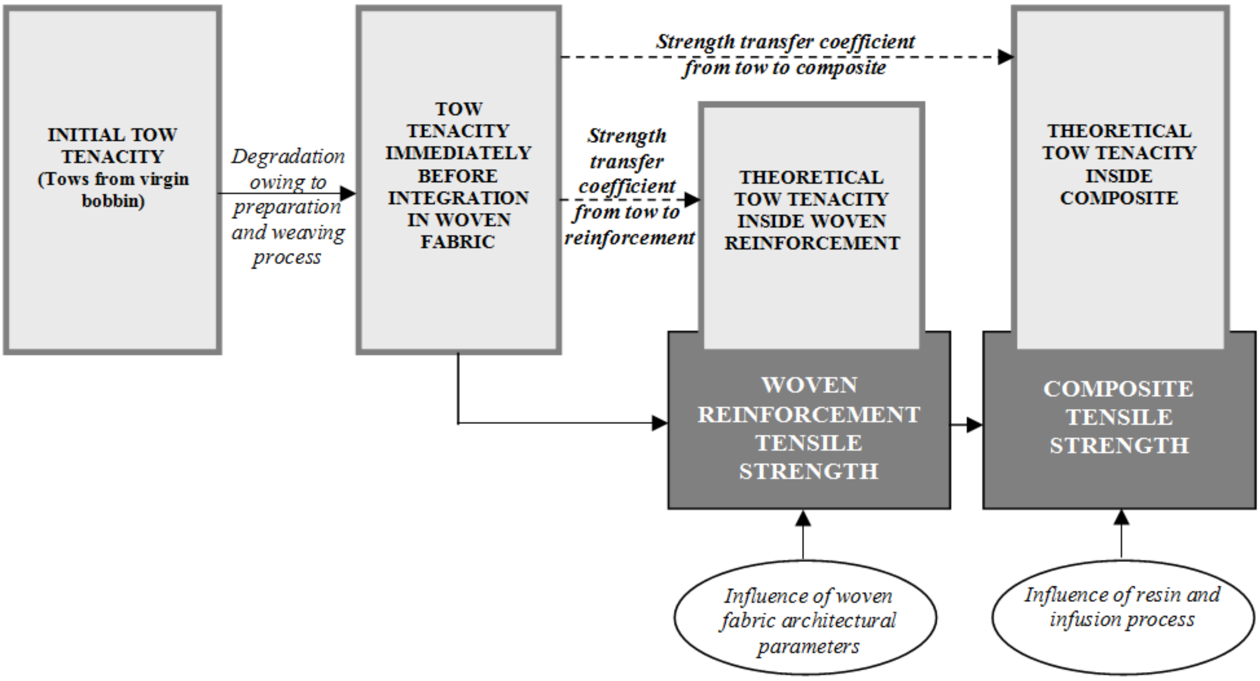

Fig. 3.1: Schematic diagram of strength transfer from tow to textile composite

3.2 Carbon tows

Multifilament tows; HexTow IM7-GP, supplied by Hexcel were chosen for weaving of the three variants. They were used in both the warp and weft directions. These tows are composed of PAN based carbon multifilaments having tow linear density of 223 Tex (0.223 g/m), while diameter of each filament is 5.2 µm having density 1.78 g/cm^3.

The tensile strength of carbon tows was experimentally determined. In order to figure out the real effect of weave architecture on strength transfer from tow to reinforcement/composite, it is important that the initial warp tow strength values be corrected for the degradation imparted by the weaving process (abrasion with heddles and loom parts, tow to tow friction, stretching and bending during shed formation and stresses imparted during the beat up process etc.). For this purpose warp tow samples were carefully extracted from length between cloth fell and heald frames on the loom and from different areas along the reinforcement width. Weft tows are not subjected to similar stresses during the weaving operation, therefore no correction, for initial tow strength values in the weft direction is required. 20 specimens of carbon tows each having 150 mm length were tested on MTS ½ tester. The speed of the machine for these tests was kept at 250 mm/min.

Tensile strength test results for carbon tows are reported in Table 3.1. Average breaking force for warp tow samples taken from the loom is slightly lower than the average value for carbon tows taken directly from the bobbin (the value is 5.06% lower in case of *'on loom'* samples).

Table 3.1: Tensile strength test results for Carbon tows

Carbon tow properties (experimental)	**Virgin tows from bobbin**	**Warp tows from loom**
Breaking Force (Std. Dev.)	217.11 N (13.8)	206.12 N (43.89)
Elongation at break	2.40 %	2.40 %
Ultimate tensile strength	957 MPa	910 MPa
Tensile modulus	276 GPa	276 GPa
Tenacity	108.5 cN/Tex	103.1 cN/Tex

Fig. 3.2 shows a graphical representation of the breaking force values obtained. The standard deviation for breaking force values is higher in the case of 'on looms' samples as compared to the samples taken from 'virgin bobbins'. This difference can be explained in terms of tow to tow friction and abrasion of carbon tows with loom parts. The movement of heald frames in the vertical plane also causes warp tow strength degradation. The tows which are subjected to more frequent movements in the vertical plain owing to the weave structure, experience greater deterioration and thus the strength reduction is more pronounced. Breaking force value of an individual tow depends upon the number and location of weak points in the sample which explains high standard deviation in the case of *'on loom'* samples.

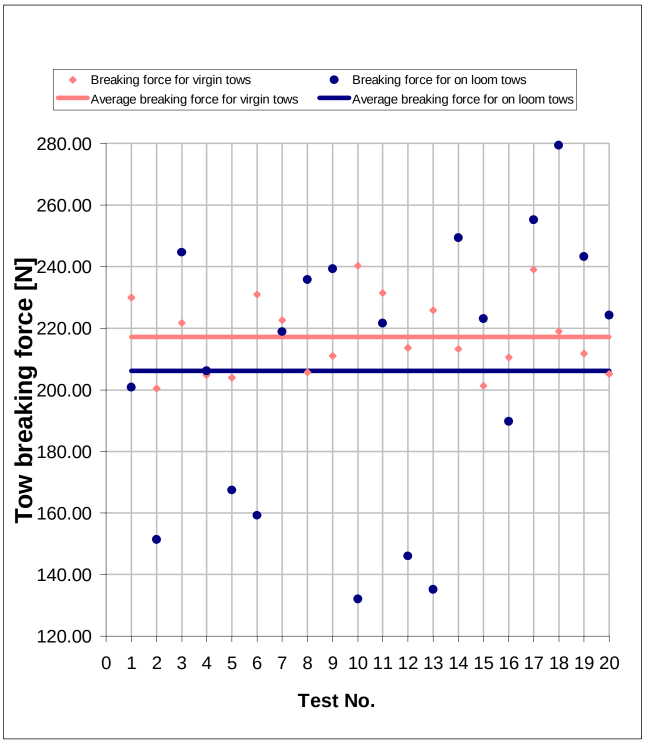

Fig. 3.2: Average values for breaking force of carbon multifilament tows taken from the bobbin and from the loom

In the case of weft tows, process induced degradation is negligible for shuttle weft insertion system.

3.3 Tensile properties of woven reinforcements

3.3.1 Conception and weaving of warp interlock fabrics

As reinforcements, three variants of angle interlock fabrics each having 5 layers, were woven (Appendices 5-7). They were manufactured from 6K carbon multifilament tows; HexTow IM7-GP, supplied by Hexcel, described in the previous section.

These reinforcements were woven on a specially modified loom described in chapter 2. All the basic structural parameters were kept the same for the three variants (number of layers, warp and weft tow densities and linear densities of tows) except for the binding depth *(y)*, which was decreased progressively from the first to the third variant. Structural parameters of these reinforcements are given in Table 3.2.

Table 3.2: Basic parameters of interlock reinforcements

No.	**Parameter**		**1st Variant**	**2nd Variant**	**3rd Variant**
1	Number of layers	Warp	1	2	4
		Weft	5	5	5
2	Tow linear density (Tex)	Warp	223	223	223
		Weft	223	223	223
3	Tow density (tows/cm)	Warp	16	16	16
		Weft	25	25	25
4	Weave structure	Binding depth of the interlocking warp (y)	5	3	2
		Binding step of the interlocking warp (x)	5	3	2
		Warp repeat (r_{wp})	6	8	12
		Weft repeat (r_{wp})	30	20	15

Fig. 3.3 shows WiseTex® based 3D graphical representations of the three reinforcement variants for better elaboration of binder path geometry.

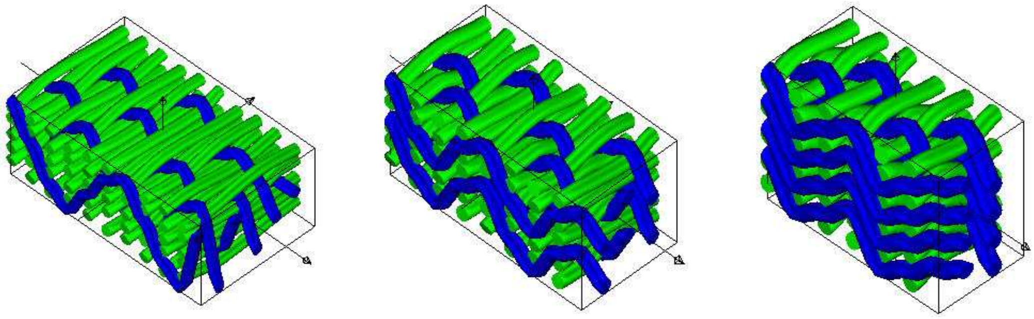

1st is not allowed;

1st variant *2nd variant* *3rd variant*

Fig. 3.3: WiseTex$^{®}$ based geometrical description of warp interlock variants

The first variant is a through the thickness/angle interlock weave, having maximum binding depth of warp binder ($y = 5$). For the second variant, the binding depth was decreased ($y = 3$), and for the last variant minimum binding depth was chosen ($y = 2$) so as to conceive a layer-to-layer/angle interlock. In this way the binding depth was gradually decreased from 1st to the third variant.

In order to have symmetrical angles of interlocking warps for all the three variants, the binding step *(x)* was varied along with the binding depth *(y)* of interlocking warps. For each variant, minimum binding step that allows symmetrical binding while maintaining structural configuration in angle interlock category, was chosen.

For all the three variants reed denting order of 4 ends/dent was chosen so that the warp density remains the same. Warp and weft densities were measured and were found to be 16 tows/cm and 25 tows/cm respectively, for all the variants. Fig. 3.4 shows surface photographs of the three reinforcements.

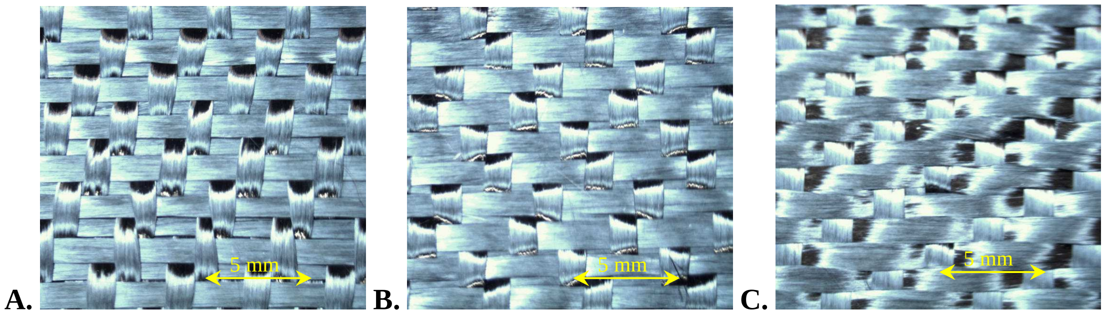

1st variant *2nd variant* *3rd variant*

Fig. 3.4: Carbon interlock reinforcement surface photographs

Crimp percentage was measured by carefully removing tows from dry reinforcement samples according to the norm [1]. 10 reinforcement samples, each 10 cm in length, were used for this purpose. Reinforcement thicknesses were measured using Sodemat$^{®}$ fabric thickness tester. While areal weights *(GSM_{fabric})* and fibre volume fractions *(FVF)* were calculated using mathematical formulae given below

$$GSM_{fabric} = \frac{P \times Tex}{10} \left\{ \frac{100}{100 - c} \right\} \tag{3.1}$$

$$FVF = \left\{ \frac{GSM_{fabric}}{1000 \times \rho \times T} \right\} \times 100 \tag{3.2}$$

Where:

GSM_{fabric} = Areal weight of the fabric reinforcement;

FVF = Fibre volume fraction % age;

P = Total number of tows per cm in the considered direction (warp or weft);

Tex = Tow linear density in the considered direction (warp or weft) in 10^{-6} Kg/m;

c = Tow crimp % age in the considered direction (warp or weft);

ρ = Carbon fibre density in g/cm^3;

T = Thickness of the composite or reinforcement in mm.

These properties are summarized in Table 3.3.

Table 3.3: Structural characteristics and properties of angle interlock dry reinforcements

No.	Characteristic/property	U.M.		1st Variant	2nd Variant	3rd Variant
1	**Crimp (*c*)**	%	Warp	5.1	3.5	1.6
			Weft	0.7	0.7	1.0
2	**Areal weight (*GSM*)**	g/m^2	Warp	374.9	369.3	362.5
			Weft	561.5	561.6	563.1
			Reinforcement	936.4	930.9	925.6
3	**Thickness (*T*)**	mm	Reinforcement	2.3	1.7	2.0
4	**Fibre volume fraction (*FVF*)**	%	Warp	9.4	12.4	10.5
			Weft	13.8	18.6	16.1
			Reinforcement	23.2	31.0	26.6

With the decreasing binding depth from the first to the third variant, the crimp %age in the warp direction as well as the mass of warp tows also decreases in the reinforcement. Weft tow crimp % age is almost the same for the first two variants. The third variant shows a slightly higher degree of undulation in weft tows. This higher crimp in the weft direction for the third variant does not affect the decreasing trend of total areal weight that decreases with the binding depth of warp tows, from the first to the third variant.

Tow waviness (expressed as crimp % age) has an influence on reinforcement thickness (through undulation frequency and amplitude). Compression of weft tows by the pressure applied by undulating warp tow influences compactness of the structure. This particular phenomenon also influences fabric thickness. Other factors which might influence thickness of the reinforcement include number of layers, warp and weft tow densities and linear densities of warp and weft tows etc. In the three reinforcements under discussion, these factors have been kept constant. In view of this it is logical to expect that the thickness would decrease from first to the third variant. But this is not so and the first variant has the highest value of thickness while the second one has the lowest thickness. This implies that the first variant is the least compact and the second one is the most compact structure. The structural geometry i.e., number of warp tows placed in one vertical column and the order of warp binders seems to have played role in determining the thickness of the reinforcements. While referring to Fig. 3.3 it can be noticed that weft tows are placed in columns of 5 tows each while there are 1, 2 and 4 warp tows per column for 1st, 2nd and 3rd variant respectively.

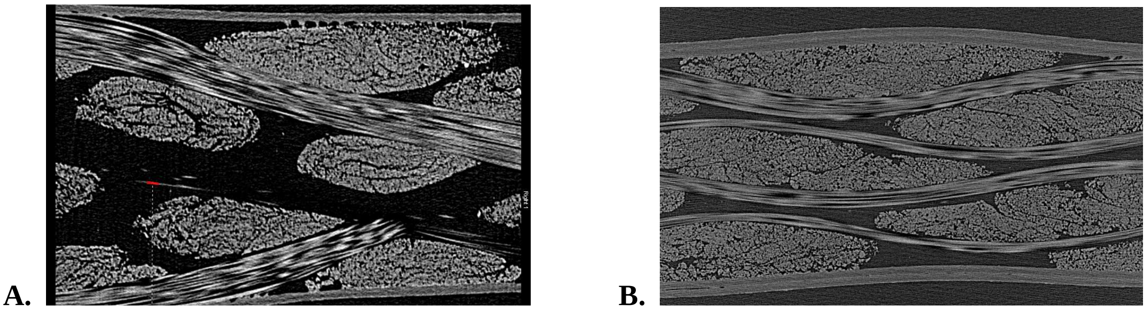

Fig. 3.5: Photomicrographs of longitudinal sections A) 1st Variant B) 3rd Variant

Observations on photomicrographs given in Fig. 3.5 reveal that compression being applied on weft tows in the three variants varies as the pressure being applied by the warp binder changes with the binder path. In the 1st variant the weft tows are least compressed while they are more compressed in the 2nd and 3rd variants (Fig. 3.5-A and B). This phenomenon is responsible for greater thickness and more porosity i.e., greater fibre less area in the 1st variant as can be seen in the longitudinal section in Fig. 3.5-A.

The first two variants were conceived so that two consecutive warp binders in the reinforcement traversed the weft layers in opposite direction. This type of construction can be referred to as jaw type ordering of warp binders as shown in Fig. 3.6-A. Jaw type ordering gave the first two variants structural integrity which implies less mobility for weft tows when the reinforcement is bent or moulded. The 3rd variant was conceived as traditional twill type structure. A typical twill type construction is shown in Fig. 3.6-B. Traditional twill type structures are less compact and allow mobility of weft tows when the reinforcement is bent or made to adopt the form of a mould.

Differences in structural integrity and mobility of weft tows might also explain why the 3rd variant has greater thickness as compared to the 2nd one which is the most compact structure owing to the combined effect of binder path ($y = 3$) and jaw type construction.

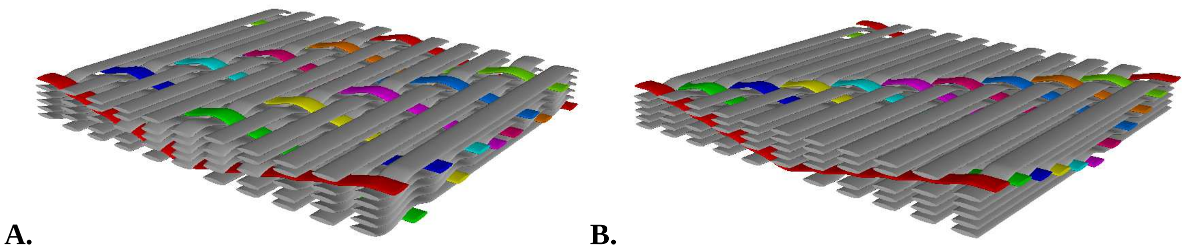

Fig. 3.6: Different warp orders in a through the thickness angle interlock

A) Jaw type construction B) Twill type construction

Reinforcement thickness directly influences the fibre volume fraction in the three variants as all the reinforcements have similar warp and weft tow linear densities (Tex = 10^{-6} Kg/m) as well as equal warp and weft tow densities (tows/cm). The 2nd variant having the least thickness has the greatest fibre volume fraction while the 1st variant having the greatest thickness has the least value of fibre volume fraction.

3.3.2 Tensile Testing of warp interlock fabrics

The tensile properties of dry specimens of woven reinforcements were measured using ZWICK 1474 tester. 5 samples for each variant in warp and weft directions, each having a width of 2.5 cm were tested. An existing norm for tensile tests of unimpregnated glass fabrics; NF ISO 4606 [2] was followed, since a norm does not exist for the tensile strength testing of multilayer carbon reinforcements. According to the norm, for each variant, two rectangular pieces of reinforcements having dimensions 20 x 25 cm, one having warp tows in length direction and the other one having weft tows along its length were chosen. These pieces were pasted with thick card board strips each of which was 5 cm long, at the two ends of the reinforcement pieces, at a distance of 15 cm, using SR 8100 epoxy resin and SD 8824 hardener supplied by Sicomin®. Afterwards reinforcement samples were cut so that 5 samples each for warp and weft directions, having dimensions 4 cm x 25 cm were obtained for each variant. Tows lying at the edges along the length direction were removed carefully by hand, from each sample. In this way parallel tows along the length direction in 2.5 cm width area were obtained. Thus the final dimensions of samples were 2.5 cm x 25 cm with all the length direction tows parallel to each other and lying along the tensile loading direction. Some of these samples are shown in Fig. 3.7.

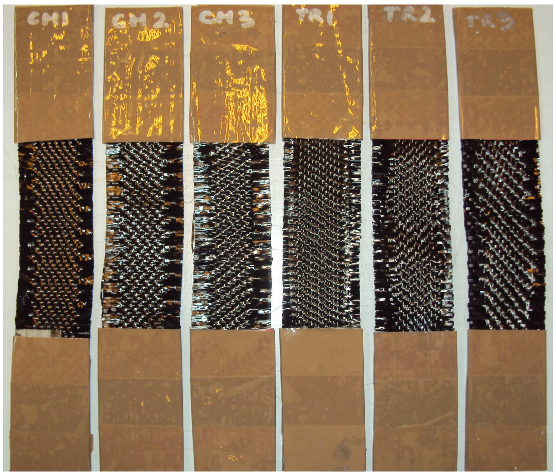

Fig. 3.7: Woven reinforcement samples

These samples were mounted on the tensile strength tester as shown in Fig. 3.8. The length of samples between the jaws was 15 cm so that 5 cm length of a sample at each end having card board strip was gripped by the jaws. This arrangement ensures optimum grip of the samples, prevents their slippage in clamps during tensile loading as well as any damage to the reinforcement due to clamping pressure of jaws. The crosshead speed for the tests was kept at 5 cm/min.

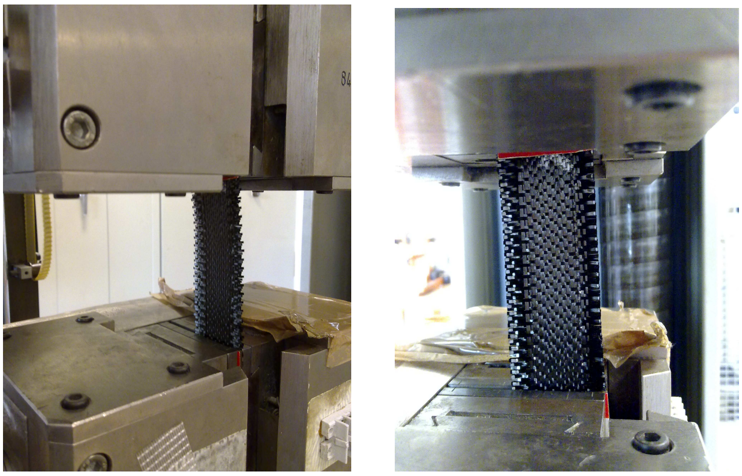

Fig. 3.8: Woven reinforcement samples mounted on ZWICK 1474 Tester

Table 3.4 shows the values of ultimate tensile strength, ultimate strain, maximum force and Young's modulus for dry carbon reinforcements.

Table 3.4: Tensile properties of dry carbon reinforcements

Variant	**Ultimate Tensile Strength** [MPa]		**Ultimate Strain** [%]		**Force max (F_w)** [N]		**Young's Modulus** **[**GPa]	
	Warp	Weft	Warp	Weft	Warp	Weft	Warp	Weft
1st	194.2	412.7	7.2	2.9	11166.6	23731.4	5.1	19.0
2nd	368.0	471.8	8.0	2.7	15638.5	20053.3	6.4	22.4
3rd	345.7	519.0	2.6	3.7	17285.4	25947.8	17.1	19.4

The ultimate tensile strength in the weft direction is generally higher as compared to warp direction in case of all the three variants. This is primarily because of the difference in warp and weft densities (16 tows/cm in warp as against 25 tows/cm for weft). Another reason is the fact that during weft insertion through a shuttle, weft tows do not undergo similar deterioration as warp tows during weaving process.

Comparing the ultimate strength in warp direction for the three variants, we notice that the maximum value is exhibited by the second variant (368 MPa), followed by the third variant that shows 6% loss in strength from 2nd variant. The first variant is the weakest in the warp direction showing 47% loss in strength as compared to the second one. This is directly related to fibre volume fraction in the warp direction for the three variants.

The 3rd variant is the stiffest as well in warp direction as it has the least amount of crimp in warp direction. An inverse relationship exists between crimp and stiffness of the structures. On the other hand stiffness in the weft direction does not vary much and remains almost the same for the three variants, since crimp for the three variants is almost the same.

Fig. 3.9 shows typical stress-strain curves for these variants in warp and weft directions.

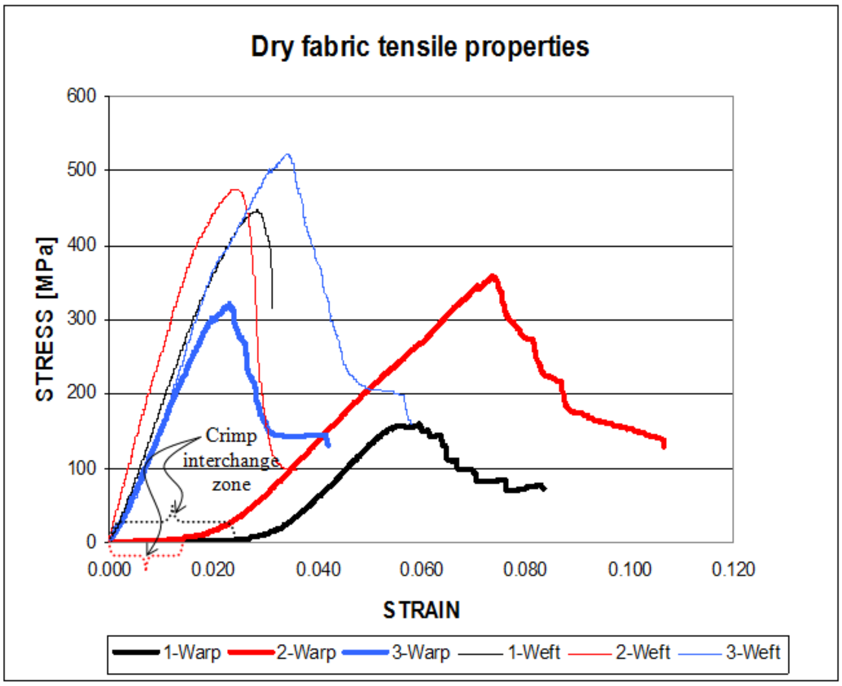

Fig. 3.9: Typical stress strain curves for three variants of dry reinforcements tested in warp and weft directions

Two types of curves can be seen in Fig. 3.9.

J shaped curves; Curves with initial crimp interchange region for tensile loading in warp direction for the 1st and 2nd variant. These curves can be divided in two zones.

- ***Crimp Interchange Zone;*** is the zone in which strain increases rapidly at low stresses. In this zone highly crimped warp tows straighten and lose crimp. Crimp interchange zone is conspicuous in the case of 1st and 2nd variants where warp crimp is high whereas for the 3rd variant, this zone is non existent. The initial crimp interchange region is due to high crimp in warp direction for these variants. Warp crimp interchange region is longer for 1st variant as compared to the second one. It can be deduced from the curves that higher the crimp in warp tows longer is the crimp interchange region in the curve.

- ***Stiff Zone;*** is the zone in which the load bearing straightened warp tows resist the applied load. This zone is characterized by high stiffness and rigidity. The stiff zone is followed by ultimate rupture. All the reinforcements undergo rupture in much the same way. Owing to low elasticity of carbon tows, the filaments give in and break, due to which multifilament tows on the surface of the reinforcement appear to have grown wider, distorted and ruffled.

Curves without crimp interchange region; for tensile loading in weft direction for all the three variants and for 3rd variant warp direction loading. The absence of crimp interchange region is reminiscent of low crimp percentages. These materials have higher moduli of elasticity and are stiffer. Absence of crimp also underscores greater efficiency in the loading direction as the tows resist the applied tensile load as soon as it is applied.

3.4 Carbon interlock based composites

3.4.1. Manufacturing of composite samples

Resin impregnation of reinforcement samples was carried out using VARTM process as shown in Fig. 3.10. The resin used was epoxy resin ‘EPOLAM 5015’.

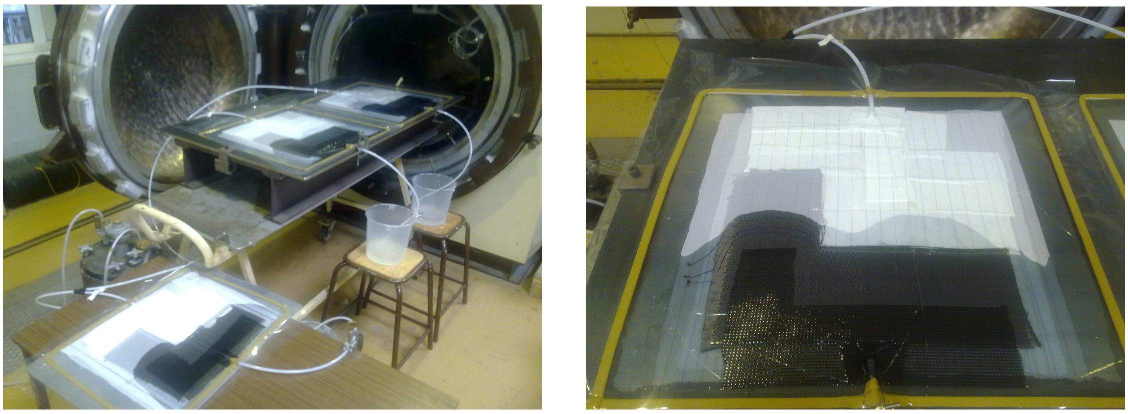

Fig. 3.10: Resin impregnation process of carbon reinforcements using VARTM technology

Fig. 3.11 shows transversal and longitudinal sections of resin infused composites made from the three reinforcement variants.

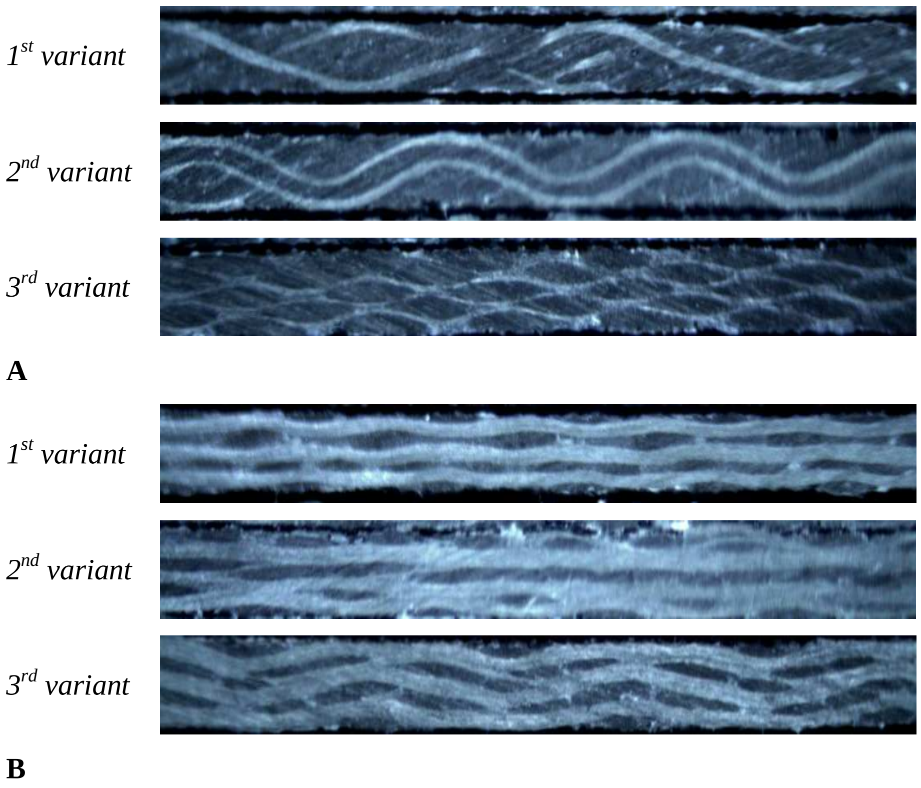

Fig. 3.11: Photomicrographs of cross sectional views

A) Longitudinal sections (warp direction); B) Transversal sections (weft direction)

The areal weights of composites were measured using electronic balance. Thickness of the composite samples were measured on photomicrographs using commercially available software package “Bel Microimage analyzer®”. Standard procedure was adopted for the calculation of fibre volume fractions according to the norm [3].

These values are summarized in table 3.5.

Table 3.5: Properties of carbon/epoxy composites

	U.M.		**1st Variant**	**2nd Variant**	**3rd Variant**
Areal weight of composite (*GSM*)	g/m²		1741.6	1833.1	2088.8
Thickness (*T*)	Mm		1.45	1.50	1.70
Fibre volume fraction (*FVF*)	%	Warp	14.7	13.9	12.2
		Weft	21.6	20.9	18.8
		Total	36.3	34.8	31.0

Resin impregnation using VARTM technology influences each variant differently in warp and weft directions. Application of vacuum during resin infusion causes the thickness of the three reinforcements to decrease. The degree of compression undergone is different for each variant. Fig. 3.12 gives a comparison of this thickness variation in the three variants.

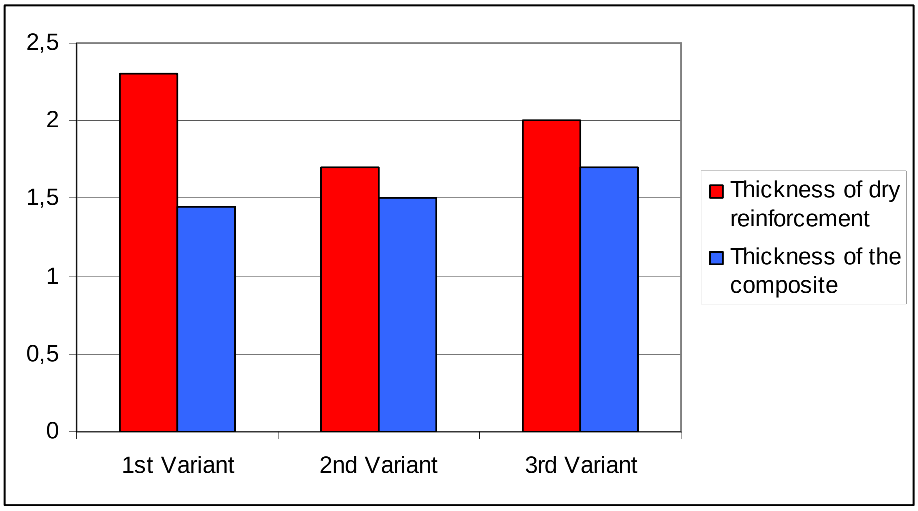

Fig. 3.12: Comparison of reinforcement and composite thickness for the three variants

In order to better appreciate these changes in thickness upon resin impregnation and their different extents in the three variants it is important to keep in mind the basic structural parameters and architectural arrangements of warp and weft tows in the reinforcements. These factors determine the degree and severity of any change that occurs during subsequent material handing and processing. Some of these factors have been discussed in detail in section 1.3.1.

It can be seen from Fig. 3.12 that the 1st variant undergoes greatest change in thickness owing to the existence of fibre less voids (refer to Fig. 3.5-A). The 2nd variant undergoes smallest change in thickness as it is a compact structure with fewer fibre-less voids (refer to Fig. 3.5-B). For the 3rd variant the change in thickness is moderate as it is conjectured to be a moderately compact structure.

3.4.2. Tensile testing of composite samples

The composites prepared from each reinforcement variant were cut into 5 specimens of 2.5 cm x 25 cm in warp and weft directions according to the norm [4]. ZWICK 1474 tester was used for tensile strength tests. The distance between jaws was 15 cm while constant loading rate of 5 mm/min. was maintained for tensile testing.

Table 3.6 shows the values of ultimate tensile strength, ultimate strain, maximum force and Young's modulus for carbon/epoxy composites made from three reinforcement variants.

Table 3.6: Tensile properties of carbon/epoxy composites

Variant	**Ultimate tensile strength** [MPa]		**Ultimate normal strain** [%]		**Force max.** [N]		**Young Modulus** [GPa]	
	Warp	Weft	Warp	Weft	Warp	Weft	Warp	Weft
1st	223.9	386.1	0.6	0.2	8117.6	13995.9	53.2	106.2
2nd	245.6	450.6	1.3	0.3	9210.1	16896.6	36.7	136.6
3rd	299.4	527.6	0.7	0.8	12722.6	22424.0	53.0	104.6

Fig. 3.13 shows typical stress-strain curves for three composite variants in warp and weft directions.

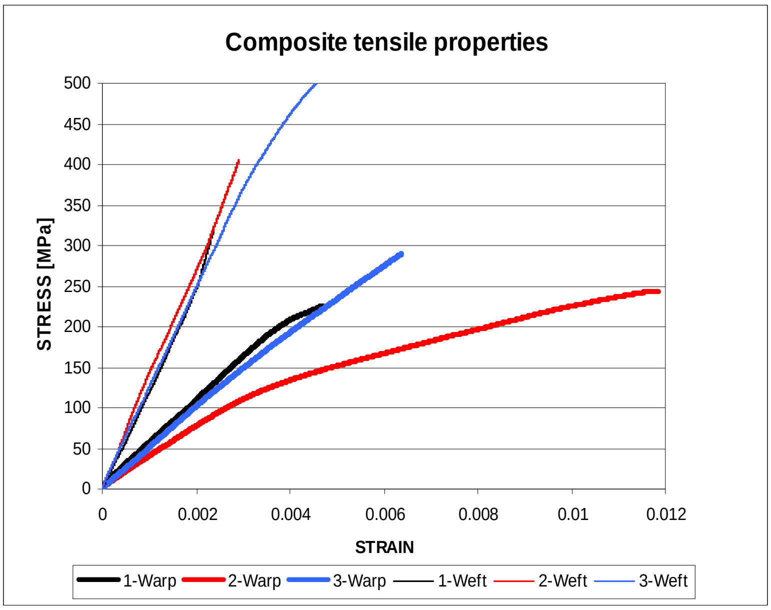

Fig. 3.13: Typical stress strain curves for three variants of carbon/epoxy composites tested in warp and weft directions

Comparing the ultimate tensile strength in warp direction for the three variants studied, we notice that the maximum value is exhibited by the 3rd variant (299.4 MPa), followed by the 2nd (245.6 MPa) and 1st (223.9 MPa). An indirect relationship exists between the tensile strength and crimp of warp tows in the said composite structures. If the fibre volume fractions for the three composite variants be compared it seems that the role played by crimp is relatively more important than the role of fibre volume fraction.

As was the case with dry reinforcements, the tensile strength and stiffness of each variant in the weft direction is significantly higher than in warp direction owing to the differences in fibre volume fraction in warp and weft directions.

The fibre volume fractions for the three variants do not vary much in the weft direction. Moreover in all the three reinforcements weft crimp is very low. In spite of that the ultimate tensile strength of the composites in the weft direction increases gradually from 1st to the 3rd variant.

It can be hypothesized that this is due, in large part, to warp tow path. The binder tow is highly crimped in the 1st variant, which causes the collimation or stacking of weft tows under the binder, giving rise to inhomogeneous distribution of fibre content in the weft direction and creation of fibre less voids which are filled in by the resin. The phenomenon of collimation of weft tows reduces with the reduction in warp tow crimp. Moreover in a through the thickness structure, highly crimped warp causes local compression and kinks on the weft tows. These kinks might be responsible for damage initiation in weft tows during tensile loading. In the 3rd variant which is a layer-to-layer/angle interlock, the warp tows are not severely crimped thus compression applied on the weft tows is not as marked as in the case of 1st variant. Lower crimp of warp binder also translates into lower collimation and local deformations of weft tows. That is why the mechanical properties in the weft direction improve gradually from the 1st to the 3rd variant as the warp binder crimp reduces gradually.

A comparison of all the key mechanical properties of reinforcements and their composites are given in Fig. 3.14

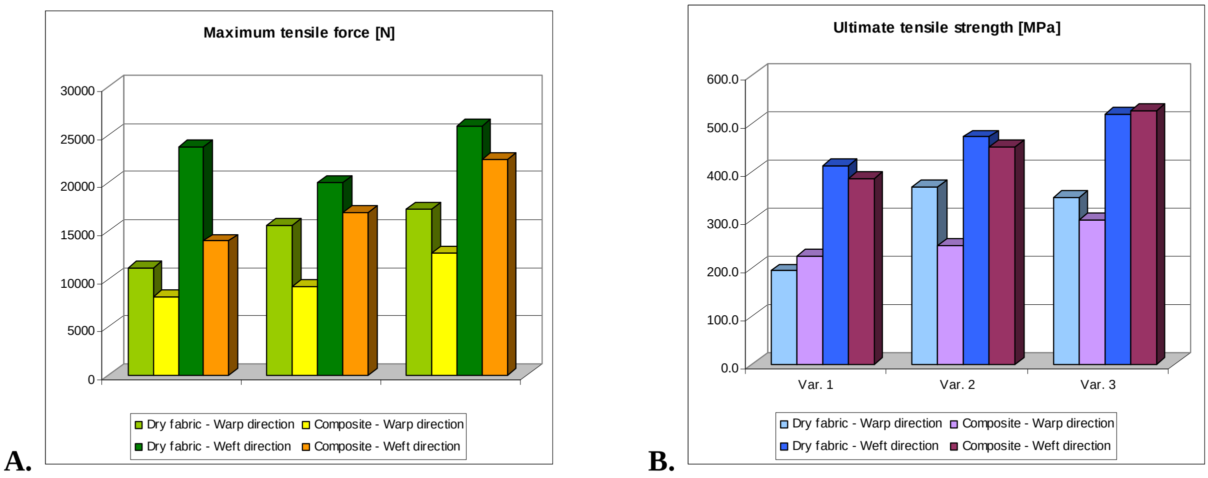

Fig. 3.14: Comparison of dry reinforcement and composite tensile properties in warp and weft directions

3.5 *Strength Transfer from tow to textile composites*

In order to evaluate the transfer of mechanical properties from tow to woven interlock reinforcement/textile composite, a coefficient called 'strength transfer coefficient' (*C)* has been proposed. It is defined as the ratio between 'theoretical' tenacity of individual tows inside the reinforcement (Tf_2) and the initial tenacity of tow i.e., the tenacity before weaving (Tf_1). This 'theoretical' tenacity is calculated by dividing reinforcement/composite sample tenacity in the applied load direction by the number of tows inside woven sample. The tenacity so calculated has been named "theoretical" because it is not the real tenacity of the individual tows extracted from the reinforcement. It can only be real if tows are parallel and without interlacements.

In a woven structure, the 'strength transfer coefficient' expresses the influence of the reinforcement architectural parameters on tensile properties of the reinforcement.

The strength transfer coefficient is given mathematically as:

$$C = \frac{Tf_2}{Tf_1} \tag{3.3}$$

Where:

Tf_1 = Tow tenacity before its integration in woven reinforcement and is expressed in N/Tex;

Tf_2 = Theoretical tow tenacity after its integration in woven reinforcement, including the influence of weave structure and is expressed in N/Tex.

As used in literature, tenacity denotes the strength of a multifilament tow of given size and it is generally synonymous to ultimate tensile strength. The mathematical relation for 'initial tow tenacity' 'Tf_1' is:

$$Tf_1 = \frac{F_{bkg(t)}}{Tex} \tag{3.4}$$

Where:

$F_{bkg(t)}$ = Average tensile strength of tow (N);

Tex = Linear density of tow (g/1000m)

In case of a woven reinforcement, 'theoretical tow tenacity' 'Tf_2' can be calculated as

$$Tf_2 = \frac{F_{bkg(f)}}{P \times b \times Tex} \tag{3.5}$$

Where:

$F_{bkg(f)}$ = average tensile strength of the woven fabric reinforcement (N);

P = tow density in the direction of applied load (tows/cm);

b = width of the woven reinforcement (cm);

Tex = linear density of tows (g/1000m)

For a composite material made by impregnating a woven reinforcement in a polymeric resin, following relation stands for 'Tf_2'

$$Tf_2 = \frac{F_{bkg(c)}}{P \times b \times Tex} \tag{3.6}$$

Where

$F_{bkg(c)}$ = Average tensile strength of the composite (N)

All the other symbols have the same significance as for relation 3.5

Replacing relations (3.4) and (3.5) for Tf_1 and Tf_2 in relation (3.3), we obtain the following formula for 'strength transfer coefficient' from tow to reinforcement ($C_{t\text{-}f}$):

$$C_{t-f} = \frac{F_{bkg(f)}}{P \times b \times F_{bkg(t)}} \tag{3.7}$$

An analogous formula for 'strength transfer coefficient' from tow to composite ($C_{t\text{-}c}$) can be given as

$$C_{t-c} = \frac{F_{bkg(c)}}{P \times b \times F_{bkg(t)}} \tag{3.8}$$

For the three variants under discussion, 'strength transfer coefficient' has been used to calculate the influence of weave structure on tensile properties of the reinforcement and the composite. These values are reported in Table 3.7.

Table 3.7: Strength transfer coefficient

Variant	**Strength transfer coefficient from tow to dry reinforcement C_{t-f}**		**Strength transfer coefficient from tow to composite C_{t-c}**		**Difference C_{t-c} - C_{t-f}**	
	Warp Direction	Weft direction	Warp Direction	Weft direction	Warp direction	Weft Direction
1st	1.35	1.75	0.98	1.03	-0.37	-0.89
2nd	1.90	1.48	1.12	1.41	-0.78	-0.44
3rd	2.10	1.91	1.54	1.65	-0.55	-0.73

As mentioned earlier, in the case of strength transfer coefficient in the weft direction, average breaking strength value for the samples taken from virgin bobbins ($F_{bkg(t)}$ = 217.11 N) was used to calculate initial weft tow tenacity (Tf_1 = 1.08 N/Tex) as weft tows do not undergo prior to insertion damage and degradation on shuttle looms.

Fig. 3.15 shows variation of strength transfer coefficient from tow to textile composite in warp and weft directions for the three woven architectures.

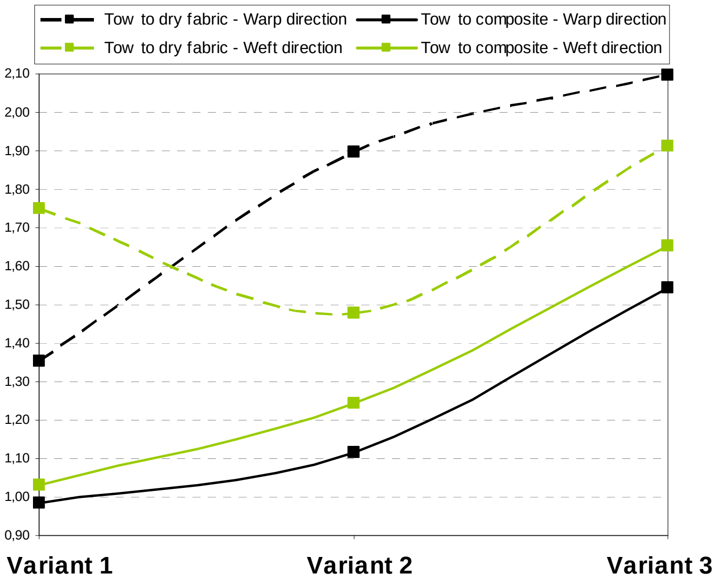

Fig. 3.15: Variation of strength transfer coefficient with reinforcement architecture

Strength transfer coefficient value when exceeds unity, it implies gain in strength due to the integration in woven reinforcement. On the contrary values inferior to unity imply that the integration of tow inside the woven reinforcement has negatively influenced the strength of a single tow, and it has decreased after its integration in the reinforcement.

In the case of composites made from the first variant, warp strength transfer coefficient is less than unity (0.98) which signifies a net loss of strength in warp tows. This can be explained in terms of warp tow crimp geometry. Crimp amplitude is particularly high in case of the first variant and this is the cause of strength loss in warp tows as high crimp percentage reduces the efficiency of the composite in the loading direction. The strength transfer coefficient increases progressively as crimp amplitude in warp decreases from first to the third variant. For the second and third variant the warp strength transfer coefficient is greater than unity which implies a net gain of strength, after the integration of carbon tows in the reinforcement. Strength transfer coefficient is significantly high for the third variant which has layer to layer binding (1.54)

Strength transfer coefficients vary in much the same way in the weft direction as in the warp direction for the three variants (Fig. 3.15). But the values are higher than those for the warp direction. This is because of lower crimp and much higher fibre volume fractions in the weft direction as compared to the warp direction, for all the three variants. Strength transfer coefficients in the weft direction increase gradually from 1st to the 3rd variant, as with the decreasing crimp amplitude in the warp direction the collimation and compression of weft tows gradually decreases.

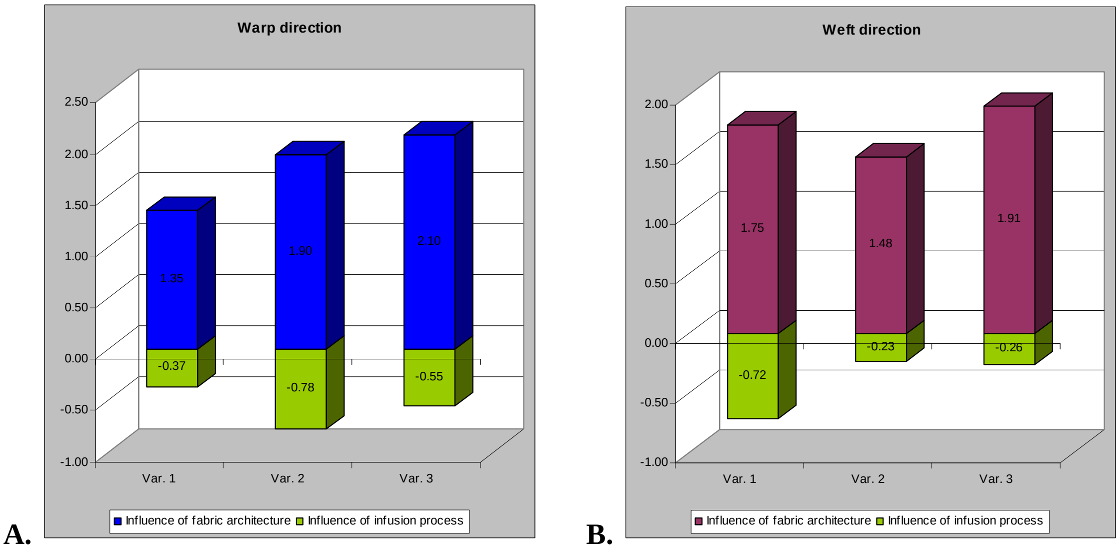

Fig. 3.16: Strength transfer gain/loss from carbon tow to composite

A) In warp direction, B) In weft direction

Fig. 3.16 shows the influence of resin impregnation on the strength transfer coefficients. Strength transfer coefficients are generally higher for dry reinforcements and are reduced considerably after resin impregnation.

This loss in strength should be explained in terms of geometrical and dimensional changes occurring in the woven reinforcement due to VARTM. As mentioned earlier in order to have an idea about these changes and gauge their influence upon composite mechanical properties, it is useful to keep in mind original reinforcement architectural characteristics. These particular architectural characteristics determine the extent to which dimensions are changed when VARTM is carried out.

The scale given in Table 3.8 will be followed for the attribution of particular nomenclature describing loss of strength as reinforcement is impregnated to form a composite. This scale is by no means a standard but only serves to better organise the discussion on influence of resin impregnation on the reinforcement.

Table 3.8: Attribution of nomenclature for the loss of strength as a reinforcement is impregnated into a composite

Range of difference $C_{t\text{-}c} - C_{t\text{-}f}$	**Designation**
0 ~ -0.25	Low
-0.25 ~ -0.50	Moderate
-0.50 ~ -0.75	Considerable
-0.75 ~ -1.00	High

For the 1st variant the loss in strength in the weft direction may be termed as high ($C_{t\text{-}c} - C_{t\text{-}f} = -0.89$), whereas it is only moderate in the warp direction ($C_{t\text{-}c} - C_{t\text{-}f} = -0.37$). As discussed earlier this structure undergoes greatest change in thickness upon resin impregnation (Fig. 3.12). The loss in strength in weft direction may be attributed to severe compression of the structure and resultant pressure of through the thickness warp binder on collimated weft tows. Collimation might also have resulted in resin rich pockets around the bundles (collimations) of weft tows in the structure which serve as damage initiation zones when tensile loading is applied.

On the contrary in the 2nd variant, loss in warp direction is considerably high ($C_{t\text{-}c} - C_{t\text{-}f} = -0.78$) whereas in the weft direction it is moderate ($C_{t\text{-}c} - C_{t\text{-}f} = -0.44$). Since this structure has undergone lowest change in thickness upon resin impregnation (Fig. 3.12), it can be conjectured that phenomena contributing to strength loss are different from the 1st variant as a small change in thickness imply fewer alterations in geometry upon impregnation. Compression due to bending pressure applied by binder warp tows upon weft tows should be a minor factor due to lower binding depth ($y = 3$), near absence of collimation of weft tows (Fig. 3.5-B), compactness of structure and insignificant loss in thickness upon resin impregnation (Fig. 3.12). Undulating warp tows however become fragile upon resin impregnation and zones where they enter and come out of the reinforcement might become zones of damage initiation. Considerably high loss in strength in warp direction seems to have caused mostly by this factor.

It was observed that the change in thickness for the 3rd variant was moderate (Fig. 3.12). Moderate changes in geometry upon impregnation translate into moderate loss of strength in both the warp $(C_{t\text{-}c} - C_{t\text{-}f} = -0.55)$ and weft $(C_{t\text{-}c} - C_{t\text{-}f} = -0.73)$ directions.

3.6 Conclusion

3D interlock woven reinforcement variants have been studied for evaluation of the changes that a carbon tow undergoes after weaving in order to understand the deformation mechanisms and transfer of strength from a multifilament tow to the composite.

Average breaking strength of warp tows is reduced due to abrasion and friction during weaving process. In order to quantify this reduction in strength, tensile strength of samples obtained from loom and from virgin bobbins was compared. It was found that this reduction in strength due to damages incurred during weaving was much lower than that reported in previous researches [5, 6]. In order to quantify the influence of binder path upon the strength transfer from a tow to an interlock reinforcement and finally to a composite, three closely related variants were conceived and woven on a modified weaving loom. It was found that the warp binder path influences not only properties in the warp direction, as is traditionally believed but in the weft direction as well. Arrangement of weft tows i.e., their reorganisation and resultant fibre-less voids also depend on the warp binder path. An additional weaving parameter which can influence the compactness of the structure is warp ordering in a through the thickness interlock structure. For similar weave design and fibre volume fractions in warp and weft, jaw type constructions were found to be more compact, stable and had greater bending rigidity as against twill type constructions. It means that jaw type constructions are easier to handle as they are less fragile. This is an important property during manual handling and lay-up. But owing to higher bending rigidity these structures are less ‘mouldable’ than twill type structures which readily adopt the form of the mould.

It was found that the dynamics of strength transfer for 3D interlock reinforcements woven using carbon multifilament tows are rather different from 2D traditional fabrics. The binding depth of interlocking warp plays an important role in determining the efficiency of the reinforcement in the loading direction. Increasing binding depth i.e. crimp amplitude of interlocking warp tows reduces the breaking strength of the composite in the warp direction. A mathematical index; strength transfer coefficient from tow to textile composite has been defined and calculated for woven reinforcements and composites, which enables us to determine the strength transfer from tows to the final structure. It is evident from the study presented here that the crimp amplitude plays an important role in determining the value of this coefficient. For through the thickness interlock reinforcement having high crimp amplitude in warp, a net loss of strength from tow to composite was observed as the strength transfer coefficient is less than unity. By decreasing crimp amplitude of interlocking warp tows, the strength transfer coefficient increases. For layer to layer geometries the strength transfer coefficient becomes greater than unity which signifies a net gain in strength as the tow is integrated in the 3D reinforcement. The binder path also influences properties in the weft direction. This is because of the fact that changing binder path implies changes in warp and weft interactions at interlacement points. Warp binders apply pressure on weft tows and they can cause them to stack together hence influencing properties in weft direction through reorganisation of weft and creation of fibre-less voids.

The strength transfer coefficients for dry reinforcements and composites have been compared in respective directions (warp and weft) for all the three variants. In all the cases loss in strength has been registered as reinforcement is impregnated to form a composite. However the extent of this loss is different and varied. This difference has been correlated to the particular reinforcement geometry and changes it has undergone upon resin impregnation.

It can be concluded that the evolution of mechanical properties from a tow to the reinforcement and finally to its composite depends on particular structural properties and response of the structure to different processing parameters.

3.7 *References*

[1] "ASTM D3883 - 04 Standard Test Method for yarn crimp and yarn take-take up in woven fabrics," West Conshohocken, PA, USA: ASTM, 2008.

[2] "NF ISO 4606-Verre textile-Tissus-Détermination de la force de rupture en traction et de l'allongement à la rupture par la méthode de la bande," AFNOR, 1996.

[3] "ASTM D3171 - 09 Standard Test Methods for Constituent Content of Composite Materials," West Conshohocken, PA, USA: ASTM, 2010.

[4] "NF EN ISO 527-4 Plastiques - Détermination des propriétés en traction," in Partie 4 : Conditions d´essai pour les composites plastiques renforcés de fibres isotropes et orthotropes: CEN, 1997.

[5] L. Lee, S. Rudov-Clark, A. P. Mouritz, M. K. Bannister, and I. Herszberg, "Effect of weaving damage on the tensile properties of three-dimensional woven composites," Composite Structures, vol. 57, pp. 405-413, 2002.

[6] S. Rudov-Clark, A. P. Mouritz, L. Lee, and M. K. Bannister, "Fibre damage in the manufacture of advanced three-dimensional woven composites," Composites Part A: Applied Science and Manufacturing, vol. 34, pp. 963-970, 2003.

PART 2:

REAL TIME IN SITU STRUCTURAL HEALTH MONITORING (SHM) OF TEXTILE COMPOSITES – NEW SENSING SYSTEM

Chapter 4

State Of The Art

4.1. Existing Sensing Systems in Textiles and Composites

Recently, high performance composites reinforced with 3D structures have found wide applications in various industrial areas such as aerospace, aircraft, automobile, civil engineering etc. Good quality and reliability are basic requirements for advanced composite structures which are often used under harsh environments. To improve their performance, the cure monitoring of technological process is clearly necessary. At the same time, in service non destructive evaluation (NDE) is also needed to keep these structures operating safely and reliably.

NDE techniques have been developed in the past including ultrasonic scanning, acoustic emission (AE), shearography, stimulated infrared thermography (SIT), Fibre Brag Grating (FBG) sensors and vibration testing etc. [1]. The challenge today is to develop new low cost techniques which can perform online structural health assessment starting from the manufacture of composite structure to the real service of these structures in the field. Moreover, the NDE techniques have to be integrated in the design phase and sensors should be inserted during the fabrication of composites, in order to improve accuracy and reduce their costs. The classical NDE techniques are difficult to adapt. They are not well suited for on line structural health monitoring, because of difficulties in making in situ implementation. Moreover, it is important to understand the stress strain conditions during damage infliction. The record of stress-strain history prior to damage infliction also helps in understanding the cause of irreversible damage [2].

One possible solution is to use intelligent textile materials and structures which provide real possibility for on line and in situ monitoring of structural integrity. These materials not only perform traditional structural material’s functions, but also have actuating, sensing and microprocessing capabilities. Such intelligent materials are made by coating or treating textile yarns, filaments or fabrics with nanoparticles or conductive & semi conductive polymers giving them special properties [3-8].

A review of piezoresistive sensing approaches already being applied to measure strain in fabrics/composites shows that several diverse sensing mechanisms exist. These approaches may be categorized on the basis of manufacturing technology and materials as follows:

- Self-sensing in carbon composites [2,9-18];
- Semi conductive coatings [3, 19-24];
- Nanotube networks [25-33];

None of these have gained universal acceptance either as standard in structural health monitoring of composites or for the fabrication of intelligent textiles. In the following a review of these techniques and their potential for structural health monitoring of composites is discussed in detail.

4.1.1. Self-sensing in carbon composites

Electrical techniques have long been established as a non-invasive way to monitor damage in carbon fibre-reinforced composites under static and dynamic loading conditions as carbon fibre reinforced composites offer a unique possibility of using carbon tows as sensing network because of their conductivity.

In the case of CFRP (Carbon fibre reinforced polymers) or hybrid glass/carbon FRP it is possible to use the material itself or a part of this material as sensor since carbon is electrically conductive ($1.5 \text{ X } 10^{-5}$ Ω-m) embedded in an insulating matrix (10^{13}-10^{15} Ω-m). The measurement of global electrical resistance appears to be a valuable technique that can be used to measure the fibre fracture and delamination process associated with the modification of resistive tracks in the laminates.

Dielectric analysis [18] for cure monitoring of thermoset resins and measurement of complex impedance of CFRP cross-ply [17] during tensile loading for damage detection such as fibre failure or matrix cracking are some of the examples which demonstrate the usage of this technique in research.

Abry et al. [13, 14] have worked extensively on the detection of in-situ damage in CFRP by use of AC and DC electrical property measurements. Monotonic tests under post buckling bending conditions were performed on cross ply [0/90] and [90/0] carbon/epoxy laminates. The monitoring of electrical resistance and capacitance changes, linked to the modifications of conduction paths in the composites and occurrence of voids during loading allowed the detection of damage growth (Fig. 4.1-A & B and Fig. 4.2-A & B).

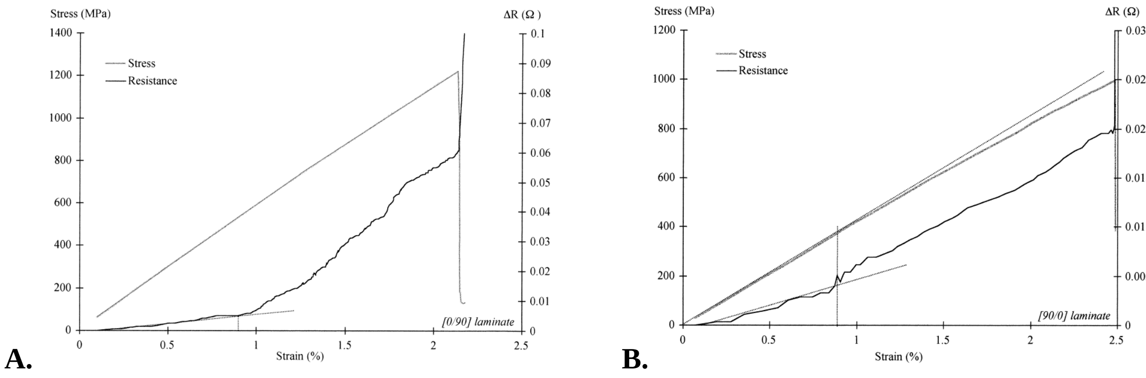

Fig. 4.1: (A) Changes in stress and electrical resistance as a function of the applied strain during a flexural monotonic loading for [0/90] composite. (B) Changes in stress and electrical resistance as a function of the applied strain during a flexural monotonic loading for [90/0] composite [13, 14].

It was found that DC electrical conduction can be used to detect fibre failure, but AC measurements are more suitable for monitoring matrix cracks (delamination, fibre /matrix de-bonding or transverse cracks). The combined use of these two methods will enable the detection as well as the qualitative identification of various damage mechanisms. Therefore measurement of the electrical resistance (DC experiments) and AC properties (resistance and capacitance) provide means to monitor the in-situ evolution of damage nucleation and growth in cross ply CFRP laminates particularly for internal damage. A critical change of resistance or capacitance variation can be defined as the warning for health monitoring during monotonic or cyclic loading. It is important to note the complementary aspects of these AC and DC measurements.

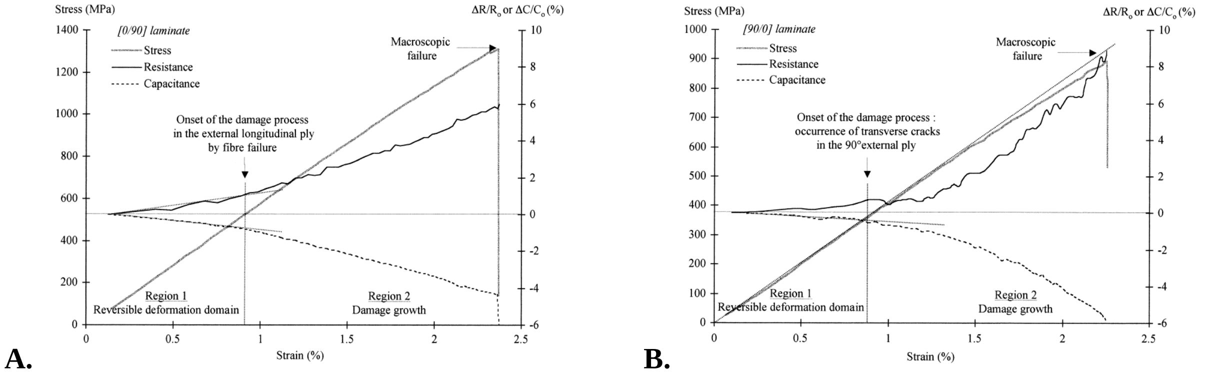

Fig. 4.2: (A) Changes in stress and AC measurements as a function of applied strain during flexural monotonic loading for [0/90] composite (B) Changes in stress and AC measurements as a function of applied strain during flexural monotonic loading for [90/0] composite [13, 14].

However such an approach can only be used for conductive fibre based composites and can not be applied to composites with non-conductive fibres such as glass and aramid fibres.

It is important to understand and interpret the failure mechanisms of the composite beforehand for later use of the technique for condition monitoring**.** Any anomaly in the failure mechanism can threaten the sensing mechanism's validity and efficacy.

A network of electrodes must be installed throughout the structure in order to extract the local information. These electrodes must be robust enough to withstand the environmental stresses.

Even in carbon fibres composites, some matrix-dominated damage may not be detected by the fibre network. Thus, more versatile technique is needed for in situ damage sensing of fibre-reinforced composites.

4.1.2. Semi conductive coatings

Concerning semi conductive coatings, they have mostly been used for intelligent textiles and flexible electronic equipment, to date, such as silicon flexible skins with regular textiles [34, 35], flexible transistors [36-40] and other smart textile applications to detect physiological condition of the wearer [4-7, 19, 21]. Such coatings on fabric, yarn or fibres are easy to realize and can be made wash resistant.

Huang et al. [4, 5] have shown the feasibility of using yarn based sensors for tracking respiratory signals. Resistance changes of these sensors were evaluated under variable loading. The wrapping process was adopted to fabricate the yarn-based sensors as shown in Fig. 4.6. Three different kinds of fibres, which included piezo-resistive, elastic and polyester fibres, were used to assemble the yarn. The piezo-resistive fibre chosen was commercially available carbon-coated fibre (CCF) RESISTAT F901 (resistivity 3×10^5 Ω/cm). The fabrication process started with the integration of polyester fibres with elastic fibres into a composite core yarn at first. The length of the elastic fibre was stretched three times in the process. Then the CCF was wrapped on the core yarn by using the single and double wrapping approaches as shown in Fig. 4.3.

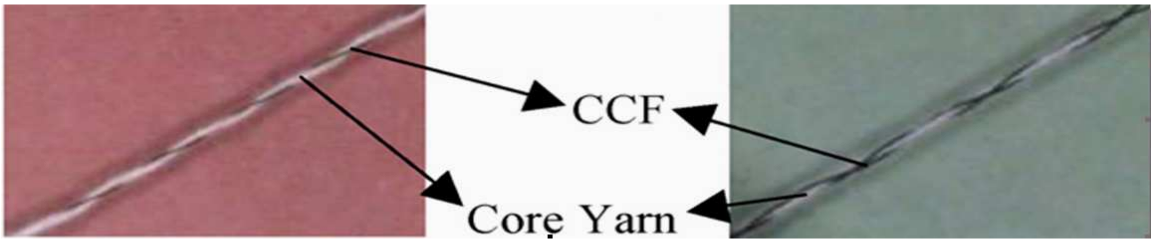

Fig. 4.3: Structure of yarn-based sensors:
single wrapping (on left) and double wrapping (on right) [4]

It is shown that the relationship between resistance and strain of the single CCF fibre can be described as a linear function (Fig. 4.4). Due to the symmetric structure, the double wrapping yarn provides higher linearity in the resistance curve and thus can be served as a better sensing element (Fig. 4.5). It was also found that the sensitivity of double wrapping yarn is lower because the lateral force might compress the core yarn such that the shape of the core yarn is changed to alleviate the deformation of the CCFs.

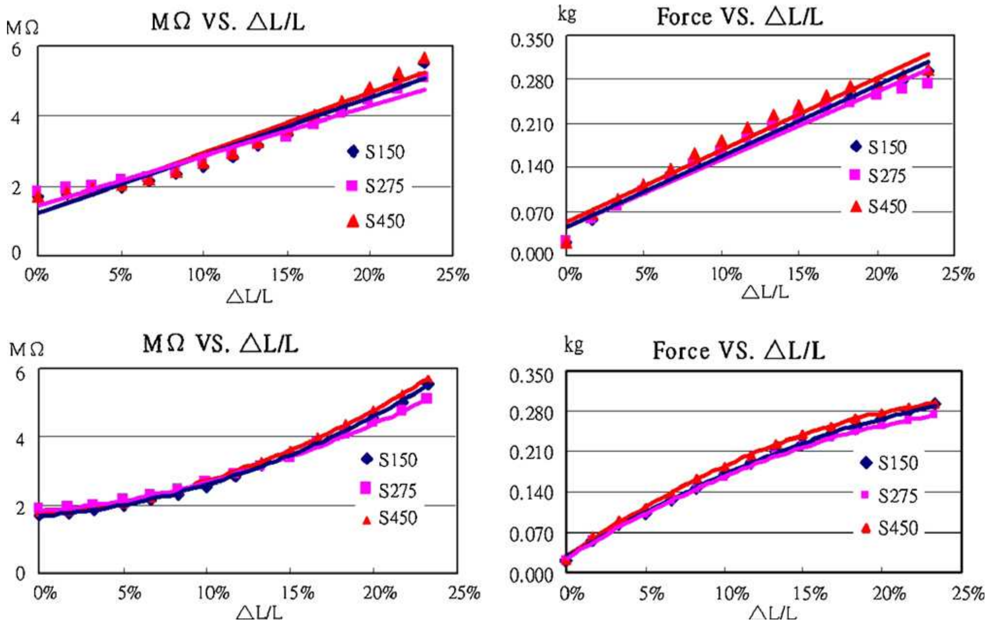

Fig. 4.4: The elongation curves of single wrapping yarns [4]

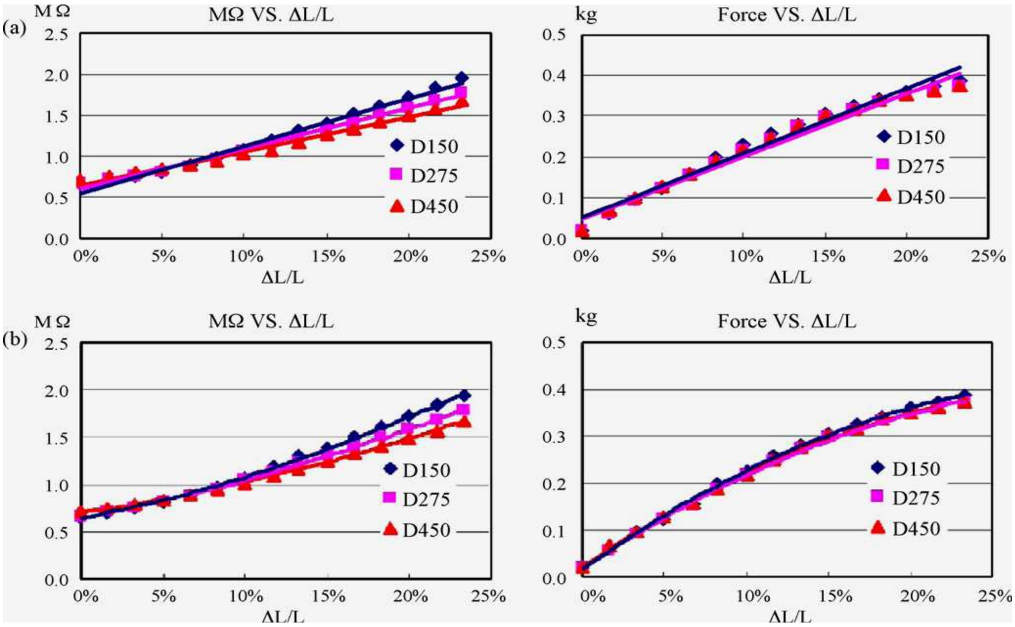

Fig. 4.5: The elongation curves of double wrapping yarns [4]

Various researchers have used piezoresistive coatings on textile surfaces to be used as sensing mechanisms [41-48]. The approach is to coat a thin layer of piezo-resistive material, such as polypyrrole or a mixture of rubbers and carbons, on conventional fabrics to form fabric-based sensors (Fig. 4.6). The function of such sensors is similar to that of flexible strain gauges which can measure strains when they are subjected to tensile stress.

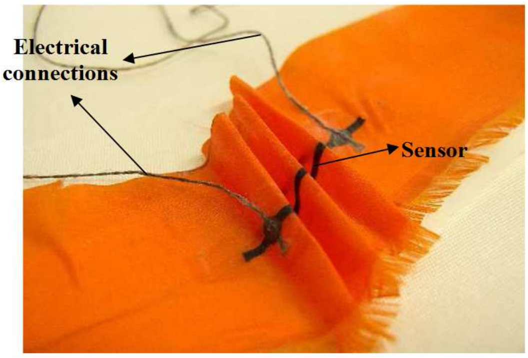

Figure 4.6: Nylon fabric coated with piezoresistive coating to serve as a sensor, with electrical connections [19]

In their annual research report, Patra et al. [49] have reported about the development of methods to inkjet print highly conductive polymer ink which is a suspension of Poly (3, 4 ethylenedioxythiophene) - poly (4-styrenesulfonate) (PEDOT-PSS)), onto fabric for use as sensors. They have monitored the response of these printed sensors to stress, fabric orientation and structure and to environmental variables such as humidity and temperature. In Fig. 4.7 an increase in the resistance of the PEDOT printed fabric with strain is shown. The gauge factor is positive and is about 5. This value is quite similar to those of metals.

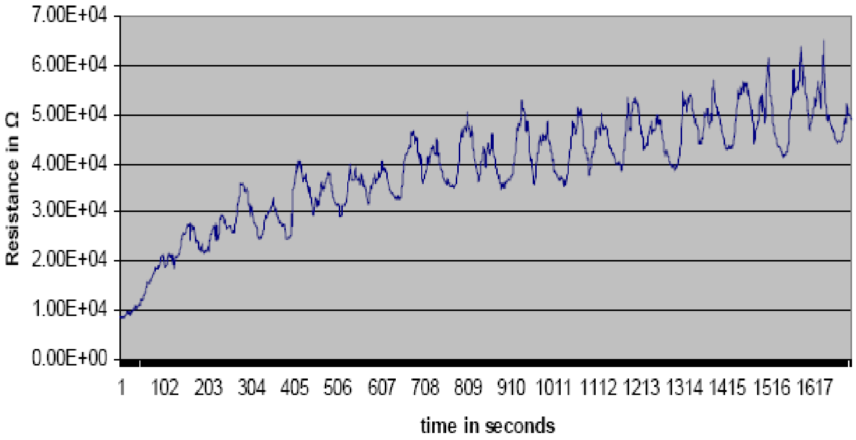

Figure 4.7: Variation in Resistance of PEDOT-PSS coated fabrics vs time within 25 repeated cycles of strain and relaxation [49]

One interesting application in the field of composites consists of coating of glass fibre tows with carbon powder to locally modify electrical properties for damage sensing [12].

It can be deduced that applications of these piezoresistive coatings are quite varied. Their peculiar properties make them an interesting choice for damage sensing. These coating techniques need to be further developed and exploited as percolation networks for sensing in structural health monitoring applications of composites.

4.1.3. Nanotube Networks

In their review, Fiedler et al. [8] proposed the use of conductive networks of nanotubes for both strain and damage sensing. Nanotubes have been investigated in detail for use as sensing mechanisms, both for smart textile applications and for structural health monitoring of composites.

Since the nanotube electronic property is a strong function of its atomic structure, mechanical deformations [50-55] or chemical doping can induce strong changes in conductance. Such changes can be easily detected by electron current signals, and these properties make CNTs extremely small sensors sensitive to their chemical and mechanical environments.

In the area of piezoresistive nanotube strain sensors, Darhap et al. [3] investigated the use of thin films of randomly oriented carbon nanotubes and measured resistance changes using a four-point-probe. They noted a linear change in the sheet resistance when subjected to tension or compression.

Zhang et al. [25] reported that multi-walled carbon nanotube-reinforced composites can be utilized as strain sensors. The sensitivity of their nano composite strain sensor was reported to be 3.5 times higher than a traditional strain gage.

They suggested that the instantaneous change in resistance with strain can be utilized for self-diagnostics and real-time health monitoring. This piezoresistive behaviour has also been demonstrated by Kang et al. [30, 54] who used single-walled nanotube polymer composite films for strain sensing and examined their static and dynamic behaviour. By extending the sensor to a long strip they created a ‘‘neuron sensor”. They have suggested that a neural system the form of a grid could be attached to the surface of a structure to form a sensor network, enabling structural health monitoring. The common feature among many reports of strain or vapour sensing is that a change in volume due to chemical, thermal or mechanical loading results directly in resistance changes.

Thostenson and Chou [27] established that the change in the size of reinforcements, from conventional micron sized fibre reinforcement to carbon nanotubes with nanometer-level diameters, enables unique opportunity for the creation of multi-functional in situ sensing capability. This implies a multi scale combination of different reinforcements, as carbon nanotubes can penetrate matrix-rich areas between fibres in individual bundles as well as between adjacent plies and can achieve a percolating nerve-like network of sensors throughout the arrays of fibres in a composite, as illustrated in Fig. 4.8.

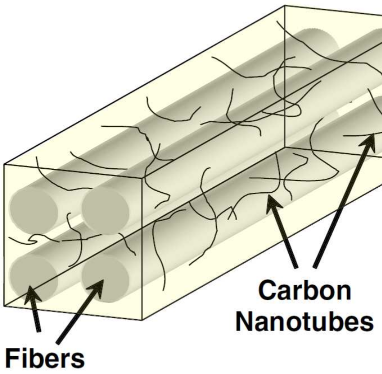

Fig. 4.8: Three-dimensional model showing the penetration of nanotubes throughout a fibre array due to their relative scale. [27]

A percolating network was formed by first dispersing carbon nanotubes in an epoxy polymer matrix using calendaring approach and then infusing it throughout a fibre preform. Authors have demonstrated that these percolating networks of carbon nanotubes are remarkably sensitive to initial stages of matrix-dominated failure and can detect in situ damage. Through key experiments designed to promote different failure modes they have demonstrated that it is feasible to identify the nature and progression of damage (Fig. 4.9).

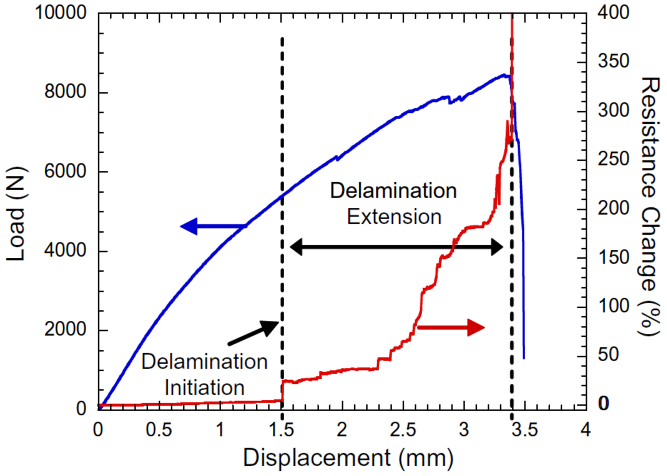

Fig. 4.9: Load/displacement and resistance response of a five-ply unidirectional composite with the centre ply cut to initiate delamination [27]

Fig. 4.9 shows result from a five-ply unidirectional composite where the centre ply was cut so that the shear stresses accumulate at the broken fibre ends and initiate ply delamination during tensile loading. At low strain there is a linear increase in the specimen resistance with deformation.

A sharp increase in resistance occurs when the ply delamination is initiated. As the delamination grows with increasing stress there is a large increase in resistance marked by increases in the slope of the resistance curve.

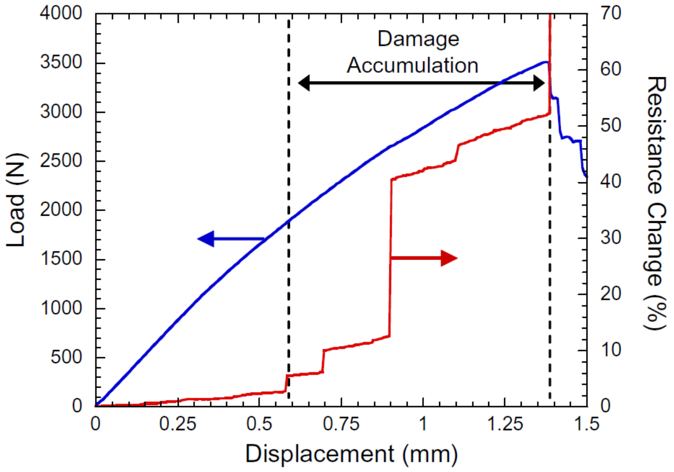

Fig. 4.10: Load/displacement and resistance response of a (0/90)s cross-ply composite showing accumulation of damage due to micro cracks [27]

Fig. 4.10 shows the strain and electrical resistance of a cross-ply symmetric laminate. During initial loading there is a linear increase in resistance with strain. Upon the initiation of micro cracking in the 90° plies there is a sharp change in the electrical resistance. From the first initiation of cracking to the ultimate fracture of the laminate, resistance changes are marked by sharp step increases which according to the authors, might correspond to the accumulation of micro cracks. Linear variation in electrical resistance with deformation between the step increases can also be noted. For both cases, there is a linear increase in resistance with deformation prior to damage initiation, indicating strong potential for both strain and damage detection. After the onset of damage and subsequent reloading of damaged structures there is a remarkable shift in the sensing curve, indicating irreversible damage. Authors have opined that these findings hold promise for development of automatic self-healing approaches for polymers and development of enhanced life prediction methodologies.

A particularly attractive feature for development of nanotube percolating networks for sensors in fibre-reinforced composites is that the nanotubes are considerably smaller than the structural reinforcement. In Thostenson and Chou's [27] work the network of sensors formed in the composite occupied less than 0.15% of the volume. Incorporation of in situ nanotube based sensing capability is thus non-invasive to the structural properties of the laminate.

Despite their advantages and enormous potential, significant challenges still exist in their development, for example the efficient growth of macroscopic-length carbon nanotubes, controlled growth of nanotubes on desired substrates, durability of nanotube based sensors and actuators, effective dispersion in polymer matrices and their orientation. Therefore, there is a need to develop both experimental and analytical techniques to bridge the nano and macro scales towards optimization so as to use nanotube networks as sensors inside macro scale (fabric) or meso scale (tow) composites [28].

4.2. Structural Health Monitoring

4.2.1. Fundamental Definitions

4.2.1.1. Damage

Damage can be defined as changes introduced into a system that adversely affect its current or future performance. Implicit in this definition is the concept that damage is not meaningful without a comparison between two different states of the system, one of which is assumed to represent the initial, and often undamaged, state. In structural and mechanical systems the definition of damage will be limited to changes to the material and/or geometric properties of these systems, including changes to the boundary conditions and system connectivity, which adversely affect the current or future performance of these systems [56].

4.2.1.2. Defect/flaw

In terms of length-scales, all damage begins at the material level. Although not necessarily a universally accepted terminology, such damage is referred to as a defect or flaw and is present to some degree in all materials. Under appropriate loading scenarios, the defects or flaws grow and coalesce at various rates to cause component and then system-level damage [56].

4.2.1.3. Failure

As the damage grows, it will reach a point where it affects the system operation to a point that is no longer acceptable to the user. This point is referred to as failure. In terms of time-scales, damage can accumulate incrementally over long periods of time such as that associated with fatigue or corrosion damage accumulation. On relatively shorter time-scales, damage can also result from scheduled discrete events such as aircraft landings and from unscheduled discrete events such as enemy fire on a military vehicle or natural phenomena hazards such as earthquakes [56].

4.2.1.4. Performance

Health monitoring is a concept that requires a comprehensive and quantitative description of performance covering a large spectrum of limit states that may govern throughout the life cycle of a composite material. There are four principle limit states defined as:

- Utility and functionality
- Serviceability and Durability
- Safety and stability at failure
- Safety at conditional limit states

Each limit state incorporates a number of limit events that should be considered in design and evaluation. The proper subjective as well as objective and quantitative indices for limit events determine the attainment of a limit state. Most limit events are governed by defects in design, materials or fabrication, or by various loading events associated with some probabilistic model.

The critical remaining issue related to the definition of performance is the formulation of objective, quantitative criteria for each limit event, and then find appropriate tests, measurements and simulation methods for assurance that the desired performance limits will not be exceeded in the limit events expected during the life cycle of the composite part. The concept of health monitoring promises to provide the data and information for various types of composites to serve for formulating objective performance indices. The importance of unambiguous and quantitative indices for ensuring performance is quite evident; performance limit states and the corresponding limit events serve as critical foundations for performance based design and evaluation [58].

4.2.1.5. Health

Engineers use various indices for defining health depending on purpose. Although it is pragmatic to use deterministic indices that are mainly related to "structural safety" most engineers recognize the need for a broader definition that relates to the definition of performance discussed earlier. After all, the main purpose for evaluation of health is the prognosis of future performance.

It is thus desirable to define the health of a composite part as its system reliability to possess adequate capacity against any probable demands that may be imposed on it in conjunction with the limit states defined previously. It is important to emphasize that system reliability should cover the entire spectrum of limit states and limit events and not just "structural safety" [58].

4.2.1.6. Health Monitoring

Health monitoring is the tracking of any aspect of a structure's health by reliably measured data and analytical simulations in conjunction with heuristic experience so that the current and expected future performance of the composite part for at least the most critical limit events, can be described in a pro-active manner. The single most important distinction of health monitoring from a typical in-depth composite part evaluation and testing practice is the minimum standards that are required for analytical modelling for reliable computer simulations, and how the measurements, loads and tests are designed and implemented in conjunction with the analytical simulations [58, 59].

4..2.1.7. Structural Identification

Structural identification is defined as the development of an analytical conceptualization leading to an analytical model of a composite structure that is quantified, tested and validated by correlating model simulations with corresponding measurements from the structure. It serves as both the starting point and the core of health monitoring. Applications of the structural identification principle provide the most reliable manner of characterizing a structure for analysis and decision making as it goes through its life cycle. The structural identification principle is what should guide engineers in determining the minimum number of measurements needed to accurately and completely characterize a structure so that its health may be reliably evaluated at the serviceability and safety limit states [58, 59].

Structural identification provides the most objective and reliable manner of documenting the global mechanical properties of a structural system and assessing its physical condition, load-rating, vulnerability, maintenance and retrofit needs etc. The "characterization" is also used by the engineers to describe the concept. It offers an understanding of all the critical mechanisms of flexibility, energy dissipation and inertia; the three-dimensional response kinematics; the resistance mechanisms; the critical structure regions; the mechanisms of resistance at the critical regions, the localized force, deformation and accumulated damage states at the critical regions. This information is essential to reliably assess and identify the available capacities of stiffness, strength stability, deformability, hardening and energy dissipation in the structure.

The following steps are essential for structural identification of a structure:

a. Collecting information, conceptualizing and a-priori modelling to best represent the existing knowledge about the structure.
b. Experiment design based on analytical and preliminary experimental studies.
c. Full scale modal and controlled load tests are conducted to identify, verify and evaluate global and local behaviour. These tests are conducted in conjunction with in-depth visual inspections of the composite structure, local NDE techniques, and in many cases material testing to identify and assess the extent of any existing deterioration and damage.
d. Processing and conditioning of the resulting experimental data to mitigate any errors and assure its quality.
e. Progressive calibration of analytical models by adjusting mechanical properties and boundary and continuity conditions to reflect the physical parameters measured from the full scale states.
f. Utilization of the calibrated model as a basis for management decisions.

4.2.2. Structural Health Monitoring

The process of implementing a damage detection and characterization strategy for engineering structures is referred to as Structural Health Monitoring (SHM). Here damage is defined as changes to the material and/or geometric properties of a structural system, including changes to the boundary conditions and system connectivity, which adversely affect the system’s performance. The SHM process involves the observation of a system over time using periodically sampled dynamic response measurements from an array of sensors, the extraction of damage-sensitive features from these measurements, and the statistical analysis of these features to determine the current state of system health. For long term SHM, the output of this process is periodically updated information regarding the ability of the structure to perform its intended function in light of the inevitable aging and degradation resulting from operational environments. After extreme events, such as earthquakes or blast loading, SHM is used for rapid condition screening and aims to provide, in near real time, reliable information regarding the integrity of the structure [56-59].

The classical methods for periodical maintenance use many NDE techniques which require extensive human involvement and expensive procedure. Moreover, this kind of periodical inspection cannot give any information concerning accidents and failures occurring between two successive overhauls. In order to overcome such shortcomings it is now possible to use ‘sensitive’ material. A material or a structure is said to be ‘sensitive’ when it includes sensors providing real time information about the material itself, or its environment. Continuous health monitoring of materials would result in improved durability and safety of structures.

The basic idea is to build a system similar to the human nervous system, with a network of sensors placed in critical areas where structural integrity must be maintained. Mathematical algorithms based on a "neural network" then can be trained to recognize patterns of electrical signals that represent damage, such as fibre strains or breakage and matrix cracks. In broadest terms, therefore, SHM comprises a distributed network of sensors that are deployed as integral parts of a structure and capable of collecting and sending information to an interrogator or electronic monitoring device [60].

Damage identification is carried out in conjunction with five closely related disciplines that include [56-58]:

- Structural Health Monitoring (SHM);
- Condition Monitoring (CM);
- Non-Destructive Evaluation (NDE);
- Statistical Process Control (SPC) and
- Damage Prognosis (DP).

Typically, SHM is associated with online–global damage identification in structural systems such as aircrafts and buildings.

CM is analogous to SHM, but addresses damage identification in rotating and reciprocating machinery, such as those used in manufacturing and power generation.

NDE is usually carried out off-line in a local manner after the damage has been located. There are exceptions to this rule, as NDE is also used as a monitoring tool for in situ structures such as pressure vessels and rails. NDE is therefore primarily used for damage characterization and as a severity check when there is *à priori* knowledge of the damage location.

SPC is process-based rather than structure-based and uses a variety of sensors to monitor changes in a process, one cause of which can be structural damage.

Once damage has been detected, DP is used to predict the remaining useful life of a system.

4.3. References

[1] S. Black, “Structural health monitoring: Composites get smart,” available at: http://www.compositesworld.com/articles/structural-health-monitoring-composites-get-smart, (consulted on 07/09/2009)

[2] S. Wang and D. D. L. Chung, "Self-sensing of flexural strain and damage in carbon fiber polymer-matrix composite by electrical resistance measurement," Carbon, vol. 44, pp. 2739-2751, 2006.

[3] P. Dharap, L. Zhiling, S. Nagarajaiah, and E. V. Barrera, "Nanotube film based on single-wall carbon nanotubes for strain sensing," Nanotechnology, vol. 15, pp. 379-382, 2004.

[4] C.-T. Huang, C.-L. Shen, C.-F. Tang, and S.-H. Chang, "A wearable yarn-based piezo-resistive sensor," Sensors and Actuators A: Physical, vol. 141, pp. 396-403, 2008.

[5] C.-T. Huang, C.-F. Tang, M.-C. Lee, and S.-H. Chang, "Parametric design of yarn-based piezoresistive sensors for smart textiles," Sensors and Actuators A: Physical, vol. 148, pp. 10-15, 2008.

[6] D. De Rossi, F. Carpi, F. Lorussi, R. Paradiso, E. P. Scilingo, and A. Tognetti, "Electroactive fabrics and wearable man-machine interfaces," in Wearable Electronics and Photonics: Woodhead Publishing Limited, UK, 2005.

[7] E. P. Scilingo, F. Lorussi, A. Mazzoldi, and D. De Rossi, "Strain-sensing fabrics for wearable kinaesthetic-like systems," IEEE sensors journal, vol. 3, pp. 460-467, 2003.

[8] B. Fiedler, F. H. Gojny, M. H. G. Wichmann, W. Bauhofer, and K. Schulte, "Can carbon nanotubes be used to sense damage in composites?," Annales de chimie, vol. 29, pp. 81-94, 2004.

[9] R. Schueler, S. P. Joshi, and K. Schulte, "Damage detection in CFRP by electrical conductivity mapping," Composites Science and Technology, vol. 61, pp. 921-930, 2001.

[10] I. De Baere, W. V. Paepegem, and J. Degrieck, "Electrical resistance measurement for in situ monitoring of fatigue of carbon fabric composites," International Journal of Fatigue, vol. 32, pp. 197-207, 2010.

[11] A. S. Kaddour, F. A. R. Al-Salehi, S. T. S. Al-Hassani, and M. J. Hinton, "Electrical resistance measurement technique for detecting failure in CFRP materials at high strain rates," Composites Science and Technology, vol. 51, pp. 377-385, 1994.

[12] N. Muto, Y. Arai, S. G. Shin, H. Matsubara, H. Yanagida, M. Sugita, and T. Nakatsuji, "Hybrid composites with self-diagnosing function for preventing fatal fracture," Composites Science and Technology, vol. 61, pp. 875-883, 2001.

[13] J. C. Abry, S. Bochard, A. Chateauminois, M. Salvia, and G. Giraud, "In situ detection of damage in CFRP laminates by electrical resistance measurements," Composites Science and Technology, vol. 59, pp. 925-935, 1999.

[14] J. C. Abry, Y. K. Choi, A. Chateauminois, B. Dalloz, G. Giraud, and M. Salvia, "In-situ monitoring of damage in CFRP laminates by means of AC and DC measurements," Composites Science and Technology, vol. 61, pp. 855-864, 2001.

[15] K. Schulte and C. Baron, "Load and failure analyses of CFRP laminates by means of electrical resistivity measurements," Composites Science and Technology, vol. 36, pp. 63-76, 1989.

[16] M. Kupke, K. Schulte, and R. Schüler, "Non-destructive testing of FRP by D.C. and A.C. electrical methods," Composites Science and Technology, vol. 61, pp. 837-847, 2001.

[17] K. Schulte and H. Wittich, "The electrical response of strained and/or damaged polymer matrix composites," in 10th Int. Conference on Composite Materials. vol. 5, K. Street and A. Poursatip, Eds. Whistler B.C., Canada, 1995, pp. 315-325.

[18] D. Karanbuehl, H. Aandahl, N. M. Haralampus-Grynaviski, W. Newby, D. Hood, G. Boiteux, G. Seytre, J. P. Pascault, A. Maazouz, J. F. Gerard, H. Sautereau, J. F. Chailan, A. C. Loos, and J. D. MacRae, "Use of in situ dielectric sensing for intelligent processing and health monitoring," in Third

International Conference on Intelligent Materials. vol. SPIE 2779, P. F. Gobin and J. Tatibouet, Eds. Lyon, France, 1996, pp. 112-117.

[19] C. Cochrane, V. Koncar, M. Lewandowski, and C. Dufour, "Design and Development of a Flexible Strain Sensor for Textile Structures Based on a Conductive Polymer Composite," Sensors and Actuators A, vol. 7, pp. 473-492, 2007.

[20] W. Zhang, R. S. Blackburn and A. A. Dehghani-Sanij, "Carbon Black Reinforced Epoxy Resin Nanocomposites as Bending Sensors," Journal of composite materials, vol. 43, pp. 367-376, 2009.

[21] A. Dittmar, R. Meffre, F. D. Oliveira, C. Gehin, and G. Delhomme, "Wearable Medical Devices Using Textile and Flexible Technologies for Ambulatory Monitoring," in IEEE Engineering in Medicine and Biology 27th Annual Conference Shanghai, China, 2005, pp. 7161-7164.

[22] A. S. Lim, Q. An, T.-W Chou and Erik T. Thostenson, "Mechanical and electrical response of carbon nanotube-based fabric composites to Hopkinson bar loading," *Composites Science and Technology*, doi:10.1016/j.compscitech.2010.12.025, article in press.

[23] D. S. Hecht, H. Liangbing, and G. George, "Electronic properties of carbon nanotube/fabric composites," Current Applied Physics, vol. 7, pp. 60-63, 2007.

[24] S. Peng, J. O'Keeffe, C. Wei, K. Cho, J. Kong, R. Chen, N. Franklin, and H. Dai, "Carbon Nanotube Chemical and Mechanical Sensors," in 3rd International Workshop on Structural Health Monitoring, 2003, pp. 1-8.

[25] W. Zhang, J. Suhr, and N. Koratkar, "Carbon nanotube/polycarbonate composites as multifunctional strain sensors," Nanotechnology, vol. 6, pp. 960-964, 2006.

[26] E. T. Thostenson and T. W. Chou, "Carbon nanotube-based health monitoring of mechanically fastened composite joints," Composites Science and Technology, vol. 68, pp. 2557-2561, 2008.

[27] E. T. Thostenson and T. W. Chou, "Carbon nanotube networks: sensing of distributed strain and damage for life prediction and self healing," Advanced Materials, vol. 18, pp. 2837–2841, 2006.

[28] C. Li, E. T. Thostenson, and T. W. Chou, "Sensors and actuators based on carbon nanotubes and their composites: A review," Composites Science and Technology, vol. 68, pp. 1227-1249, 2008.

[29] C. Li and T. W. Chou, "Modeling of damage sensing in fiber composites using carbon nanotube networks," Composites Science and Technology, vol. 68, pp. 3373-3379, 2008.

[30] I. P. Kang, M. J. Schulz, J. H. Kim, and V. Shanov, "A carbon nanotube strain sensor for structural health monitoring," Smart Material Structure, vol. 15, pp. 737-748, 2006.

[31] H. Zhao, Y. Zhang, P. D. Bradford, Q. Zhou, Q. Jia, F. G. Yuan and Y. Zhu, "Carbon nanotube yarn strain sensors," Nanotechnology, vol. 21, pp. 1-5, 2010.

[32] K. J. Loh, J. P. Lynch, and N. A. Kotov, "Nano-engineered inductively coupled carbon nanotube wireless strain sensor," available at: http://www.seminarprojects.com/Thread-nanoengineered-inductively-coupled-carbon-nanotube-wireless-strain-sensor#ixzz1BqyDrkhi (consulted on 23/01/2011))

[33] S. S. Lee, J. H. Lee, I. K. Park, S. J. Song, and M. Y. Choi, "Structural health monitoring based on electrical impedance of a carbon nanotube neuron," Key Engineering Materials, vol. Advanced Non-destructive evaluation, pp. 140-145, 2006.

[34] R. B. Katragadda and Y. Xu, "A Novel Intelligent Textile Technology Based on Silicon Flexible Skins," in Electrical & Computer Engineering ISWC Wayne State University, Detroit, Michigan, USA, 2005, pp. 78-81.

[35] R. B. Katragadda and Y. Xu, "A novel intelligent textile technology based on silicon flexible skins," Sensors and Actuators A: Physical, vol. 143, pp. 169-174, 2008.

[36] J. B. Lee and V. Subramanian, "Weave patterned organic transistors on fiber for E-textiles," IEEE Transactions on Electron Devices, vol. 62, pp. 269, 2005.

[37] E. M. Guerra, G. R. Silva and M. Mulato, "Extended gate field effect transistor using V_2O_5 xerogel sensing membrane by sol–gel method," Solid State Sciences, vol. 11, pp. 456-460, 2009.

[38] M. C. Choi, Y. Kim and C. S. Ha, "Polymers for flexible displays: From material selection to device applications," Progress in Polymer Science, vol. 33, pp. 581-630, 2008.

[39] C. Kagan, "Flexible Transistors," available at: https://www.technologyreview.com/InfoTech/12259/?a=f (consulted on 22/01/2011)

[40] E. Fortunato, N. Correia, P. Barquinha, L. Pereira, G. Goncalves, R. Martins, "High-Performance Flexible Hybrid Field-Effect Transistors Based on Cellulose Fiber Paper," IEEE Electron Device Letters, vol. 29, pp. 988-990, 2008.

[41] F. Carpy , D. De Rossi, F. Lorussi, A. Mazzoldi, E. P. Scilingo and A. Tognetti,, "Electroactive fabrics for distributed, conformable and interactive systems,," in IEEE Sensors Journal, vol. 2, pp. 1608-1613, 2002.

[42] F. Lorussi, E. P. Scilingo, M. Tesconi, A. Tognetti, and D. De Rossi, "Wearable sensing garment for posture detection, rehabilitation and tele-medicine," in 4th International IEEE MBS Special Topic Conference on Information Technology Applications in Biomedicine, Birmingham, UK, 2003, pp. 228–290.

[43] T. D. R. Wijesiriwardana, S. Mukhopadhyay, K. Mitcham, "Knitted strain gauges," in SPIE Int. Symp. Microtechnologies for the New Millennium Maspalomas, Canary Islands, Spain, 2003, pp. 5116–5131.

[44] K. M. R. Wijesiriwardana and T. Dias, "Fibre-meshed transducers based real time wearable physiological information monitoring system,," in 8th International Symposium on Wearable Computers, 2004, pp. 40-47.

[45] R. Wijesiriwardana, "Inductive fiber-meshed strain and displacement transducers for respiratory measuring systems and motion capturing systems," IEEE Sensors Journal, vol. 6, pp. 571–579, 2006.

[46] S.L. Baurley, "Smart textiles for future intelligent consumer products," in IEE Eurowearable, 2003, pp. 73-75.

[47] S. Kim, S. Leonhardt, N. Zimmermann, P. Kranen, D. Kensche, E. Muller and C. Quix, “Influence of contact pressure and moisture on the signal quality of a newly developed textile ECG sensor shirt,” in 5th International Summer School and Symposium on Medical Devices and Biosensors, 2008, pp. 256-259.

[48] V. Koncar, B. Kim, E. B. Nebor and X. Joppin, “FICC (floatable intelligent and communicative clothing) project conductive fibers development,” in Eighth International Symposium on Wearable Computers, 2004, pp. 36-39.

[49] P. K. Patra, S. B. Warner, Y. K. Kim, C. H. Chen, and P. D. Calvert, "Quantum Tunneling Nanocomposite Textile Soft Structure Sensors and Actuators," University of Massachusetts Dartmouth, Project Report M04-MD07, November 2005.

[50] M. A. Wahab and K. Alam, “Performance comparison of zero-Schottky-barrier single and double walled carbon nanotube transistor,” in International Conference on Electrical and Computer Engineering, 2008, pp. 270-274.

[51] D. Kienle and A. Ghosh, “Atomistic study of the role of contact properties on nanotube conduction,” in 4th IEEE Conference on Nanotechnology, 2004, pp. 537-540.

[52] W. Tan, J. Twomey, G. Dongjie, K. Madhavan, M. Li, “Evaluation of Nanostructural, Mechanical, and Biological Properties of Collagen–Nanotube Composites,” IEEE Transactions on NanoBioscience, vol. 9, pp. 111-120, 2010.

[53] A. Behnam, J. Guo and A. Ural, “Effects of nanotube alignment and measurement direction on percolation resistivity in single-walled carbon nanotube films,” Journal of Applied Physics, vol. 102, pp. 044313 - 044313-7, 2007.

[54] I. P. Kang, J. W. Lee, G. R. Choi, J. Y. Jung, S. H. Hwang, Y. S. Choi, K. J. Yoon, M.J. Shulz, "Structural health monitoring based on electrical impedance of a carbon nanotube neuron," Key Eng Mater: Adv Nondestructive Eval, pp. 321-323:140-145, 2006.

[55] C. Zhou, “Carbon nanotube nanoelectronics and macroelectronics,” in 10th IEEE International Conference on Solid-State and Integrated Circuit Technology (ICSICT), 2010, pp. 1210-1213.

[56] C. R. Farrar and K. Worden, "An introduction to structural health monitoring," Philosophical Transactions of the Royal Society A, vol. 365, pp. 303-315, 2007.

[57] D. Balageas, "Introduction to structural health monitoring," in Structural health monitoring, D. Balageas, C. P. Fritzen, and A. Guemes, Eds. London: ISTE Ltd., 2006, pp. 13-44.

[58] A. E. Aktan, F.N. Catbas, K.A. Grimmelsman, and M. Pervizpour, "Development of a Model Health Monitoring Guide for Major Bridges," Drexel Intelligent Infrastructure and Transportation Safety Institute July 2003.

[59] O. Buyukozturk and T. Y. Yu, “Structural health monitoring and seismic impact assessment,” in *Proc. 4th Nat. Conf. Earthquake Eng.*, Istanbul, Turkey, 2003, Available at: http://web.mit.edu/istgroup/ist/documents/2003_Paper_SHM%20and%20Seismic%20Impact%20Assessment_Istanbul.pdf Consulted on 01/01/2010

[59] D. D. L. Chung, “Composites get smart,” Materials today, vol. 5, pp. 30-35, 2002.

Chapter 5

Piezo-resistive sensor for on-line SHM of composite structural parts

5.1. Introduction

Present study is aimed at designing, developing and optimizing piezoresistive sensors realized from semi conductive coatings, suited for on line structural health monitoring of composite structural parts containing 3D reinforcement. Our sensors have been designed to offer following advantages:

- They can be embedded inside the reinforcement during weaving.
- They have all the characteristics of a traditional textile material (flexible, lightweight and are capable of adopting the geometry of the reinforcement and become its integral part).
- Since these sensors are inserted during weaving process, they are subjected to similar strains as the composite itself. Measurement of resistance change with variation in sensor's length is a way of determining in situ strains in the composite material which lead to its final damage.
- The fibrous sensors are not supposed to modify the overall structural and mechanical properties of the composite as they are integrated locally and the bulk of the structure is composed of high performance multifilament tows.
- Insertion of intelligent piezoresistive sensor inside the reinforcement during weaving process is the most convenient and cost effective way of integrating a sensor for structural health monitoring (SHM) of 3D interlock woven reinforcements.

Development and optimization of such piezoresistive sensors has been carried out in order to render them sensitive enough to measure in situ strains inside the composite part. Sensitivity is important as the targeted application usually undergoes very low strains and even such low strains and/or vibrations during the life time of composite parts are critical. Often they are used in areas where structural integrity can not be compromised (aircraft wings, bodies etc).

Optimization of sensors is followed by their insertion in the reinforcement during weaving process on a special loom modified and adapted for multilayer warp interlock weaving. In a woven fabric warp direction is the same as that of weaving while weft direction is perpendicular to the warp direction. In this research work fibrous sensors are inserted in the weft direction. The reinforcement is then impregnated with epoxy resin using infusion process to form a stiff composite material.

In the first place only tensile loading was considered because for composite structures it is important to identify the behaviour of fibrous reinforcement inside the composite. This is not the case for metallic structural parts. It was important for our research work to validate the concept of in situ measurement with the sensor compatible with manufacturing method of carbon composites. The fatigue properties may also be estimated from the history recorded during the life time of composite structural part having an embedded fibrous sensor.

Since the carbon multifilament tows are conductive and may disturb the functioning of piezoresistive fibrous sensor, it is imperative to coat the sensor with an additional insulating layer. The compatibility of interfacial properties of the insulating layer with the carbon nanoparticles coated on the sensory yarn surface on one side and with the epoxy resin on the other side is very important. An insulating medium that has good adherence with the coated yarn as well as with the resin should be used.

5.2. Strain gauge development

Strain gauges are a class of sensors which are used in many types of applications. Electrical-type strain gauges convert a displacement into an electrical signal. Their output is usually a change of resistance.

In a resistive strain gauge, the stretching causes a change in geometry so as to increase the resistance of the gauge. Since the gauge material is not incompressible so the resistivity also changes with the change in geometry. The gauge factor for a resistive strain gauge is given as:

$$K = \frac{\left(dR \middle/ R \right)}{\left(dL \middle/ L \right)} = 1 + 2\nu + \frac{\left(d\rho \middle/ \rho \right)}{\left(dL \middle/ L \right)} \tag{5.1}$$

Where:

$R =$ Resistance of the gauge;

$L =$ Length of the gauge;

$\nu =$ Poisson's ratio;

$\rho =$ Resistivity of the gauge material.

Gauge factor depends on the material properties and conduction mechanism in the gauge material. For metals it ranges from 2 to 4.

For semi conductive materials much higher gauge factor values are achievable. In the following paragraph an approach for the development of flexible textile strain gauges has been described.

5.2.1. Preliminary tests

Several different semi conductive coating formulations for intelligent textile structures exist. The one chosen here was developed in GEMTEX [1]. The fundamental principle of functioning of such intelligent coatings is based on forming (and deforming) of electrical conductive paths (percolation networks) in a coated layer, made of conductive nano charges. This phenomenon is responsible for electrical resistance variation in the coated layer with change in its length. Thus textile substrates coated with such a piezoresistive layer can be used as strain gauges in composite materials.

Yarns and filaments have been coated with the conductive layer using dispersed carbon black particles (Printex® L6) in polymer (Evoprene® 007) solution, using Chloroform as a solvent and dispersing medium. In order to characterize the sensitivity and adherence of the coating on different substrates, the carbon black solution having 25% and 35% carbon black concentration was coated on different yarns and filaments (polyester, polyamide, polyethylene and cotton). Visual inspection of the surfaces of the coated yarns and filaments shows that the coating is more uniform for filaments as compared to spun yarns. Spun yarns absorb the solution so that solution penetrates inside the pores and interstices much like a dye. This particular phenomenon is a source of non homogeneity in sensor electrical and mechanical properties, as the spun yarn is non uniform as compared to filaments, the coating and thus the resistivity achieved is non uniform. Fig. 5.1 gives a comparison of resistivity values for different yarns and filaments with that of the carbon multifilament tow.

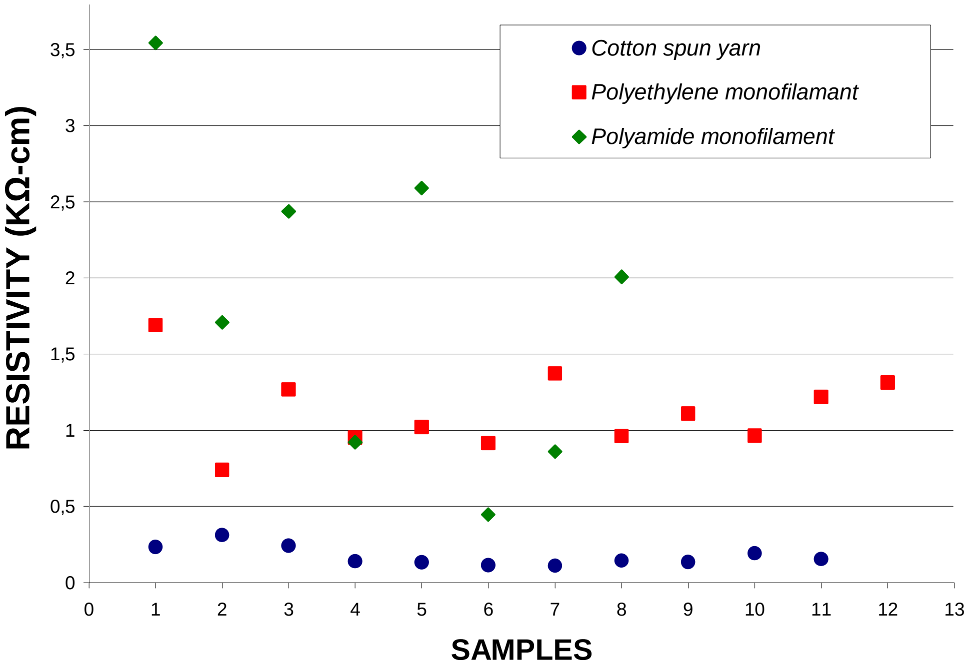

Fig. 5.1: Resistivities calculated for different substrates coated with 35% carbon black solution as compared to that of carbon multifilament tows

In order to carry out tensile tests on coated yarns and monofilaments MTS ½ tester was used which is shown in Fig. 5.2.

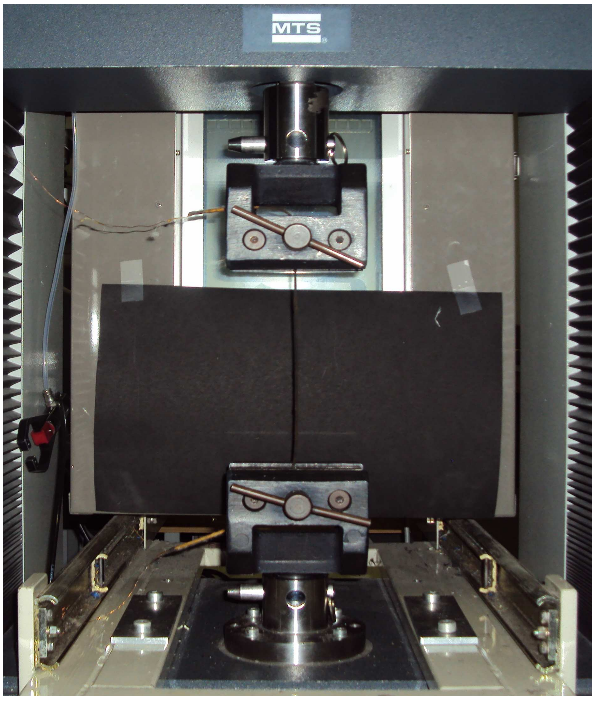

Fig. 5.2: MTS ½ tester used for preliminary tensile tests on sensor

The schematic of simple voltage divider circuit used for the measurement of resistance is shown in Fig. 5.3.

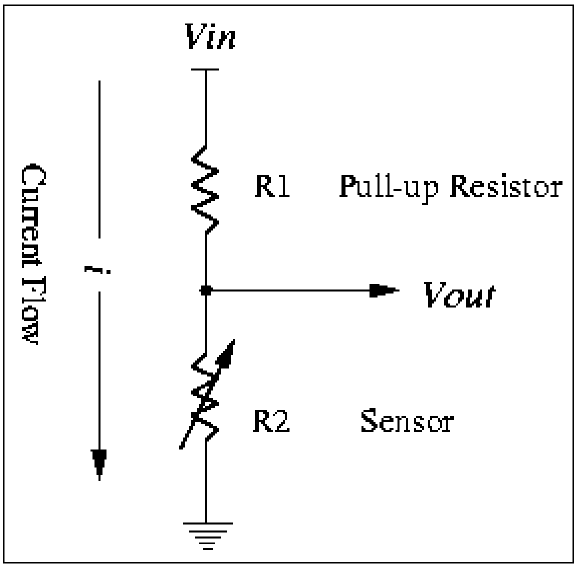

Fig. 5.3: Schematic of voltage divider circuit used for sensor resistance measurement

For the purpose of resistance variation measurement and analysis Keithley KUSB-3100 data acquisition module was employed (Fig. 5.4-A). The data acquisition module (Keithley KUSB-3100) was connected to computer interface for data acquisition and storage.

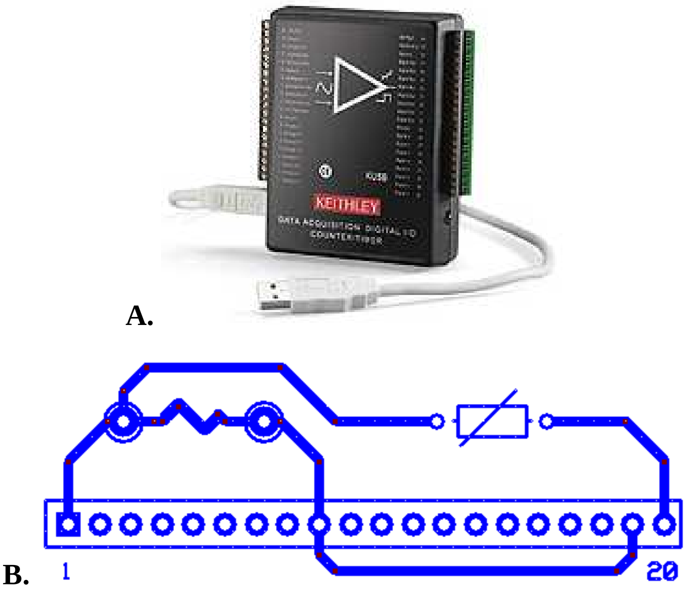

Fig. 5.4: (A) Data acquisition module Keithley KUSB 3100 (B) Circuit divider configuration

5.2.1.1. Influence of substrate

Fig. 5.5 shows some of the results obtained using different substrates for coating. The yarns were coated using 35% carbon black solution by weight. A visual inspection of the surfaces of the coated yarns and filaments shows that the coating is more uniform for monofilaments as compared to spun yarns. Cotton spun yarns absorb the solution so that solution penetrates inside the pores and interstices much like a dye. Due to this fact the initial resistance of the coating on spun yarns is much lower than monofilaments. But since the cotton spun yarns are inherently irregular, the coatings obtained are not homogenous and the results obtained for different coated yarns vary widely in their response to tensile loading.

Due to particular fineness of the Nylon monofilament it was found that slight non homogeneity in coating on the surface can result in breakdown of conductive path as is obvious from Fig. 5.5-B and as a result the behaviour of Nylon is highly inconsistent. Polyethylene monofilaments provide a reasonably good compromise as the substrate. The coatings on polyethylene are easy to achieve due to good substrate-conductive solution interfacial properties. As the curves in Fig. 5.5-C show the polyethylene coatings are reproducible as the curves for all the four samples are nearly identical as opposed to Nylon and cotton.

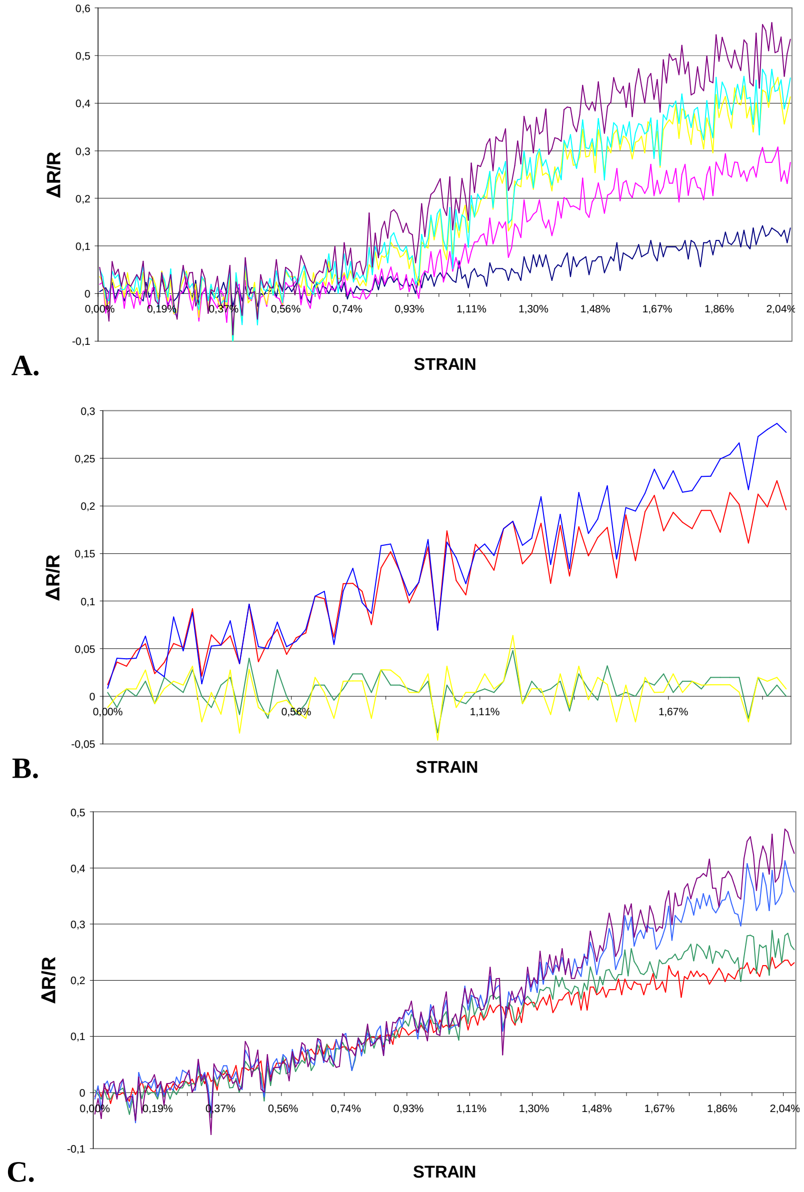

Fig. 5.5: Tensile strength tests on different yarn and filament substrates coated with 35% Carbon black solution (A) 71 Tex Cotton yarn (B) 25 Tex Nylon monofilament (C) 4823 Tex Polyethylene monofilament

5.2.1.2. Influence of loading rate

A study was carried out to characterize the influence of loading rate during tensile testing on the sensitivity of sensors. Results are shown in Fig. 5.6 and 5.7.

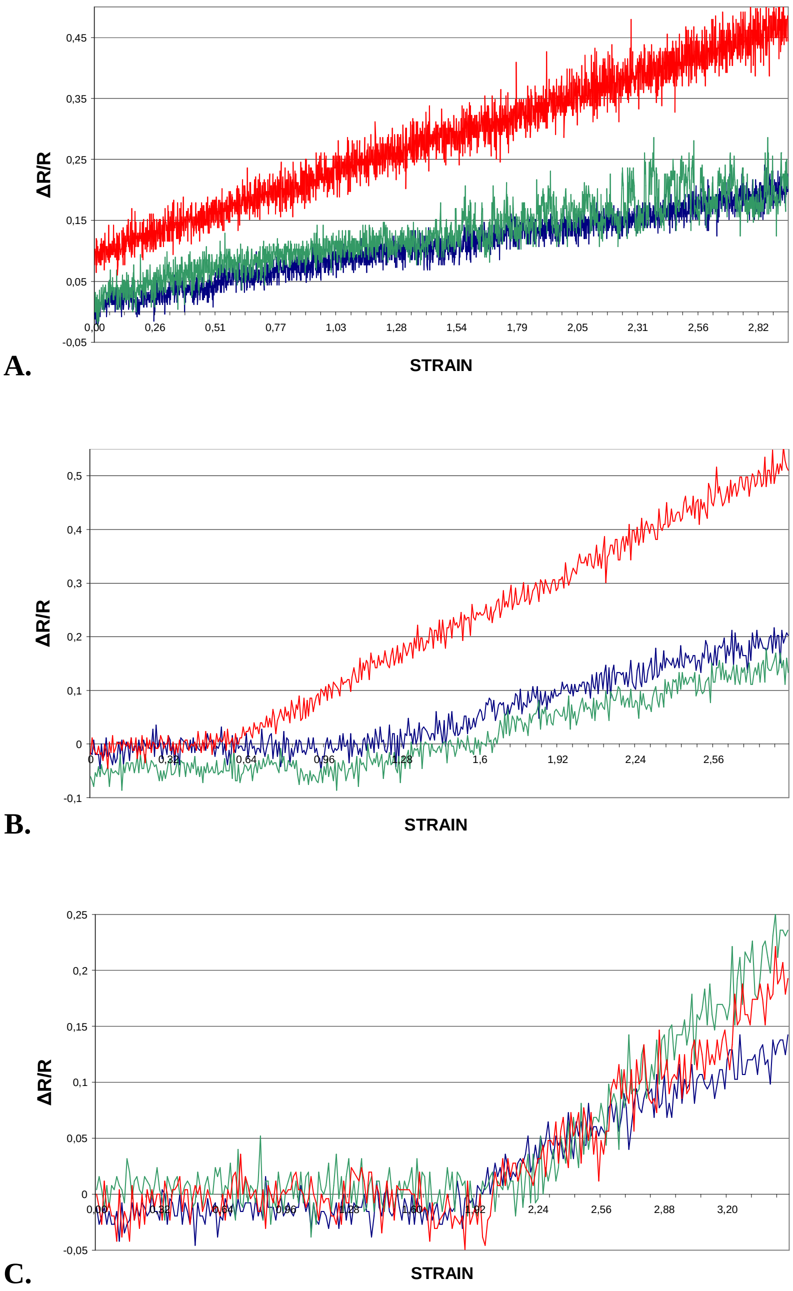

Fig. 5.6: Tensile strength tests on 71 Tex Cotton yarn substrates coated with 25% Carbon black solution at (A)10 mm/min. (B)50 mm/min.(C)100 mm/min.

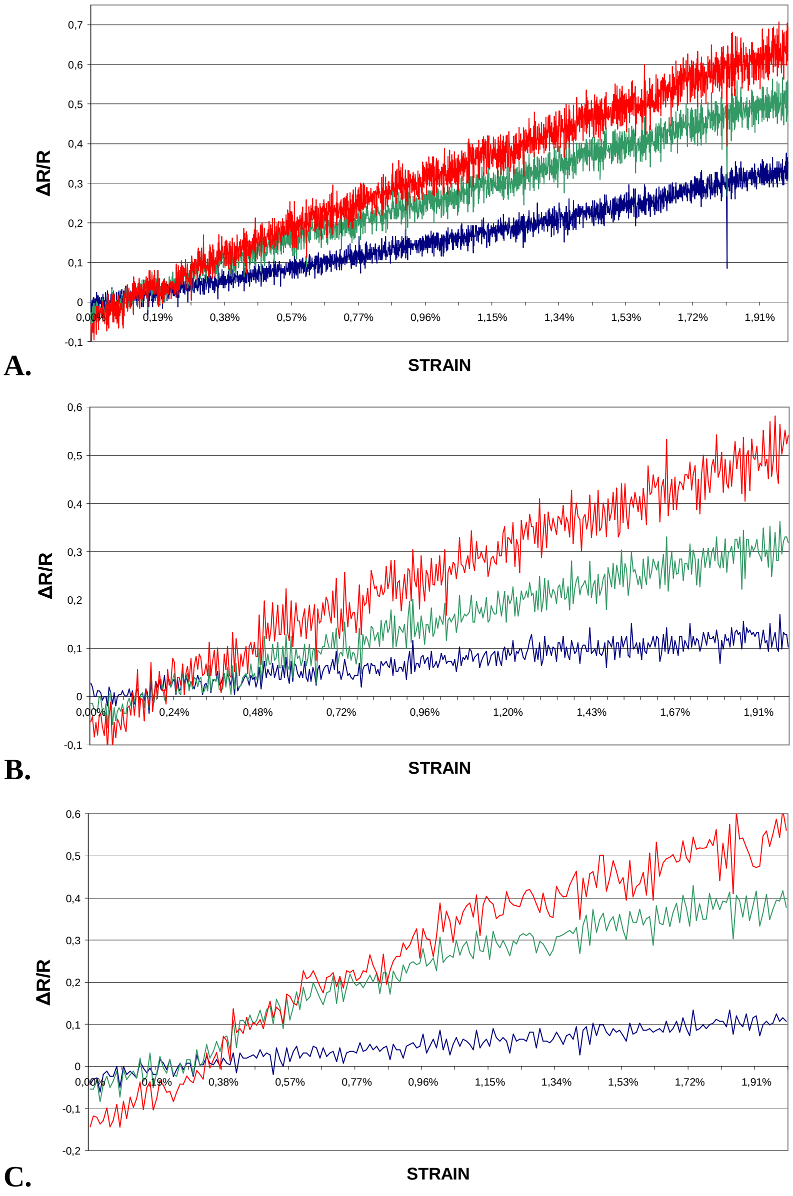

Fig. 5.7: Tensile strength tests on 380.4 Tex Cotton yarn substrates coated with 25% Carbon black solution at (A)10 mm/min. (B)50 mm/min.(C)100 mm/min.

For comparison purpose fine (71 Tex) and coarse (380.4 Tex) spun cotton yarns were chosen for substrates. These yarns were coated using 25% carbon black solution (by weight) so as to formulate more sensitive sensor coatings. These sensors were tested for their response to tensile loading at 3 different speeds i.e., at 10 mm/min, 50 mm/min and 100 mm/min (Fig. 5.6 and 5.7).

Results show that sensors are satisfactorily sensitive to tensile loading at 10 mm/min as is obvious from Fig. 5.6-A and Fig. 5.7-A. At higher loading rates the inertial force becomes more marked, influencing adversely the sensitivity of sensors in low strain regions (refer to Fig. 5.6-B, 5.6-C and Fig. 5.7-B, 5.7-C). The cotton count also influences the sensitivity of the sensors. Coarser substrate allows more carbon black solution to penetrate the yarn pores which signifies more conduction paths and lower initial resistance of the sensor. Such sensors show better results at higher speeds and their sensitivities are not influenced by higher loading rates (refer to Fig. 5.7-C).

5.2.2. Optimization of Sensor

It was found that Polyethylene proves to be the best substrate as far as resistivity and uniformity of the conductive layer are concerned. The coatings on polyethylene are easy to achieve due to good substrate-conductive solution interfacial properties. Coatings on polyethylene are reproducible and give coherent results. Therefore 2 ply polyethylene filament was chosen for sensor development.

Sensor structural and geometrical parameters along with initial electrical resistance of the sensor are shown in Table 5.1.

Table 5.1: Sensor Properties

No.	*PARAMATER*	*UM*	*VALUE*
1	Linear density of the filament	g/km	48.23
2	Diameter of the filament	mm	0.7
3	Average width of the sensor cross section	mm	1.68
4	Average thickness of the sensor cross section	mm	1.26
5	Average sensor cross sectional area	mm^2	1.66
6	Aspect ratio of the sensor	-	1.33
7	Initial Resistance of the Sensor	KΩ	43.3

The two ends of the coated Polyethylene filaments were additionally coated with silver paint and fine copper wire was attached to the two ends with the help of this paint (as shown in the Fig. 5.8-A and B). In this way, secure connections were realized enabling the reduction of the contact resistance to the minimum.

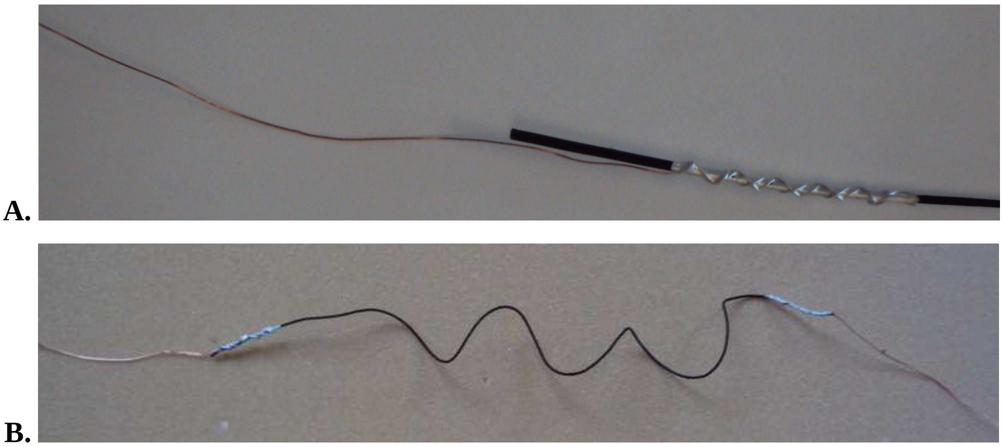

Fig. 5.8: (A) Carbon black coated sensor with polyethylene double-ply substrate and (B) Detail of connections at the ends.

Transversal and longitudinal section of the sensor obtained through SEM and tomography are shown in Fig. 5.9-A and B respectively.

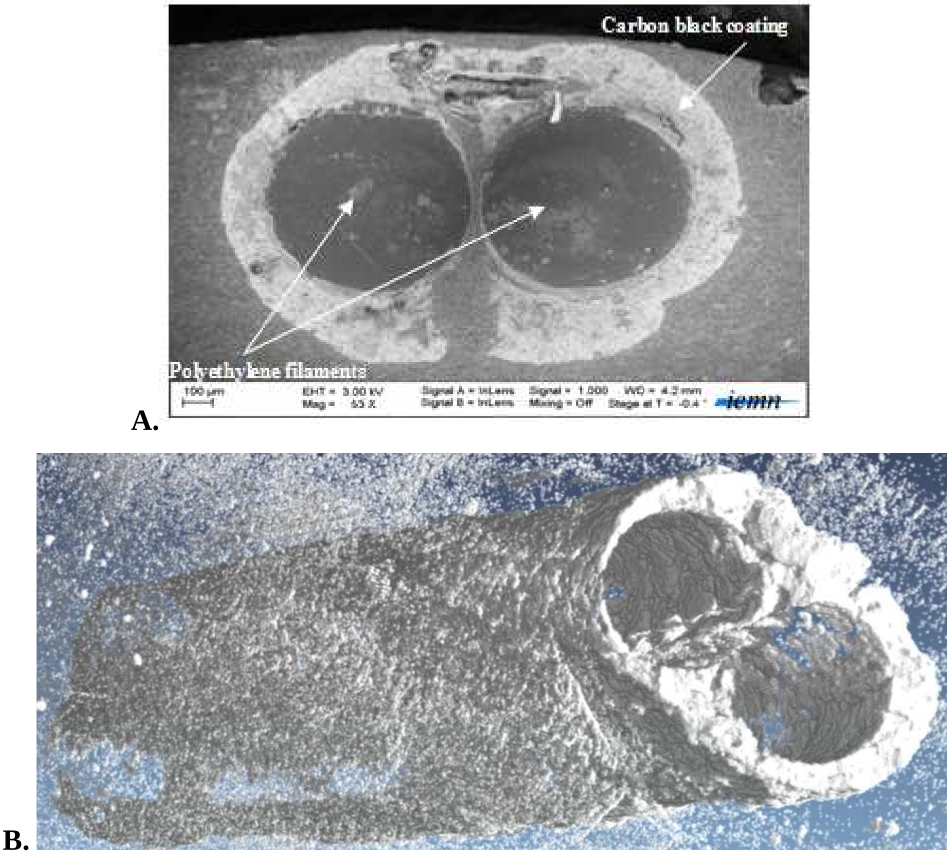

Fig. 5.9: (A) Transversal section (SEM), (B) Longitudinal section (Tomography) of the sensor

Once the sensors are optimized they are ready to be inserted in the reinforcement during weaving process. For insertion in conductive fibre based reinforcements like that woven using carbon multifilament tows, the sensor was coated with Latex Abformmasse supplied by VossChemie® so as to insulate the sensor from surrounding carbon tows.

5.3. Data Acquisition and Sensor Signal Conditioning

5.3.1. Data acquisition device

A bridge measures resistance indirectly by comparison with a similar resistance. Such a simple bridge is shown in Fig. 5.3. As is obvious from curves presented in Fig. 5.5, 5.6 and 5.7, the simple voltage divider circuit is not adequate for the measurement of resistance change in case of sensors developed here. These piezoresistive sensors produce a very small percentage change in resistance in response to physical phenomena such as strain. Moreover the output signal has considerable noise.

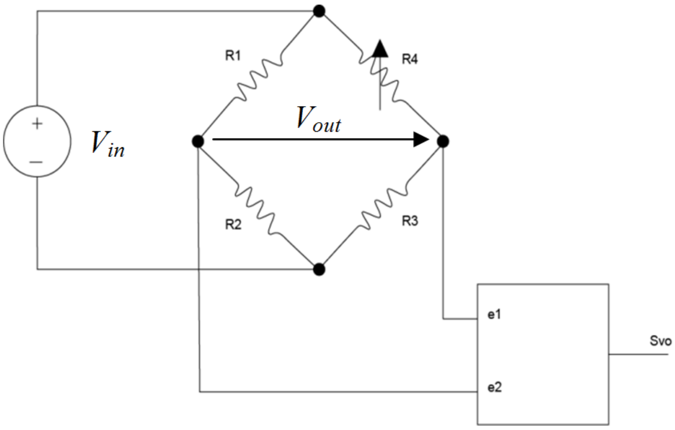

Fig.5.10: Wheatstone bridge configuration used for differential voltage variation measurement caused by resistance variation in the sensor: R4 (strain gauge) [2]

Wheatstone bridges offer an attractive solution for sensor applications as they are capable of measuring small resistance changes accurately. The Wheatstone bridge was originally developed by S.G. Christie in 1833. Typical Wheatstone bridge consists of four resisters connected to form a quadrilateral (Fig. 5.10). A source of excitation (usually a voltage source or current source) is connected across one of the diagonals, and voltage detector is connected across the other diagonal. The detector measures the difference between the outputs of two voltage dividers connected across the excitation.

In majority of sensor applications the Wheatstone bridge is used to measure the deviation in the initial value of one or more resistors as a function of physical variable to be measured. In this case the output voltage change is an indication of resistance change. This resistance change is caused by the change in length in the case of our piezoresistive sensors.

The basic relationship is given as

$$V_{out} = \frac{V_{in}(R_1R_3 - R_2R_4)}{(R_2 + R_1)(R_3 + R_4)} \tag{5.2}$$

For a balanced configuration $V_{out} = 0$ which implies that:

$$(R_1R_3 - R_2R_4) = 0 \tag{5.3}$$

The Wheatstone bridge configuration shown in Fig. 5.10 has only one varying element of resistance (sensor). Its output may be amplified by using a single precision op-amp connected in the inverting mode as shown in Fig. 5.11 But this circuit has poor gain accuracy and also unbalances the bridge due loading from RF and the op-amp bias current. The RF resisters must be carefully chosen and matched to maximize the common mode rejection (CMR). Another disadvantage is the difficulty of maximizing CMR while at the same time allowing different gain options. Moreover the output of such circuits is non-linear.

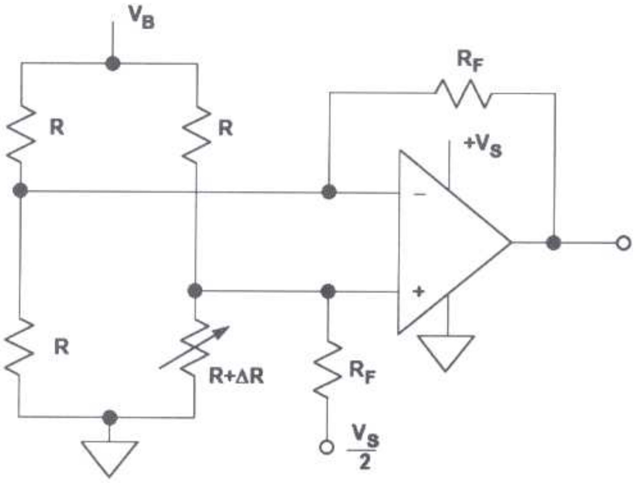

Fig. 5.11: Using a single op-amp as a bridge amplifier for a single element varying bridge [2]

The practical solution to these problems is the use of an instrumentation amplifier (in-amp). Instrumentation amplifiers are efficient ICs with following advantages:

- Gain and offset voltage of can be easily adjusted for output signal;
- Better gain accuracy set with a single resister RG;
- The bridge is not unbalanced;
- Excellent common mode rejection can be achieved;
- They are simple to use and allow us the conception of a circuit with fewer components.

Fig. 5.12 shows a commercially available instrumentation amplifier INA 101.

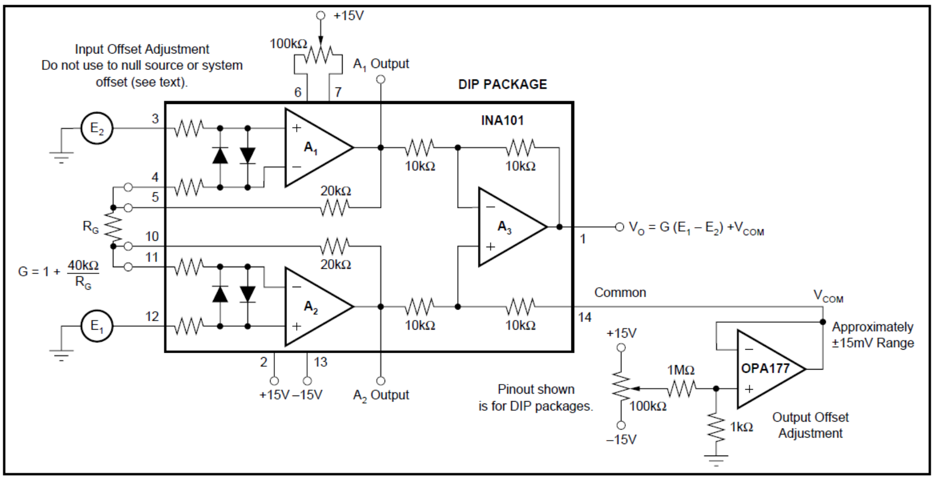

Fig. 5.12: Operational amplifier INA 101[3]

Due to the above stated advantages of inst-amps. They can be used to amplify output from a Wheatstone bridge. The data can be then fed to data acquisition module and can be displayed on computer using software interface. This data is now ready to be used and manipulated in any suitable format. Fig. 5.13 shows schematic diagram of the data amplification and acquisition set-up used.

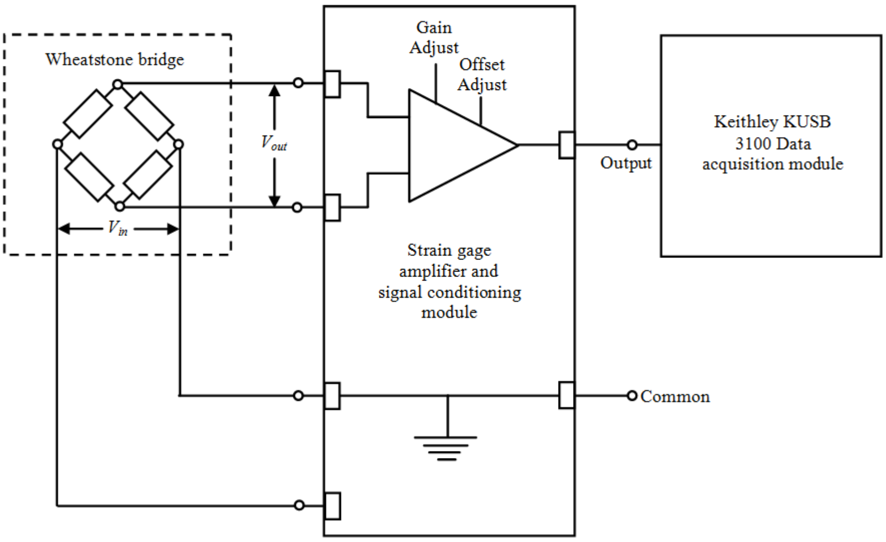

Fig. 5.13: Schematic of instrumentation amplifier connected to Wheatstone bridge

The schematic diagram and the circuit board of the module used for signal amplification and linearization are shown in Fig. 5.14-A and B respectively.

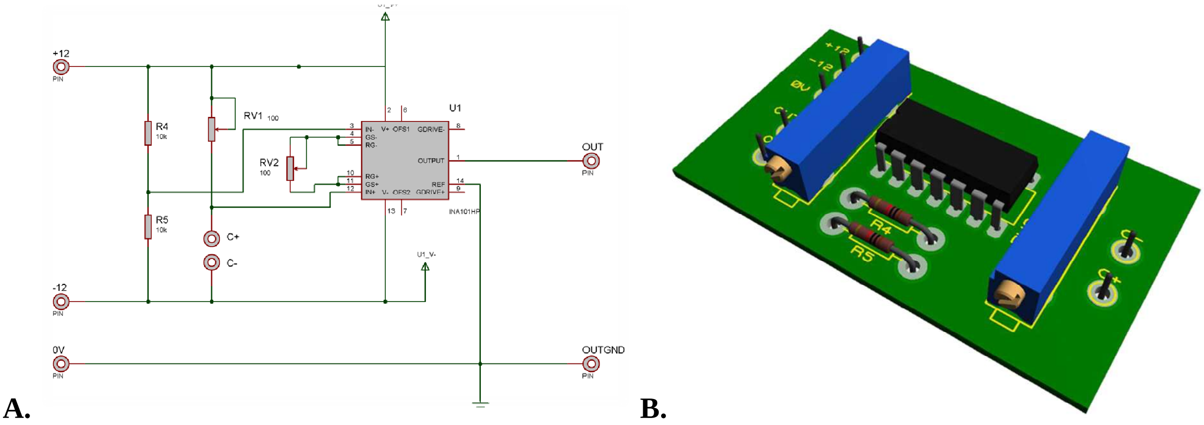

Fig. 5.14: Signal amplification and linearization Module

(A) Schematic diagram (B) Circuit board with mounted components

For the data amplification module described above, the output voltage is given as

$$V_{out} = G(E_1 - E_2) \tag{5.4}$$

Where:

$$G = 1 + \frac{40K\Omega}{RG} \tag{5.5}$$

RG is the variable resistance which allows gain adjustment.

Normalized resistance can be given as

$$\frac{\Delta R}{R} = \frac{4}{\left(GV_{in}/V_{out}\right) - 2} \tag{5.6}$$

5.3.2. Prior to Insertion Calibration of sensor

The sensor was tested on MTS ½ tester (Fig. 5.15). For all the tests presented in this section, quasi static tensile loading at a constant test speed of 5mm/min was carried out.

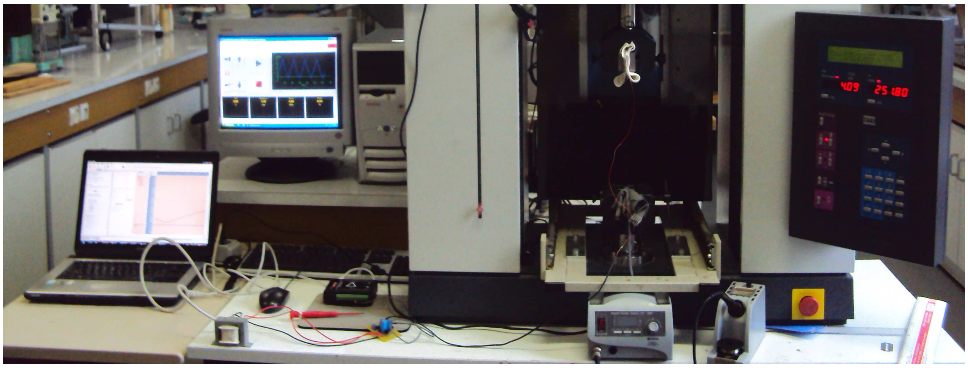

Fig. 5.15: Tensile strength test on MTS ½ tester using data acquisition module Keithley 3100

For the purpose of output voltage data acquisition during the tests performed on the composite samples, Keithley® KUSB-3100 data acquisition module was employed in conjunction with the amplification and linearization module described earlier (Refer to Fig. 5.13).

The data acquisition module when connected to a computer shows the voltage variation data in real time via the software interface (Keithley QuickDAQ). The data was saved on computer hard disk for further treatment. The resistance variation data thus obtained for different test results was treated for noise reduction using a low pass filter.

The resultant stress-strain-resistance relationship curve up to 2.75 % elongation of the out of composite sensor (before insertion in the reinforcement) is shown in Fig. 5.16. It may be noticed in Fig. 5.16 that the stress vs. strain curve has the same shape as ΔR/R vs. strain curve. This validates electromechanical properties of our fibrous sensor for strains ranging from 0 to 2.75%.

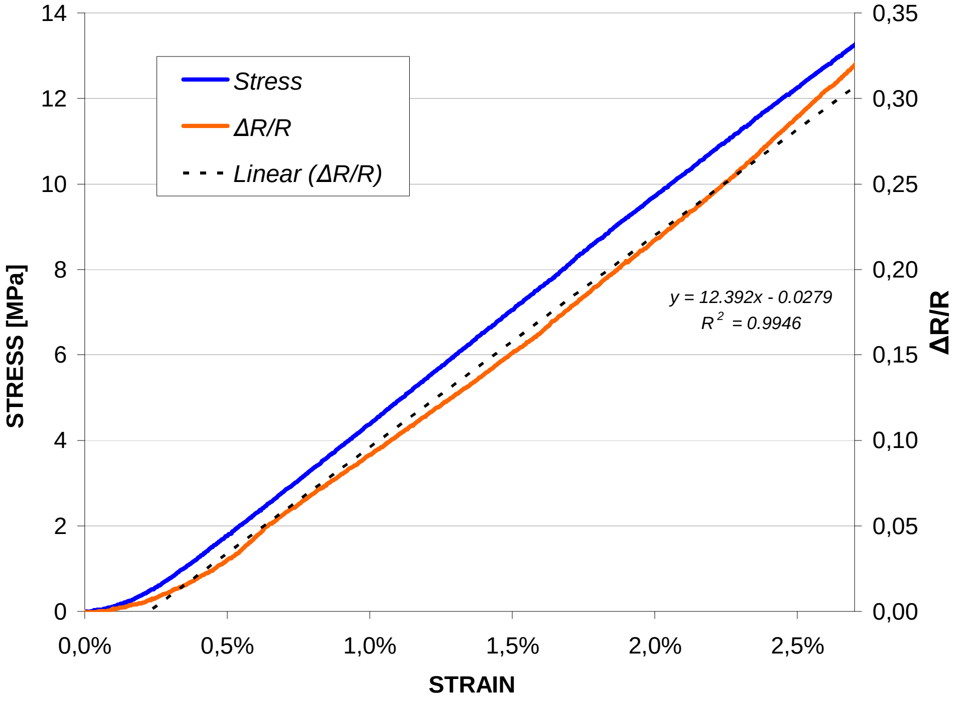

Fig. 5.16: Normalized resistance and stress against strain for sensor outside composite

Fig. 5.17 shows the hysteresis behaviour of the sensor outside the composite for 2 cycles at 2.5% extension followed by compression in each cycle. The sensor follows the extension and compression cycles albeit with considerable hysteresis.

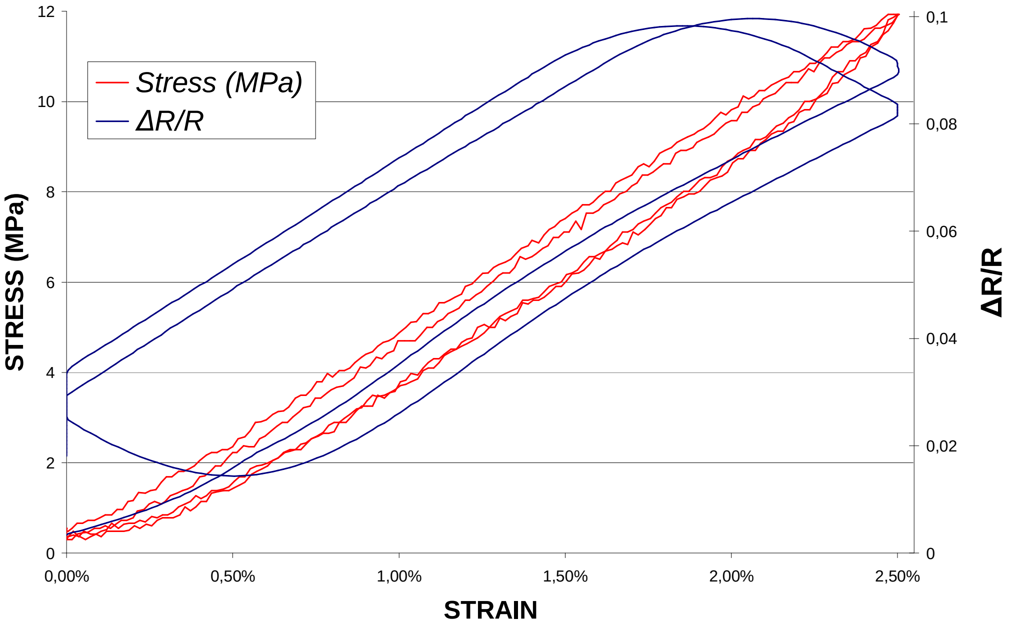

Fig. 5.17: Normalized Resistance and Stress against Strain for Sensor outside composite (Hysteresis 2 cycles at 2.5% extension)

For further details on the calculation of stress, consult Appendix 8.

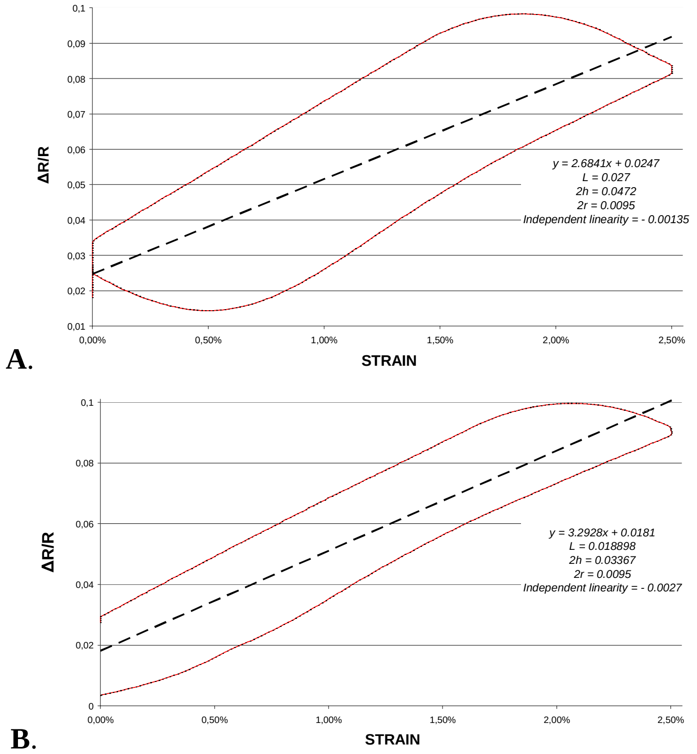

Fig. 5.18: Comparison of the two cycles for 2.5% extension (A) 1st cycle (B) 2nd cycle

Comparison of 1st and 2nd cycles presented in Fig. 5.18-A and B respectively, shows that the hysteresis is higher for the first cycle and considerably lower for the 2nd one.

In Fig. 5.19, the hysteresis results of the sensor for 10 cycles have been given. The sensor underwent 0.5 % extension followed by compression in each cycle. The sensor follows the extension and compression patterns in each cycle.

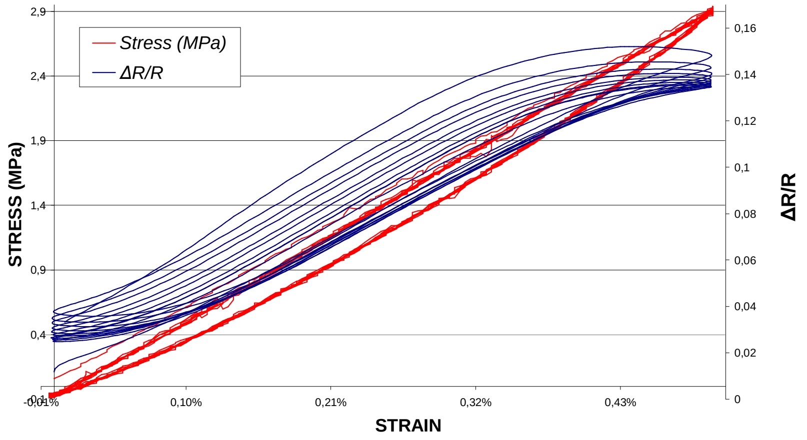

Fig. 5.19: Normalized Resistance and Stress against Strain for Sensor outside composite (Hysteresis 10 cycles at 0.5% extension)

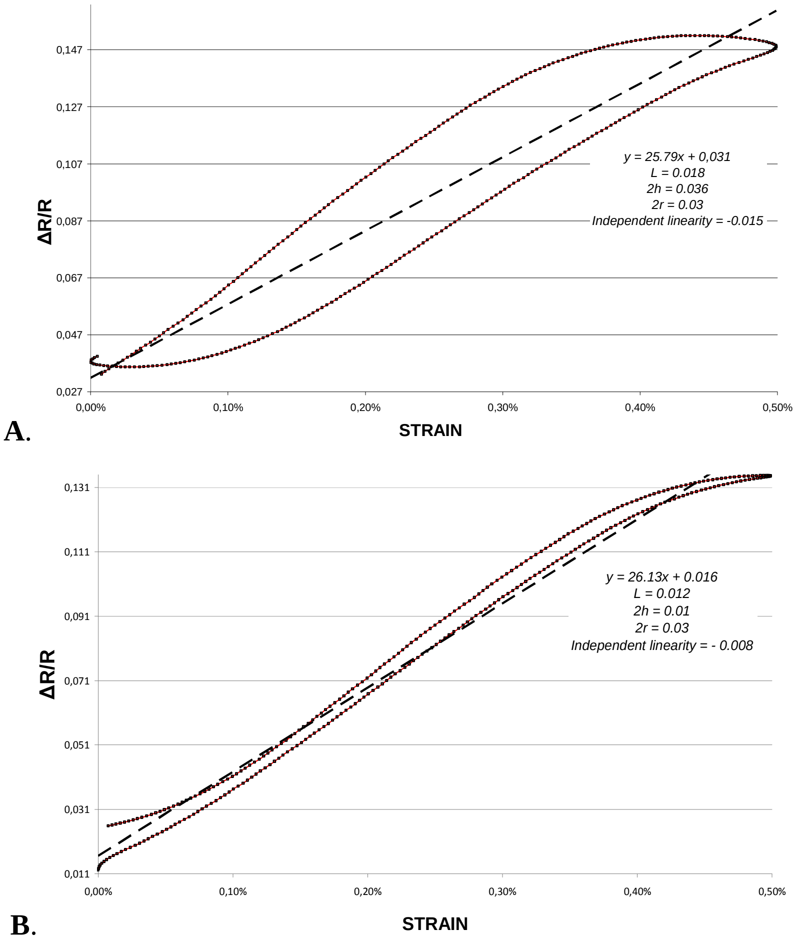

Fig. 5.20: Comparison of first and last cycle for 0.5% extension (A) 1st cycle (B) 10th cycle

A comparison of curves given in Fig. 5.20-A and B shows that the hysteresis is high for the first cycle which reduces gradually and for the 10th cycle the sensor exhibits almost linear behaviour.

Fig. 5.21 gives a comparison of linearity and hysteresis errors for the two hysteresis tests descried above.

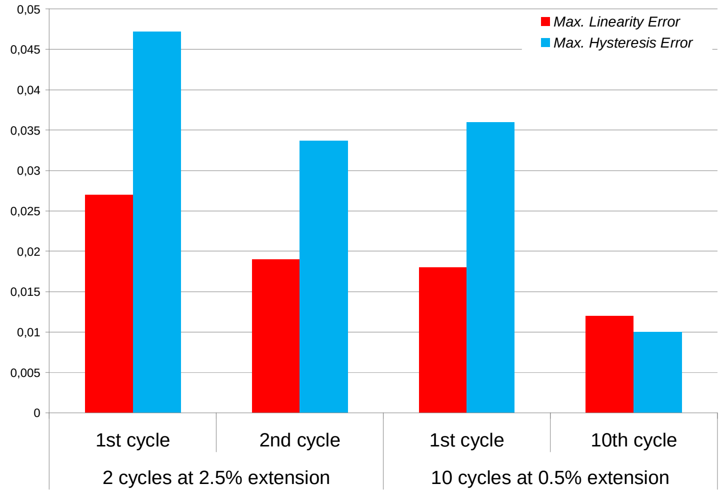

Fig. 5.21: Comparison of linearity and hysteresis errors

In Fig. 5.22 a comparison of repeatability errors is given.

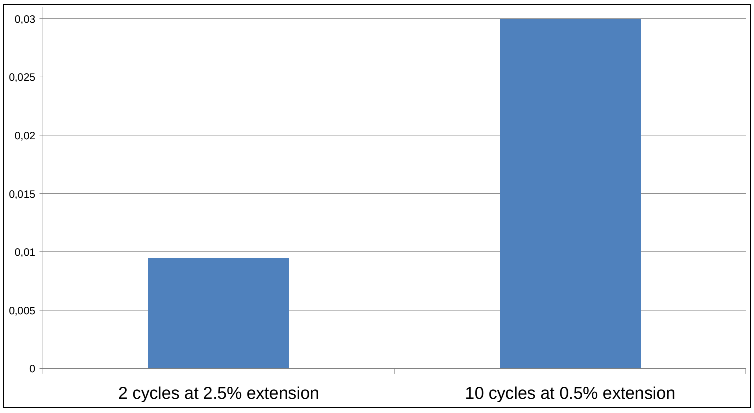

Fig. 5.22: Comparison of repeatability errors

A comparison of hysteresis and linear errors shows that their values are higher for two cycle extension carried out at 2.5% extension as compared to 10 cycle extension carried out at 0.5% extension. Moreover these errors are always high for the first cycle and then they reduce gradually so that for the 10th cycle, their value is very low. Due to this phenomenon the repeatability error is higher for 10 cycle extension as compared to 2 cycle extension as the sensor behaviour deviates considerably from 1st to the 10th cycle.

In Table 5.2, the calculated values of all the errors relevant to sensor performance have been listed.

Table 5.2: Sensor characteristics

No.	***PARAMATER***	***VALUE***
1	Max linearity error for 1st cycle (2.5%)	0.027
2	Max. linearity error for 2nd cycle (2.5%)	0.019
3	Max. hysteresis error for 1st cycle (2.5%)	0.047
4	Max. hysteresis error for 2nd cycle (2.5%)	0.033
5	Max repeatability error (2.5%)	0.0095
6	Independent linearity for 1st cycle (2.5%)	-0.0013
7	Independent linearity for 2nd cycle (2.5%)	-0.0027
8	Sensitivity or gauge factor (2.5%)	12.39
9	Max linearity error for 1st cycle (0.5%)	0.018
10	Max linearity error for 10th cycle (0.5%)	0.012
11	Max. hysteresis error for 1st cycle (0.5%)	0.036
12	Max. hysteresis error for 10th cycle (0.5%)	0.01
13	Max repeatability error (0.5%)	0.03
14	Independent linearity for 1st cycle (0.5%)	-0.015
15	Independent linearity for 10th cycle (0.5%)	-0.008

5.4. Reinforcement architecture and sensor insertion

5.4.1. Reinforcement manufacturing process

An orthogonal/layer to layer interlock structure with 13 layers was woven on a modified conventional loom (ARM Patronic B60).

200 Tex Multifilament carbon tows (6K) supplied by Hercules Inc. were used in warp and weft. The reinforcement and composite parameters have been listed in Table 5.3.

Table 5.3: Reinforcement and composite specifications

No.	***PARAMETER***	***VALUE***
1	Linear density of warp tow	200
2	Linear density of weft tow	200
3	Average thickness of reinforcement	6.5
4	Warp tows density	24
5	Weft tows density	169
6	Areal weight	3908
7	Fibre volume fraction	34.16

Sensors can be inserted in warp or weft directions during weaving. Given the technical complications associated with sensor insertion in warp direction during weaving on a loom, insertion in weft direction has been carried out for preliminary studies. The placement of sensor in the reinforcement was decided so that the sensor was inserted in the middle of the structure. Moreover, since the sensor is inserted during the weaving process it follows the same trajectory as the carbon tows inside the reinforcement. In Fig. 5.23 off the loom dry reinforcement photograph has been shown. Latex coated sensor connections can be seen protruding from the reinforcement.

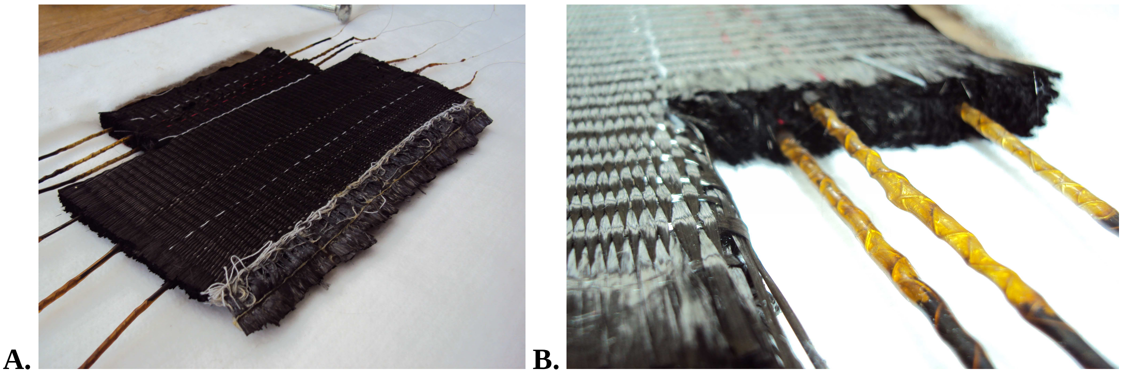

Fig. 5.23: Reinforcement with protruding sensor connections

5.4.2. Composite manufacturing process

After weaving, the reinforcement was carefully removed from the loom and was impregnated using vacuum bag infusion process in order to make the composite part stiff. The resin employed was epoxy EPOLAM 5015. The two connections of the sensor which remain outside the reinforcement at the two ends were carefully separated from the rest of the mould. This was done by creating two vacuum sub moulds inside the larger mould so that the resin may not impregnate the two connections of the sensor (Fig. 5.24-A and B).

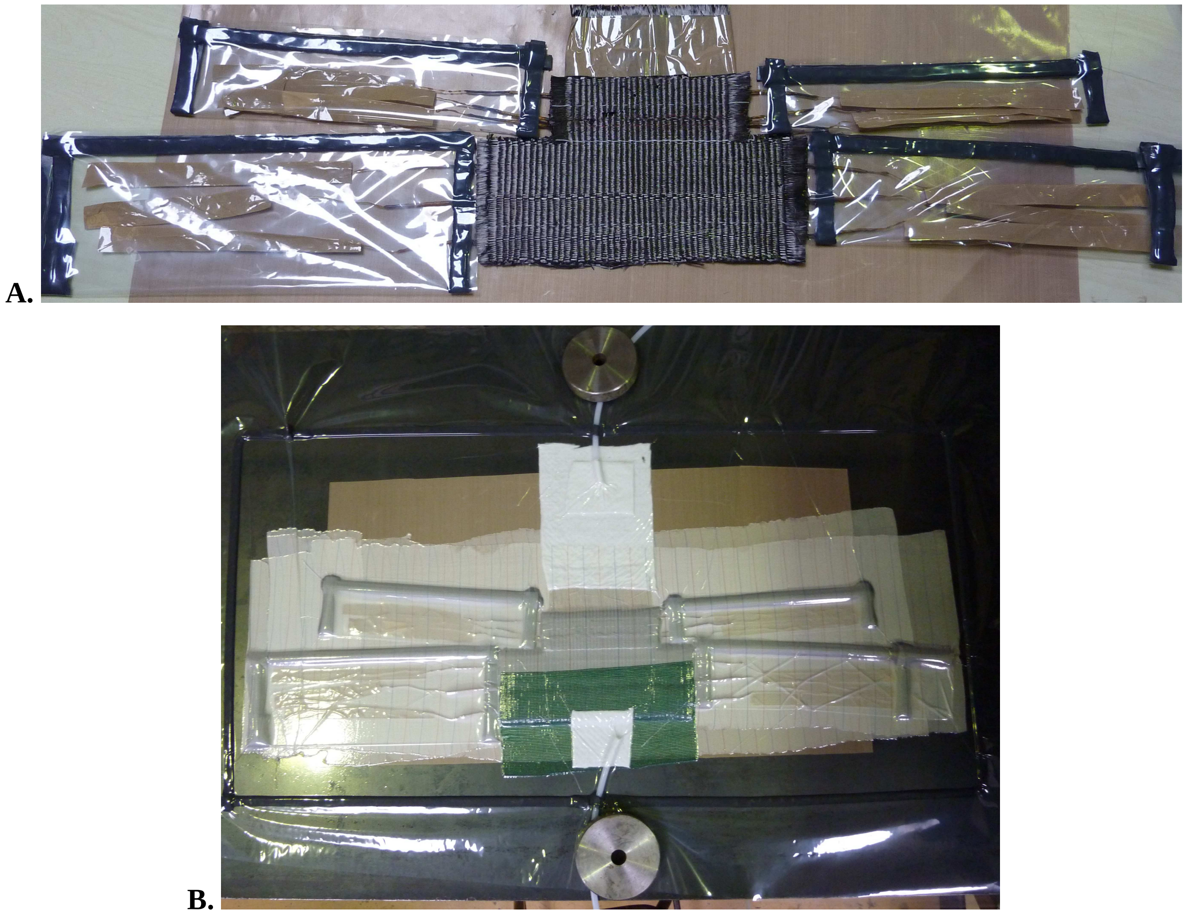

Fig. 5.24: (A) Preparation of sub moulds for vacuum bag infusion
(B) Vacuum bag infusion of the reinforcement with sub moulds

The impregnated composite samples were cut into slabs of “25 cm × 2.5 cm” each, as shown in Fig. 5.25. Samples were prepared according to the norm. In this way each composite specimen of “25 cm × 2.5 cm” had one sensor in the centre.

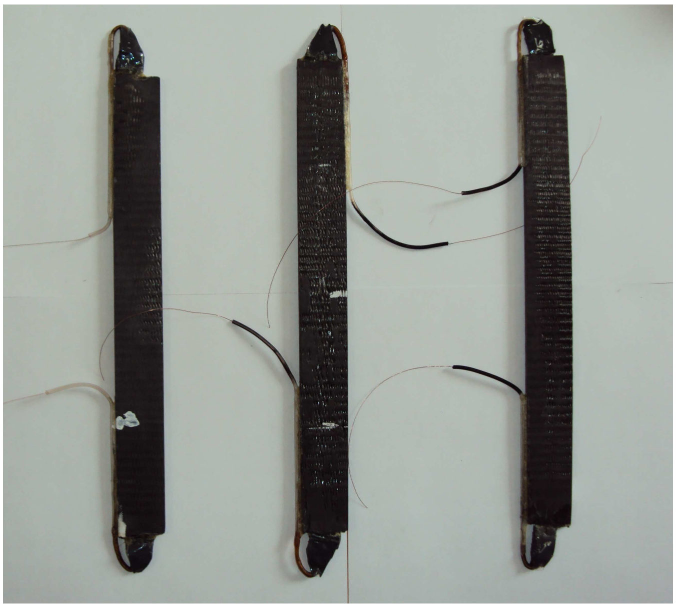

Fig. 5.25: Composite specimens for tensile testing with integrated textile sensor

Fig. 5.26 shows the composite cross section. Weft tows can be seen undulating in the layer to layer configuration.

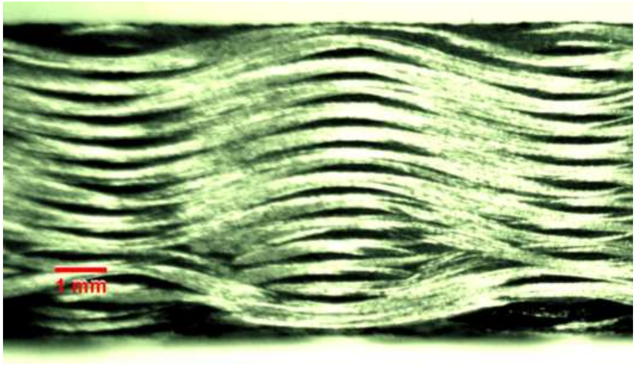

Fig. 5.26: Composite cross section in the weft direction

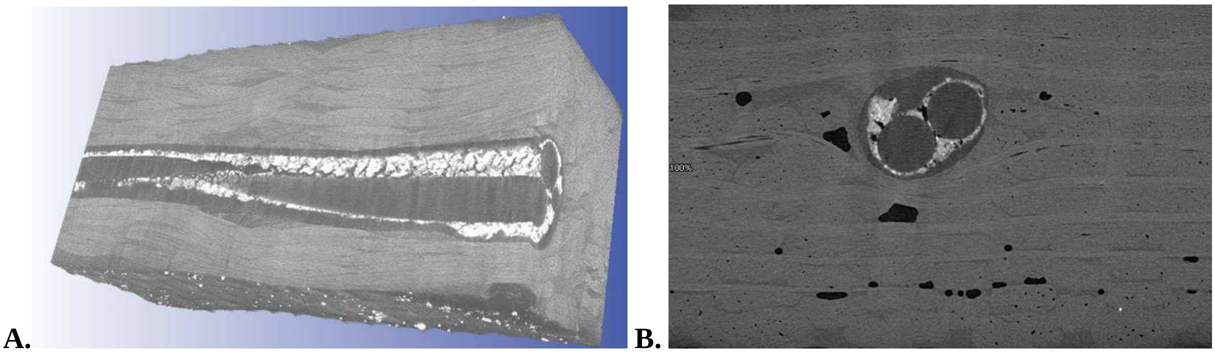

Fig. 5.27: Composite tomographical images (A) weft direction (B) warp direction

5.5. Local measurements and results

5.5.1. On-line measurements - Discussions

The composite specimens were tested on Instron 8500 tester (Fig. 5.28). Tensile strength tests were performed on the composite specimens according to ISO 527-4 [4] in the weft direction i.e., the direction parallel to the inserted sensor. The same Wheatstone bridge was used for resistance variation measurement. The configuration of the testing equipment was also kept the same. The composite structural part specimen was tested at constant test speed of 5 mm/min. The composite underwent traction until rupture.

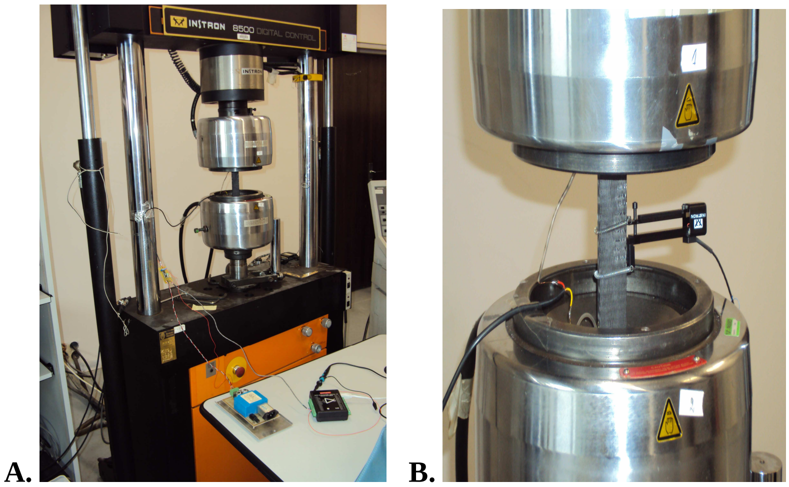

Fig. 5.28: Instron 8500 tensile strength tester with specimen loaded for tensile testing

Resultant stress-strain-resistance relationship curve is shown in Fig. 5.29.

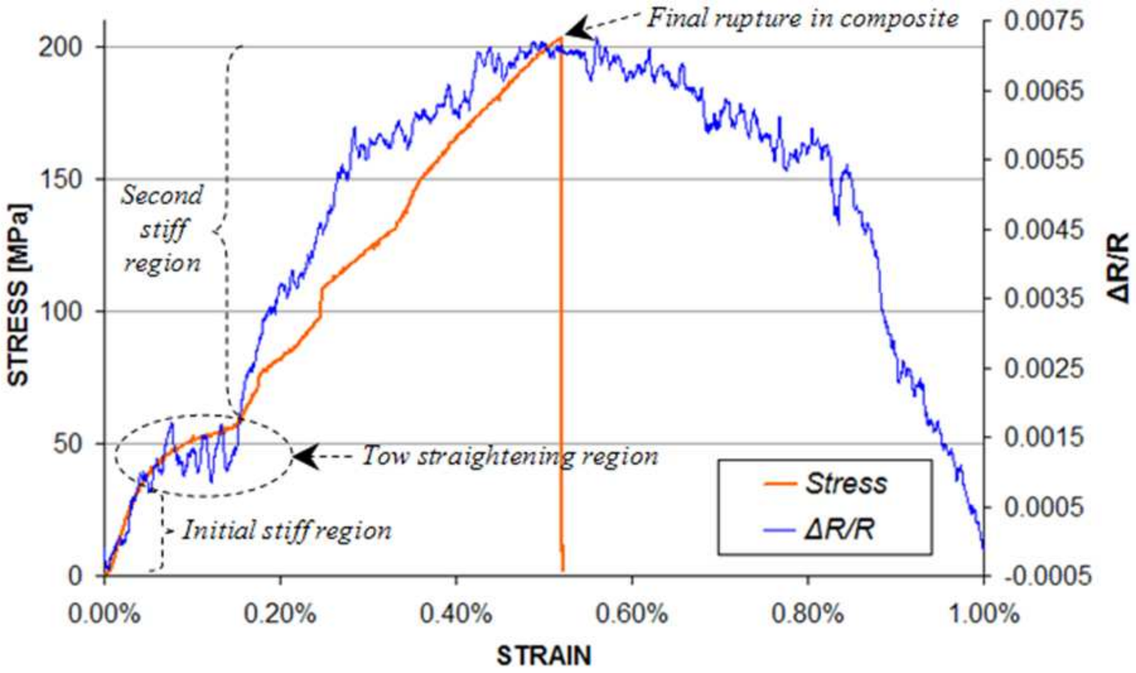

Fig. 5.29: Normalized Resistance and Stress against Strain for Sensor inside composite

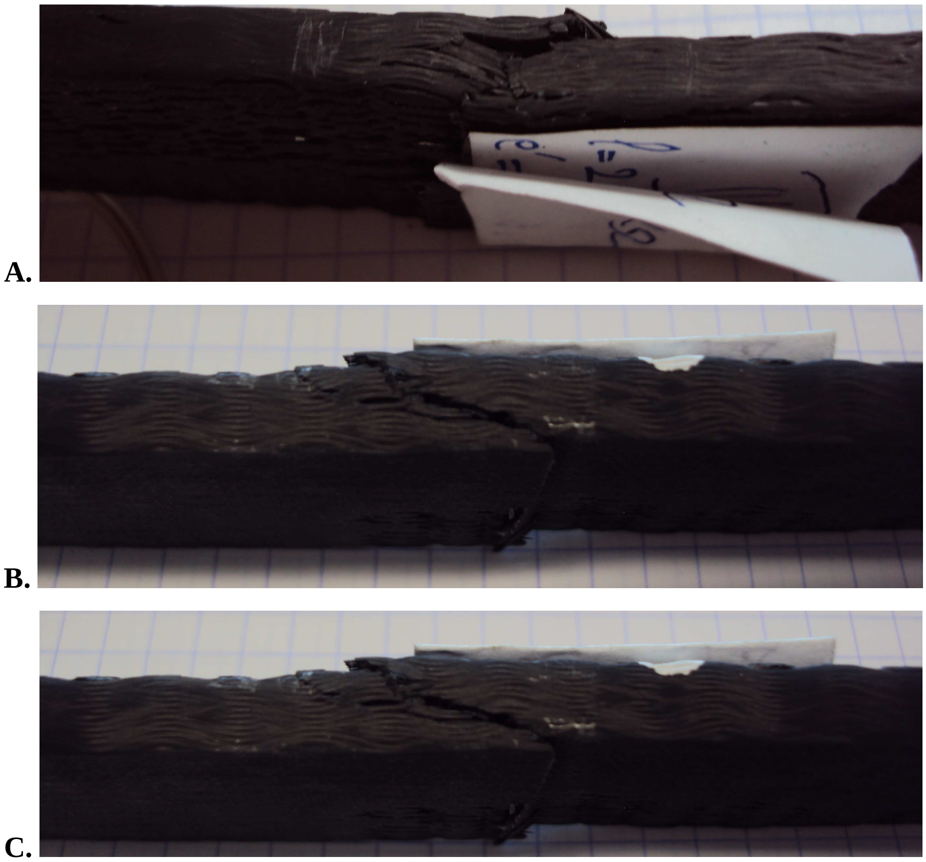

Fig. 5.30: Broken composite samples after tensile strength tests

From Fig. 5.29 it can be observed that the normalized resistance follows the stress-strain curve. The stress-strain-resistance curve can be divided into three regions namely; the initial stiff region where the composite exhibits toughness against the applied load represented by high slope. The second region is called the tows straightening region. It is followed by the second stiff region and finally the point of rupture. The rupture occurred at the strain of 0.52 %, after which the tensile strength tester came back to its initial position at the same speed (5mm/min.). Since the fibrous sensor has not been broken, ΔR/R decreased until 0 as the tester returned to its initial position. However this decrease was not linear because the sensor was still intact while the resin-sensor interface was partially damaged which caused its non linear behaviour.

From the composite micrograph in weft direction given in Fig. 5.26 and also from the photographs in Fig. 5.30, it can be noticed that the weft tows are highly crimped. In the initial stiff region micro cracks start appearing as the composite specimen undergoes traction but the interface at resin and multifilament tows is still intact. That’s why the composite exhibits rigid behaviour. In Fig. 5.29 it can be observed that after the initial stiff region the highly crimped tows tend to straighten due to increasing tensile load in the second region. In this region the micro cracks give way to relative slippage of highly crimped tows in their sockets i.e., the resin-tow interface is relatively weakened. This region called the tow straightening region is enclosed in an ellipse in Fig. 5.29. The region will be characterized by high Poisson contraction. It can also be remarked that the sensor resistance follows the stress strain curve but in the second region the electrical resistance curve is noisier as compared to other regions of the curve which might signify the slippage of tows as well as the sensor in their sockets. This second region is followed by the third region called the second stiff region where the tows are locked in their sockets. In this region the tows resist the applied load and exhibit stiff behaviour as they regain some of their initial stiffness after the straightening of tows in the second region. The electrical resistance varies almost linearly with the applied load, in this region.

The third region is followed by the point of rupture of the composite. After this point ΔR/R, having attained the highest value at the point of rupture, starts dropping down. The fact that the sensor resistance attains its initial value after the rupture signifies that the sensor, owing to its elastic properties, is not destroyed with the composite.

In Fig. 5.31, a comparison of the electrical resistance variation for identical, integrated (sensor embedded in the composite) and unintegrated (sensor before insertion) has been given.

Initially the sensors behave essentially the same way as is obvious from the two curves. The two curves part ways at around 0.20% elongation which roughly coincides with the beginning of third region namely; the second stiff region in Fig. 5.29. Unlike in situ sensor the out-of-composite sensor has linear resistance-strain relationship.

This difference in the two curves signifies the differences in the milieu around the two sensors. The out of composite sensor is unconstrained while the in situ sensor is constrained by the reinforcement and resin inside the composite as it has to follow the deformation pattern of the composite.

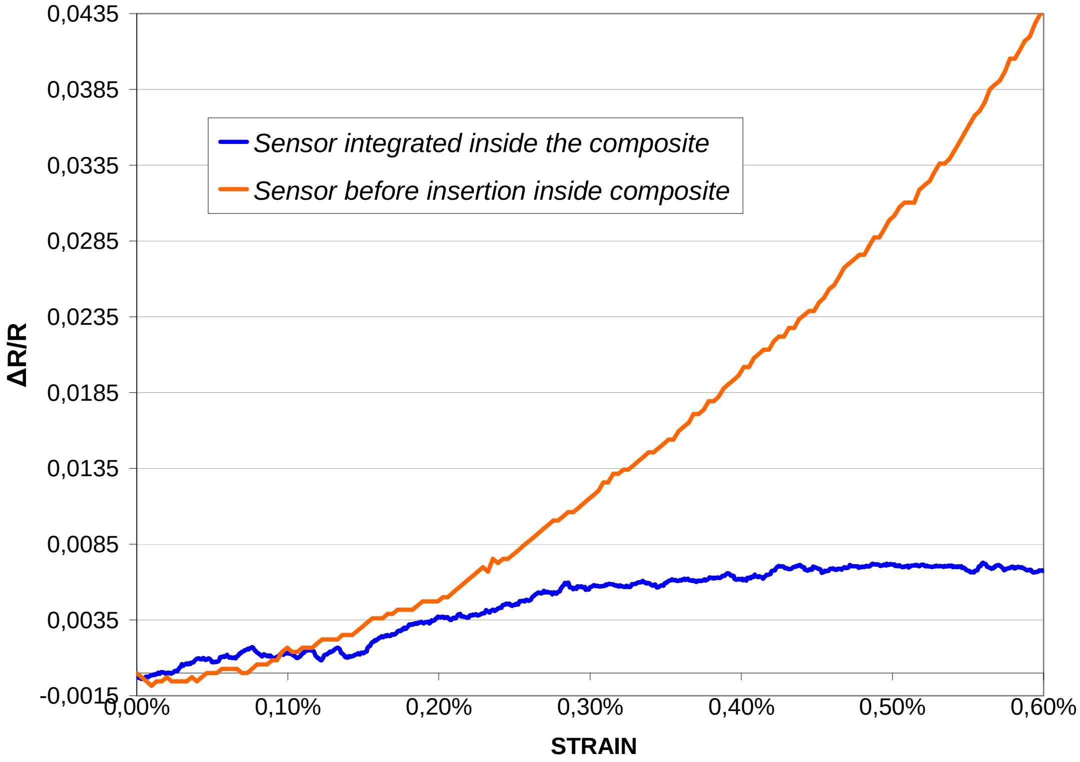

Fig. 5.31: Normalized Resistance against Strain for integrated and out of composite sensors

In Fig. 5.32-A and B, photographs of specimens which underwent these tensile tests are shown. The mode of rupture for all the samples is nearly the same. There is a single zone of rupture half way along the length of samples where tows give in to applied traction in rather brittle fashion. Tow pull out can also be seen in some of the samples but does not seem to be the dominant mode of rupture (Fig. 5.32-A). Low strain to failure is due to low fibre pullout during failure. The initial crack seems to have rendered the structure weak. The crack then propagated in the structure till the complete fracture of tows at the zone of rupture (Fig. 5.32-B).

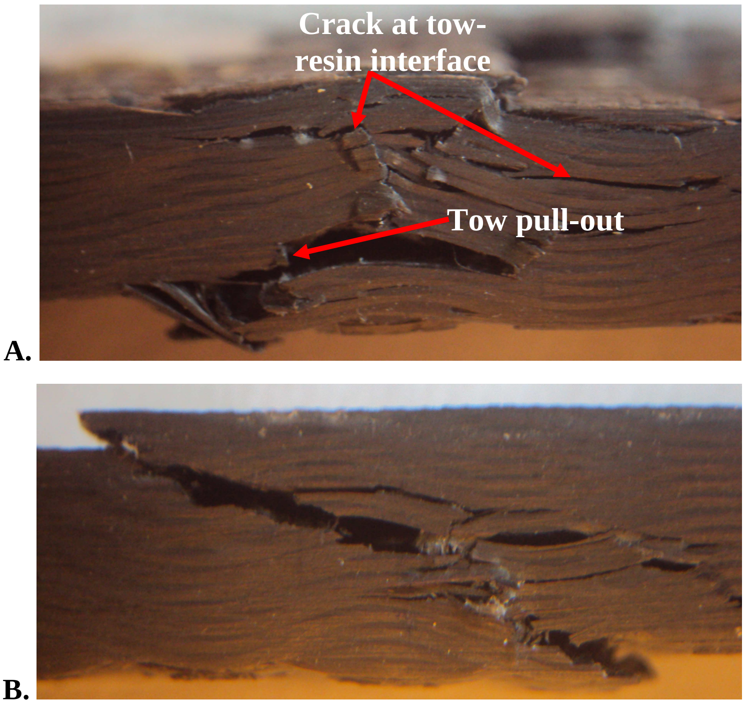

Fig. 5.32: Surface photographs on composite samples taken after tensile strength tests A) Weft tow pull-out and crack at tow-resin interface B) Complete transversal rupture

Fig. 5.33 shows tomographical images of the samples which underwent traction. Sensor cross section and its path at and near the zone of rupture can be observed.

In Fig. 5.33-A, B and C, it can be observed that the sensor-resin interface has a lot of voids. These are caused by poor resin-sensor interfacial properties. The insulating medium on the sensor surface needs to have good adherence with the epoxy resin and the carbon fibre reinforcement. Damage that occurred at the main rupture zone has propagated along the sensor interface giving rise to debonding of the sensor. A kink in the sensor can be observed (Fig. 5.33-A) which is caused by the relaxation of sensor as it tries to regain its original dimensions after the tensile loading damages the composite sample. The insulation coating around the sensor renders it thick as well which is undesirable as thick insulation coatings might adversely affect the mechanical properties of the reinforcement inside the composite.

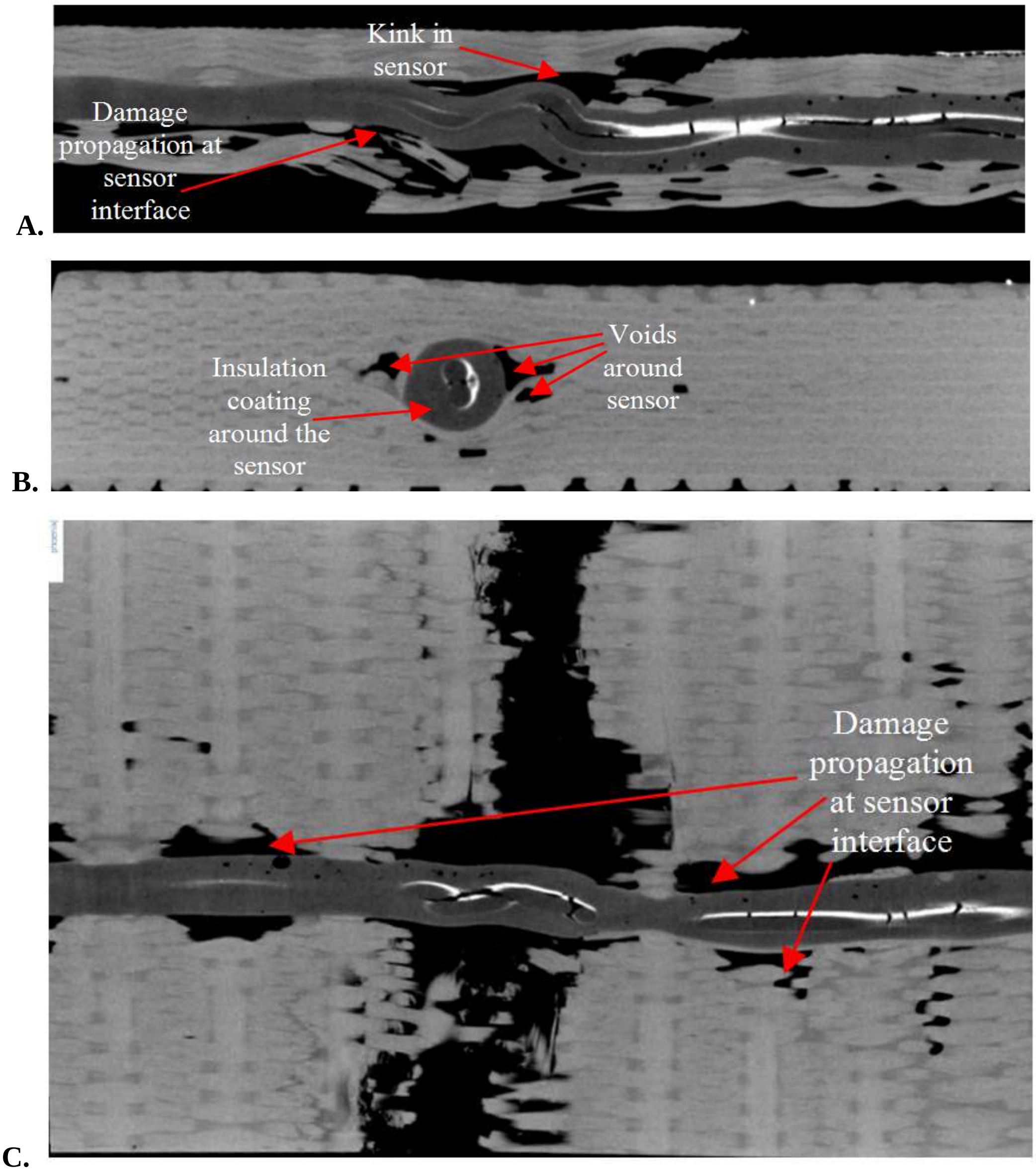

Fig. 5.33: Tomographical images of sensor inside a tested sample near the zone of rupture A) Longitudinal section B) Transversal section C) Top view

5.6. Conclusion

In conclusion, the sensor developed for in situ measurements on carbon fibre composite structures is capable of detecting strain in the structure. The electrical resistance variation in the sensor follows the deformation pattern of the composite, mainly due to its sensitivity to its environment and because of the fact that it is integrated in the structure and follows the fibre architecture of the reinforcement. It has been shown that the integrated textile sensors inside the reinforcement can be used as in situ strain gages for the composite materials. Moreover, if the placement of these sensors inside the reinforcement is carefully chosen, they can be used to follow the local deformation pattern so as to better understand the deformation mechanisms and predict life time of the composite parts. At present the sensors have been tested for tensile loading. Tensile strength tests were chosen to demonstrate the basic features of this novel SHM approach. In the future these sensors will be used for bending and fatigue tests on similar 3D carbon fibre woven reinforcement based composites.

However optimisation of sensors needs to carried out in order to prepare thinner sensors having negligible affect on reinforcement geometrical and mechanical properties. For carbon fibre based reinforcements which require an insulation coating on the sensor surface, a better and finer coating needs to be applied.

In view of the test results presented, it can be concluded that these sensors can be used for in situ health monitoring of various types of composites especially for different deformation modes of 3D or multilayer reinforcements in which different layers don't necessarily deform in homogenous manner. For instance, the fibrous sensors may well be used for the detection of transverse strains and for the detection of interlaminer slippage.

5.7. References

[1] C. Cochrane, V. Koncar, M. Lewandowski, and C. Dufour, "Design and development of a flexible strain sensor for textile structures based on a conductive polymer composite," Sensors and Actuators A, vol. 7, pp. 473-492, 2007.

[2] "Sensor signal conditioning," in Sensor Technology Handbook, J. Wilson, Ed.: Newnes, Dec. 2004.

[3] "http://www.datasheetdir.com/INA101+Instrumentation-Amplifiers," consulted on 06/05/2010.

[4] "NF EN ISO 527-4 Plastiques - Détermination des propriétés en traction," in Partie 4 : Conditions d´essai pour les composites plastiques renforcés de fibres isotropes et orthotropes: CEN, 1997.

GENERAL CONCLUSION AND FUTURE DEVELOPMENTS

This report is divided into two parts. The first part deals with the weaving of carbon and glass multifilament tows to form 3D interlock reinforcements, modelling of reinforcement geometry and influence of geometry and weaving parameters on global tensile properties through the calculation of strength transfer coefficients. The second part is concerned with the development of piezoresistive sensors for on line local structural health monitoring of composites reinforced with 3D woven interlock reinforcements.

In the first chapter of this report, an overview of the 3D weaving, 3D interlock reinforcements, and their classification and modelling techniques has been presented. A state of the art of failure mechanisms of 3D woven composites and influence of weaving on mechanical properties of woven composites due to degradation imparted on tows is also given. A survey of the literature has shown that there are various classification methods which can be used to assign well defined nomenclature to a vast variety of interlock structures. An overview of the approaches adopted for the modelling of woven fabrics/reinforcements shows that diverse techniques can be used for the modelling. They depend upon the scale and structure to be modelled, as well as the kind of information intended to be extracted from the model. Geometries modelled by these approaches are different from the real structures, weaving parameters and weavability limits and manufacturing constraints. Therefore, for realistic geometrical modelling of reinforcements, it is important to have better knowledge of real geometries and weaving parameters. The state of the art of the global failure mechanisms of 3D woven composites shows that an extensive research work has already been carried out on the failure mechanisms during tensile loading of 3D woven composites. Most of this work is related to orthogonal woven structures. Moreover, none of the studies discuss the influence of interlocking warp amplitude on the tensile properties. On the other hand, literature review shows that tow degradation due to abrasion and friction during weaving negatively influences the tow tensile strength and modulus. The weaving damage has little effect on tensile modulus, whereas its impact is reported to be quite significant on tensile strength.

Chapter 2 deals with the development of geometrical model of woven interlock reinforcements. An approach for the characterization of initial (before weaving) and final (after weaving) geometry of multifilament tows is presented. A weaving parameter called ‘relative fractional cover’ has been defined allowing the determination of cross sectional geometries of tows. Once shape functions are assigned, an analytical approach can be used to calculate all the basic fabric geometry parameters. This is followed by the description of 3D interlock reinforcements weaving on a modified conventional loom. Technical issues faced in their weaving, along with some proposed solutions, are given in detail. This section is followed by the weaving of layer to layer/orthogonal and angle interlock samples from glass and carbon multifilament tows. Their analysis and validation of geometrical modelling approach on the basis of visual observations and physical tests is described. It has been demonstrated that the geometrical modelling approach predicts all the basic parameters of the reinforcement from technological data available to the weaver.

Chapter 3 deals with the study of global mechanical deformations in 3D woven interlocks. Three angle interlock reinforcements were woven from 6K carbon multifilament tows. These reinforcements were designed so that all the structural parameters were kept the same except for binding depth *(y)* and binding step *(x)*. The study aimed at evaluating mechanical changes that occur along the complete manufacturing line starting from a so called virgin tow obtained from bobbin to the formation of the composite. A novel parameter called the 'strength transfer coefficient' is proposed for evaluating the influence of the reinforcement architectural parameters on tensile properties of the reinforcement.

It was found that the average breaking strength obtained for 'on loom' samples was 5.06% lower than for the samples obtained from virgin bobbin. Afterwards, tensile strength tests were performed on woven fabric reinforcements. A novel approach for the tensile testing of dry interlock reinforcements was adopted as no precedent of such tests was found in the literature. It was found that the binding depth and step i.e., the warp binder path influence tensile properties not only in warp direction but in the weft direction as well. By reducing the binding depth of warp the pressure on the weft tows and their collimation is reduced considerably. Consequently the 3rd variant which was conceived to have minimum binding $(y = 2)$ depth was the strongest in the weft direction (519 MPa). Moreover warp binder path determines the fibre packing and compactness of the structure which ultimately influences the thickness and fibre volume fraction of the reinforcement. That's why the 2nd variant having an intermediate binding depth $(y = 3)$ is the strongest in the warp direction (368 MPa).

For the composites manufactured from these reinforcements, it was found that the compactness of the structure played an important role in determining ultimate resin impregnation and final thickness of the composite. These factors, in turn, influence fibre volume fraction and tensile strength of the composites. While comparing the change in thickness incurred due to infusion, it was found that the highest percentage change occurred in the 1st variant. It may be explained by the fact that this is the least compact structure owing to through the thickness binding of interlocking warp. The 2nd variant being the most compact underwent least change. This is due to relatively lower binding depth of interlocking warp $(y = 3)$ and jaw type construction. The 3rd variant having lowest binding depth of interlocking warp $(y = 2)$ exhibits highest strength in both the warp and weft directions.

Strength transfer coefficient has been calculated for all the reinforcements in the warp and weft directions. It shows that for the 1st variant, the value is less than unity in warp direction which signifies a net loss in strength as a tow is integrated in the composite. For all other variants, the value is greater than unity in both the warp and weft directions. The strength transfer coefficient in the warp and weft directions increases with the decreasing binding depth and attains the maximum value for the 3rd variant which signifies a positive impact of the integration of the tow in the woven reinforcement. Such structures are stronger in both the warp and weft directions. This coefficient is one of many factors which can help in the designing of reinforcement most suitable for a special composite structural part.

Part 2 of the thesis is composed of two chapters. Chapter 4 gives state of the art of sensing system for local in situ deformations that are used in intelligent textiles and structural health monitoring of composites. In first section of this chapter, state of the art of several diverse mechanisms such as semi-conductive coatings, nano-tube networks dispersed in matrices and self sensing in carbon composites is described. It has been highlighted that the use of semi conductive coatings for SHM offers much promise and needs to be explored further. The second section of this chapter deals with structural health monitoring. It can be concluded from the state of the art that a signal acquisition and conditioning system are as indispensable for a health monitoring system as a sensing mechanism.

Chapter 5 deals with the development of flexible textile sensors to serve as a strain gauge inside a composite structure for its on-line local structural health monitoring. This development is followed by sensor insertion in the reinforcement during weaving, data acquisition, conditioning and final analysis of the test results.

A nano particle based composite coating developed in our laboratory was adopted for the purpose of the realization of suitable sensors. The volume percentage of carbon black, textile fibre substrate and the thickness of the coating were optimised for the realization of a sensitive and flexible strain gauge, able to detect very low local deformations (less than 1% of the composite length) in a 3D interlock reinforcement based composite. Polyethylene was used as the substrate and a double ply was employed to reduce the initial resistance to a detectable level. The final sensor having initial resistance of 1KΩ/cm homogeneously was inserted in weft direction in layer to layer/orthogonal interlock reinforcement during weaving. The sensor was inserted in 7^{Th} layer of 13 layers of reinforcement, so that it was in the centre of the reinforcement. A strain gauge amplifier and signal conditioning module was also developed and was used in conjunction with commercially available Keithley KUSB 3100 data acquisition module. The sensor was connected in Wheatstone bridge configuration. The test results obtained from quasi static tensile loading of composite samples are promising as the sensor was able to detect very low strain (0.52% at break). Since the sensor was inserted as a weft during weaving, it was able to follow the deformation pattern only in weft direction of the composite sample. It can be surmised that the number and location of sensors inside the reinforcement can be chosen ‘strategically’ according to the reinforcement geometry and expected stress conditions during service life of the composite part.

This system can also be employed for detecting other modes of deformations such as bending and fatigue due to repeated deformations & vibrations.

The research work presented here holds promises for further development of efficient and reliable on line local structural health monitoring tools for composite parts. The sensors can be optimized for use in nearly any reinforcement. The sensor structure and applied conductive piezo resistive coatings & materials with data amplification and conditioning module could be modified according to the modes and velocity of deformations. Moreover, sensing mechanisms with different sensitivity levels will have to be developed for different stress conditions such as ballistic impacts and crash.

Appendix 1:

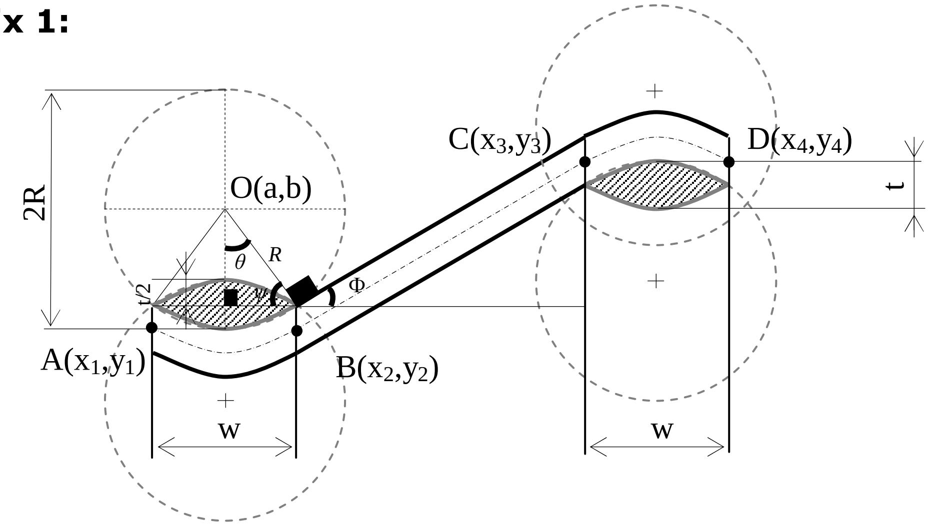

$$90° + \theta + \psi = 180°$$

$$\theta + \psi = 90° \qquad (1)$$

$$90° + \Phi + \psi = 180°$$

$$\Phi + \psi = 90° \qquad (2)$$

Solving (1) and (2):

$$\theta = \Phi$$

From the above Figure

$$Tan\theta = \frac{w/2}{R - t/2} \qquad (3)$$

Where

$$R^2 = \left(\frac{w}{2}\right)^2 + \left(R - \frac{t}{2}\right)^2$$

$$R = \left(\frac{w^2 + t^2}{4t}\right) \qquad (4)$$

Putting (4) in (3):

$$\theta = Tan^{-1}\left(\frac{2wt}{w^2 - t^2}\right)$$

Which also implies that

$$\Phi = Tan^{-1}\left(\frac{2wt}{w^2 - t^2}\right)$$

Appendix 2:

6 Layers of 3 Layers Orthogonal Interlock with layer-to-layer binding.

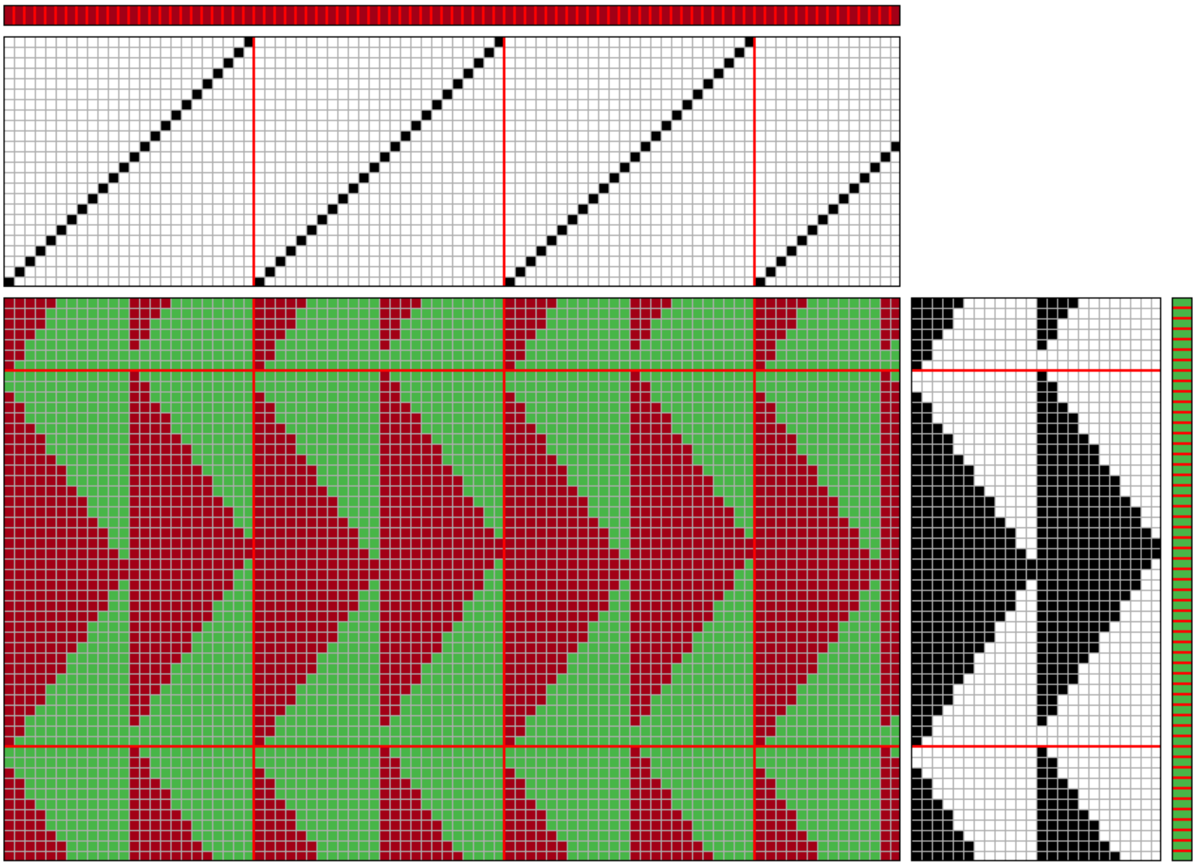

Appendix 3:

8 Layers Orthogonal interlock with layer-to-layer binding.

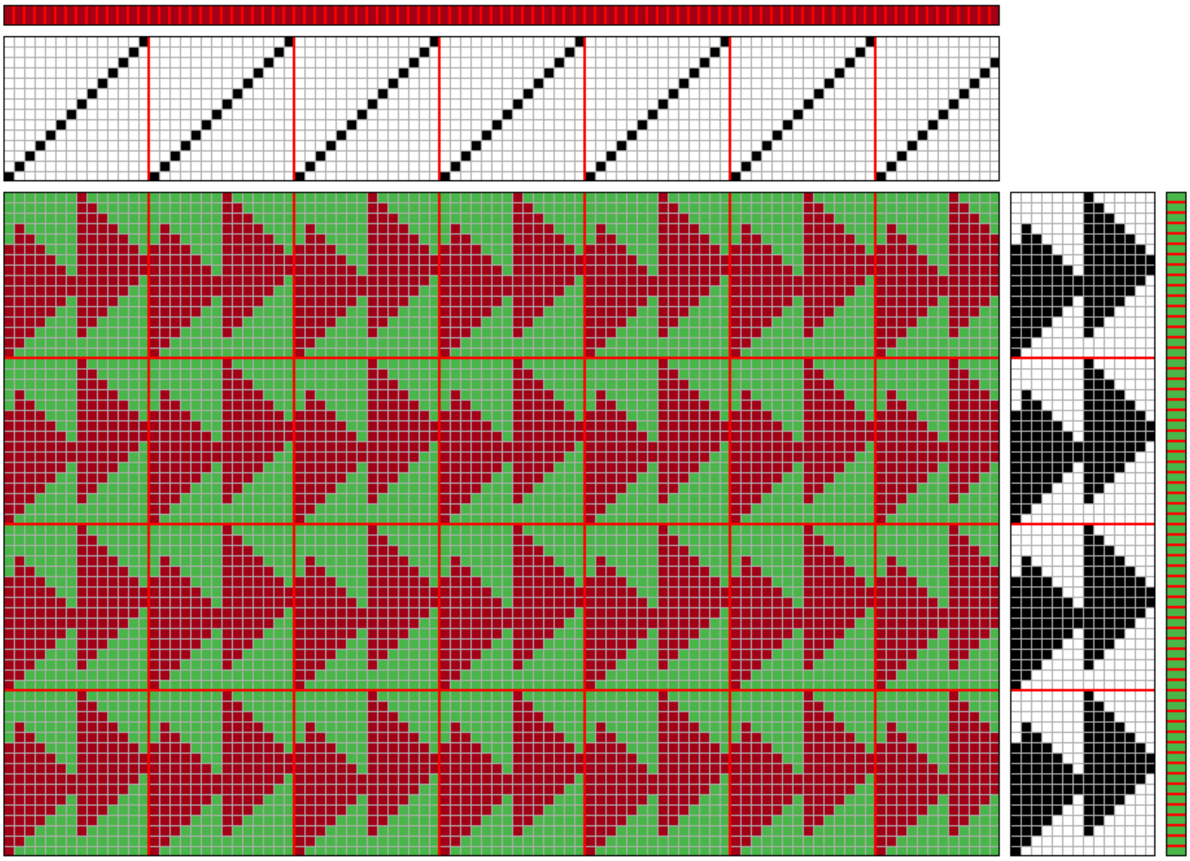

Appendix 4:

13 Layers Orthogonal interlock with layer-to-layer binding.

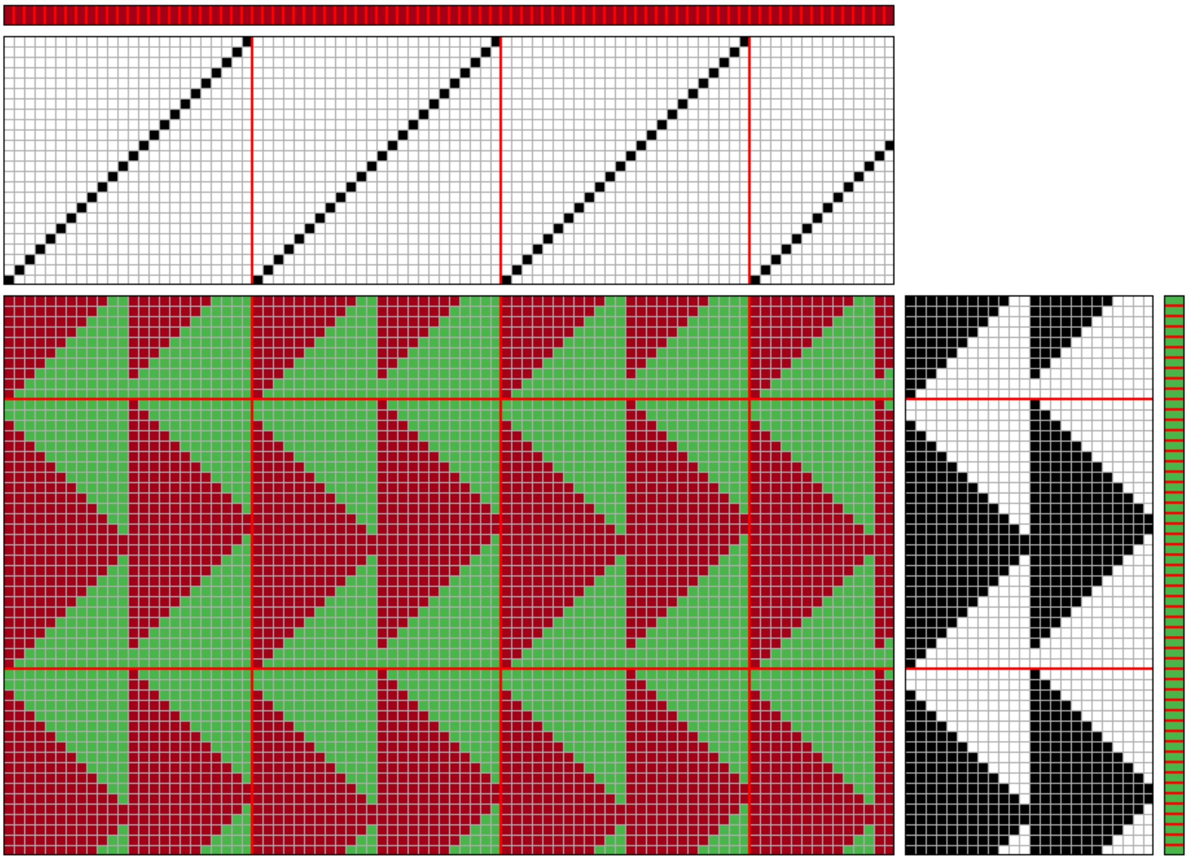

Appendix 5:

5 Layers angle interlock, through-the-thickness binding (1st variant).

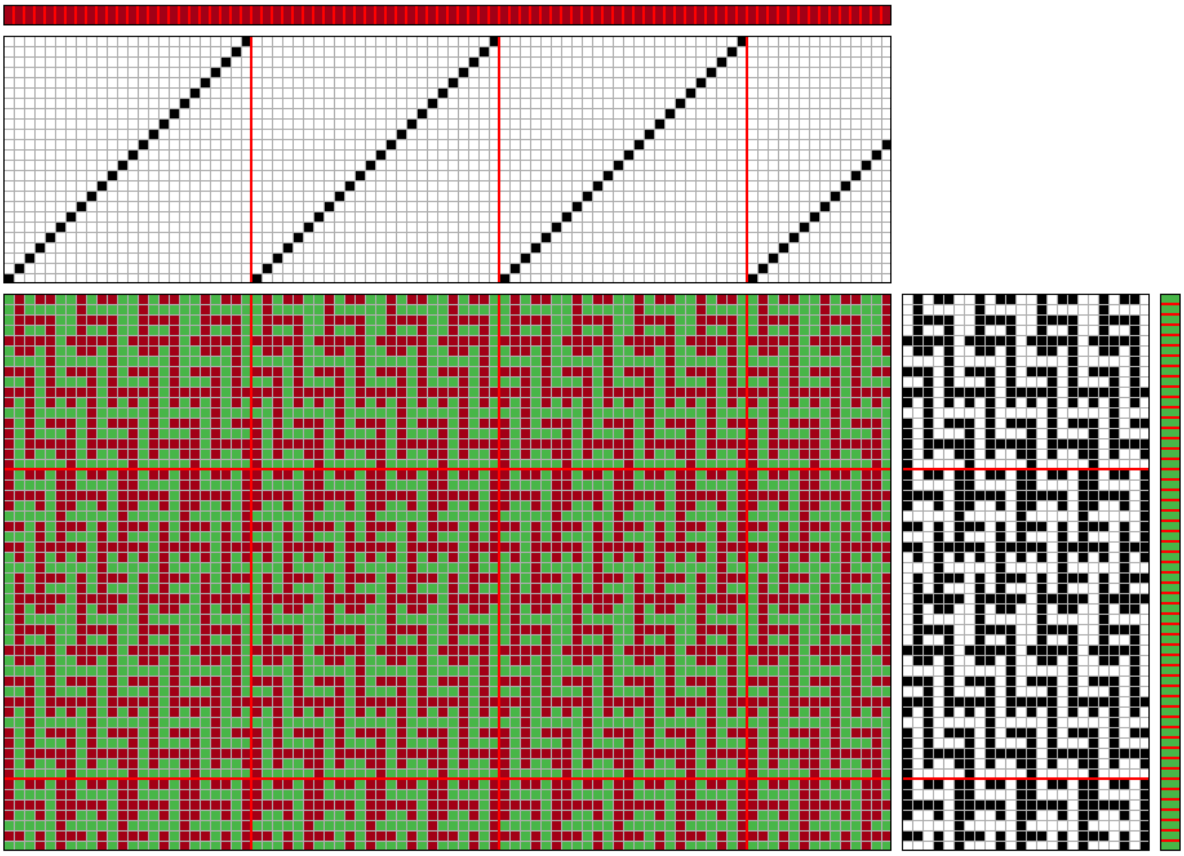

Appendix 6:

5 Layers angle interlock, intermediate-thickness-binding (2nd variant).

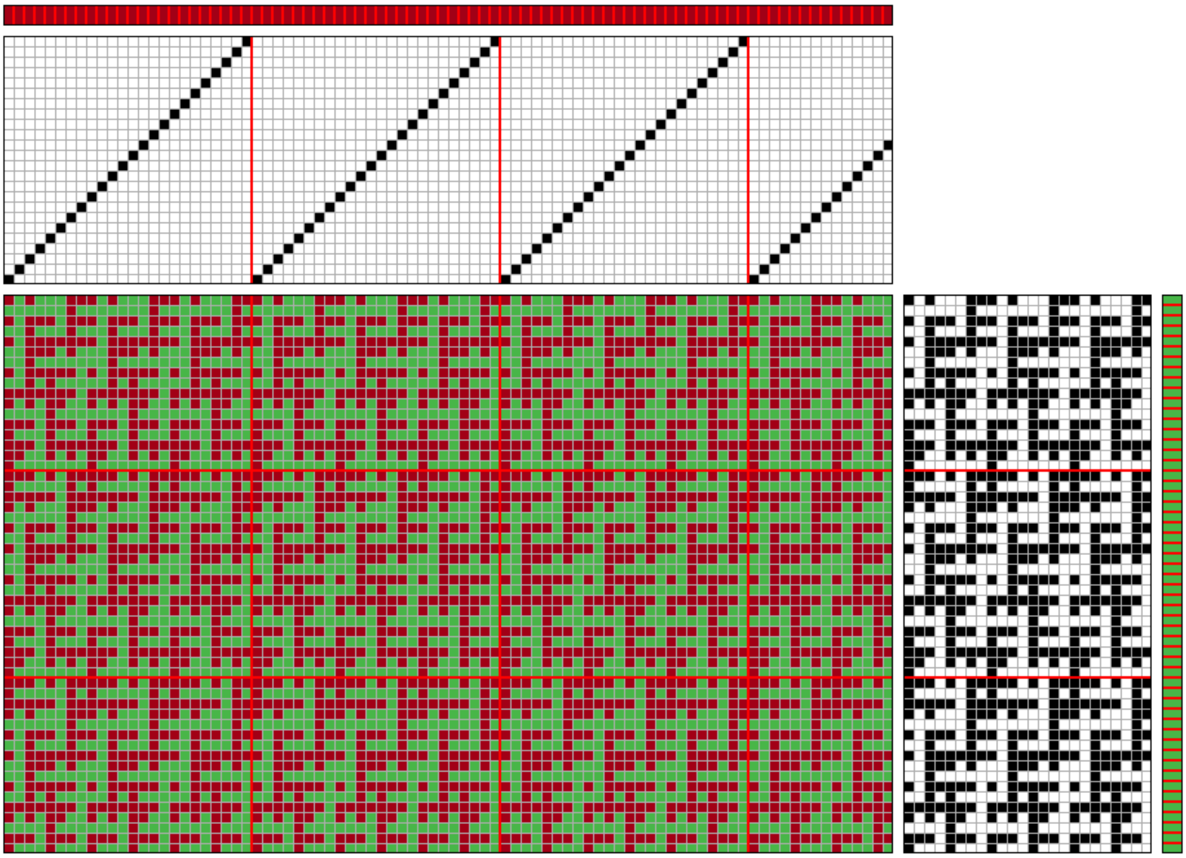

Appendix 7:

5 Layers angle interlock, layer-to-layer binding (3rd variant).

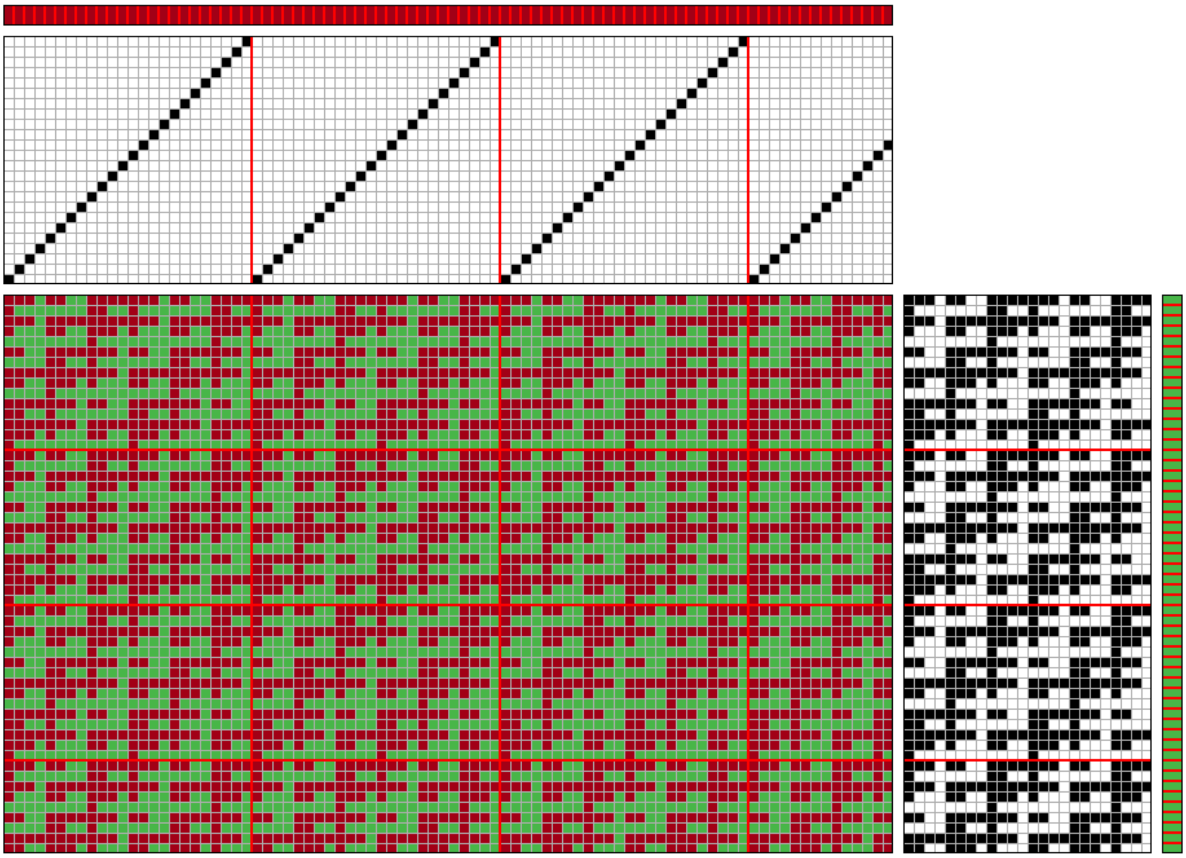

Appendix 8:

$$Stress = \frac{Force}{Area}$$

Force is directly measured by the tensile strength tester whereas the sensor area is calculated as area of an ellipse. The width (w) and thickness (t) of the sensor can be calculated from the SEM photograph given in Fig. 5.9 (A).

Therefore:

$$Area = \frac{\pi \times w \times t}{4}$$

Where;

$$w = 1.68$$

$$t = 1.26$$

$$Area = \frac{\pi \times 1.68 \times 1.26}{4}$$

$$Area = 1.66 mm^2$$

Geometrical modelling and characterization of 3D warp interlock composites and their on-line structural health monitoring using flexible textile sensors

Abstract: This thesis is divided in two parts. In the first part a geometrical modelling approach has been developed in tandem with weaving parameters. The reinforcements were woven on a modified conventional loom to study the geometry of these structures. Their weaving has been described in detail. The weaving parameters have been correlated to the modelling approach. The meso structural modelling approach is capable of predicting essential reinforcement geometrical characteristics at meso structural level without being too complicated. Furthermore, mechanical characterization of 3D interlock reinforcements has been carried out in such a way that a track of mechanical properties during the complete production cycle has been maintained. A novel parameter called strength transfer coefficient was proposed which allows better understanding of the influence of structural parameters on the final properties of the composite.

In the second part of the thesis an online structural health monitoring system which is composed of a textile based sensor and signal amplification and treatment module, has been developed. This system is capable of detecting structural deformations in the composite as the sensor is integrated during the manufacturing of the reinforcement and can follow its deformation pattern when composite is subjected to tensile loading in a real time.

Modélisation géométrique et caractérisation des composites renforcés avec des tissu 3D interlock-mesure in-situ par des capteurs textiles

Résumé : Ce mémoire de thèse de doctorat est structuré en deux parties. Dans la 1ère partie, une nouvelle approche traitant la caractérisation géométrique et mécanique est décrite. La modélisation géométrique de tissu 3D interlock est corrélée avec les paramètres de tissage afin de mieux prendre en compte ces paramètres. Le tissage de tissu 3D interlock est décrit en détail. Par la suite, une étude a été menée pour mieux comprendre les changements qui se produisent dans une mèche de carbone lorsque cette dernière est intégrée dans un renfort. Un coefficient de transfert des propriétés mécaniques a été proposé permettant une meilleure compréhension de l'influence des paramètres structuraux sur les propriétés d'un composite.

Dans la 2eme partie du mémoire, un système de mesure in situ pour les composites a été développé. Ce système comporte un capteur souple et un module de traitement de données et d'amplification des signaux. Le capteur fibreux développé durant nos recherches a été inséré pendant le tissage comme un fil de trame. Le système a été testé sur une plaque en composite, contenant les renforts en 3D interlock, en traction. Le capteur suit fidèlement les déformations de la plaque composite jusqu'à la rupture.

Keywords: Weaving, Interlock reinforcement, geometrical modelling, mechanical characterisation, carbon tows, on line structural health monitoring, textile sensor, tensile properties

Université des Sciences et Technologie de Lille (USTL)
Laboratoire GEMTEX de l'Ecole Nationale Supérieure des Arts et Industries Textiles
2, allée Louise et Victor Champier BP30329. 59056 Roubaix (France)